

**Biophysical characterization of ligand binding and release of *Anthereae polyphemus*
Pheromone Binding Protein 1 (ApolPBP1)
and
Exploring the nickel proteome**

by

Suman Mazumder

A dissertation submitted to the Graduate Faculty of
Auburn University
in partial fulfillment of the
requirements for the Degree of
Doctor of Philosophy

Auburn, Alabama
August 3, 2013

Keywords: NMR, ApolPBP1, Fluorescence spectroscopy,
Delipidation, HSQC

Copyright 2013 by Suman Mazumder

Approved by

Smita Mohanty, Major Professor & Co-chair, Associate Professor of Chemistry & Biochemistry
Eduardus Duin, Co-chair, Associate Professor of Chemistry & Biochemistry
Holly Ellis, Associate Professor of Chemistry & Biochemistry
Peter Livant, Associate Professor of Chemistry & Biochemistry
Steven Mansoorabadi, Assistant Professor of Chemistry & Biochemistry

Abstract

In moths, pheromone binding proteins (PBPs) transport the hydrophobic pheromone molecules to the membrane-bound receptors across the aqueous sensillar lymph to trigger the neuronal response. We showed here that, recombinant *Antheraea polyphemus* PBP1 (ApolPBP1) expressed with hydrophobic molecule(s) endogenous to the *Escherichia coli* which keeps the protein in the ligand-bound conformation at high pH but switches to the ligand-free conformation at low pH. Two molecular switches are considered to play a role in this mechanism: (i) protonation of His70 and His95 situated at one end of the binding pocket and (ii) switch of the unstructured C-terminus at the other end of the binding pocket to a helix that enters the pocket at low pH. Here, we show the role of the histidine-driven switch in ligand release and the role of C-terminus in ligand binding or releasing for ApolPBP1 by binding of 1-aminoanthracene (AMA) by fluorescence spectroscopy and solution NMR. Mutation of His70 and His95 to alanines drives the equilibrium toward the ligand-bound conformation even at low pH thus eliminating the pH-induced histidine-dependent switch which exists in the wild type protein. The C-terminal truncated proteins exist only in the bound conformation at all pH levels and failed to undergo pH- or ligand-dependent conformational switching. Our studies revealed that these proteins can bind ligand even at low pH in contrast to the wild type protein. Although C-terminal truncated proteins could bind ligands even at low pH, they had reduced affinity for the ligand at both low and high pH compared to that of wild-type ApolPBP1. This indicates that apart from helping in the ligand releasing mechanism, the C terminus might have a role in the

ligand binding mechanism and/or preventing the early escape of the ligand from the binding pocket. Our results are in contrast to those reported, where C-terminal truncated proteins had similar or increased pheromone binding affinity at both high and low pH. We also examined the role of three charged residues (Asp132, Glu137 and Glu141) present inside the C-terminus tail. We discovered that, single mutations (D132N, E137Q and E141Q) and double mutations (D132NE137Q and E137QE141Q) have no effect on the conformation of the protein. They behaved as the wild type protein.

Most of the bacteria and some plant species require nickel for the production of many essential enzymes inside their cells. In this current study we are trying to find out and characterize small nickel containing proteins from an Archaea, *Methanothermobacter marburgensis*. We also tried to use a metallobiome approach and discover any nickel-containing proteins that have not been characterized before. In the nickel-hyperaccumulating plant *Streptanthus polygaloides* the goal was to test if ICP-EAS was sensitive enough to detect the nickel-containing proteins during the purification steps. This detection method works really well and several nickel protein containing fractions have been isolated. More purification steps will be needed however to obtain pure proteins and to fully characterize them.

Acknowledgments

I highly acknowledge my profound gratitude to my advisor Dr. Smita Mohanty, Co-Chair and Major Professor for her guidance, support, encouragement, and help throughout the entire period of my graduate research work at Auburn University. I would like to convey my heartfelt gratitude to Dr. Evert Duin, Co-Chair, for his invaluable guidance, support, encouragement, persistence, and supervision for the completion of my graduate study. I am also very much thankful to my committee members; Dr. Holly Ellis, Dr. Peter Livant, Dr. Steven Mansoorabadi, and Dr. Jacek Wower, for their valuable comments and instructive suggestions towards my research and dissertation.

I am also very much thankful to Dr. Rik Blumenthal, Graduate Program Officer at the Dept. of Chemistry & Biochemistry, Dr J. V. Ortiz, Chair of the Dept. of Chemistry & Biochemistry and Dr. George Flowers, Dean of the Graduate School, for all the help they provided during a very tough situation in my life.

I would like to thank my current lab partners, Divya Prakash, Xiao Xiao, Selamawit Ghebreamlak and former lab partners Dr. Uma Katre, Dr Shigeki, Dr Monimoy Banerjee, Dr Chengdong Huang, Pricilla Ward, Dr. David Zoetway and Bhaven Sayania for their generous support and help during my graduate work.

I would like to specially thank Dr. Mohiuddin Ovee, a priceless friend, for the help and mental support he provided during my stay in Auburn.

I am also grateful to the Department of Chemistry and Biochemistry at Auburn University for providing me the opportunity to carry out my dream. I would like to thank Malone-Zallen Graduate Research Fund for their support during my graduation work.

I would also like to thank the United States Department of Agriculture PECASE Presidential Early Career Award for Scientists and Engineers Award 2003-35302-12930, and grant 2011-65503-20030, National Science Foundation grant IBS-0628064, and National Institutes of Health grant DK082397 for their funding to Dr. Smita Mohanty, which financially supported my research in her lab.

Finally, special thanks are given to my family for always being there to be supportive. I am indebted to my parents and my wife for their continuous love, understanding, endurance and encouragement through my life. I also want to thank all my friends at Auburn and in India who directly or indirectly contributed to the success of my study.

Table of Contents

Abstract	ii
Acknowledgments	iv
List of Tables	x
List of Figures	xi
List of Abbreviations	xviii
Chapter 1 Introduction	1
1.1 Nuclear Magnetic Resonance (NMR)	1
1.1.1 Introduction.....	1
1.1.2 Basics of NMR.....	2
1.1.3 Protein NMR.....	8
1.2 Odorant Binding Proteins (OBPs)	13
1.2.1 Introduction.....	13
1.2.2 Chemical communication in insects and Pheromone Binding Proteins	13
1.2.3 <i>Antheraea polyphemus</i> Pheromone binding protein1 (ApolPBP1)	21
1.3 Objective of the Study	28
References.....	29
Chapter 2 Effect of Delipidation and pH on the conformation of ApolPBP1	33
2.1 Introduction.....	33
2.2 Materials and Methods.....	36

2.2.1 Cloning and Overexpression.....	36
2.2.2 Purification.....	36
2.2.3 Delipidation.....	37
2.2.4 Mass Spectrometry.....	37
2.2.5 NMR Measurements	38
2.3 Results.....	39
2.3.1 Expressed and purified protein	39
2.3.2 Effect of Delipidation on the Conformation of ApolPBP1.....	41
2.3.3 Effect of pH on ApolPBP1 conformation.....	50
2.4 Discussion.....	55
References.....	57
Chapter 3 Role of Histidine residues in ligand binding and release	60
3.1 Introduction.....	60
3.2 Materials and Methods.....	62
3.2.1 Cloning and Overexpression.....	62
3.2.2 Delipidation, Mass spectrometry and NMR measurement.....	62
3.2.3 AMA binding studies by Fluorescence.....	63
3.3 Results and Discussions.....	64
3.3.1 Expressed and purified protein	64
3.3.2 Effect of Histidine mutation.....	66
3.3.3 AMA Binding Studies by Fluorescence	71
3.4 Conclusions.....	74
References.....	78

Chapter 4 Role of C-terminus in ligand binding and/or releasing	82
4.1 Introduction.....	82
4.2 Materials and Methods.....	86
4.2.1 Cloning, Overexpression & Purification of C-terminus deleted proteins.....	86
4.2.2 Cloning, Overexpression & Purification of C-terminus mutant proteins	86
4.2.3 NMR Measurements	87
4.2.4 Fluorescence Spectroscopy	88
4.2.5 AMA Binding Studies	88
4.3 Results.....	90
4.3.1 Expression and purification of C-terminus deleted proteins.....	90
4.3.2 Role of C-terminus in Ligand Binding and Release	97
4.3.3 Effect of pH and ligand on the conformation of ApolPBP1 C-terminus deleted mutants.....	107
4.3.4 AMA binding studies by fluorescence.....	117
4.3.5 Effect of mutations on C-terminus.....	121
4.4 Discussion	157
References.....	163
Chapter 5 Exploring the nickel proteome	165
5.1 Introduction.....	165
5.1.1 Exploring the nickel proteome in <i>Methanothermobacter marburgensis</i>	165
5.1.2 Exploring the nickel proteome in the plant <i>Streptanthus polygaloides</i>	169
5.2 Materials and methods	174
5.2.1 Growth of <i>Methanothermobacter marburgensis</i> cells.....	174
5.2.2 Harvest and sonication of <i>M. marburgensis</i> cells.....	175

5.2.3 Protein purification and metal ion detection	175
5.2.4 Purification from the plant material	176
5.2.5 Sequencing of protein bands	177
5.3 Results.....	177
5.3.1 Purification of different protein fractions from <i>M. marburgensis</i>	177
5.3.2 Purification of different protein fractions from plant material	187
5.4 Discussion and Future direction.....	196
References.....	197

List of Tables

Table 1.1 Properties of some selected nuclei of biological NMR importance	3
Table 3.1 Dissociation constants ($K_{[AMA]}$) for the binding of AMA to different ApolPBP1 samples, determined using the increase in AMA fluorescence at 480 nm	70
Table 4.1 Dissociation constant (K_d) values for the binding of AMA to various mutants of ApolPBP1, determined using the increase in AMA fluorescence at 480 nm	117
Table 5.1 NCBI-BLAST search for the protein bands from 15% gel	193

List of Figures

Figure 1.1 Energy splitting as a function of magnetic field strength.....	4
Figure 1.2 Schematic representation of a NMR experiment.....	7
Figure 1.3 Schematic representation of HSQC experiment.....	11
Figure 1.4 2D ^1H - ^{15}N HSQC spectrum of uniformly ^{15}N -labeled Calbindin $\text{D}_{9\text{K}}$	12
Figure 1.5 Different types of semiochemicals	15
Figure 1.6 Schematic representation of pheromone transport in insects by Pheromone binding proteins	18
Figure 1.7 Sequence alignments of PBPs from different moth species	19
Figure 1.8 Phylogenetic tree of different moth PBPs generated using Clustal W2.....	20
Figure 1.9 Sequence and secondary structure of <i>Antheraea polyphemus</i> Pheromone binding protein1 (ApolPBP1)	22
Figure 1.10 Binding pocket of ApolPBP1	23
Figure 1.11 NMR structure of ApolPBP1 at pH 5.2.....	25
Figure 1.12 NMR structure of ApolPBP1 at pH 6.3.....	25
Figure 1.13 NMR structure of ApolPBP1 at pH 4.5.....	26
Figure 1.14 NMR structure of BmorPBP at pH 6.5.....	26
Figure 1.15 NMR structure of BmorPBP at pH 4.5.....	27
Figure 1.16 X-ray crystallography structure of BmorPBP at pH 7.5.....	27
Figure 2.1 Mass spec analysis of pure ApolPBP1	40
Figure 2.2 2D $\{^1\text{H}, ^{15}\text{N}\}$ HSQC spectrum of Undelipidated and Delipidated ApolPBP1 at pH 6.5 and pH 4.5.....	42

Figure 2.3 Deconvoluted ESI-mass spectra of ApolPBP1wt under non-denaturing conditions ...	44
Figure 2.4 Two dimensional $\{^1\text{H}, ^{15}\text{N}\}$ HSQC spectrum of Undelipidated and Delipidated ApolPBP1 at pH 6.5	46
Figure 2.5 Expanded region of the $\{^1\text{H}, ^{15}\text{N}\}$ HSQC spectra of delipidated ApolPBP1, pH 6.5, upon titration with 6E, 11Z-hexadecadienyl acetate (<i>A. polyphemus</i> pheromone)	48
Figure 2.6 One-dimensional slices from the 1H axis of the twodimensional $\{^1\text{H}, ^{15}\text{N}\}$ HSQC spectra of ApolPBP1 upon titration with 6E, 11Z-hexadecadienyl acetate	49
Figure 2.7 A. Expanded region of the two-dimensional $\{^1\text{H}, ^{15}\text{N}\}$ HSQC spectrum of undelipidated ApolPBP1.....	51
Figure 2.7 B. Expanded region of the two-dimensional $\{^1\text{H}, ^{15}\text{N}\}$ HSQC spectrum of delipidated ApolPBP1 at pH 6.5 and 4.5.....	52
Figure 2.8 Expanded region of the two-dimensional $\{^1\text{H}, ^{15}\text{N}\}$ HSQC spectrum of pH titration of delipidated ApolPBP1 from pH 4.5 to pH 6.5.....	53
Figure 2.9 Expanded region of the two-dimensional $\{^1\text{H}, ^{15}\text{N}\}$ HSQC spectrum of pH titration of delipidated ApolPBP1 from pH 6.5 to 4.5.....	54
Figure 2.10 Pictorial representation of ApolPBP1 with/ without the ligand and at high and low pH.....	56
Figure 3.1 Mass spec analysis of pure ApolPBP1H70A/H95A	65
Figure 3.2 A. Two-dimensional $\{^1\text{H}, ^{15}\text{N}\}$ HSQC spectra of undelipidated ApolPBP1H70A/H95A	67
Figure 3.2 B. Two-dimensional $\{^1\text{H}, ^{15}\text{N}\}$ HSQC spectra of undelipidated ApolPBP1H70A/H95A	68
Figure 3.3 Extended portion from the overlap of two-dimensional $\{^1\text{H}, ^{15}\text{N}\}$ HSQC spectra of undelipidated ApolPBP1H70A/H95A.....	69
Figure 3.4 Extended region of the $\{^1\text{H}, ^{15}\text{N}\}$ HSQC spectra of delipidated ApolPBP1 H70A/H95A.....	70
Figure 3.5 Fluorescence intensities of different ApolPBP1 proteins upon addition of AMA, measured at 480 nm.....	72
Figure 3.6 ApolPBP1 at pH 6.3, showing His-70 and His-95 at one end of the binding pocket...	75
Figure 3.7 ApolPBP1 at high and low pH	76
Figure 3.8 Schematic representations of ApolPBP1wt and ApolPBP1H70A/H95A	77

Figure 4.1 A. SDS-PAGE analysis of unlabeled ApolPBP1 Δ P129-V142	91
Figure 4.1 B. SDS-PAGE analysis of unlabeled ApolPBP1H70A/H95A Δ P129-V142.....	92
Figure 4.1 C. SDS-PAGE analysis of unlabeled ApolPBP1D132N, ApolPBP1E137Q and ApolPBP1E141Q.....	93
Figure 4.1 D. SDS-PAGE analysis of unlabeled ApolPBP1D132NE137Q and, ApolPBP1E137QE141Q.....	94
Figure 4.2 A. Mass spec analysis of pure ApolPBP1 Δ P129-V142	95
Figure 4.2 B. Mass spec analysis of pure ApolPBP1H70A/H95A Δ P129-V142.....	96
Figure 4.3 A. Two-dimensional $\{^1\text{H}, ^{15}\text{N}\}$ HSQC spectra of delipidated ApolPBP1 Δ P129-V142 at pH 6.5.....	98
Figure 4.3 B. Two-dimensional $\{^1\text{H}, ^{15}\text{N}\}$ HSQC spectra of delipidated ApolPBP1H70A/H95A Δ P129-V142 at pH 6.5.....	96
Figure 4.3 C. Two-dimensional $\{^1\text{H}, ^{15}\text{N}\}$ HSQC spectra of delipidated ApolPBP1 Δ P129-V142 At pH 4.5.....	99
Figure 4.3 D. Two-dimensional $\{^1\text{H}, ^{15}\text{N}\}$ HSQC spectra of delipidated ApolPBP1H70A/H95A Δ P129-V142 at pH 4.5.....	101
Figure 4.4 A. Two-dimensional $\{^1\text{H}, ^{15}\text{N}\}$ HSQC spectra of delipidated (black color) and undelipidated (red color) ApolPBP1 Δ P129-V142 at pH 6.5	103
Figure 4.4 B. Two-dimensional $\{^1\text{H}, ^{15}\text{N}\}$ HSQC spectra of delipidated (black color) and undelipidated (red color) ApolPBP1H70A/H95A Δ P129-V142 at pH 6.5.....	104
Figure 4.4 C. Two-dimensional $\{^1\text{H}, ^{15}\text{N}\}$ HSQC spectra of delipidated (black color) and undelipidated (red color) ApolPBP1 Δ P129-V142 at pH 4.5	105
Figure 4.4 D. Two-dimensional $\{^1\text{H}, ^{15}\text{N}\}$ HSQC spectra of delipidated (black color) and undelipidated (red color) ApolPBP1H70A/H95A Δ P129-V142 at pH 4.5.....	106
Figure 4.5 A. Expanded regions of the two-dimensional $\{^1\text{H}, ^{15}\text{N}\}$ HSQC spectra of delipidated ApolPBP1 Δ P129-V142	108
Figure 4.5 B. Expanded regions of the two-dimensional $\{^1\text{H}, ^{15}\text{N}\}$ HSQC spectra of delipidated ApolPBP1H70A/H95A Δ P129-V142.....	109
Figure 4.6 A. Expanded region of the two-dimensional $\{^1\text{H}, ^{15}\text{N}\}$ HSQC spectra of delipidated ApolPBP1 Δ P129-V142 at pH 6.5.....	111

Figure 4.6 B. Expanded region of the two-dimensional $\{^1\text{H}, ^{15}\text{N}\}$ HSQC spectra of delipidated ApolPBP1 Δ P129-V142 at pH 4.5.....	112
Figure 4.6 C. Expanded region of the two-dimensional $\{^1\text{H}, ^{15}\text{N}\}$ HSQC spectra of delipidated ApolPBP1H70A/H95A Δ P129-V142 at pH 6.5.....	113
Figure 4.6 D. Expanded region of the two-dimensional $\{^1\text{H}, ^{15}\text{N}\}$ HSQC spectra of delipidated ApolPBP1H70A/H95A Δ P129-V142 at pH 4.5.....	114
Figure 4.7 A. Resonance corresponding to Leu-68 showing the phenomenon of intermediate exchange.....	115
Figure 4.7 B. One-dimensional slices from the ^1H axis taken in the midpoint of the resonance corresponding to Leu-68.....	116
Figure 4.8 Increase in the fluorescence intensities of different ApolPBP1 samples upon addition of AMA monitored at 480 nm.....	118
Figure 4.9 Relative fluorescence intensities of delipidated ApolPBP1 mutants upon addition of 5 μM AMA to 1 μM protein samples.....	119
Figure 4.10 A. Two-dimensional $\{^1\text{H}, ^{15}\text{N}\}$ HSQC spectra of undelipidated ApolPBP1D132N in 50 mM sodium phosphate buffer at pH 4.5.....	122
Figure 4.10 B. Two-dimensional $\{^1\text{H}, ^{15}\text{N}\}$ HSQC spectra of undelipidated ApolPBP1D132N in 50 mM sodium phosphate buffer at pH 6.5.....	123
Figure 4.10 C. Two-dimensional $\{^1\text{H}, ^{15}\text{N}\}$ HSQC spectra of undelipidated ApolPBP1E137Q in 50 mM sodium phosphate buffer at pH 4.5.....	124
Figure 4.10 D. Two-dimensional $\{^1\text{H}, ^{15}\text{N}\}$ HSQC spectra of undelipidated ApolPBP1E137Q in 50 mM sodium phosphate buffer at pH 6.5.....	125
Figure 4.10 E. Two-dimensional $\{^1\text{H}, ^{15}\text{N}\}$ HSQC spectra of undelipidated ApolPBP1E141Q in 50 mM sodium phosphate buffer at pH 4.5.....	126
Figure 4.10 F. Two-dimensional $\{^1\text{H}, ^{15}\text{N}\}$ HSQC spectra of undelipidated ApolPBP1E141Q in 50 mM sodium phosphate buffer at pH 6.5.....	127
Figure 4.11 A. Expanded region of Two-dimensional $\{^1\text{H}, ^{15}\text{N}\}$ HSQC spectra of undelipidated ApolPBP1D132N and ApolPBP1wt proteins at pH 6.5.....	128
Figure 4.11 B. Expanded region of Two-dimensional $\{^1\text{H}, ^{15}\text{N}\}$ HSQC spectra of undelipidated ApolPBP1D132N and ApolPBP1wt proteins at pH 4.5.....	129
Figure 4.11 C. Expanded region of Two-dimensional $\{^1\text{H}, ^{15}\text{N}\}$ HSQC spectra of undelipidated ApolPBP1E137Q and ApolPBP1wt proteins at pH 6.5.....	130

Figure 4.11 D. Expanded region of Two-dimensional $\{^1\text{H}, ^{15}\text{N}\}$ HSQC spectra of undelipidated ApolPBP1E137Q and ApolPBP1wt proteins at pH 4.5	131
Figure 4.11 E. Expanded region of Two-dimensional $\{^1\text{H}, ^{15}\text{N}\}$ HSQC spectra of undelipidated ApolPBP1E141Q and ApolPBP1wt proteins at pH 6.5	132
Figure 4.11 F. Expanded region of Two-dimensional $\{^1\text{H}, ^{15}\text{N}\}$ HSQC spectra of undelipidated ApolPBP1E141Q and ApolPBP1wt proteins at pH 4.5	133
Figure 4.12 A. Two-dimensional $\{^1\text{H}, ^{15}\text{N}\}$ HSQC spectra of undelipidated ApolPBP1D132NE137Q in 50 mM sodium phosphate buffer at pH 4.5	135
Figure 4.12 B. Two-dimensional $\{^1\text{H}, ^{15}\text{N}\}$ HSQC spectra of undelipidated ApolPBP1E137QE141Q in 50 mM sodium phosphate buffer at pH 4.5	136
Figure 4.12 C. Two-dimensional $\{^1\text{H}, ^{15}\text{N}\}$ HSQC spectra of undelipidated ApolPBP1D132NE137Q in 50 mM sodium phosphate buffer at pH 6.5	137
Figure 4.12 D. Two-dimensional $\{^1\text{H}, ^{15}\text{N}\}$ HSQC spectra of undelipidated ApolPBP1E137QE141Q in 50 mM sodium phosphate buffer at pH 6.5	138
Figure 4.13 A. Expanded region of Two-dimensional $\{^1\text{H}, ^{15}\text{N}\}$ HSQC spectra of undelipidated ApolPBP1D132NE137Q and ApolPBP1wt proteins at pH 4.5	139
Figure 4.13 B. Expanded region of Two-dimensional $\{^1\text{H}, ^{15}\text{N}\}$ HSQC spectra of undelipidated ApolPBP1E137QE141Q and ApolPBP1wt proteins at pH 4.5.....	140
Figure 4.13 C. Expanded region of Two-dimensional $\{^1\text{H}, ^{15}\text{N}\}$ HSQC spectra of undelipidated ApolPBP1D132NE137Q and ApolPBP1wt proteins at pH 6.5	141
Figure 4.13 D. Expanded region of Two-dimensional $\{^1\text{H}, ^{15}\text{N}\}$ HSQC spectra of undelipidated ApolPBP1E137QE141Q and ApolPBP1wt proteins at pH 6.5.....	142
Figure 4.14 A. Two-dimensional $\{^1\text{H}, ^{15}\text{N}\}$ HSQC spectra of delipidated ApolPBP1D132NE137Q in 50 mM sodium phosphate buffer at pH 4.5	143
Figure 4.14 B. Two-dimensional $\{^1\text{H}, ^{15}\text{N}\}$ HSQC spectra of delipidated ApolPBP1D132NE137Q in 50 mM sodium phosphate buffer at pH 6.5	144
Figure 4.14 C. Two-dimensional $\{^1\text{H}, ^{15}\text{N}\}$ HSQC spectra of delipidated ApolPBP1E137QE141Q in 50 mM sodium phosphate buffer at pH 4.5.....	145
Figure 4.14 D. Two-dimensional $\{^1\text{H}, ^{15}\text{N}\}$ HSQC spectra of delipidated ApolPBP1E137QE141Q in 50 mM sodium phosphate buffer at pH 6.5.....	146
Figure 4.15 A. Expanded region of Two-dimensional $\{^1\text{H}, ^{15}\text{N}\}$ HSQC spectra of delipidated ApolPBP1D132NE137Q at pH 4.5 and 6.5 and ApolPBP1wt protein at pH 4.5	147

Figure 4.15 B. Expanded region of Two-dimensional $\{^1\text{H}, ^{15}\text{N}\}$ HSQC spectra of delipidated ApolPBP1E137QE141Q at pH 4.5 and 6.5 and ApolPBP1wt protein at pH 4.5.....	148
Figure 4.16 A. Two-dimensional $\{^1\text{H}, ^{15}\text{N}\}$ HSQC spectra of undelipidated ApolPBP1D132NE137QE141Q in 50mM sodium phosphate buffer at pH 6.5	150
Figure 4.16 B. Overlapping between the HSQC spectra of Undelipidated ApolPBP1 at pH 6.5 and ApolPBP1D132NE137QE141Q at pH 6.5	151
Figure 4.16 C. Extended region of HSQC spectra of Undelipidated ApolPBP1 at pH 6.5 and ApolPBP1D132NE137QE141Q at pH 6.5	152
Figure 4.17 A. Two-dimensional $\{^1\text{H}, ^{15}\text{N}\}$ HSQC spectra of undelipidated ApolPBP1D132NE137QE141Q in 50mM sodium phosphate buffer at pH 4.5	153
Figure 4.17 B. Overlapping between the HSQC spectra of Undelipidated ApolPBP1 at pH 6.5 and ApolPBP1D132NE137QE141Q at pH 4.5	154
Figure 4.17 C. Overlapping between the HSQC spectra of Undelipidated ApolPBP1 at pH 4.5 and ApolPBP1D132NE137QE141Q at pH 4.5	155
Figure 4.17 D. Overlapping between the HSQC spectra of Undelipidated ApolPBP1D132NE137QE141Q at pH 6.5 and ApolPBP1D132NE137QE141Q at pH 4.5	156
Figure 4.18 Schematic representations of the c-terminus deleted (ApolPBP1 Δ P129-V142 and ApolPBP1H70A/H95A Δ P129-V142) proteins with compared to the ApolPBP1wt protein	161
Figure 4.19 Schematic representations of the single mutant and double mutant proteins with compared to the ApolPBP1wt protein	162
Figure 5.1 Overview of the nickel trafficking proteins in <i>E. coli</i>	167
Figure 5.2 Schematic representations of different mechanisms for metal intake and distribution for non-hyperaccumulator and hyperaccumulator plants	171
Figure 5.3 The latex of <i>Sebertia acuminata</i>	172
Figure 5.4 Metal concentrations from different run of <i>M. marburgensis</i> after Sephacryl run	178
Figure 5.5 Ni profile of the different protein peaks with the after Sephacryl column run	179
Figure 5.6 Ni profile of the different protein peaks with the after the Q-sepharose column.....	181
Figure 5.6 Mono-Q profile for the B peak obtained from the Q-sepharose column step.....	183

Figure 5.7 15% SDS-PAGE analysis of the fractions of peak B (from Q-sepharose column) after Mono-Q run	184
Figure 5.8 Ni profile of different protein peaks of Peak A after Mono-Q run	185
Figure 5.9 15% SDS-PAGE analysis of different protein peaks from peak A (from Q-sepharose) after Mono-Q run	186
Figure 5.10 Ni profile of different protein fractions from <i>Streptanthus polygaloides</i> after running into DEAE-sepharose column	188
Figure 5.11 Ni profile of the protein peaks after running into Superdex™ 100 column.....	190
Figure 5.12 15% SDS-PAGE gel analysis of the fractions 28 and 30.....	191
Figure 5.13 Coverage map of Band 1, 3, 4 and 5 (of the fractions 28 and 30) from SDS-PAGE gel	192
Figure 5.14 Ni ion profile after the Superdex-100 run for the DEAE-filtrate	195

List of Abbreviations

NMR	Nuclear Magnetic Resonance
TMS	Tetramethylsilane
HSQC	Heteronuclear Single Quantum Coherence
COSY	Correlation Spectroscopy
TOCSY	Total Correlation Spectroscopy
2D	Two Dimensional
3D	Three Dimensional
4D	Four Dimensional
INEPT	Insensitive Nuclei Enhanced by Polarization Transfer
OBPs	Odorant Binding Proteins
GOBPs	General-odorant Binding Proteins
PBPs	Pheromone Binding Proteins
ApolPBP1	<i>Antheraea polyphemus</i> Pheromone-Binding Protein1
BmorPBP	<i>Bombyx mori</i> Pheromone-Binding Protein
AperPBP1	<i>Antheraea pernyi</i> Pheromone-Binding Protein1
AvelPBP	<i>Argyrotaenia velutinana</i> Pheromone-Binding Protein
LdisPBP1	<i>Lymantria dispar</i> Pheromone-Binding Protein1
OnubPBP	<i>Ostrinia nubilalis</i> Pheromone-Binding Protein
CrosPBP	<i>Choristoneura rosaceana</i> Pheromone-Binding Protein

Chapter 1

Introduction

1.1 Nuclear Magnetic Resonance (NMR)

1.1.1 Introduction

Nuclear Magnetic Resonance (NMR) was first described by Isidor Rabi in 1938.¹ Rabi was awarded the Nobel Prize for his work. In 1946, Felix Bloch and Edward M Purcell expanded this technique on liquids and solids, for which they shared the Nobel Prize in 1952. They observed that some nuclei could absorb radiofrequency energy when placed in a magnetic field of a strength specific to the identity of the nuclei. When this absorption occurs, the nucleus is described as being in resonance. Different nuclei that have nonzero spin within a molecule resonate at different (radio) frequencies for the same magnetic field strength. The observation of magnetic resonance of the nuclei present in a molecule allows discovering essential chemical and structural information of the molecule, which is possible even for the complex macromolecules.

NMR is a technique known for its great variety of applications. It is a well-known technique for structure determination of biomolecules, such as proteins. NMR can also provide detailed information on dynamics of the macromolecules, and can provide information on the kinetic aspects of interactions of a biomolecule with its ligand. NMR can also provide information on the reaction state and the chemical environment of molecules. In addition to that, NMR is a non-destructive process. Thus the ability to gather both structural and dynamic information is the most important attribute of NMR in the context of structural molecular biology.²

1.1.2 Basics of NMR

Nuclei of some atoms possess a property called angular momentum or spin. For some of the nucleus (such as ^{12}C) these spins are paired. As a result, the nucleus of that particular atom has no overall spin. On the contrary, in some atoms (such as ^1H and ^{13}C) the nuclei do possess an overall spin. Thus, the overall spin (I) is important. According to the basic principle of quantum mechanics, the maximum observable component of the angular momentum of a nucleus possessing a spin is a half-integral or integral multiple of $h/2\pi$, where h is Planck's constant. Thus when a nucleus has a positive charge and is spinning, it generates a small magnetic field. The nucleus therefore possesses a magnetic moment, μ , which is proportional to its spin, I (Eq. 1.1).

$$\mu = \gamma I h / 2\pi \quad \text{Eq. 1.1}$$

where, γ is the gyromagnetic ratio and has a characteristic value for every nucleus. The properties of some biologically important nuclei are described in Table 1.1.

As observed, altogether there are $2I + 1$ possible states of the nucleus with spin quantum number I . In the absence of an external magnetic field, these states have the same energy level, i.e. field splitting is zero. However, if a uniform external magnetic field, B_0 , is applied, these states correspond to states of different potential energy. The difference in energy between two states (the transition energy) at an applied magnetic field B_0 can be found from Eq. 1.2.

$$\Delta E = h\nu = \mu B_0 / I \quad \text{Eq. 1.2}$$

The energy levels for a spin $1/2$ nucleus such as ^1H are shown in Figure 1.1 as a function of applied magnetic field strength (B_0).³

Nucleus	<i>I</i>	γ (rad T ⁻¹ s ⁻¹)	Natural abundance (%)
¹ H	1/2	2.6752×10^8	99.99
² H	1	4.107×10^7	0.012
¹² C	1/2	6.728×10^7	1.07
¹⁴ N	1	1.934×10^7	99.63
¹⁵ N	1/2	-2.713×10^7	0.37
¹⁷ O	1/2	-3.628×10^7	0.038
¹⁹ F	1/2	2.518×10^8	100
³¹ P	1/2	1.0839×10^8	100

Table 1.1 Properties of some selected nuclei of biological NMR importance. Taken from reference 3.

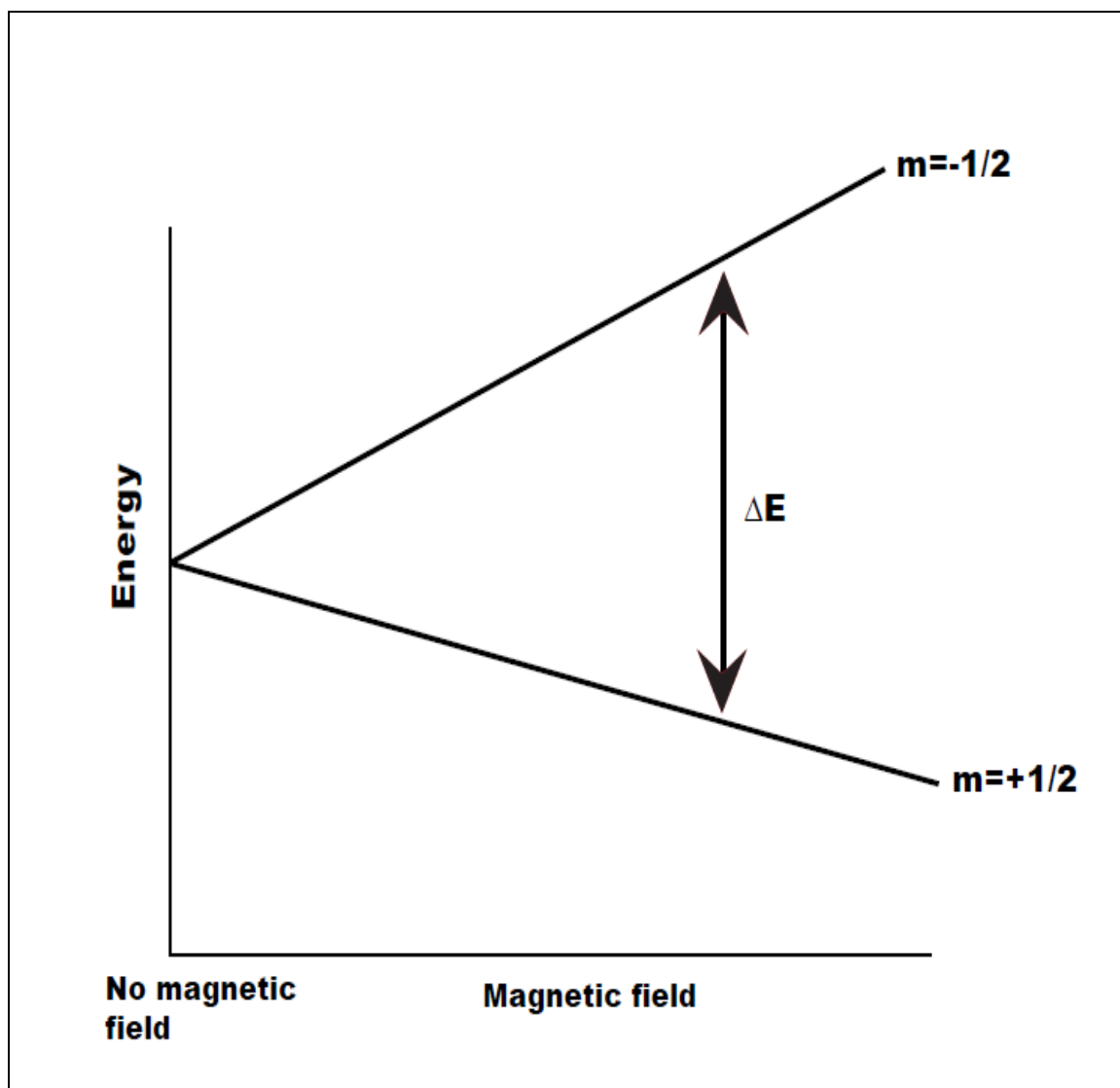


Figure 1.1 Energy splitting as a function of magnetic field strength. Taken from reference 3.

The nucleus is spinning on its axis. In the presence of the external magnetic field (B_0), this axis of rotation will precess around the magnetic field. The precession frequency of a nucleus, termed as the Larmor frequency (Eq. 1.3):

$$\nu = \gamma B_0 / 2\pi \quad \text{Eq. 1.3}$$

The Larmor frequency depends on the applied magnetic field and the nature of the nucleus.

When a spin 1/2 nucleus, such as ^1H or ^{13}C is under the influence of an external magnetic field, it will have two orientations, i.e., a lower energy and a higher energy orientation. The populations of both the energy levels follow the Boltzmann distribution. The lower energy level contains a larger number of nuclei than the higher energy level. It is possible to excite the nuclei in the lower energy level to the higher energy level with the precise electromagnetic radiation. The radiation frequency required depends on the difference in energy between the energy levels (Eq. 1.2). To reestablish the Boltzmann distribution of the higher number of nuclei in the ground state, various relaxation processes (Spin-Spin and Spin-Lattice) take place that allow the nuclei from the higher energy state to come back to the lower energy state. The nuclei absorb radio frequency and flip to the higher energy levels. The nuclei in different chemical environments (within the same molecule) do not identically experience the same external magnetic field. Depending on their local chemical environment, different nuclei in a molecule resonate at slightly different frequencies. The chemical shift is reported as a relative measure from some reference resonance frequency, and measured in parts per million (ppm). For the nuclei ^1H and ^{13}C , tetramethylsilane (TMS) is commonly used as a reference. The chemical shift is independent of the frequency of the spectrometer. The process of determining the resonating frequencies of the nuclei in a particular molecule is called resonance assignment. There is also an effect of

electrons shielding of the nucleus which results in reducing the effective magnetic field. As a result, energy of a lower frequency is required to induce the transitions between spin states. On the other hand, when the electrons are not within the close proximity of a nucleus, the nucleus is deshielded and feels a stronger magnetic field requiring more transition energy to achieve resonance. Normally, nuclei attached to electron withdrawing groups tend to resonate at higher frequencies.

In one dimensional NMR spectrum a single chemical shift coordinate along X axis is available. In two dimensional experiments, both the X and the Y axes have chemical shift scales. By looking at the peaks and matching them to the X and Y axes, information of chemical shifts of the nuclei are obtained. Several 2D experiments are available to obtain useful information of a protein structure, HSQC, COSY, TOCSY etc. The Heteronuclear Single Quantum Coherence (HSQC) experiment is used frequently and has significant contribution in protein NMR. It was invented by Geoffrey Bodenhausen and D. J. Ruben in 1980.⁴ The resulting spectrum is two-dimensional with one axis for ^1H and the other for a heteronucleus (a nucleus other than a proton, most often ^{13}C or ^{15}N). The spectrum contains a peak for each unique proton attached to the heteronucleus. Thus, if the chemical shift of a specific proton is known, the chemical shift of the heteronucleus can be determined, and vice versa. In the 3D experiments, X, Y, and Z axes all have chemical shift scales. 3D NMR experiments are combination of two 2D experiments (Figure 1.2). In the same way, a 4D experiment is obtained by combining three 2D experiments (or two 3D experiments) in an analogous fashion. These experiments are widely used for protein structure determination.

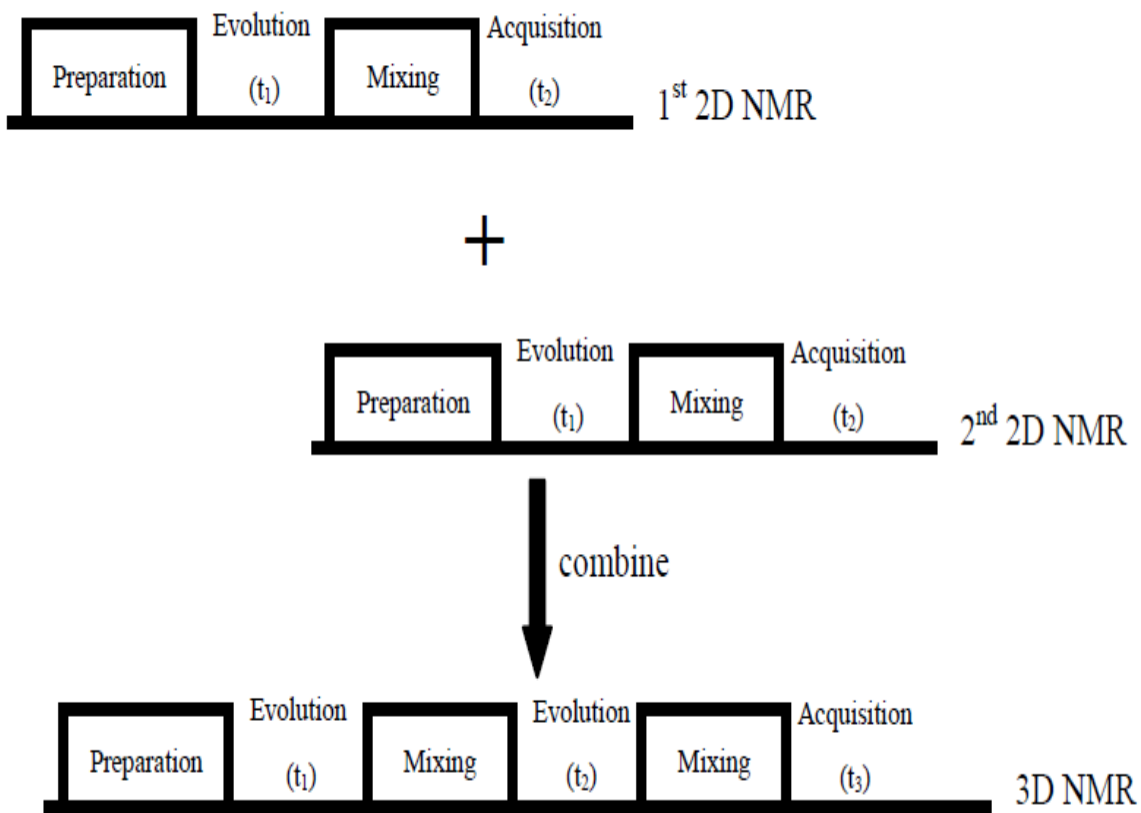


Figure 1.2 Schematic representation of a 3D NMR experiment from the combination of two 2D NMR experiments. Taken from reference 3.

1.1.3 Protein NMR

NMR spectroscopy is used to obtain information about the structure and dynamics of proteins. This field was pioneered by Richard R. Ernst and Kurt Wüthrich,⁵ among others. This technique also provides information regarding structural, functional and kinetic aspects of protein-ligand interaction. Biomolecular NMR is a key technique for studying the various mechanisms involved in different cellular pathways, because it can acquire both the structural and dynamics data of proteins or protein-ligand complexes in solution under physiological conditions. NMR also serves as a tool in studying weak and transient interactions, which are associated with many biological functions. The first major step in biological NMR spectroscopy of complex biomolecules, such as in protein NMR structure determination, is the complete assignment of the spectrum. To identify and assign each amino acid residue, a number of two dimensional or higher (three-dimensional or four-dimensional) NMR experiments are adopted. Among many other 2D experiments, HSQC is one of the most frequently used. A HSQC experiment correlates the chemical shifts of the nuclei that are directly connected, i.e., two different kinds of nuclei. The HSQC experiment was first performed by Geoffrey Bodenhausen and D. J. Ruben in 1980.⁴ In a 2D-HSQC spectrum one axis is ^1H and the other is a heteronucleus most often ^{13}C or ^{15}N . The HSQC experiment involves the transfer of magnetization on the proton to the second nucleus, which may be ^{15}N or ^{13}C , via an INEPT (Insensitive Nuclei Enhanced by Polarization Transfer) step. After a time delay (t_1), the magnetization is transferred back to the proton via a retro-INEPT step and the signal is then recorded. In HSQC, a series of experiments is recorded where the time delay t_1 is incremented. The ^1H signal is detected in the directly measured dimension in each experiment, while

the chemical shift of ^{15}N or ^{13}C is recorded in the indirect dimension which is formed from the series of experiments (Figure 1.3).

The HSQC experiment is a highly-sensitive 2D-NMR experiment and the ^{15}N -HSQC spectrum has improved resolution compared to multiple-quantum correlation experiments.^{6,7} The ^{15}N -HSQC experiment is one of the most regularly recorded experiments for the determination of protein structures by NMR. The HSQC experiment can be performed using the natural abundance of the ^{15}N but natural abundance of ^{15}N isotope is very low (less than 1%). So normally for the protein NMR, isotopically labeled protein samples are used. Such labeled proteins are usually produced by expressing the protein in bacterial cells grown in the presence of ^{15}N -labeled media. Each residue of the protein (except proline) has an amide proton attached to nitrogen in the peptide bond (backbone of the polypeptide chain). The HSQC provides the correlation between the nitrogen and amide proton. So each amide group yields a peak in the HSQC spectra which in turn represents each residue of the polypeptide chain. So a HSQC spectrum consists of an observable peak from each residue of a protein, with the exception of proline residues which lack a free amide proton. Also the N-terminal residue (which has an NH_3^+ group and maybe the 2nd residue from N-terminus end also) is not observable in the HSQC spectrum due to fast exchange with the solvent. In addition to the backbone amide peaks, side-chains with nitrogen-bound protons (such as asparagine, glutamine etc.) will also produce peaks. These side-chain peaks and sometimes the backbone peaks have a distinctive appearance in the HSQC spectrum. In a typical HSQC spectrum, the NH_2 -peaks from the side-chain of asparagine and glutamine appear as doublets on the top right corner. The side-chain nitrogen peaks from tryptophan are usually shifted downfield and appear near the bottom left corner. The backbone amide peaks of glycine normally appear near the top of the spectrum (Figure 1.4).⁸

If the protein is folded properly, the peaks in the HSQC spectrum are usually well-dispersed and most of the individual peaks can be distinguished from each other. A large cluster of overlapped peaks around the middle of the spectrum indicate the presence of significant unstructured elements in the protein which means that the protein is not folded properly or might be denatured. The HSQC spectrum is also called the finger print region of a protein. Any kind of change in the protein conformation, e.g., due to pH or temperature changes or binding of a ligand molecule, is observed in the HSQC spectrum. HSQC is a very important tool to study protein-ligand interactions. Once the HSQC is completely assigned, it is possible to visualize the change in chemical shift positions of each residue involved in the binding. This process is useful for ligand binding studies as it will show which amino acid residues are involved in the binding by showing any conformational change upon ligand binding. The HSQC experiment is also used for dynamic studies of protein-ligand interactions.

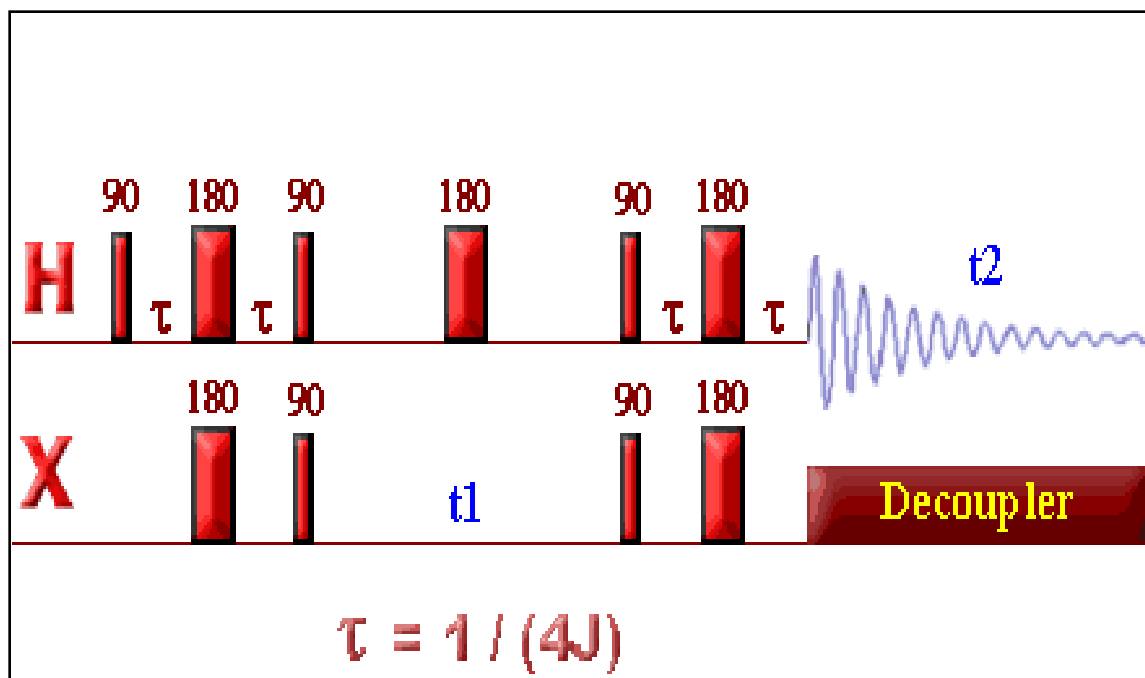


Figure 1.3 Schematic representation of the HSQC experiment.

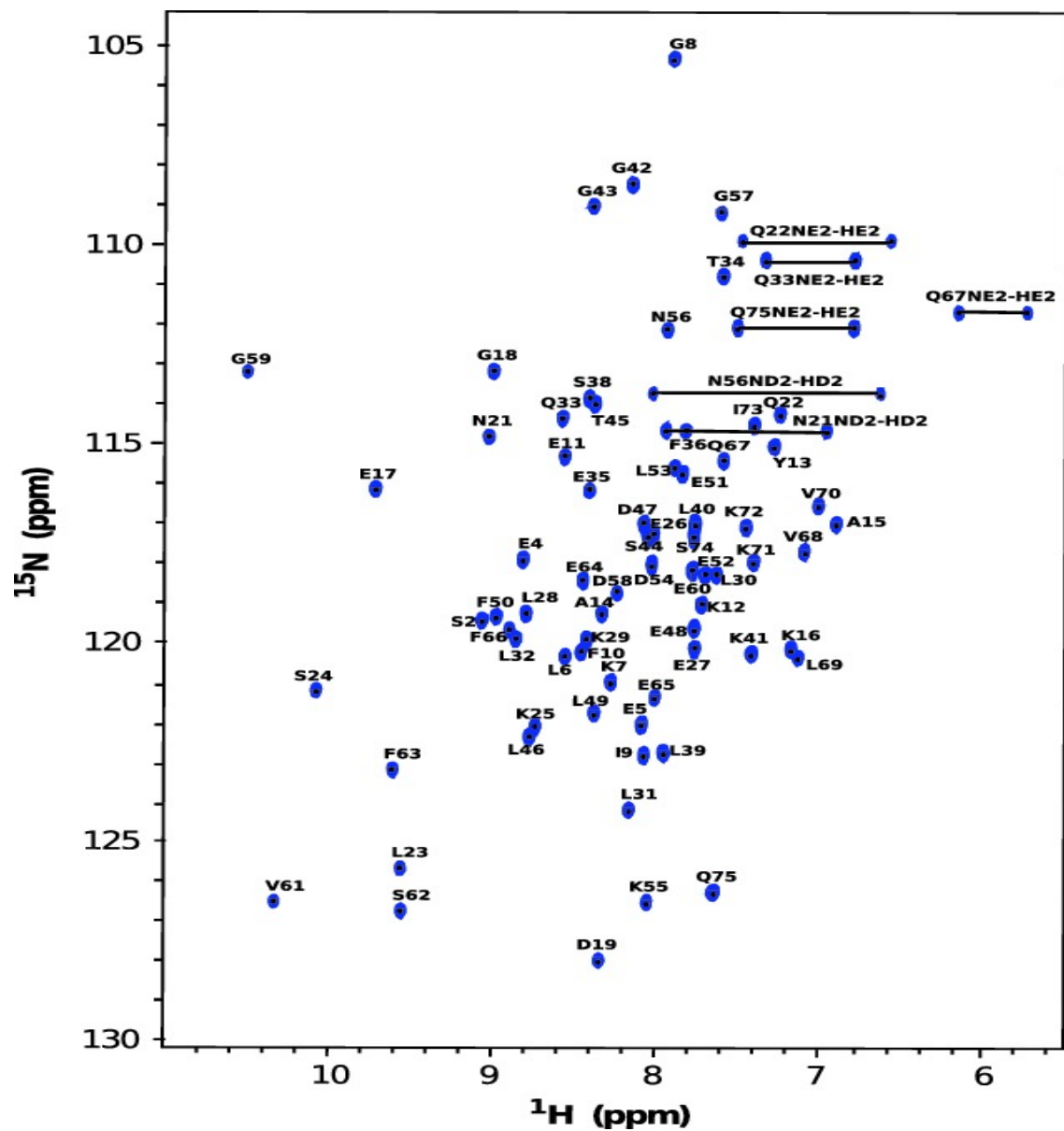


Figure 1.4 2D ^1H - ^{15}N HSQC spectrum of uniformly ^{15}N -labeled Calbindin $\text{D}_{9\text{K}}$. Taken from reference 8.

1.2 Odorant Binding Proteins (OBPs)

1.2.1 Introduction

Odorants are organic volatile compounds that initiate the signaling process in olfaction. Carriers for the odorant molecules are called odorant-binding proteins (OBPs).⁹ OBPs are low-molecular-weight water soluble proteins. They belong to the superfamily of soluble proteins called “lipocalins”. OBPs are present in high concentration in the nasal mucus of vertebrates and in the sensillar lymph of insects. OBPs play a major role in the signaling cascade of olfaction in all animals. OBPs are divided into two families: pheromone binding proteins (PBPs) which are species-specific and associate with pheromone-sensitive neurons, and general-odorant binding proteins (GOBPs), which appear to associate with general-odorant-sensitive neurons. In moths PBPs are found in males only, while GOBPs are found in both sexes. GOBPs are believed to respond to a range of volatile plant and food odorants.¹⁰ The olfactory system enables almost every animal to detect and discriminate between thousands of odorants present in the environment. In fact, it has been observed that as much as 4% of the genome of many higher eukaryotes is devoted to encoding the proteins that can detect “smell”.^{11,12}

1.2.2 Pheromone Binding Proteins (PBPs) and Chemical communication in insects

Insects are the most diverse group of animals on earth, with approximately five million species described to date.¹³ All insects have some common adaptations that maximize fitness in their respective habitats. One such fundamental adaptation is the ability to respond to environmental signals, i.e., the ability to detect external chemical compounds via a chemical sensor. Chemical communication, also known as chemoreception, is an important phenomenon in insects that controls intra and interspecies interactions, helps them to maintain the sexual

relationships or protects them against possible attacks. The sophisticated olfactory system of insects is able to sense volatile odorants released by prey, host plants or conspecific (belonging to the same species) animals. It is known that insects rely heavily on chemical signals for communication. These signals are often called semiochemicals or infochemicals.¹⁴⁻¹⁶ Semiochemicals is a name derived from Greek word *semeon*, which means “a signal”. Semiochemicals can be divided into two groups based on who "sends" a message and who "receives" it: **Pheromones** (combination of two Greek words; *pherein* means “to carry” and *hormon* means “to excite”), are the chemical signals that carry information from one member to another member of the same species.¹⁷ Pheromones were discovered by German scientist Peter Karlson and Swiss scientist Martin Luscher in 1959.¹⁸ These include sex attractants, trail marking compounds, alarm substances, and many other intraspecific messages. **Allelochemicals or allomones** (combination of two Greek words *allos* and *hormon* means “to attract others”) are signals that are produced and released by a member of one species but affect the behavior of a member of a different species and include defensive signals such as repellents, location of suitable host plants, and a vast array of other substances that regulate interspecific behaviors (Figure 1.5).¹⁹

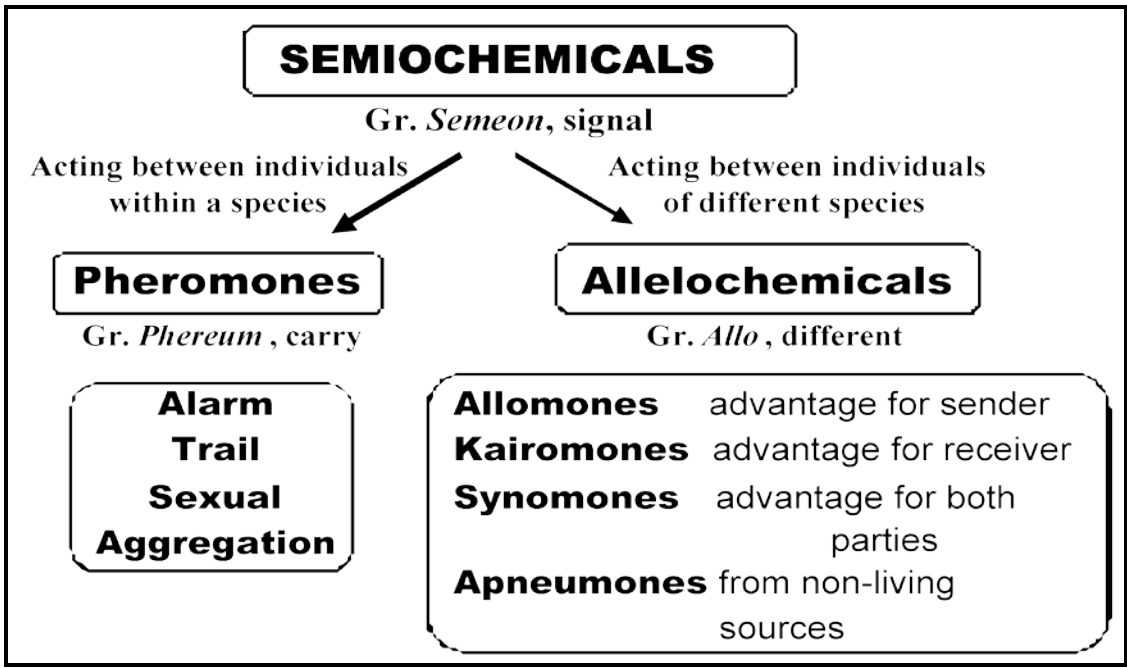
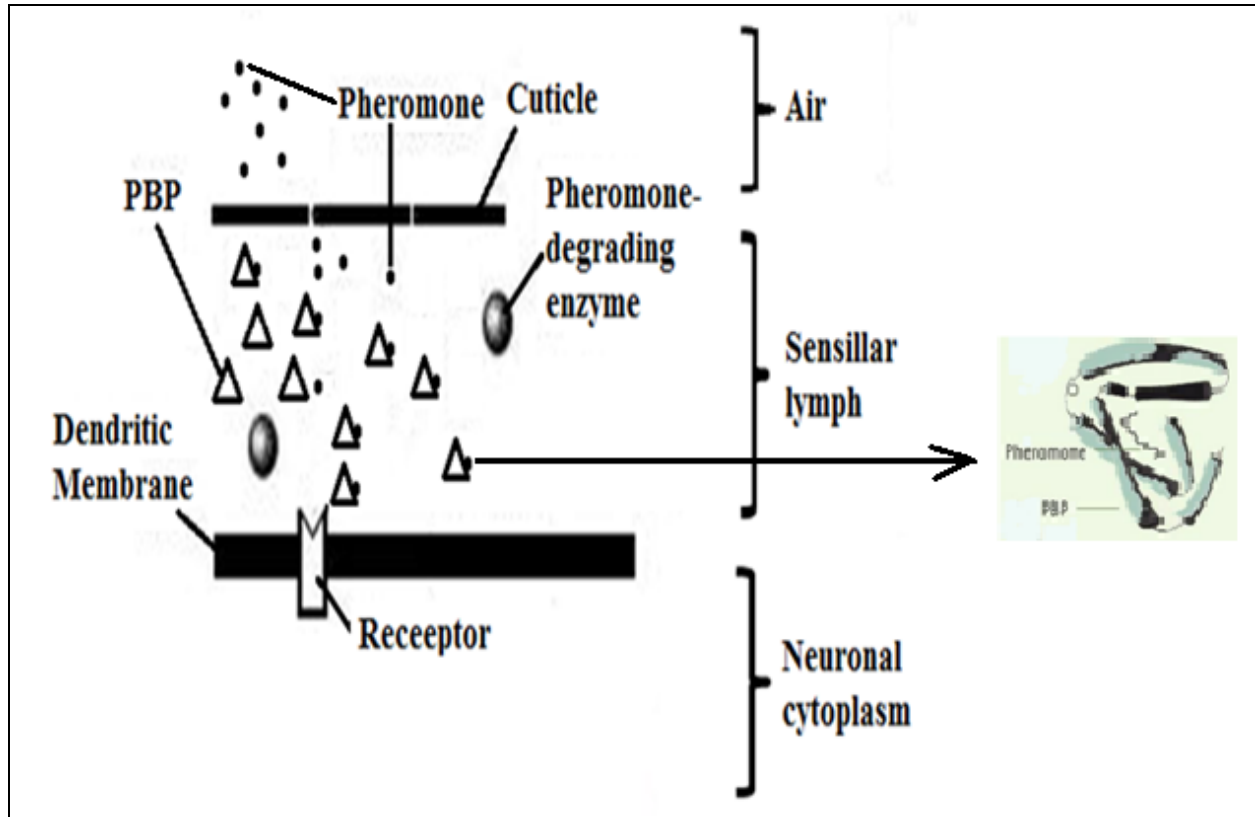


Figure 1.5 Different types of semiochemicals. Copied from reference 15.

Pheromones, a class of semiochemicals that when released by one member of a species, elicits behavioral response in another member of the same species, serve as chemical stimuli in intraspecies communication. In lepidopteran moths, like other insect species, sex pheromones secreted by females are detected with extreme selectivity and specificity by the males of the same species, initiating the mating process. The male moths are capable of distinguishing between closely related pheromones of different species.^{9,20} The organs responsible for olfaction are the sensory hair (sensilla trichoidea) on the surface of the moth's antennae. The pheromone binding proteins (PBPs), the carrier protein for the pheromone molecules, are present in high concentration in the sensillar lymph fluid of the male antenna. PBPs transport the hydrophobic pheromone molecules across the aqueous sensillar lymph to membrane bound receptors (ion channels) (Figure 1.6).^{21,22} PBPs are water soluble and acidic in nature. The molecular weight of these proteins ranges between 14-16 kDa. PBPs are observed to be present in male moths only. The first PBP to be identified, cloned, and expressed in the bacterial system was from the giant silk moth *Antheraea polyphemus*^{23,24} and was named *Antheraea polyphemus* Pheromone-binding protein1 (ApolPBP1). Until now, PBPs have been isolated from at least eight moth species that share about 50% sequence identity (Figure 1.7), with six conserved cysteine residues in each, forming three disulfide bridges that are important for the protein structure and formation of the hydrophobic binding pocket for the pheromone molecules.²⁵ The closeness between different PBPs are shown by drawing a phylogenetic tree in Figure 1.8.

Insects are ideal systems to study olfaction. Olfaction is species specific in all animals. It is very sensitive also. Moreover some insects are pests, causing economical harm to the humans. Some insects are resistant to insecticides. Using too much insecticide can be hazardous for human health. Disruption of sexual mating in insect can be done via sensory inhibition. Hence

getting structural and mechanistic information of pheromone binding and release would be an important step towards achieving bio-rational crop protection. Thus we can achieve species specific, environmental friendly, bio-rational crop protection.



Neuronal Response

Figure 1.6 Schematic representation of pheromone transport in insects by Pheromone binding proteins.

```

ApolPBP1 SPEIMKNLSNNFGKAMDQCKDELSLPDSVVADLYNFWKDDYVMTDRLAGCAINCLATKLD 60
ApolPBP2 SPEIMKNLCMNYGKTMQCKQELGLPDSVINDLYNFWKDDYVMTDRLAGCAINCLSTKLD 60
ApolPBP3 SQEIMKTMTLTFKGLDACKKEMDLPDVTVDVDFNNFWKEDYVVTNRDAGCAIVCLASKIN 60
AperPBP1 SPEI IKNLSQNFCKAMDQCKQELNIPDSVIADLYNFWKDDYVMTDRLAGCAINCMATKLD 60
BmorPBP  SQEVMKNLSLNF GKALDECKKEMTLTDAINEDFYNFWKEGYEIKNRETGCAIMCLSTKLN 60
BmorPBP2 SRDVMTNLSIQFAKPLEACKKEMGLTETVLKDFYNFWIEDYEFTRNTGCAILCMSKLE 60
BmorPBP3 SSEAMRHIATGFIRVLDECKQELGLTDHILTDMYHFWKLDYSMMTRETGCAIICMSKLD 60
AvelPBP  SQDVIKGMTLNF RKGLDECKKEMNLPDSINADFYNFWKDDHVL SNRDTGCAIMCLSSKLE 60
CrosPBP  SADVVKGMTLNF GKLEECKKEMNLPDSINADFYNFWKDDHVL TNRTGCAIMCLSSKLE 60
OnubPBP  SQDVMKQMTINFGKALDTCRKELDLPDSINADFYNFWKEGYELSNRQTGCAIMCLSSKLD 60
LdisPBP1 SKEVMKQMTINFAKPM EACKQELNVPDAVMQDFNFWKEGYQITNREAGCVILCLAKKLE 60
* : : : : : : : * : * : : : : * : * * . : . * : * * . * * : : * : :

```

```

ApolPBP1 VVDPDGNLHHGNAKDFAMKHGADETM AQQQLVDI IHGCEKSAP-PNDDKCMKTIDVAMCFK 119
ApolPBP2 IVDPDGNLHHGNAKEFAMKHGADDGMAQQQLVDI IHRCEKSTP-PNDDKCTKTMDIAMCFK 119
ApolPBP3 LVDSMGILIHGSAHEFAKQH GADDNMAKQLSDTLHTCETIIG-TGNDECTRALHVANCFK 119
AperPBP1 VVDPDGNLHHGNAKEFAMKHGADASMAQQQLVDI IHGCEKSAP-PNDDKCMKTIDVAMCFK 119
BmorPBP  MLDPEGNLHHGNAMEFAKKHGADETM AQQQLVIDI IHGCEKSTP-ANDDKCIWTLGVATCFK 119
BmorPBP2 LMDGDYNLHHGKAHEFARKHGADETM AKQLVDLIHGCSQSVA-TMPDECERTLKVAKCFI 119
BmorPBP3 LIDGDGKLHHGNAQAYALKHGAATEVA AKLVEVIHGCEKLHE-SIDDQCSRVEVAKCFR 119
AvelPBP  LVS-DGKLHHGNTFDYAKQHGADETV AQQQLVDLIHSCEKSLP-DLEDPCM KVLEWAKCFK 118
CrosPBP  LVS-DGKLHHGNTLEYAKQH GADDTVAQQQLVDLIHNCEKALP-DLEDPCM KVLEWAKCFK 118
OnubPBP  LVDPEGKLHHGNTEFAKKH GADDSMAKQLVELIHKCEGSVA-DDPDACMKVLDIAKCFK 119
LdisPBP1 LLDQDMNLHHGKAMEFAMKHGADEAM AKQLLDIKHSCEKVITIVADDP CQTMLNLMAMCFK 120
: : . * * * . : : * : * * * : * : * : * * . * * : * * *

```

```

ApolPBP1 KEIHKLNWVPNMDLVIGEVLAEV 142
ApolPBP2 KEIHKLNWVPNMDLVVCEVLAVV 142
ApolPBP3 VEMHKLDWAPSMDLIIGELLAEI 142
AperPBP1 KEIHKLNWVPDMDVVLGEVLAEV 142
BmorPBP  AEIHKLNWAPSM DVAVGEILAEV 142
BmorPBP2 AEIHKLKWAPDV ELLMAEVLNEV 142
BmorPBP3 TGVHELHWAPKLDVIVGEVMTEI 142
AvelPBP  TEIHKLNWAPSVEVLAAEMLAEV 141
CrosPBP  IEIHKLNWAPSM DVLAGEMLAEI 141
OnubPBP  AEIHKLNWAPSM DLIVAEVLAEV 142
LdisPBP1 AEIHKLWAPTLDVAVGELLADT 143
: * : * . * * : : : * : :

```

Figure 1.7 Sequence alignment of PBP s from different moth species. Amino acid residues marked as star (*) are conserved among the moth species, whereas residues marked as double dot (:) are similar kind of amino acids. PBP s from moth species *Antheraea polyphemus* (ApolPBP1, ApolPBP2 and ApolPBP3), *Bombyx mori* (BmorPBP, BmorPBP2 and BmorPBP3), *Antheraea pernyi* (AperPBP1), *Argyrotaenia velutinana* (AvelPBP), *Ostrinia nubilalis* (OnubPBP), *Choristoneura rosaceana* (CrosPBP) and *Lymantria dispar* (LdisPBP1) are aligned using Clustal W2.

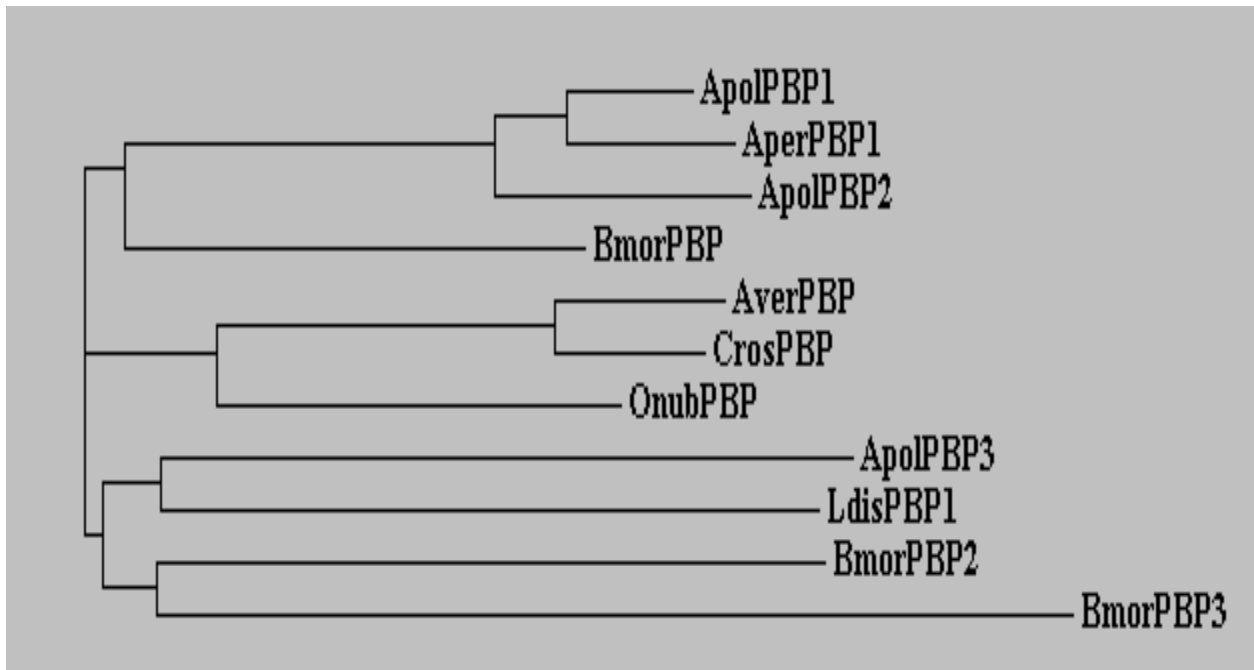
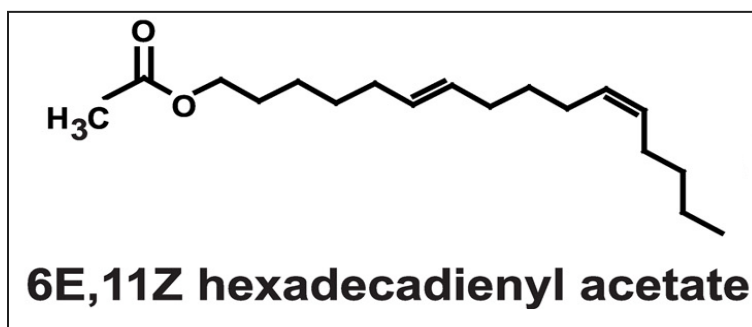


Figure 1.8 Phylogenetic tree of different moth PBPs generated using Clustal W2, showing the closeness/ distance between them.

1.2.3 *Antheraea polyphemus* Pheromone binding protein1 (ApolPBP1)

There are three subtypes of pheromone binding proteins (PBP) found in *Antheraea polyphemus*. They are: ApolPBP1, ApolPBP2 and ApolPBP3. Here we will only discuss ApolPBP1. ApolPBP1 is a highly water soluble protein. ApolPBP1 has a molecular weight of ~15.9 kD. It consists of 142 amino acid residues (Figure 1.9). ApolPBP1 has six conserved cysteine residues, which form three disulfide bonds that stabilize the protein structure (Cys19-Cys54, Cys50-Cys108 & Cys97-Cys117). These disulfide bonds help maintain the 3-dimensional structure and shape of this protein (Figure 1.10). ApolPBP1 has 6 α -helices. ApolPBP1 binds to the pheromone molecule 6E, 11Z-hexadecadienyl acetate. ApolPBP1 has about 67% sequence identity with another lepidopteran moth *Bombyx mori* PBP (BmorPBP).



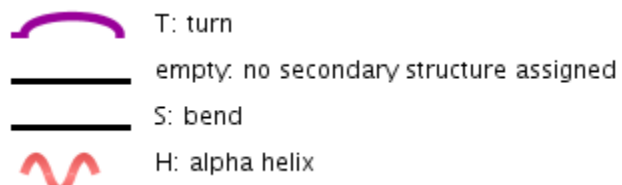
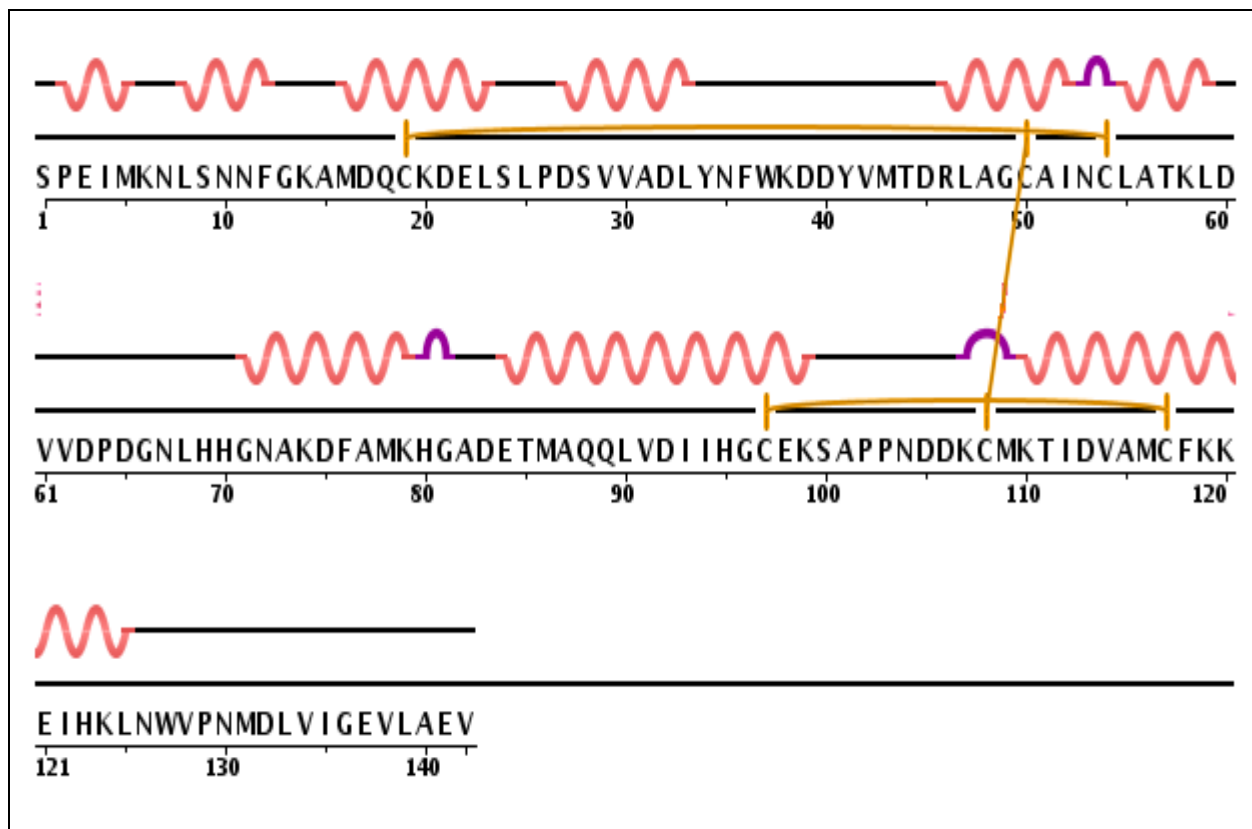


Figure 1.9 Sequence and secondary structure of *Antheraea polyphemus* Pheromone binding protein1 (ApolPBP1). Yellow lines are showing disulfide bond between Cys residues.

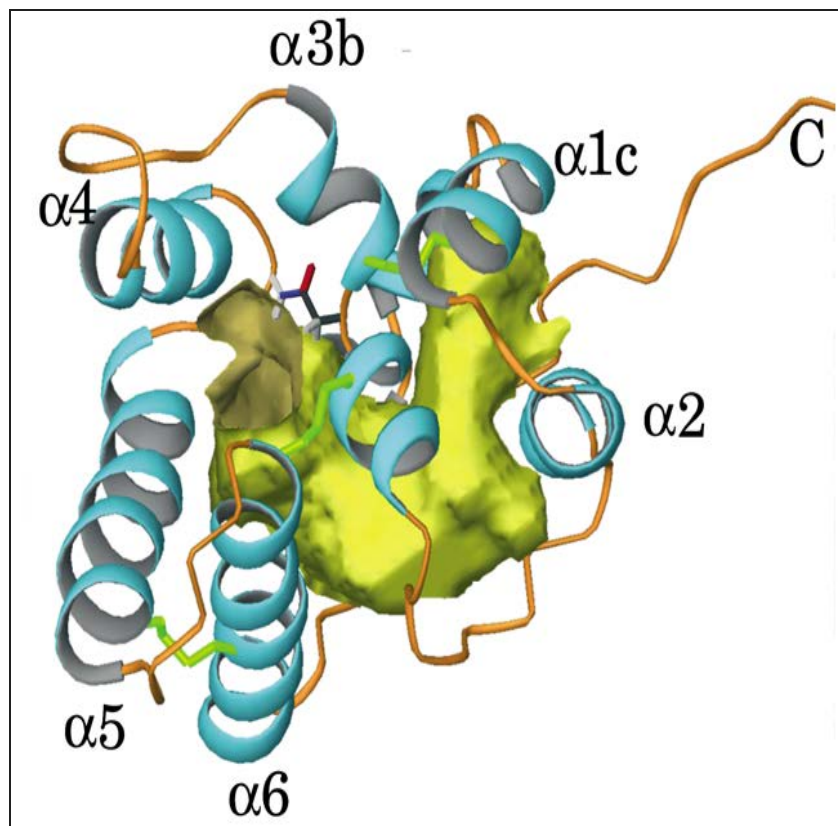


Figure 1.10 Binding pocket of ApolPBP1. Copied from reference 27.

It was proposed that ApolPBP1 can exist in two conformations:

The “**ligand binding or form B**” conformation at pH >6.0, characterized by an unstructured C-terminal tail, and the “**ligand releasing or form A**” conformation at pH <6.0, in which the C-terminus occupies the binding pocket as the 7th α -helix. Structures have already been solved for ApolPBP1 and BmorPBP at both high and low pH.²⁶⁻³² These structures however did not support the model as proposed. It has been found that, ApolPBP1 at pH 5.2 exists in two conformations (or mixed conformation), i.e. the same protein has both the ligand-bound and free conformations (Figure 1.11).²⁶ Whereas ApolPBP1 at pH 6.3 has the ligand-bound conformation with an unstructured C-terminal tail exposed to the solvent (Figure 1.12).²⁷ The NMR structure of ApolPBP1 at pH 4.5 showed that, the protein was in the ligand-free conformation with the C-terminal helix occupying the binding cavity (Figure 1.13).²⁸ Similar results were obtained for BmorPBP. At pH 6.5, the protein showed the ligand-bound conformation (Figure 1.14)²⁹ and at pH 4.5, it showed the ligand-free conformation (Figure 1.15).³⁰ But the crystal structure of BmorPBP at pH 7.5 shows the delipidated protein in the ligand-free conformation (Figure 1.16).³¹ Thus, different structures of ApolPBP1 and BmorPBP are contradictory to each other, implying that the same protein at a low or high pH may or may not have the C-terminal helix internalized in the binding cavity.

Two molecular switches have been proposed to be responsible for the ligand binding and release. The first one is the, protonation and subsequent repulsion of His-70 and His-95 situated at one end of the binding pocket to open the pocket at pH values below 6.0. The other one is the formation of a 7th helix by the C-terminal dodecapeptide, which occupies the binding pocket at low pH.

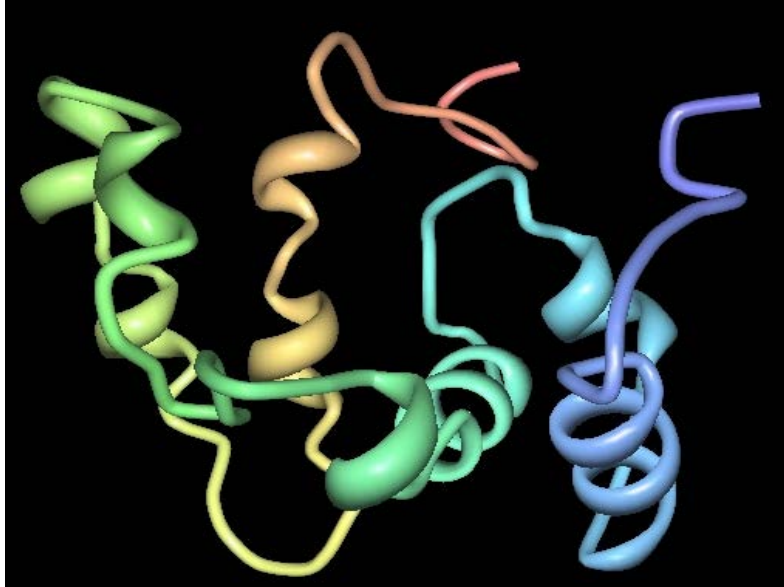


Figure 1.11 NMR structure of ApolPBP1 at pH 5.2. Adapted from reference 26.

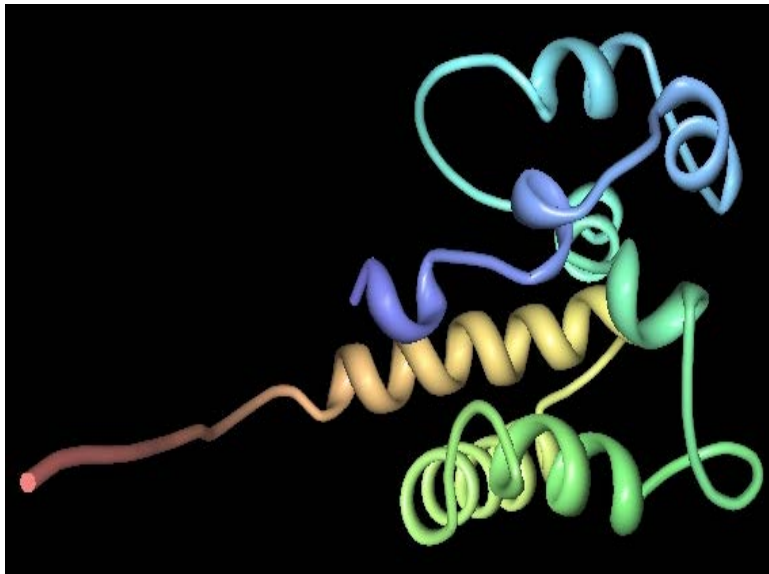


Figure 1.12 NMR structure of ApolPBP1 at pH 6.3. Adapted from reference 27.

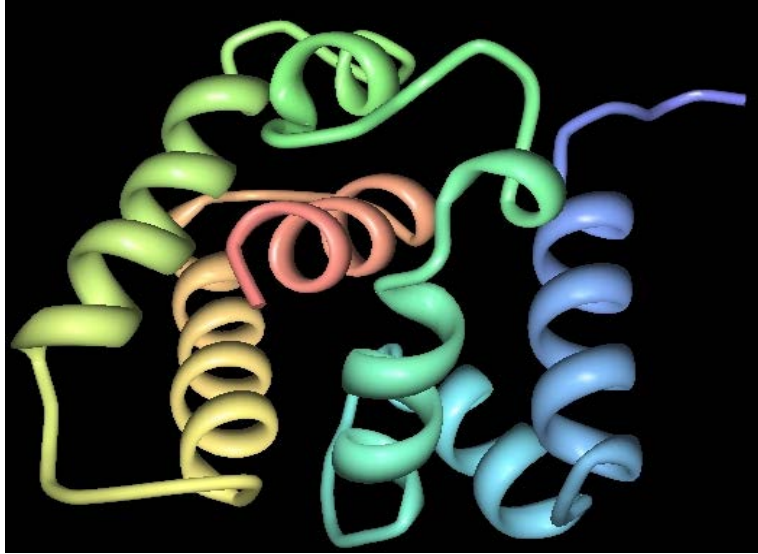


Figure 1.13 NMR structure of ApolPBP1 at pH 4.5. Adapted from reference 28.

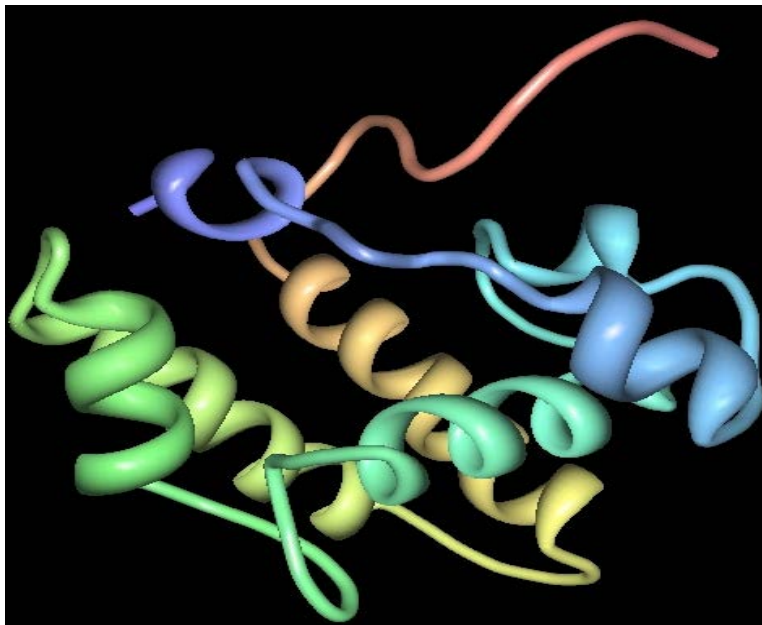


Figure 1.14 NMR structure of BmorPBP at pH 6.5. Adapted from reference 29.

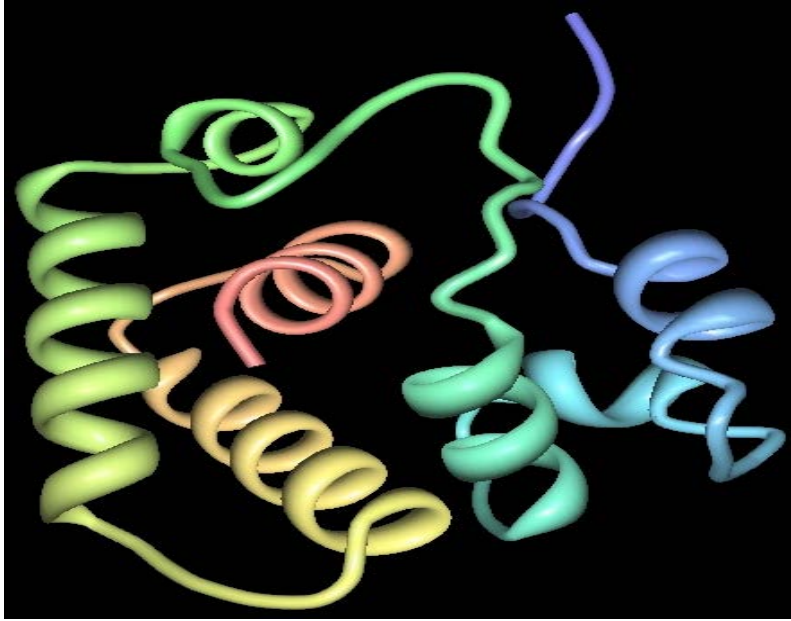


Figure 1.15 NMR structure of BmorPBP at pH 4.5. Adapted from reference 30.

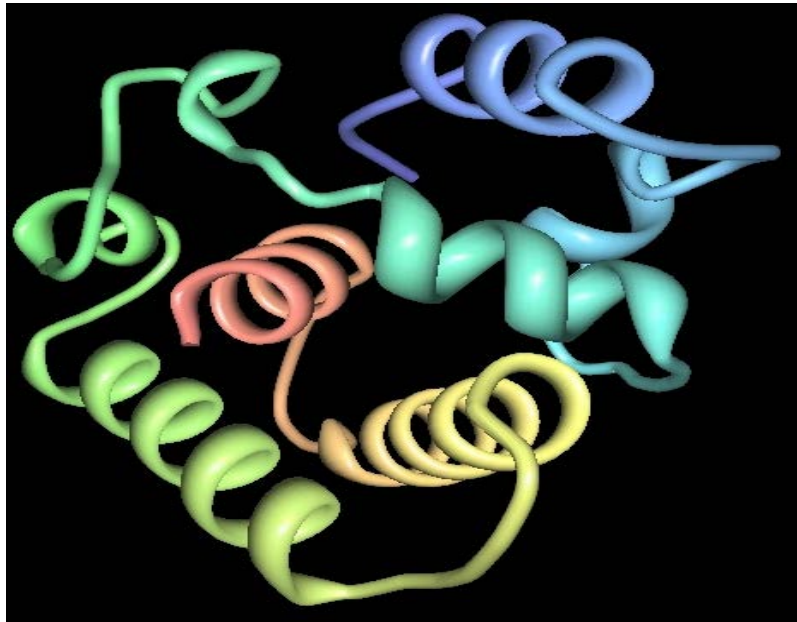


Figure 1.16 X-ray crystal structure of BmorPBP at pH 7.3. Adapted from reference 31.

1.3 Objective of the Study:

The differences in the structures of PBPs led us to conclude that there might be differences in ligand release models at low pH for ApolPBP1 than BmorPBP. In a recent investigation,²⁸ the ApolPBP1 at pH 4.5 was shown to have the same closed conformation as that of BmorPBP, with the C-terminal dodecapeptide segment tucked into the binding cavity after forming the seventh α -helix. However, there was a significant difference in the ApolPBP1 sample preparation in this study,²⁸ which included a delipidation step during purification of the recombinant protein. It is noteworthy here that many previous biochemical^{24,33,34} and biophysical investigations^{26,27,29,30,35} on either BmorPBP or ApolPBP1 have been conducted on the undelipidated protein, *i.e.* without carrying out the delipidation step. The objective of this study is to understand the mystery beneath the differences between structures of these undelipidated and delipidated moth PBPs, *i.e.* to understand the effect of delipidation and pH on PBP conformation. We carried out a detailed investigation to clarify the effect of delipidation, pH, and ligand on the conformation of ApolPBP1, as a representative member of the moth PBP family. Moreover, the previously proposed ligand release model of involvement of the pH-induced histidine-driven conformational switch at low pH^{26,32,36} was verified by the mutation of His70 and His95 to alanine in ApolPBP1. We also investigated the role of the C terminus tail in ligand binding and releasing by mutating the C-terminus tail of ApolPBP1. To gain insight into the role of pH and ligand on the conformational switches, a detailed biophysical characterization using solution NMR and fluorescence spectroscopy experiments of the mutants was carried out.

Reference:

- (1) Rabi I.I., Zacharias J.R., Millman S., and Kusch P. (1938) "A New Method of Measuring Nuclear Magnetic Moment". *Physical Review* 53, 318.
- (2) Roberts, G. C. K. (1993) NMR of macromolecules. A practical Approach. *Oxford University Press*.
- (3) Cavanagh, J., Fairbrother, W. J., Palmer, A. G., Skelton, N. J., and Rance, M. (2006) Protein NMR spectroscopy: principles and practice. *Academic Press*; 2nd Ed.
- (4) Bodenhausen, G. and Ruben, D. J. (1980) Natural abundance nitrogen-15 NMR by enhanced heteronuclear spectroscopy. *Chem. Phys. Lett.* 69, 185-189.
- (5) Wüthrich K (December 1990) "Protein structure determination in solution by NMR spectroscopy". *J. Biol. Chem.* 265, 22059–62.
- (6) Bax, A., Ikura, M., Kay, L. E., Torchia, D. A., and Tschudin R. (1990) Comparison of Different Modes of Two-Dimensional Reverse-Correlation NMR for the Study of Proteins. *J. Magn. Reson.* 86, 304–318.
- (7) Norwood, T. J., Boyd, J., Heritage, J. E., Soffe, N., and Campbell, I.D. (1990) Comparison of techniques for ^1H -detected heteronuclear $^1\text{H}^{15}\text{N}$ Spectroscopy. *J. Magn. Reson.* 87, 488–501.
- (8) Oktaviani, N. A., Otten, R., Dijkstra, K., Scheek, R. M., Thulin, E., Akke, M., and Mulder, F. A. A. (2011) 100% complete assignment of non-labile ^1H , ^{13}C , and ^{15}N signals for calcium-loaded calbindin D_{9k} P43G *Biomol NMR Assign.* 5, 79–84.
- (9) Pelosi, P. and Maida, R. (1995) Odorant-binding proteins in insects. *Comp. Biochem. Physiol. B* 111, 503–514.

- (10) Vogt, R. G., Prestwich, G. D. and Lerner, M. R. (1991) Odorant-binding-protein subfamilies associate with distinct classes of olfactory receptor neurons in insects. *J. Neurobiol.* 22, 74–84.
- (11) Buck, L. and Axel, R. (1991) A novel multigene family may encode odorant receptor: A molecular basis for odor recognition. *Cell* 65, 175–187.
- (12) Firestein, S. (2001) How the olfactory system makes sense of scents. *Nature* 413, 211–218.
- (13) Gullan, P. J., and Cranston, P. S. (2010) *The Insects. Ed. 4.* Wiley-Blackwell: UK.
- (14) Wood, W., F., (1983) Chemical ecology: chemical communication in nature. *Journal of Chemical Education* 60, 531.
- (15) Norin, T., (2007) Semiochemicals for insect pest management. *Pure and Applied Chemistry* 79, 2129-2136.
- (16) Perna, J., and Aksela, M., (2011) Learning Organic Chemistry through a Study of Semiochemicals. *Journal of Chemical Education* 88, 1644–1647.
- (17) Law, J., H., and Regnier, F., E., (1971) Pheromones. *Ann. Rev. Biochem.* 40, 533.
- (18) Karlson, P. and Luscher, M. (1959) ‘Pheromones’: a New term for a Class of Biologically Active Substances. *Nature* 183, 56.
- (19) Brown, Jr., W. L., Eisner, T., and Whittaker, R. H. (1970) Allomones and Kairomones: Transspecific Chemical Messenger. *Bioscience* 20, 21.
- (20) Roelofs, W. L. (1995) Chemistry of sex attraction. *Proc. Natl Acad. Sci., U.S.A.* 92, 44–49.

- (21) Sato, K., Pellegrino, M., Nakagawa, T., Nakagawa, T., Vosshall, L. B., and Touhara, K. (2008) Insect olfactory receptors are heteromeric ligand-gated ion channels. *Nature* 452, 1002–1006.
- (22) Wicher, D., Schäfer, R., Bauernfeind, R., Stensmyr, M. C., Heller, R., Heinemann, S. H., and Hansson, B. S. (2008) *Drosophila* odorant receptors are both ligand-gated and cyclic-nucleotide-activated cation channels. *Nature* 452, 1007-1011.
- (23) Raming, K., Krieger, J., and Breer, H. (1989) Molecular cloning of an insect pheromone-binding protein. *FEBS Lett.* 256, 215–218.
- (24) Prestwich, G. D. (1993) Bacterial expression and photoaffinity labeling of a pheromone binding protein. *Protein Sci.* 2, 420–428.
- (25) Ring, J. R., Prusti, R. K., and Mohanty, S. (2008) Chemical communication: a visit with insects. *Curr. Chem. Biol.* 2, 83–96.
- (26) Zubkov, S., Gronenborn, A. M., Byeon, I. J., and Mohanty, S. (2005) Structural Consequences of the pH-induced Conformational Switch in *A. polyphemus* Pheromone binding Protein: Mechanisms of Ligand Release. *J. Mol. Biol.* 354, 1081–1090.
- (27) Mohanty, S., Zubkov, S., and Gronenborn, A. M. (2004) The Solution NMR Structure of *Antheraea polyphemus* PBP Provides New Insight into Pheromone Recognition by Pheromone-binding Proteins. *J. Mol. Biol.* 337, 443–451.
- (28) Damberger, F.F., Ishida, Y., Leal, W.S., Wüthrich, K. (2007) Structural basis of ligand binding and release in insect pheromone-binding proteins: NMR structure of *Antheraea polyphemus* PBP1 at pH 4.5. *J.Mol.Biol.* 373, 811-819.

- (29) Lee, D., Damberger, F. F., Peng, G., Horst, R., Güntert, P., Nikonova, L., Leal, W. S., and Wüthrich, K. (2002) NMR structure of the unliganded *Bombyx mori* pheromone-binding protein at physiological pH. *FEBS Lett.* 531, 314–318.
- (30) Horst, R., Damberger, F., Luginbühl, P., Güntert, P., Peng, G., Nikonova, L., Leal, W. S., and Wüthrich, K. (2001) NMR structure reveals intramolecular regulation mechanism for pheromone binding and release. *Proc. Natl. Acad. Sci., U.S.A.* 98, 14374–14379.
- (31) Lautenschlager, C., Leal, W. S., and Clardy, J. (2005) Coil-to-helix transition and ligand release of *Bombyx mori* pheromone-binding protein. *Biochem. Biophys. Res. Commun.* 335, 1044–1050.
- (32) Sandler, B. H., Nikonova, L., Leal, W. S., and Clardy, J. (2000) Sexual attraction in the silkworm moth: structure of the pheromone-binding-protein–bombykol complex. *Chem. Biol.* 7, 143–151.
- (33) Wojtasek, H., and Leal, W. S. (1999) Conformational Change in the Pheromone-binding Protein from *Bombyx mori* Induced by pH and by Interaction with Membranes. *J. Biol. Chem.* 274, 30950–30956.
- (34) Du, G., and Prestwich, G. D. (1995) Protein Structure Encodes the Ligand Binding Specificity in Pheromone Binding Proteins. *Biochemistry* 34, 8726–8732.
- (35) Damberger, F., Nikonova, L., Horst, R., Peng, G., Leal, W. S., and Wüthrich, K. (2000) NMR characterization of a pH-dependent equilibrium between two folded solution conformations of the pheromone-binding protein from *Bombyx mori*. *Protein Sci.* 9, 1038–1041.
- (36) Xu, W., and Leal, W. S. (2008) Molecular switches for pheromone release from a moth pheromone-binding protein. *Biochem. Biophys. Res. Commun.* 372, 559–564.

Chapter 2

Effect of delipidation and pH on the conformation of ApolPBP1

2.1 Introduction

Higher organisms have developed many complex cellular signaling systems to serve in intracellular and intercellular communication. Some of these signaling systems also function in interspecies as well as intraspecies communications, also known as chemical communication or chemoreception or olfaction. Chemical communication is mediated via small, volatile chemical compounds. Chemical signaling or chemoreception is a very important phenomenon in insects. Chemical communication/olfaction helps insects in their common behavioral processes such as feeding and mating. Insect olfactory system, situated at the boundary of the outside environment and the nervous system inside the insects, is accountable for correctly coding the sensory information from thousands of odor molecules. The insect olfactory system can distinguish among thousands of odor molecules of many different structures and respond to a specific odor. Thus, insect olfactory system is highly sensitive and very specific in its response. A Pheromone is a special type of odor molecule that triggers behavioral response in another member of the same species. In lepidopteron insects, such as- moths and butterflies, sex pheromones produced by females are detected by males of the same species. These hydrophobic compounds are then transported to the membrane-bound receptors across the aqueous sensillar lymph by the pheromone-binding proteins (PBPs).¹⁻⁵ The first PBP to be identified, cloned, and expressed in the bacterial system was from the giant silk moth *Antheraea polyphemus*.^{6,7} PBPs are highly water soluble proteins and acidic in nature. These small proteins have a molecular mass of 14-16 kDa.

The insect PBPs that have been studied so far are believed to have two conformations: (i) “ligand releasing” form or “form A” at low pH and (ii) “ligand binding” form or “form B” at high pH.⁸ It has been proposed that, the moth PBPs go through a conformational switch from “form B” to “form A” at low pH near the membrane-bound receptor/ion channels to release the pheromone molecule.⁸⁻¹³ PBPs isolated from different moth species have shown to have 50% sequence identity. Among them, PBPs from moths *Bombyx mori* (BmorPBP) and *Antheraea polyphemus* (ApolPBP1) are shown to have 67% sequence identity. All the moth PBPs have six conserved cysteine residues forming three disulfide bonds which are important to form the binding pocket and the overall architecture of PBP.¹⁴ The conformation of BmorPBP at pH 6.5 (BmorPBP^B or “form B”) consists of six helices encasing the binding pocket with an unstructured C-terminal tail that extends to the solvent.¹¹ However at pH 4.5, it is reported that BmorPBP switches to another conformation (BmorPBP^A or “form A”), where the c-terminus tail is inside the binding pocket forming a 7th helix.¹⁰ ApolPBP1 shares similar structure at high pH having six helices and an unstructured C-terminal tail.¹² However, at low pH ApolPBP1 and BmorPBP exhibit different conformations according to these reports.^{10,13} At pH 5.2, ApolPBP1 does not contain the internalized C-terminal helix and exists in two conformations.¹³ In another report though, at pH 4.5 ApolPBP1 is known to have structural similarities to BmorPBP, having an internalized C-terminal helix inside the binding pocket.¹⁵ However there is a stark difference in the ApolPBP1 sample preparation in this study¹⁵ than the previous one¹³ where a delipidation step was included in the latter. In another study on x-ray crystallographic structure of BmorPBP at 7.5, the C-terminus is inside the binding pocket as a helix even at higher pH.¹⁶

All the previous studies on either BmorPBP or ApolPBP1 have led to controversies without a clear insight as to which protein conformation is correct with regard to pH. Many of

these studies were conducted on the protein samples without carrying out the additional delipidation step,^{7-13,17} whereas for few other protein samples, an additional delipidation step was included.^{15,16} What important was that all these reports on the structures ApolPBP1 and BmorPBP contradicted with each other: (i) ApolPBP1 at low pH may or may not have the C-terminal helix^{13,15} and (ii) BmorPBP without having a delipidation procedure, had an unstructured c-terminus tail at high pH¹¹ whereas BmorPBP prepared with an additional delipidation procedure, had a internalized c-terminus helix at high pH.¹⁶

To clarify these differences between structures of these PBPs we carried out a detailed investigation to determine the effect of the delipidation protocol, ligand and pH on the conformation of ApolPBP1 using high resolution solution NMR and fluorescence spectroscopy.¹⁸

2.2 Materials and Methods

2.2.1 Cloning and Overexpression

The *ApolPBP1* gene was cloned into the NdeI and BamHI sites of the pET-21a vector previously in Dr. Smita Mohanty's laboratory. The ApolPBP1-pET-21a plasmid was transformed into *E. coli* origami cells. Overexpression and lysis was done as described previously.^{12,13} The isotope-labeled protein was expressed in M9 minimal medium with [¹⁵N] ammonium chloride (Cambridge Isotope Laboratories, MA). An overnight culture was diluted into fresh LB media with ampicillin, tetracycline and kanamycin and grown at 37 °C to an OD (optical density) at 600 nm of 0.5. Expression was induced with 1 mM IPTG (Gold Biotechnology, Inc.) and cells were incubated at 30 °C for 4 hours for unlabeled expression and for 15 hours for ¹⁵N labeled expression. Cells were then harvested using a Sorvall^R RC2-B centrifuge at 12000 rpm and 4°C. Cells were then suspended in BPER (Bacterial Protein Extraction Reagent) (Thermo Scientific) with 2 mM EDTA, 1mM PMSF and one cocktail protease inhibitor tablet (Roche) and lysed using sonication (Branson Sonifier150) pulsing for 10 seconds for 5-6 times and an interval of 1 min between each pulse. After the centrifugation, cell lysate was collected and stored at 4 °C.

2.2.2 Purification

The recombinant protein was purified by a combination of three steps: Dialysis, Anion exchange chromatography and Size exclusion chromatography. Cell lysate was dialyzed using a 3000 Da cutoff membrane in a tank filled with 20mM Tris-HCl, pH 8.0. Dialysis was carried out for 16 hours. Dialysed cell lysate was then centrifuged, filtered and subsequently injected into the DEAE column equilibrated with 20mM Tris-HCl, pH 8.0. The protein was eluted by using a salt gradient. Specific fractions containing the protein of interest were collected and concentrated using a Millipore ultrafiltration concentrator (molecular weight cutoff of 5000). The concentrated

protein sample was then loaded to a Superdex 75 column fitted to an AKTA FPLC (GE Healthcare) and was eluted in a buffer containing 20 mM Sodium-phosphate, pH 6.5 with 150 mM NaCl, 1 mM EDTA and 0.01% Sodium azide as the mobile phase. The purest fractions of ApolPBP1 was collected and concentrated accordingly.

2.2.3 Delipidation

The delipidation of ApolPBP1 was performed according to Bette *et al.* (19). The protein was first concentrated to 500 μ l using a Millipore ultrafiltration concentrator and 4.5 ml of 50 mM sodium citrate buffer pH 4.5 was added. These procedures were repeated twice, and the final volume of the protein was adjusted to 2 ml with the buffer. The protein was then incubated overnight with LipidexTM-1000 equilibrated with the 50 mM sodium citrate buffer pH 4.5, in a column shaking continuously. The temperature of incubation did not have any effect on the efficiency of delipidation as same results were obtained for the protein delipidated at 4 °C, 22 °C or 37 °C. The protein was eluted from Lipidex-1000 with sodium citrate buffer. The eluted protein was concentrated to 2 ml, incubated again overnight with fresh Lipidex-1000, and eluted with same buffer. To prepare the NMR samples, the purest fractions were exchanged to 50 mM sodium phosphate buffer, pH 6.5 or pH 4.5, with 1 mM EDTA and 0.01% sodium azide, containing 5% D₂O, and concentrated as per the protocol mentioned above. The purity of the sample was assessed by electrospray ionization-mass spectrometry.

2.2.4 Mass Spectrometry

Mass spectrometry was carried out at the Mass Spectrometry Facility, at the Department of Chemistry and Biochemistry, Auburn University. The delipidated ApolPBP1 was analyzed by electrospray ionization-mass spectrometry on a Q-ToF PremierTM (Waters) mass spectrometer.

2.2.5 NMR Measurements

All NMR data were collected at 35 °C on a Bruker Avance 600-MHz spectrometer at the Department of Chemistry and Biochemistry, Auburn University. pH titrations were carried out on 400 μ l of uniformly ^{15}N labeled 0.3 mM protein in 50 mM sodium phosphate buffer, pH 6.5 or pH 4.5, 1 mM EDTA, 0.01% NaN_3 , and 5% D_2O (used as a lock solvent) in a Shigemi tube. Two-dimensional $\{^1\text{H}, ^{15}\text{N}\}$ heteronuclear single quantum coherence (HSQC) spectra were collected for ^{15}N labeled undelipidated and delipidated samples at pH 4.5 and 6.5.

The pH titration of delipidated ApolPBP1 was carried out in the pH range of 4.5 to 6.5 while following the movement of resonance peaks in two-dimensional $\{^1\text{H}, ^{15}\text{N}\}$ HSQC spectra. The protein at pH 4.5 was titrated to pH 6.5 using 1 M NaOH. HSQC spectra were recorded at each titration point, and the movement of peaks was followed using the assignment published previously.²⁰ For the pH titration of ligand-bound protein, the delipidated ApolPBP1 samples were first incubated with an excess of ligand (1:5 palmitic acid) prior to titration from pH 6.5 to 4.5. The two-dimensional $\{^1\text{H}, ^{15}\text{N}\}$ HSQC spectra were collected at each titration point.

For ligand titration experiments, uniformly ^{15}N -labeled delipidated ApolPBP1wt (310 μ l of 220 μ M in 50mM phosphate buffer, pH 6.5, containing 5% D_2O , 1 mM EDTA, and 0.01% (w/v) NaN_3) was titrated with increasing concentrations of various ligands (0–2.2 mM), and the corresponding two-dimensional $\{^1\text{H}, ^{15}\text{N}\}$ HSQC spectra were recorded. All data were processed using NMRPipe²¹ and analyzed using NMRView.²²

2.3 Results

2.3.1 Expressed and purified protein

Unlabeled as well as ^{15}N -labeled protein was expressed and purified as mentioned above. The mass-spec analysis showed the purity of the protein (Figure 2.1), showing a single peak at 15.909 kDa.

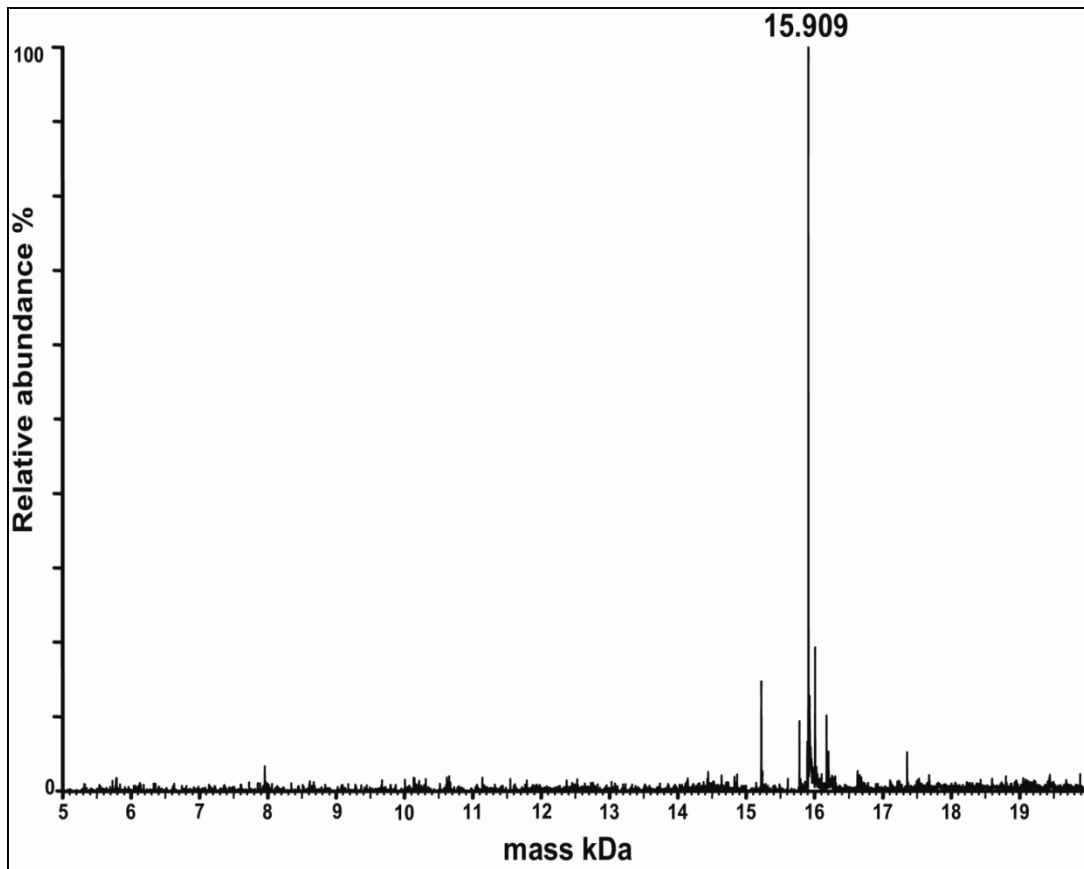


Figure 2.1 Mass spec analysis of pure and delipidated ^{15}N -labeled ApolPBP1. A sharp peak at 15,909 Da indicates the presence of pure protein. From reference 18.

2.3.2 Effect of Delipidation on the Conformation of ApolPBP1

The two-dimensional $\{^1\text{H}, ^{15}\text{N}\}$ HSQC spectrum is called the fingerprint region of a protein. The HSQC spectrum for any protein is very sensitive and this spectrum changes with any kind of environmental changes to the protein like changes in pH, temperature, or substrate binding. The changes in chemical shift positions of the residues of a protein in the HSQC spectrum may indicate a conformational change in the protein that can be either local or global. From the HSQC data, it was clear that, the HSQC spectrum of the undelipidated ApolPBP1 at pH 6.5 matched very well to that of the previously reported HSQC spectrum of ApolPBP1 at pH 6.3 suggesting the same conformation for undelipidated protein as reported previously.¹² At pH 4.5 however, the HSQC of the undelipidated protein matched very well to that of the delipidated PBP reported previously suggesting that the undelipidated PBP at low pH has the same conformation as that of delipidated ApolPBP1 at pH 4.5 (Figure 2.2A and 2.2B).¹⁵ These results indicated that the undelipidated protein went through a pH-dependent conformational change. In contrast to the above results, the delipidated ApolPBP1 didn't undergo any such conformational switch with the change in pH levels. The HSQC spectrum of the delipidated ApolPBP1 at pH 6.5 and 4.5 are exactly same and matched to that of the delipidated ApolPBP1 reported previously suggesting the same conformation as that of the previously reported conformation of delipidated ApolPBP1 at pH 4.5 (Figure 2.2C and 2.2D).¹⁵ The NMR data suggested that the undelipidated ApolPBP1 did bind to an endogenous ligand from the bacterial expression system which was ejected automatically at acidic pH of 4.5 or upon delipidation by passing through the Lipidex resin and changed conformation to the free protein.¹⁸

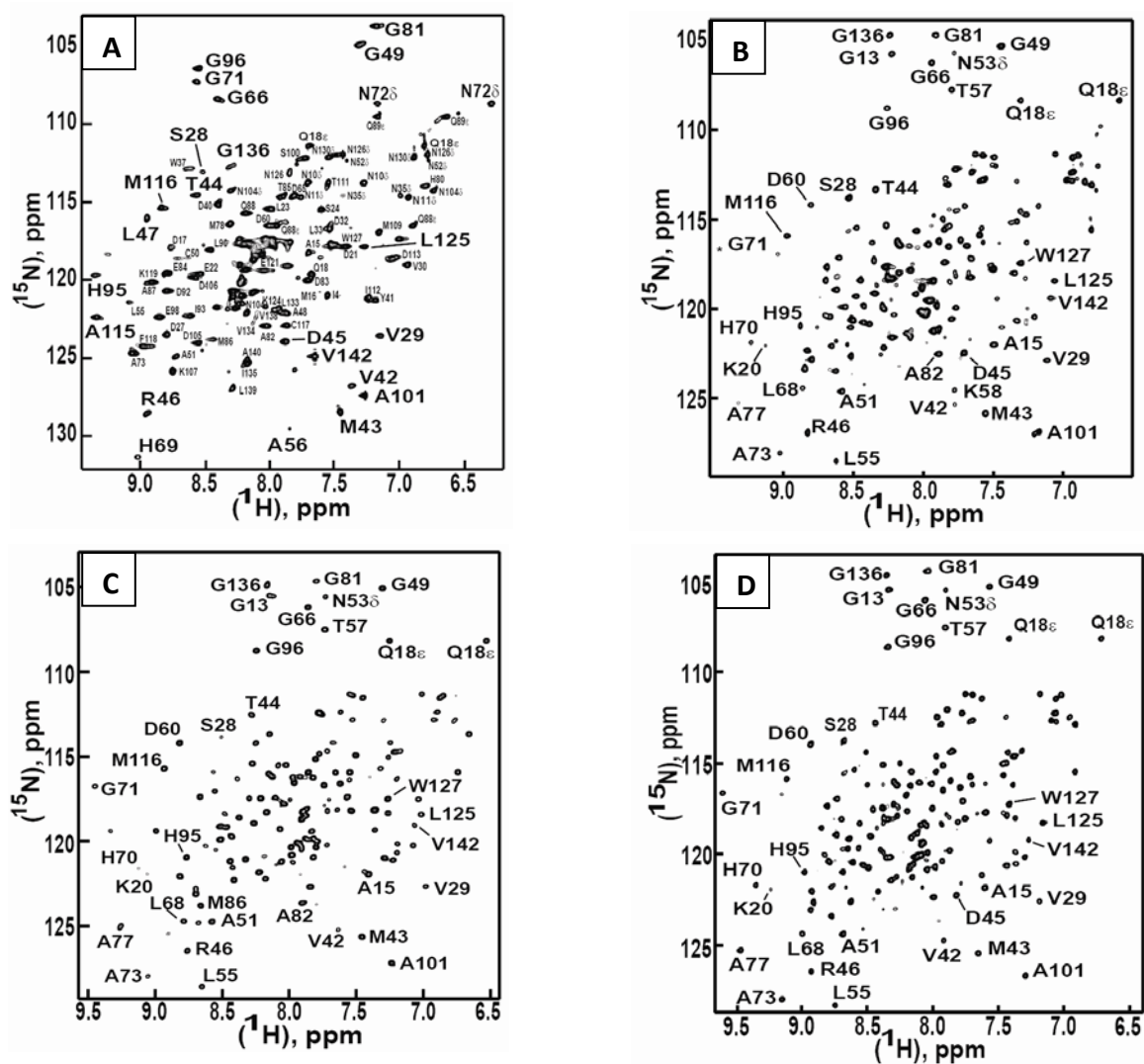


Figure 2.2 Two dimensional $\{^1\text{H}, ^{15}\text{N}\}$ HSQC spectrum of Undelipidated and Delipidated ApolPBP1 at pH 6.5 and pH 4.5. A. Undelipidated ApolPBP1 at pH 6.5. B. Undelipidated ApolPBP1 at pH 4.5. C. Delipidated ApolPBP1 at pH 6.5. D. Delipidated ApolPBP1 at pH 4.5. From reference 18.

To verify the above observation, we analyzed the undelipidated ApolPBP1 by non-denaturing ESI-MS. The deconvoluted spectrum of non-denaturing ESI-MS of undelipidated wild type protein showed two peaks: the major peak at 15908 Da corresponds to the molecular mass of the free protein (Figure 2.3 A). There is a second minor peak at 16194 Da (Figure 2.3A). The difference in mass between these two peaks was 286 which corresponded to the mass of a small molecule suggesting that the peak at 16194 Da was that of the ApolPBP1 with an endogenous ligand bound from the host expression system while the peak at 15908 Da was that of the free protein where the ligand was automatically ejected under ESI MS condition which is acidic. The second minor peak in the ESI MS was detected only under the non-denaturing conditions and was absent in the spectrum of delipidated ApolPBP1 under similar conditions (Figure 2.3B). This spectrum had only one peak that corresponds to the molecular weight of the free ApolPBP1. We also carried out a positive control for this experiment where delipidated ApolPBP1 was incubated with excess of palmitic acid and the ESI MS was carried out. This ESI MS spectrum was very similar to the undelipidated ApolPBP1 in which a second peak for ApolPBP1-palmitic acid complex was detected (Figure 2.3C). Thus, the ESI MS result was consistent with the NMR results confirming our conclusion that ApolPBP1 did bind an endogenous ligand from the host expression system. Thus, for the first time, we have shown that, PBPs expressed in the bacterial system picks up a lipid molecule from the host system and always remains in the ligand-bound conformation at pH higher than 6.0. The protein releases the ligand either at pH below 5.0 or upon delipidation changing to the ligand-free conformation.¹⁸ We concluded that this feature is very likely common for any lipid-binding protein.¹⁸

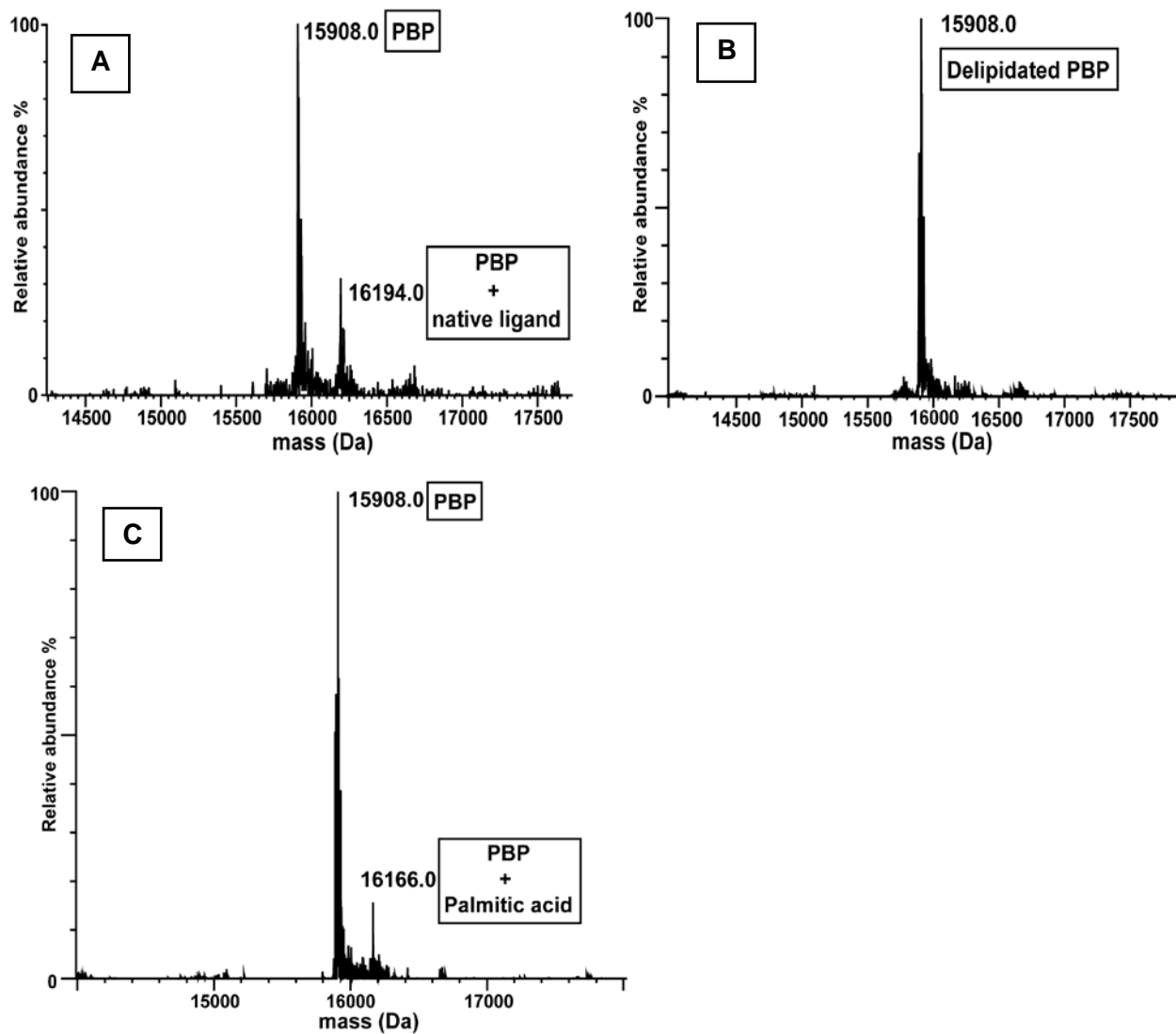


Figure 2.3 Deconvoluted ESI-mass spectra of ApolPBP1wt under non-denaturing conditions. A. Before delipidation B. After delipidation C. After incubation with excess of palmitic acid.

Based on our NMR and ESI-MS data, it is clear that the two-dimensional $\{^1\text{H}, ^{15}\text{N}\}$ HSQC spectrum for the undelipidated ApolPBP1 represents the ligand-bound conformation (Figure 2.4) whereas it's the two-dimensional $\{^1\text{H}, ^{15}\text{N}\}$ HSQC spectrum of the undelipidated ApolPBP1 at pH 4.5 or the delipidated ApolpBP1 at any pH is the ligand-free conformation of the protein (Figure 2.4).¹⁸ The undelipidated protein undergoes a conformational switch from bound to the free conformation when the pH is lowered from 6.5 to 4.5 (Figure 2.2). However, the delipidated protein remains in the free conformation at all pH levels (Figure 2.2).

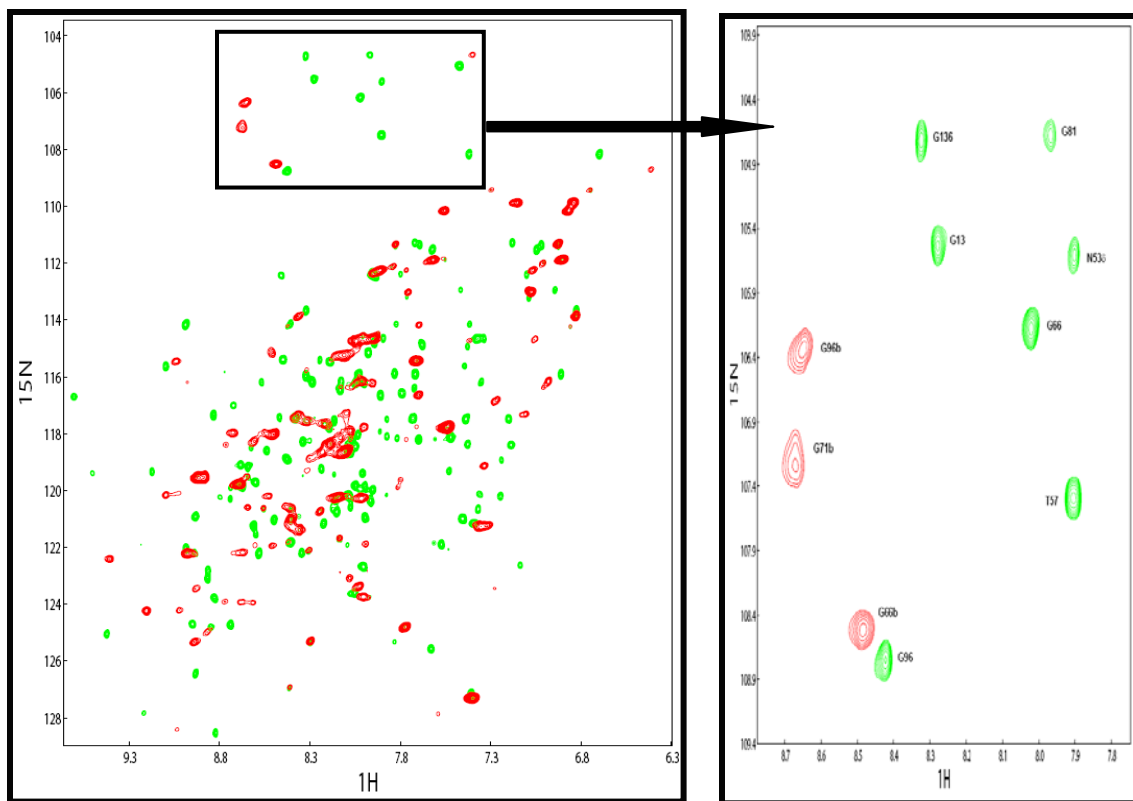


Figure 2.4 Two dimensional $\{^1\text{H}, ^{15}\text{N}\}$ HSQC spectrum of Undelipidated and Delipidated ApolPB1 at pH 6.5. HSQC spectrum in red color representing undelipidated protein whereas spectrum in green represents delipidated protein. From reference 18.

To investigate further the effect of delipidation on the structure of ApolPBP1, ligand binding studies were carried out on the delipidated protein at pH 6.5. The ligand binding experiment was started with a protein: ligand ratio of 1:0 and continued until a protein:ligand ratio of 1:10. This experiment could not go beyond a protein: ligand ratio of 1:10 because the protein precipitated out of the solution at very high ligand concentration due to increase in the alcohol content that was used to solubilize the hydrophobic ligand. And almost all the resonances in the HSQC spectrum changed their chemical shift positions indicating nonspecific protein-ligand binding.²³ During the titration experiment, the resonances belonging to the ligand-free form of the ApolPBP1 became gradually weak and finally disappeared, while the resonances belonging to the ligand-bound form appeared and became prominent with each addition of the ligand. At an approximate protein:ligand ratio of 1:1, the ligand-free form of the delipidated ApolPBP1 was completely converted into the ligand-bound form.¹⁸ Figure 2.5 shows an expanded region of the HSQC spectra of delipidated ApolPBP1 in 50mM phosphate buffer, at pH 6.5. When 6*E*, 11*Z* hexadecadienyl acetate (*A. polyphemus* pheromone molecule) is added a decrease in the intensities of the peaks corresponding to the “ligand-free” conformation is observed concomitant with an increase in the intensities of the peaks corresponding to the “ligand-bound” conformation labeled as *b* (Figure 2.5 and 2.6) (18).

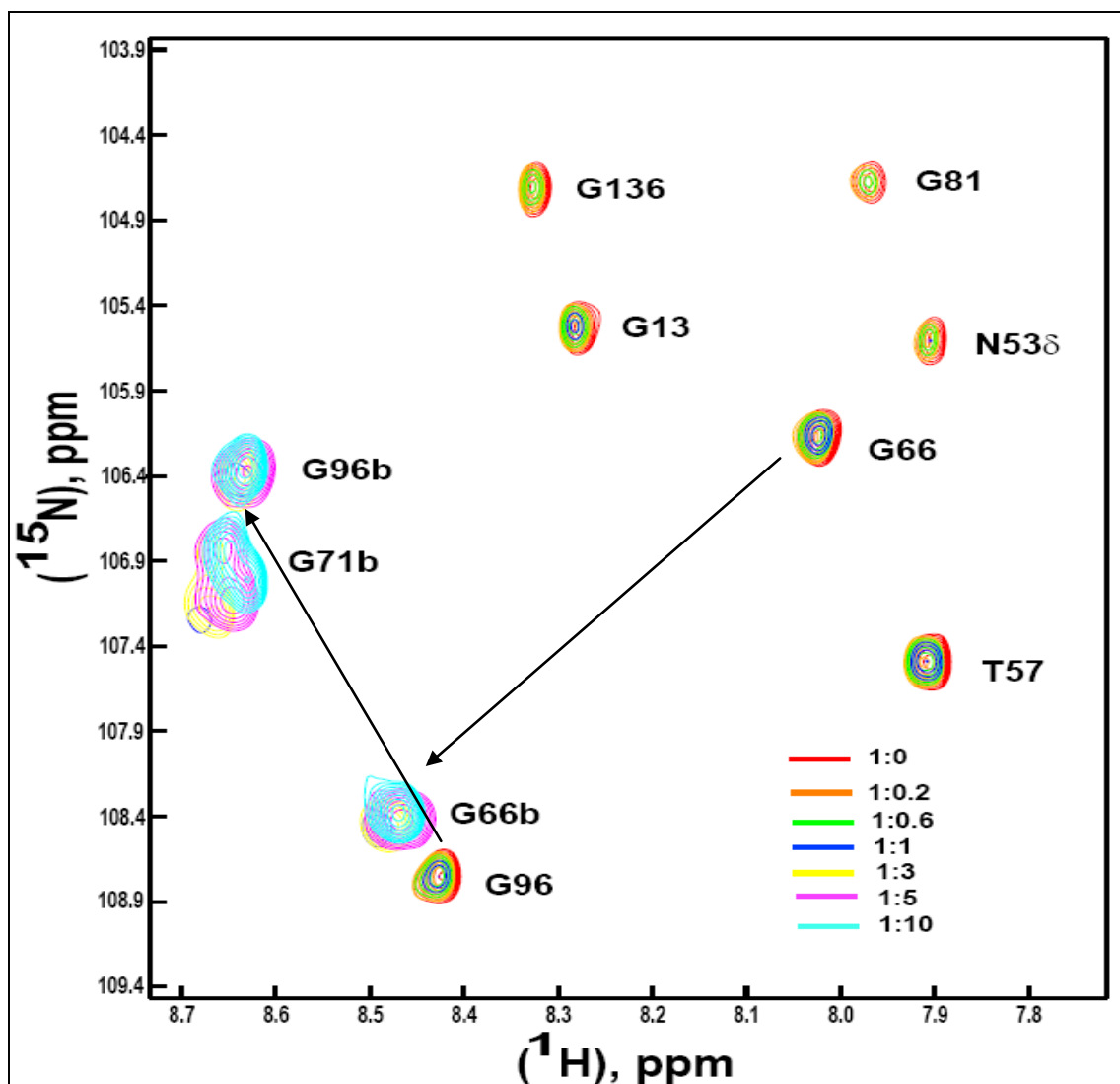


Figure 2.5 Expanded region of the $\{^1\text{H}, ^{15}\text{N}\}$ HSQC spectra of delipidated ApolPBP1, pH 6.5, upon titration with 6E, 11Z-hexadecadienyl acetate (*A. polyphemus* pheromone). Arrows showing that, the residues changing the chemical shift which indicates the protein is changing from ligand-free (G66 and G96) to ligand-bound (G66b and G96b) conformation. From reference 18.

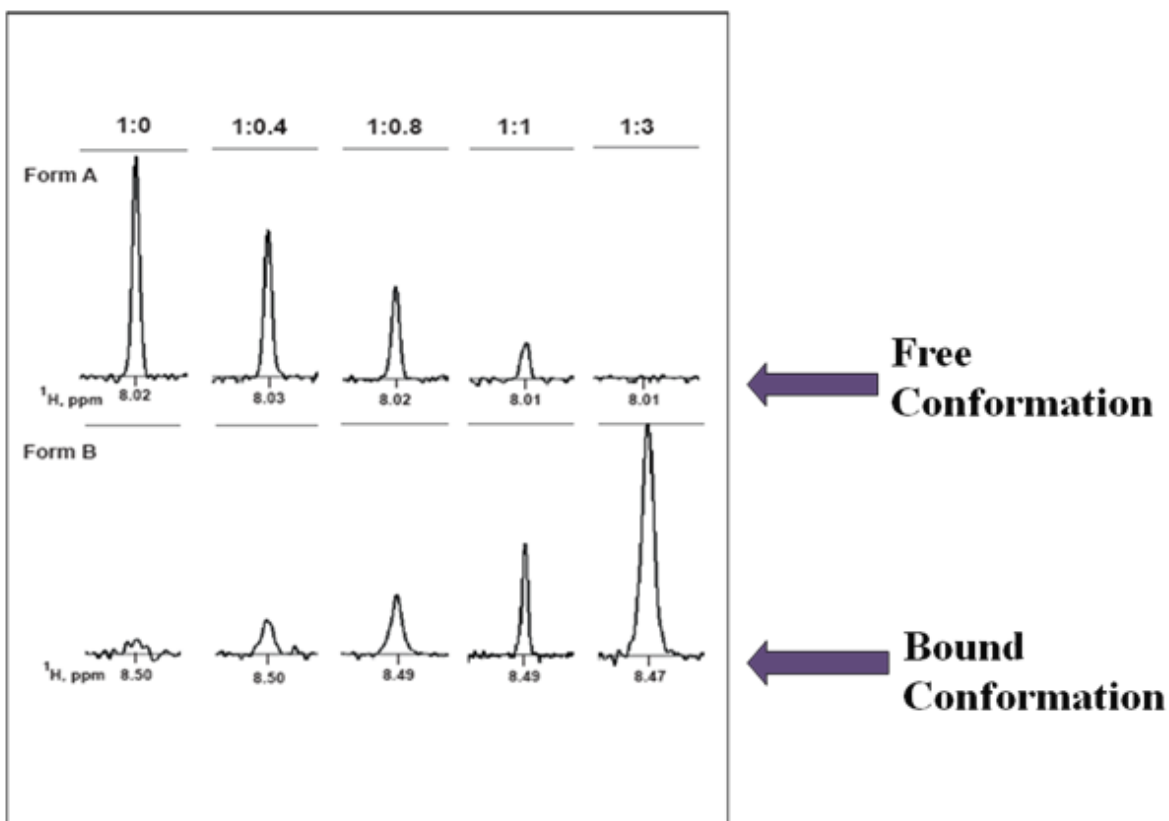


Figure 2.6 One-dimensional slices from the ^1H axis of the twodimensional $\{^1\text{H}, ^{15}\text{N}\}$ HSQC spectra of ApolPBP1 upon titration with 6*E*, 11*Z*-hexadecadienyl acetate, taken in the midpoint of the resonances corresponding to Gly66 in the free as well as the bound form. Protein: Ligand ratios are shown on the top of each pair of slices. From reference 18.

2.3.3 Effect of pH on ApolPBP1 conformation

The two-dimensional $\{^1\text{H}, ^{15}\text{N}\}$ HSQC spectra of undelipidated and delipidated ApolPBP1 showed that undelipidated protein went through a conformational change (Figure 2.7A).¹⁸ However, the delipidated protein did not change its conformation with the change in pH from high to low levels (Figure 2.7B). Thus, the delipidated ApolPBP1 is insensitive to change in pH.¹⁸ As mentioned earlier, the undelipidated ApolPBP1 at pH 6.5 is in ligand-bound conformation while at pH 4.5 in ligand-free conformation (Fig. 2.7A). In contrast, the delipidated protein remained in ligand-free conformations at all pH levels.

To investigate further, we titrated the delipidated ApolPBP1 at pH 4.5 to pH 6.5. Our data showed that, delipidated ApolPBP1 did not change its conformation, same as we observed earlier (Figure 2.8). Titration of delipidated ApolPBP1 in presence of excess ligand was also carried out from pH 6.5 to pH 4.5. The HSQC spectrum shows that, the protein at a pH above 6.0 has the ligand-bound conformation. Whereas between pH values of 5.0 and 6.0 it has the mixture of free and bound conformation, this particular observation supports the earlier report of conformational heterogeneity observed for the undelipidated ApolPBP1 at pH 5.2¹³ and undelipidated BmorPBP between pH 5.0 and 6.0.⁸ Below pH 5.0 the protein was in ligand-free conformation (Figure 2.9).

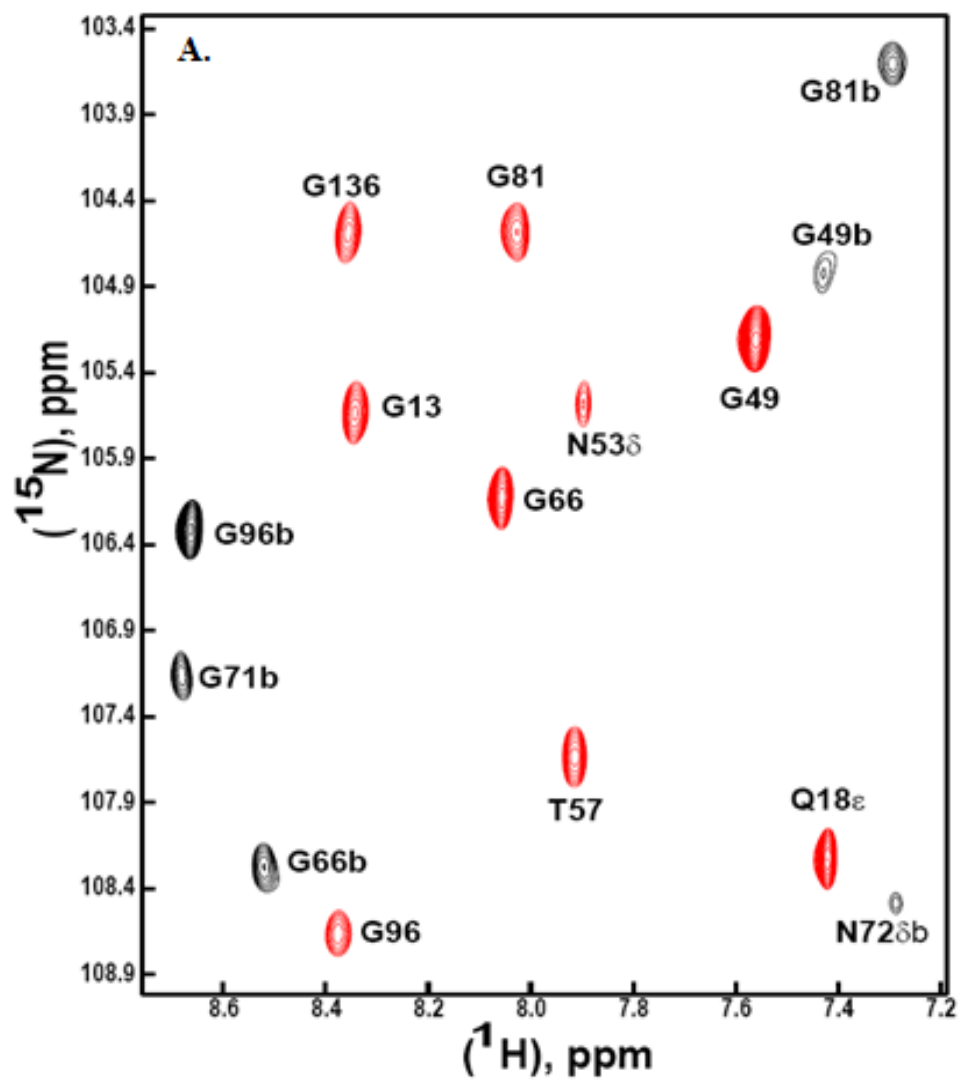


Figure 2.7 A. Expanded region of the two-dimensional $\{^1\text{H}, ^{15}\text{N}\}$ HSQC spectrum of undelipidated ApolPBP1. Resonances in black correspond to undelipidated protein at pH 6.5, which is the ligand bound conformation (labeled as b). Resonances in red correspond to undelipidated protein at pH 4.5, which belongs to ligand free conformation. From reference 18.

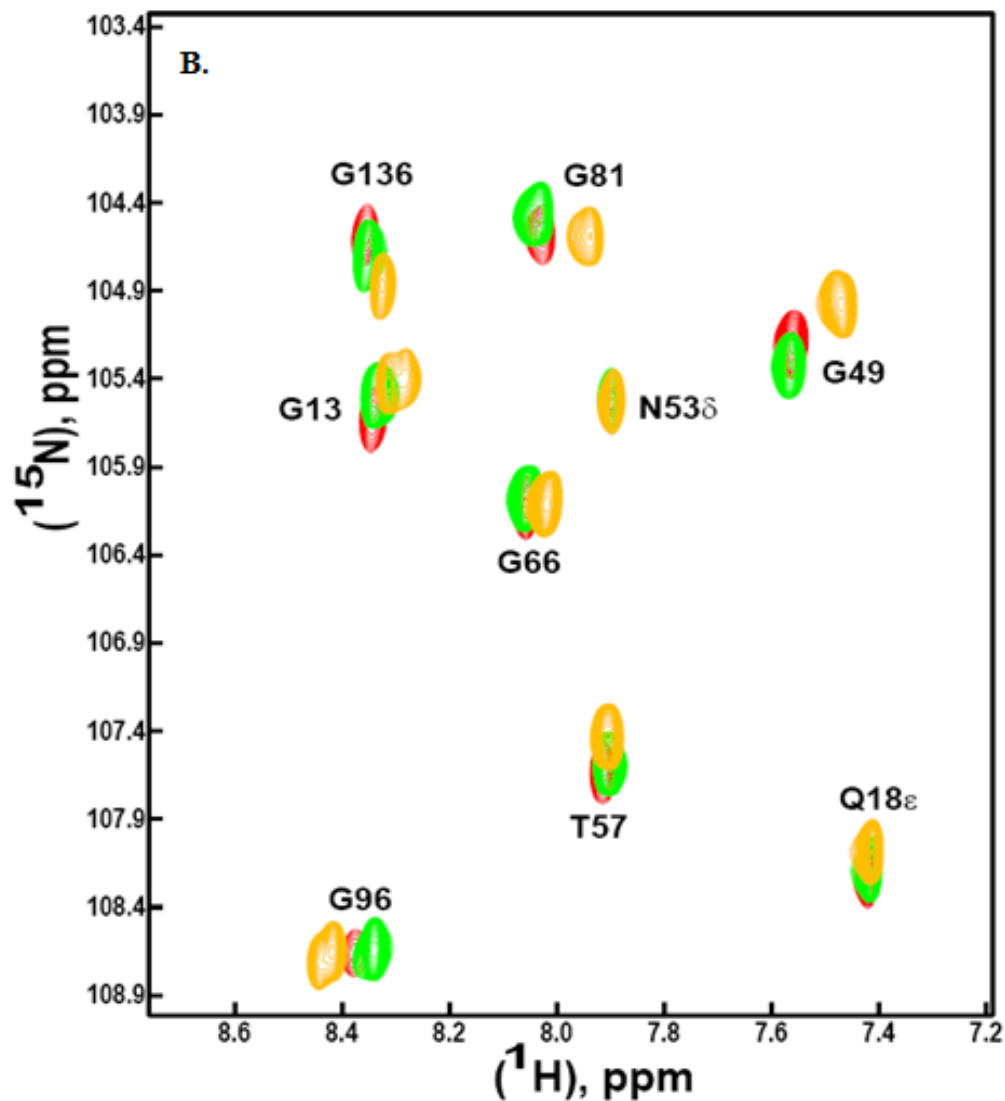


Figure 2.7 B. Expanded region of the two-dimensional $\{^1\text{H}, ^{15}\text{N}\}$ HSQC spectrum of delipidated ApolPPBP1 at pH 6.5 and 4.5, compared with undelipidated protein at pH 4.5. Resonances in yellow correspond to delipidated protein at pH 6.5, where resonances in green belong to delipidated protein at pH 4.5 and resonances in red belong to undelipidated protein at pH 4.5. All three sets showing the ligand free conformation of ApolPPBP1. From reference 18.

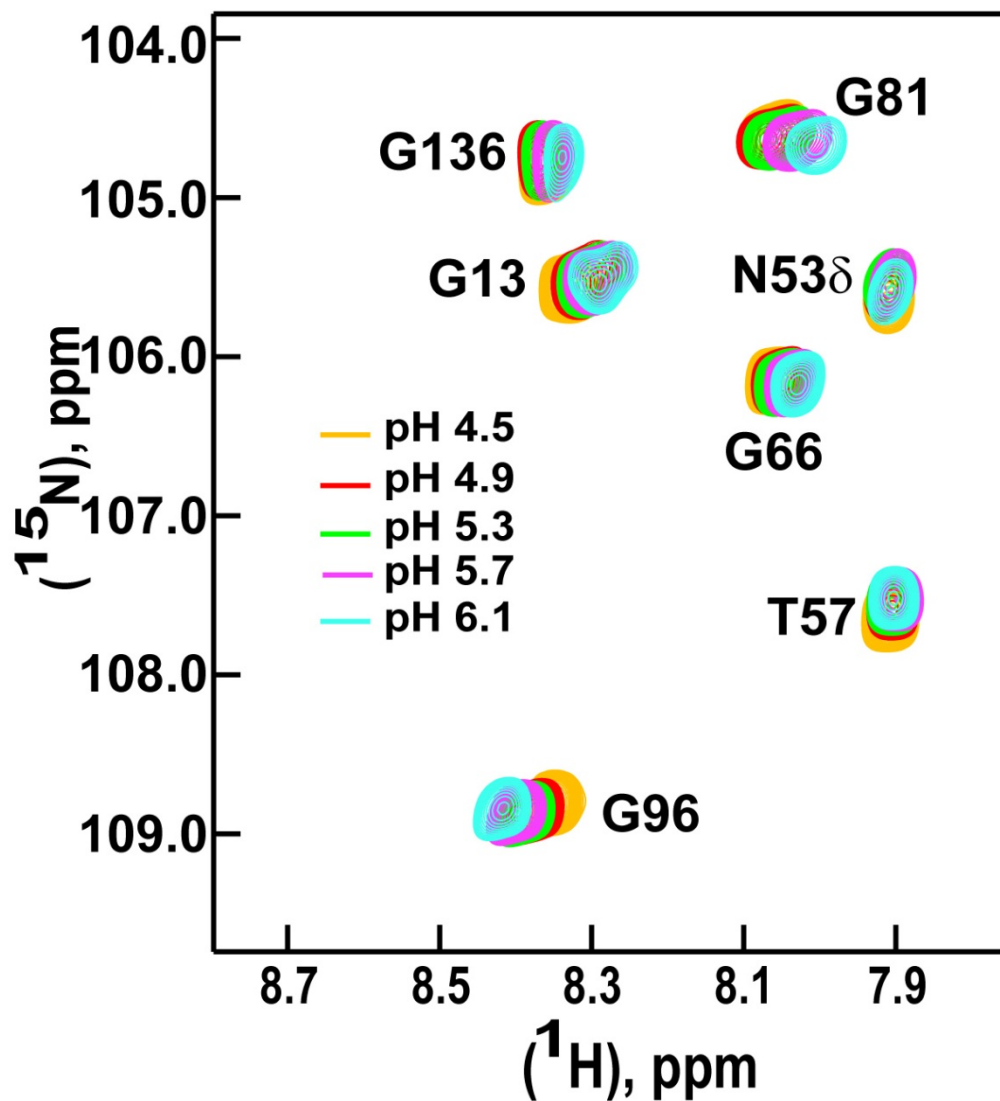


Figure 2.8 Expanded region of the two-dimensional $\{^1\text{H}, ^{15}\text{N}\}$ HSQC spectrum of pH titration of delipidated ApolPBP1 from pH 4.5 to pH 6.5. Resonances in different color correspond to different pH level as indicated. From reference 18.

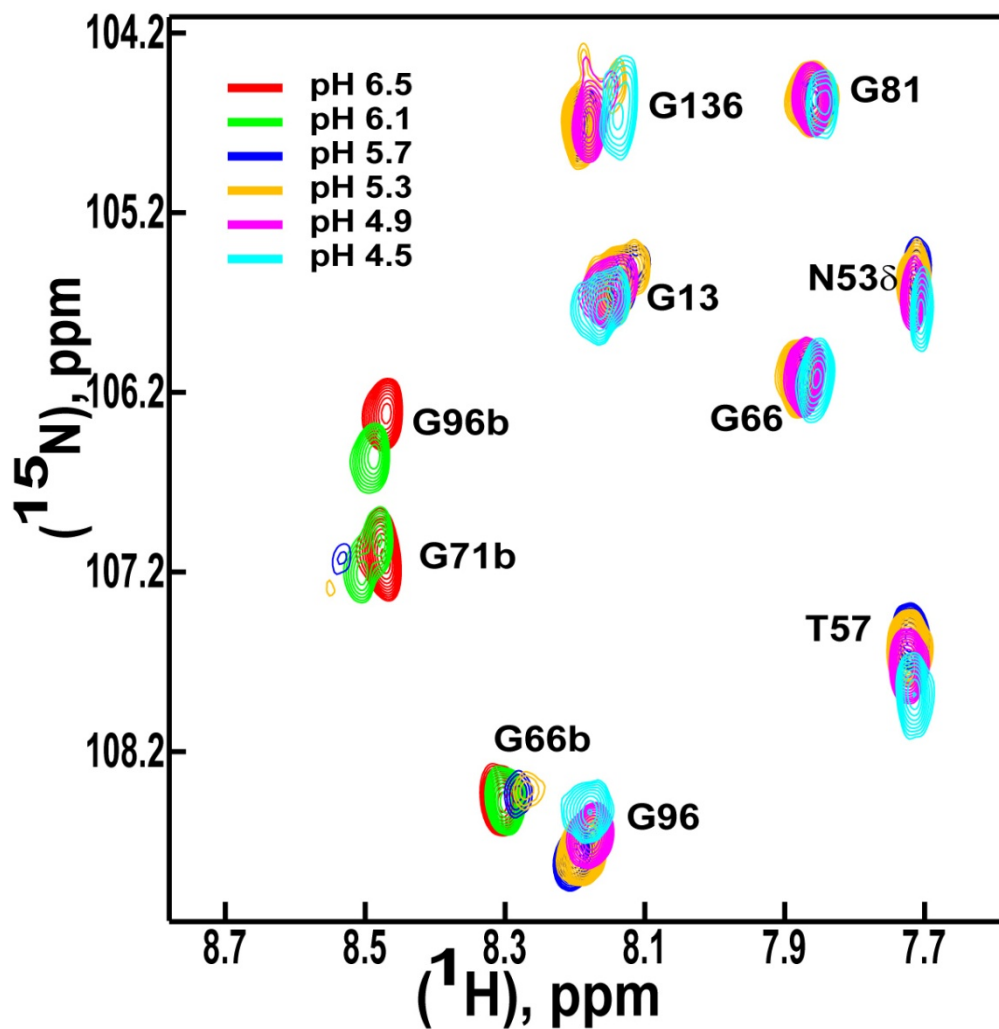


Figure 2.9 Expanded region of the two-dimensional $\{^1\text{H}, ^{15}\text{N}\}$ HSQC spectrum of pH titration of delipidated ApolPBP1 from pH 6.5 to 4.5, in presence of excess ligand (1:5 palmitic acid). Resonances in different color correspond to different pH level as indicated. From reference 18.

2.4 Discussion

We have made an important observation based on the HSQC spectrum of the undelipidated ApolPBP1 at pH 6.5 showing a single set of resonances that correspond to the ligand-bound conformation (Figure 2.6 A). Our data suggests that, for the undelipidated ApolPBP1 at pH 4.5, the major conformation is the ligand-free conformation although a few weak resonances belonging to the ligand-bound conformation (minor) are also observed at very low contour levels. Similarly, the HSQC spectrum of the delipidated ApolPBP1 at pH 4.5 shows a single set of resonances that correspond to the ligand-free conformation (Figure 2.6 B). Furthermore, at pH 6.5 the major conformation of the delipidated ApolPBP1 is the ligand-free conformation, although a few weak resonances correspond to the ligand-bound conformation (minor conformation) are observed at very low levels (Figure 2.6). These weak resonances indicate that a very small population of the ligand-bound conformation still exists even after the delipidation step is repeated several times. From this observation we can conclude that the equilibrium between two conformation shifts toward the ligand-bound conformation for the undelipidated ApolPBP1 at high pH. These observations demonstrate that the presence of a ligand favors the ligand-bound conformation and absence of a ligand favors the ligand-free conformation, respectively. Whereas high pH favors the ligand bound conformation and low pH favors the ligand free conformation (Figure 2.10).

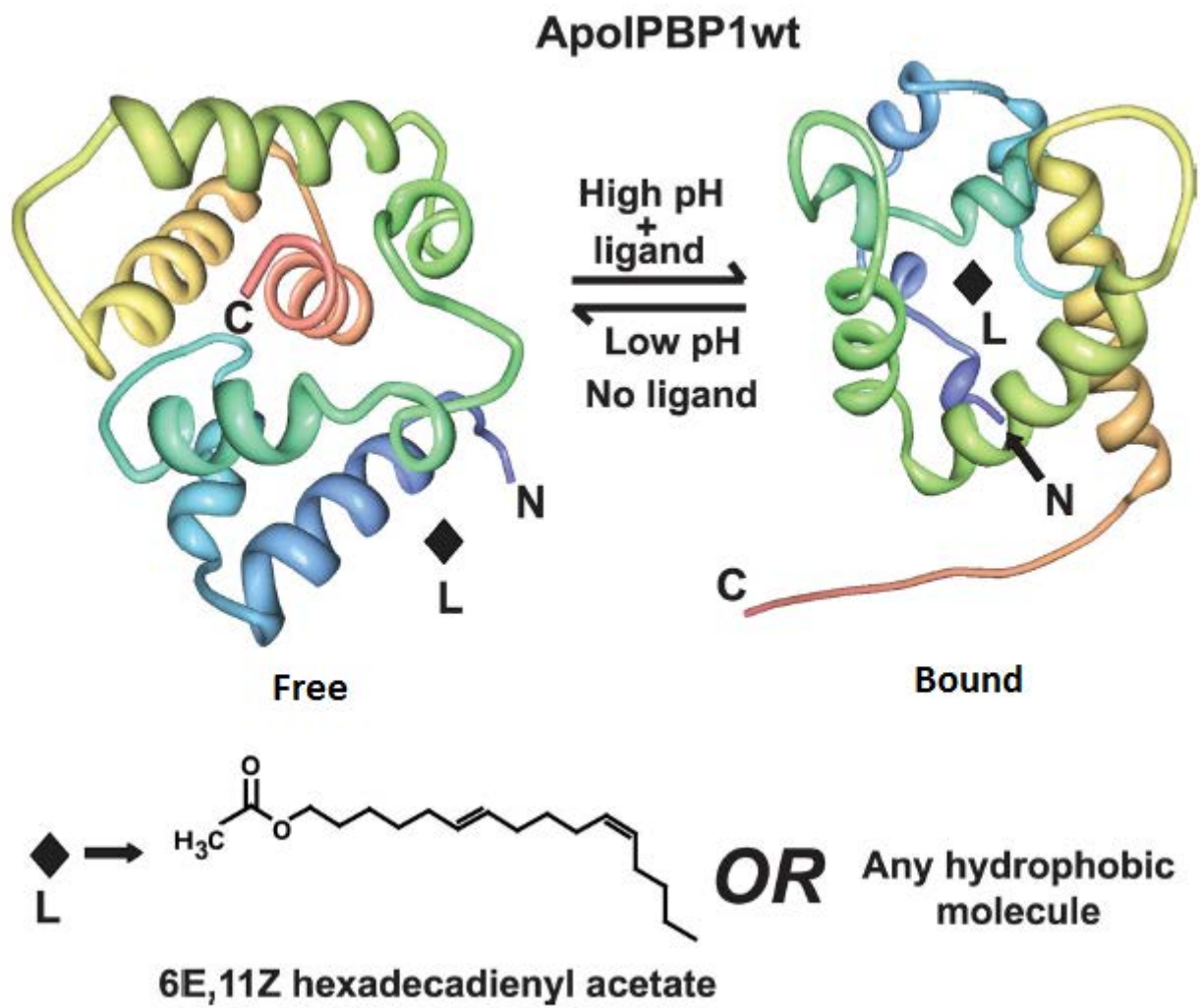


Figure 2.10 Pictorial representation of ApoIPBP1 with/ without the ligand and at high and low pH. From reference 18.

References:

- (1) Sato, K., Pellegrino, M., Nakagawa, T., Nakagawa, T., Vosshall, L. B., and Touhara, K. (2008) Insect olfactory receptors are heteromeric ligand-gated ion channels. *Nature* 452, 1002–1006.
- (2) Buck, L., and Axel, R. A (1991) novel multigene family may encode odorant receptors: amolecular basis for odor recognition. *Cell* 65, 175–187.
- (3) Wicher, D., Schäfer, R., Bauernfeind, R., Stensmyr, M. C., Heller, R., Heinemann, S. H., and Hansson, B. S. (2008) *Drosophila* odorant receptors are both ligand-gatedand cyclic-nucleotide-activated cation channels. *Nature* 452, 1007–1011.
- (4) Ronnett, G. V. and Moon, C. (2002) G proteins and olfactory signal transduction. *Annu. Rev. Physiol.* 64, 189–222.
- (5) Firestein, S. (2001). How the olfactory system makes sense of scents. *Nature* 413, 211–218.
- (6) Raming, K., Krieger, J., and Breer, H. (1989) Molecular cloning of an insect pheromone-binding protein. *FEBS Lett.* 256, 215–218.
- (7) Prestwich, G. D. (1993) Bacterial expression and photoaffinity labeling of a pheromone binding protein. *Protein Sci.* 2, 420–428.
- (8) Damberger, F., Nikonova, L., Horst, R., Peng, G., Leal, W. S., and Wüthrich, K. (2000) NMR characterization of a pH-dependent equilibrium between two folded solution conformations of the pheromone-binding protein from *Bombyx mori*. *Protein Sci.* 9, 1038–1041.
- (9) Wojtasek, H., and Leal, W. S. (1999) Conformational change in the Pheromone-binding Protein from *Bombyx mori* induced by pH and by interaction with membranes. *J. Biol. Chem.* 274, 30950–30956.

- (10) Horst, R., Damberger, F., Luginbuhl, P., Güntert, P., Peng, G., Nikonova, L., Leal, W. S., and Wüthrich, K. (2001) NMR structure reveals intramolecular regulation mechanism for pheromone binding and release. *Proc. Natl. Acad. Sci. U.S.A.* 98, 14374–14379.
- (11) Lee, D., Damberger, F. F., Peng, G., Horst, R., Güntert, P., Nikonova, L., Leal, W. S., and Wüthrich, K. (2002) NMR structure of the unliganded *Bombyx mori* pheromone-binding protein at physiological pH. *FEBS Lett.* 531, 314–318.
- (12) Mohanty, S., Zubkov, S., and Gronenborn, A. M. (2004) The Solution NMR Structure of *Antheraea polyphemus* PBP Provides New Insight into Pheromone Recognition by Pheromone-binding Proteins. *J. Mol. Biol.* 337, 443–451.
- (13) Zubkov, S., Gronenborn, A. M., Byeon, I. J., and Mohanty, S. (2005) Structural Consequences of the pH-induced Conformational Switch in *A. polyphemus* Pheromonebinding Protein: Mechanisms of Ligand Release. *J. Mol. Biol.* 354, 1081–1090.
- (14) Ring, J. R., Prusti, R. K., and Mohanty, S. (2008) Chemical communication: a visit with insects. *Curr. Chem. Biol.* 2, 83–96.
- (15) Damberger, F.F., Ishida, Y., Leal, W.S., and Wüthrich, K. (2007) Structural basis of ligand binding and release in insect pheromone-binding proteins: NMR structure of *Antheraea polyphemus* PBP1 at pH 4.5. *J.Mol.Biol.* 373, 811-819.
- (16) Lautenschlager, C., Leal, W. S., and Clardy, J. (2005) Coil-to-helix transition and ligand release of *Bombyx mori* pheromone-binding protein. *Biochem. Biophys. Res. Commun.* 335, 1044–1050.
- (17) Du, G., and Prestwich, G. D. (1995) Protein Structure Encodes the Ligand Binding Specificity in Pheromone Binding Proteins. *Biochemistry* 34, 8726–8732.

- (18) Katre, U. V., Mazumder, S., Prusti, R. K., and Mohanty, S. (2009) Ligand binding turns moth pheromone-binding protein into a pH sensor: Effect on the *Antheraea polyphemus* PBP1 conformation. *J. Biol. Chem.* 284, 32167–32177.
- (19) Bette, S., Breer, H., and Krieger, J. (2002) Probing a pheromone binding protein of the silkmoth *Antheraea polyphemus* by endogenous tryptophan fluorescence. *Insect Biochem. Mol. Biol.* 32, 241–246.
- (20) Mohanty, S., Zubkov, S., and Campos-Olivas, R. (2003) Letter to the Editor: ^1H , ^{13}C and ^{15}N backbone assignments of the pheromone binding protein from the silk moth *Antheraea polyphemus* (ApolPBP) *J. Biomol.NMR* 27, 393–394.
- (21) Delaglio, F., Grzesiek, S., Vuister, G. W., Zhu, G., Pfeifer, J., and Bax, A. (1995) NMRPipe: A multidimensional spectral processing system based on UNIX pipes. *J. Biomol. NMR* 6, 277–293.
- (22) Johnson, B. A., and Blevins, R. A. (1994) NMR View: A computer program for the visualization and analysis of NMR data. *J. Biomol. NMR* 4, 603–614.
- (23) Fielding, L. (2007) NMR methods for the determination of protein–ligand dissociation constants. *Prog. Nucl. Magn. Reson. Spectrosc.* 51, 219–242.

Chapter 3

Role of Histidine residues in ligand binding and Release

3.1 Introduction

Chemical communication is very important for most animals and especially for the survival of insects.¹⁻⁴ Male insects can detect the pheromone molecules released by the females of the same species with extreme sensitivity and specificity.^{4,5} Insect olfactory system, especially for moths and butterflies is one of the most studied systems in the field of chemical communication.⁶⁻⁸ In lepidopteran insects (moths), sex pheromones produced by females are detected by males and transported to the membrane-bound receptors (ion channels) across the aqueous sensillar lymph by the pheromone-binding proteins (PBPs).^{9,10} The previous studies on PBPs revealed that, insect PBPs bind, transport and release the pheromone molecules at olfactory receptors to initiate the neuronal response¹¹⁻¹⁶ or the PBP- pheromone complex may activate the pheromone-sensitive neurons and therefore can trigger the neuronal response.¹⁷⁻²⁰

Two molecular switches have been proposed to regulate the binding and release of the ligand from ApolPBP1. The first switch comprises of two histidine residues, His70 and His95 located at one end of the binding pocket of ApolPBP1. The second switch is the C-terminal tail situated at the opposite end of the binding pocket of ApolPBP1. The histidine switch is proposed to regulate entrance to the binding pocket through a pH dependent protonation and deprotonation mechanism.^{15,21,22} His-70 and His-95 shut the pocket at pH values above 6.0 and open it at pH values below 6.0. These two histidine residues are believed to play a very important role in the ligand release mechanism for ApolPBP1. It has been proposed that, at high pH (pH above 6.0), His-70 and His-95 are neutral in nature, leading them to shut down the end of the binding pocket

(distance between the two histidine residues is about 6.4 Å). This then helps to trap the ligand inside the binding pocket. Whereas at low pH (pH below 5.0), those two histidine residues are protonated, causing repulsion between them (at low pH the distance between the histidine residues becomes 12 Å). This phenomenon helps to open the histidine gate allowing the release of the trapped ligand from the binding pocket.

In the work presented here, we examined the above hypothesis that His-70 and His-95 regulate the closing and opening of the ApolPBP1 binding pocket at high and low pH respectively allowing the binding and releasing of the ligand.²³ To test this hypothesis, we mutated the histidine residues to alanine residues that have a neutral side chain at all pH levels. We expected that the histidine gate that is controlled by Ala-70 and Ala-95 in the ApolPBPH70A/H95A double mutant would remain shut at low pH since the alanine side chains are neutral. Consequently, the ligand would not be released even at low pH unlike the wild-type ApolPBP1. We carried out a detailed investigation of the effect of pH and ligand on the ApolPBPH70A/H95A using solution NMR and fluorescence spectroscopy.²³

3.2 Materials and Methods

3.2.1 Cloning and Overexpression

The ApolPBP1H70A/H95A gene was constructed from the ApolPBP1-pET-21a vector by site directed mutagenesis using the QuickChange site-directed mutagenesis kit from Stratagene. This work was done with the help of Dr. Uma Katre. The plasmid construct (ApolPBP1H70A/H95A-pET21a) was then transformed into the *E. coli* Origami cell line and expressed and purified as described in the previous chapter.

3.2.2 Delipidation, Mass spectrometry and NMR measurement

The mass of the ApolPBP1H70A/H95A was determined at the Mass Spectrometry Facility, at the Department of Chemistry and Biochemistry, Auburn University. The mass of the delipidated ApolPBP1H70A/H95A was analyzed by electrospray ionization-mass spectrometry on a Q-ToF PremierTM (Waters) mass spectrometer.

Delipidation of ApolPBP1H70A/H95A was done as described mentioned in the chapter 2 (section 2.2.3).

NMR data of delipidated and undelipidated ApolPBP1H70A/H95A were collected at 35 °C on a Bruker Avance 600-MHz spectrometer at the Department of Chemistry and Biochemistry, Auburn University. pH titrations were carried out on uniformly ¹⁵N labeled proteins in 50 mM sodium phosphate buffer, pH 6.5 or pH 4.5, 1 mM EDTA, 0.01% NaN₃, and 5% D₂O (used as a lock solvent) in a Shigemi tube. Two-dimensional {¹H, ¹⁵N} HSQC spectra were collected for ¹⁵N labeled undelipidated samples at pH 4.5 and 6.5. For ligand titration experiments, uniformly ¹⁵N-labeled delipidated ApolPBP1H70A/H95A (310 μl of 220 μM in 50mM phosphate buffer, pH 6.5, containing 5% D₂O, 1 mM EDTA, and 0.01% (w/v) NaN₃) was titrated with increasing concentrations of palmitic acid (0–2.2 mM), and the corresponding two-

dimensional $\{^1\text{H}, ^{15}\text{N}\}$ HSQC spectra were recorded. All data were processed using NMRPipe²⁴ and analyzed using NMRView.²⁵ All the peaks were assigned using the assignment published previously.²⁶

3.2.3 AMA binding studies by Fluorescence

The binding of AMA (1-aminoanthracene) to the ApolPBP1wt and ApolPBP1H70A/H95A at pH 6.5 and 4.5 was studied by monitoring the increase in the AMA fluorescence at 480 nm. The fluorescence spectra were recorded at the excitation wavelength of 256 nm, and emission of 400–600 nm. AMA in aqueous environments displays a weak fluorescence after excitation at 256 or 298 nm with a λ_{max} of 563 nm. The fluorescence of AMA is considerably enhanced in a hydrophobic environment like the binding cavity of PBPs with a blue shift in the λ_{max} . All the data were normalized (F_c) (y-axis) and plotted against the AMA concentration (x-axis). Then the k_D value was determined using the single site binding equation from Origin6.1-

$$y = B x / (k + x)$$

Where, B = Maximum fluorescence intensity

k = Dissociation constant

x = Ligand concentration

y = Fluorescence intensity (F_c) at specific ligand concentration

3.3 Results and Discussion

3.3.1 Expressed and purified protein

Unlabeled as well as ^{15}N -labeled protein was expressed and purified as mentioned above. The mass-spec analysis showed the purity of the protein (Figure 3.1). A single peak of ApolPBP1H70A/H95A at 15,776 Da indicates the presence of the pure double mutant protein as expected (the mass of the protein we got matched with the theoretical mass).

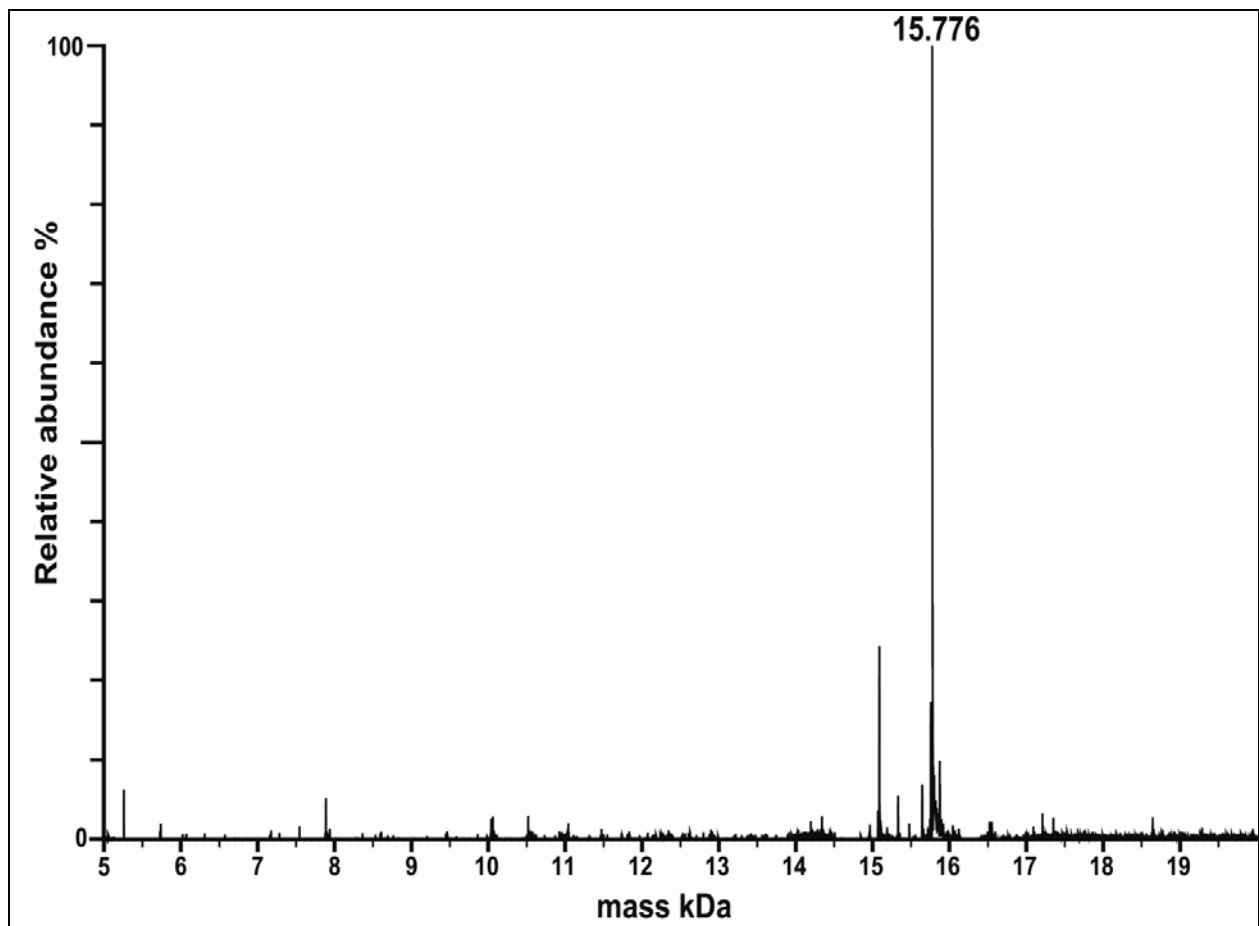


Figure 3.1 Mass spec analysis of pure and delipidated ^{15}N -labeled ApoIPBP1H70A/H95A. A sharp peak at 15,776 da indicates the presence of pure protein. From reference 23.

3.3.2 Effect of Histidine mutation

To investigate the proposed role of histidines in the pH-induced conformational switch, His-70 and His-95, located at one end of the binding pocket, were mutated to alanine. The HSQC spectrum of the undelipidated ApolPBP1H70A/H95A at pH 6.5 (Figure 3.2A) largely resembled that of the wild type protein, which is in the ligand bound conformation. However, at pH 4.5 it remained in the ligand bound conformation (Figure 3.2B) as well rather than switching to the ligand free conformation as observed in the wild type protein. The spectrum displayed some changes due to the difference in pH (Figure 3.3).

To further verify the fact that, the double mutant does not release the ligand at low pH, we carried out NMR titration studies of the delipidated ApolPBP1H70A/H95A at pH 4.5 with palmitic acid as the ligand. The delipidated ApolPBP1H70A/H95A double mutant switched from free conformation to the ligand-bound conformation upon binding to the ligand (Figure 3.4). This is data verified the fact that the ApolPBP1H70A/H95A double mutant is able to bind the ligand even at low pH since the alanine gate is shut preventing the release of the ligand. The binding affinity at pH 4.5 however was relatively lower than that at pH 6.5. We also observed that the complete conversion of the ligand free conformation to the ligand bound conformation occurred at a protein: ligand ratio of 1:3. With the above results, we successfully verified our hypothesis that His-70 and His-95 are responsible for the pH-induced conformational switch of the ligand-bound conformation of ApolPBP1 to the ligand free conformation at low pH, which is likely the mechanism of ligand release near the membrane-bound receptors.

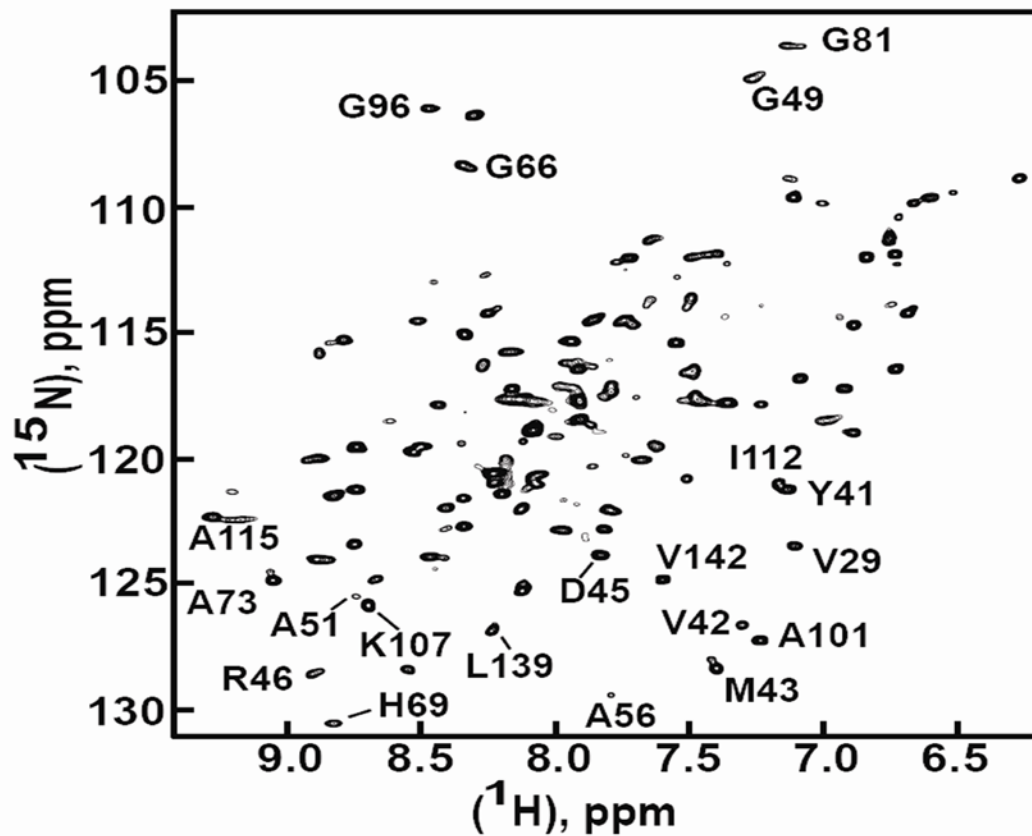


Figure 3.2 A. Two-dimensional $\{^1\text{H}, ^{15}\text{N}\}$ HSQC spectra of undelipidated ApolPBP1H70A/H95A in 50 mM sodium phosphate buffer at pH 6.5 containing 5% D_2O , 1M EDTA, and 0.01% sodium azide. The protein shown to have the ligand-bound conformation. From reference 23.

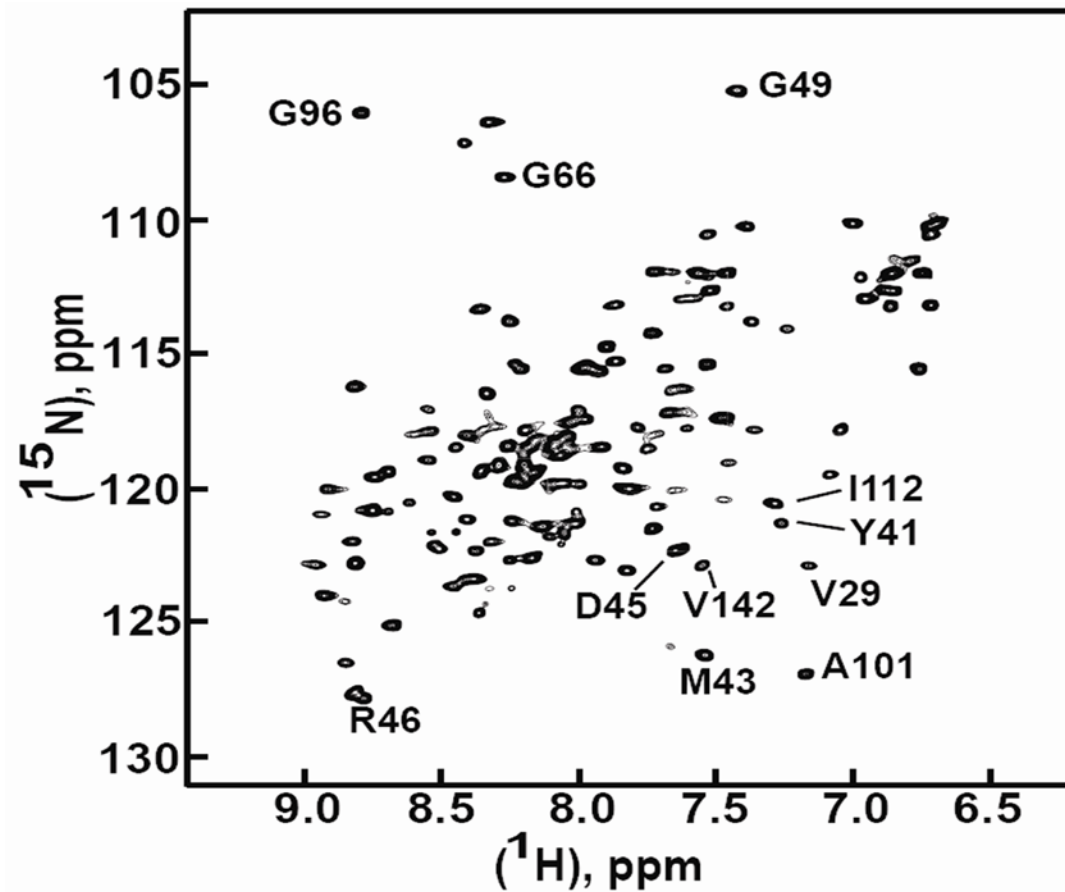


Figure 3.2 B. Two-dimensional $\{^1\text{H}, ^{15}\text{N}\}$ HSQC spectra of undelipidated ApolPBP1H70A/H95A in 50 mM sodium phosphate buffer at pH 4.5 containing 5% D_2O , 1M EDTA, and 0.01% sodium azide. The protein also shown to retain the ligand-bound conformation. From reference 23.

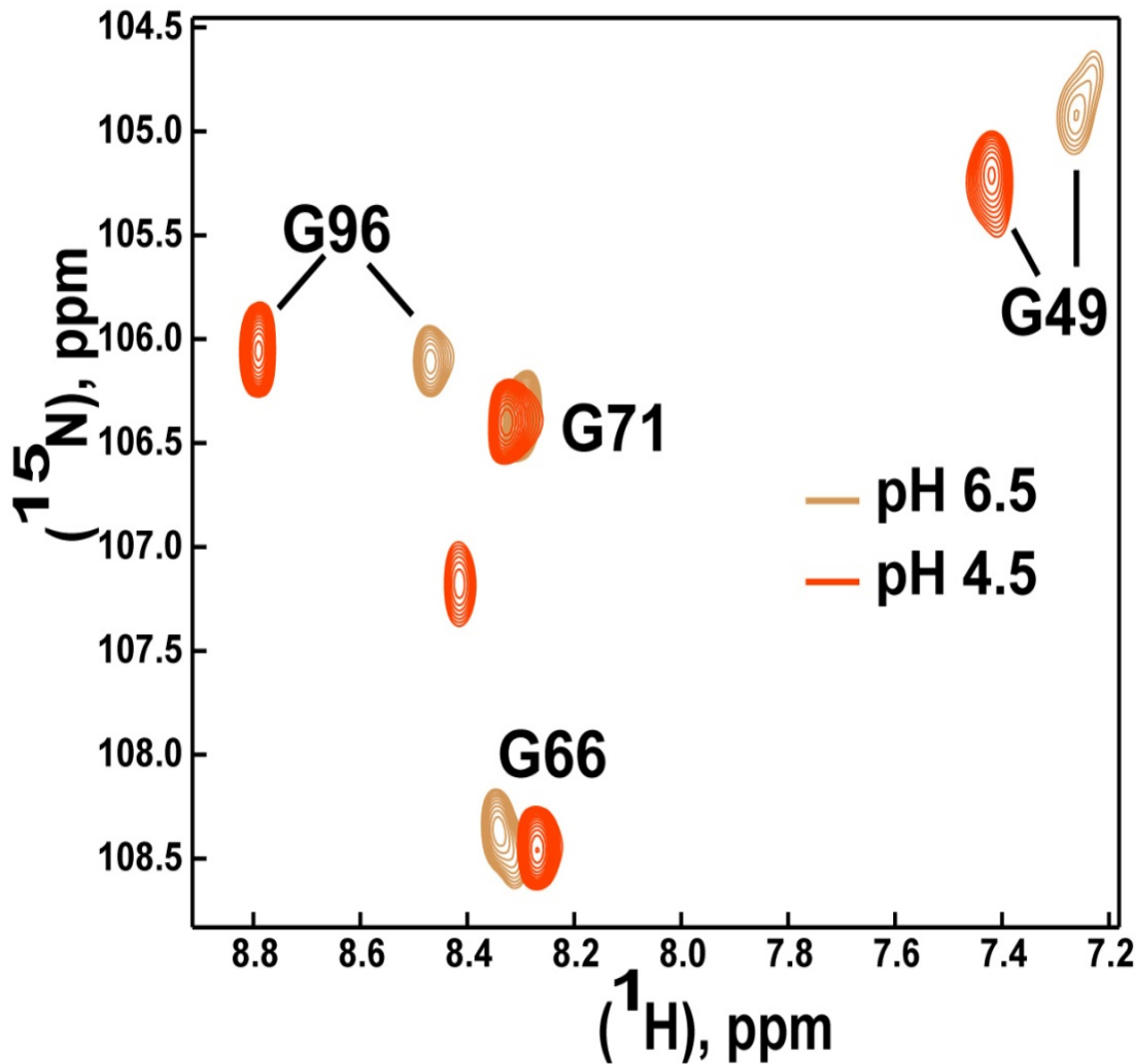


Figure 3.3 Extended portion from the overlap of two-dimensional $\{^1\text{H}, ^{15}\text{N}\}$ HSQC spectra of undelipidated ApoIPBP1H70A/H95A in 50 mM sodium phosphate buffer at pH 6.5 (grey color) and at pH 4.5 (orange color). Both the spectra is showing ligand-bound conformation. From reference 23.

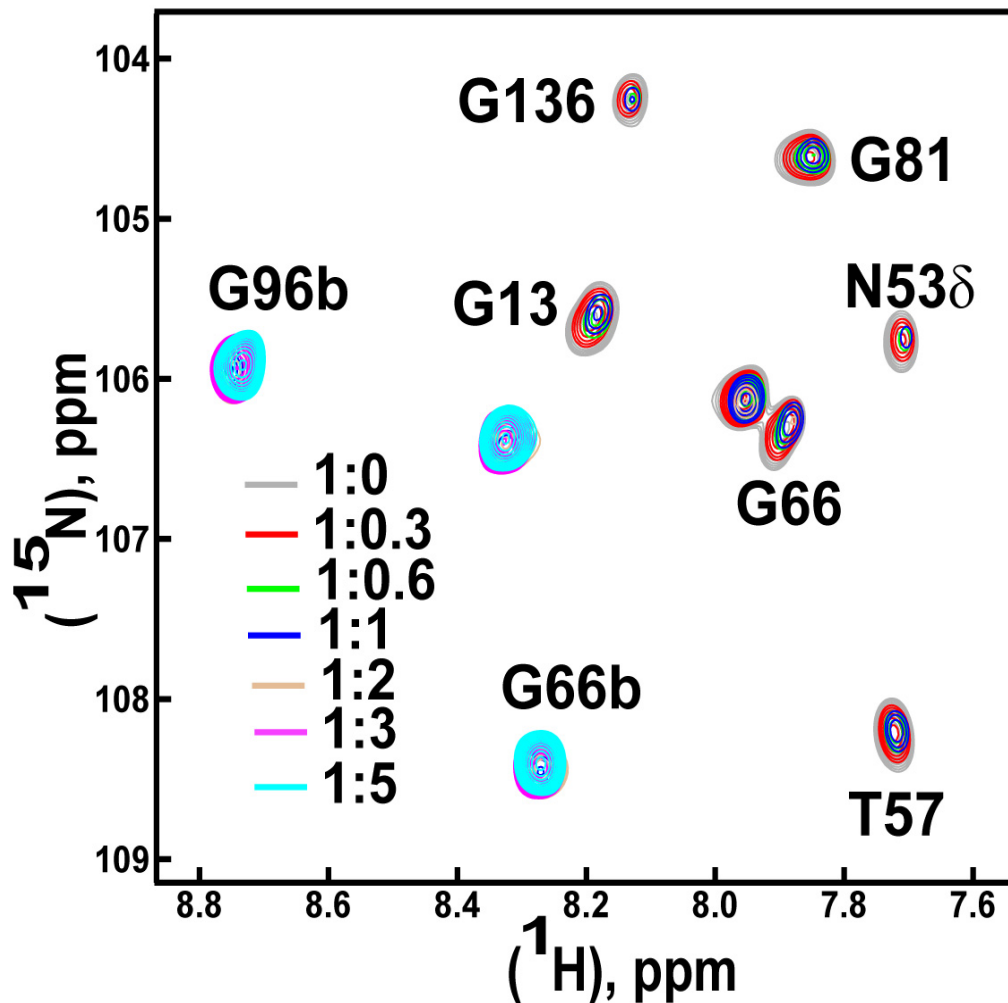


Figure 3.4 Extended region of the $\{^1\text{H}, ^{15}\text{N}\}$ HSQC spectra of delipidated ApolPBP1H70A/H95A in 50 mM sodium phosphate buffer, pH 4.5, titrated with palmitic acid, showing the disappearance of peaks corresponding to the ligand free conformation and appearance of those peaks corresponding to the ligand bound conformation labeled as b. Protein:ligand ratios are indicated on the figure with corresponding colors. From reference 23.

3.3.3 AMA Binding Studies by Fluorescence

AMA in aqueous environments displays a weak fluorescence after excitation at 256 or 298 nm with a maximum intensity (λ_{max}) of 563 nm. The fluorescence of AMA is considerably enhanced in a hydrophobic environment, similarly like the binding cavity of PBPs with a blue shift in the λ_{max} . Titration of both the undelipidated and the delipidated ApolPBP1wt as well as ApolPBP1H70A/H95A with AMA at pH 6.5 and 4.5 revealed that AMA did not bind to the wild type protein at pH 4.5. On the contrary, AMA was able to bind to ApolPBP1H70A/H95A even at pH 4.5. However, the maximum fluorescence intensity reached at saturation was about half of what it was at pH 6.5 (Figure 3.5). The delipidation also had an effect on the maximum fluorescence intensity reached at saturation; the delipidated proteins had higher intensity than their undelipidated counterparts at both pH levels (Figure 3.5). The dissociation constants (K_d) for both proteins in different conditions are listed in Table 3.1. In general, the delipidated proteins had higher affinities than their undelipidated counterparts, and the double mutant proteins had lower affinities at pH 4.5 than at pH 6.5.

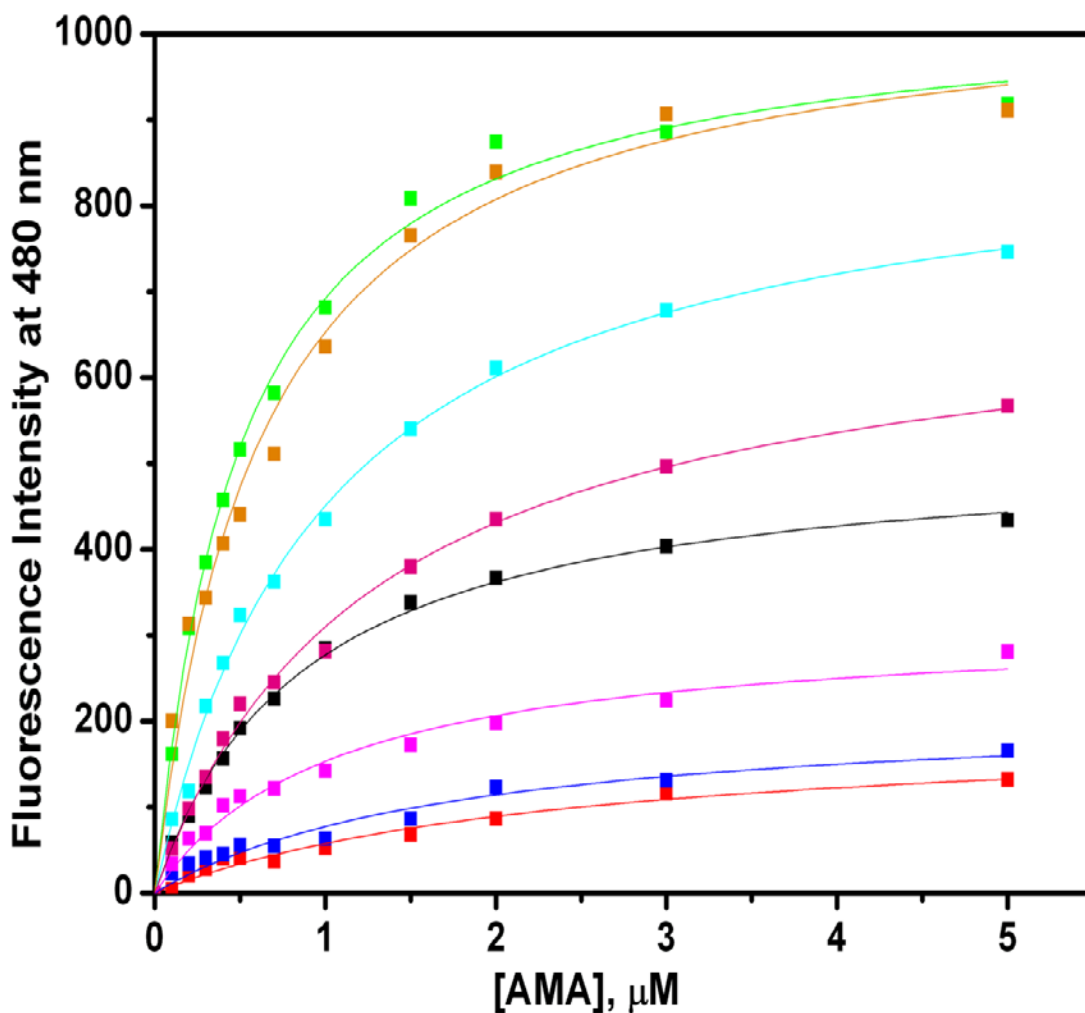


Figure 3.5 Fluorescence intensities of different ApolPBP1 proteins upon addition of AMA, measured at 480 nm. Red, Undelipidated ApolPBP1wt, pH 4.5; Blue, delipidated ApolPBP1wt, pH 4.5; Magenta, Undelipidated ApolPBP1H70AH95A, pH 4.5; Black, delipidated ApolPBP1H70AH95A, pH 4.5; Pink, Undelipidated ApolPBP1wt, pH 6.5; Cyan, Undelipidated ApolPBP1H70AH95A, pH 6.5; Orange, delipidated ApolPBP1wt, pH 6.5; Green, delipidated ApolPBP1H70AH95A, pH 6.5. From reference 23.

Protein	$K_{[AMA]}$ (nM)
Undelipidated ApolPBP1wt, pH 6.5	880 ± 100
Delipidated ApolPBP1wt, pH 6.5	500 ± 30
Undelipidated ApolPBP1H70AH95A, pH 6.5	990 ± 70
Undelipidated ApolPBP1H70AH95A, pH 4.5	1060 ± 220
Delipidated ApolPBP1H70AH95A, pH 6.5	620 ± 30
Delipidated ApolPBP1H70AH95A, pH 4.5	1290 ± 130

Table 3.1: Dissociation constants ($K_{[AMA]}$) for the binding of AMA to different ApolPBP1 samples, determined using the increase in AMA fluorescence at 480 nm. From reference 23.

3.4 Conclusions:

Our data confirm the role of His-70 and His-95 in the ligand release driven by the pH-induced conformational switch. At pH values above 6.0, the His-70 and the His-95 side chains do not carry any charge consequently the distance measured between them is 6.4 Å (Figure 3.6). But at low pH, when the His-70 and the His-95 are protonated, the distance between them is increased to 12.6 Å (Figure 3.7), opening the binding pocket for the ligand release. When the Histidine gate is permanently shut through double mutation to alanines, the ligand is unable to escape at low pH in the ApolPBP1H70A/H95A double mutant. We have shown that mutation of these two histidines to alanines keeps the protein in the ligand bound conformation (Figure 3.8) at all pH levels. Thus, the mutated protein (ApolPBP1H70A/H95A) can bind ligand even at low pH.

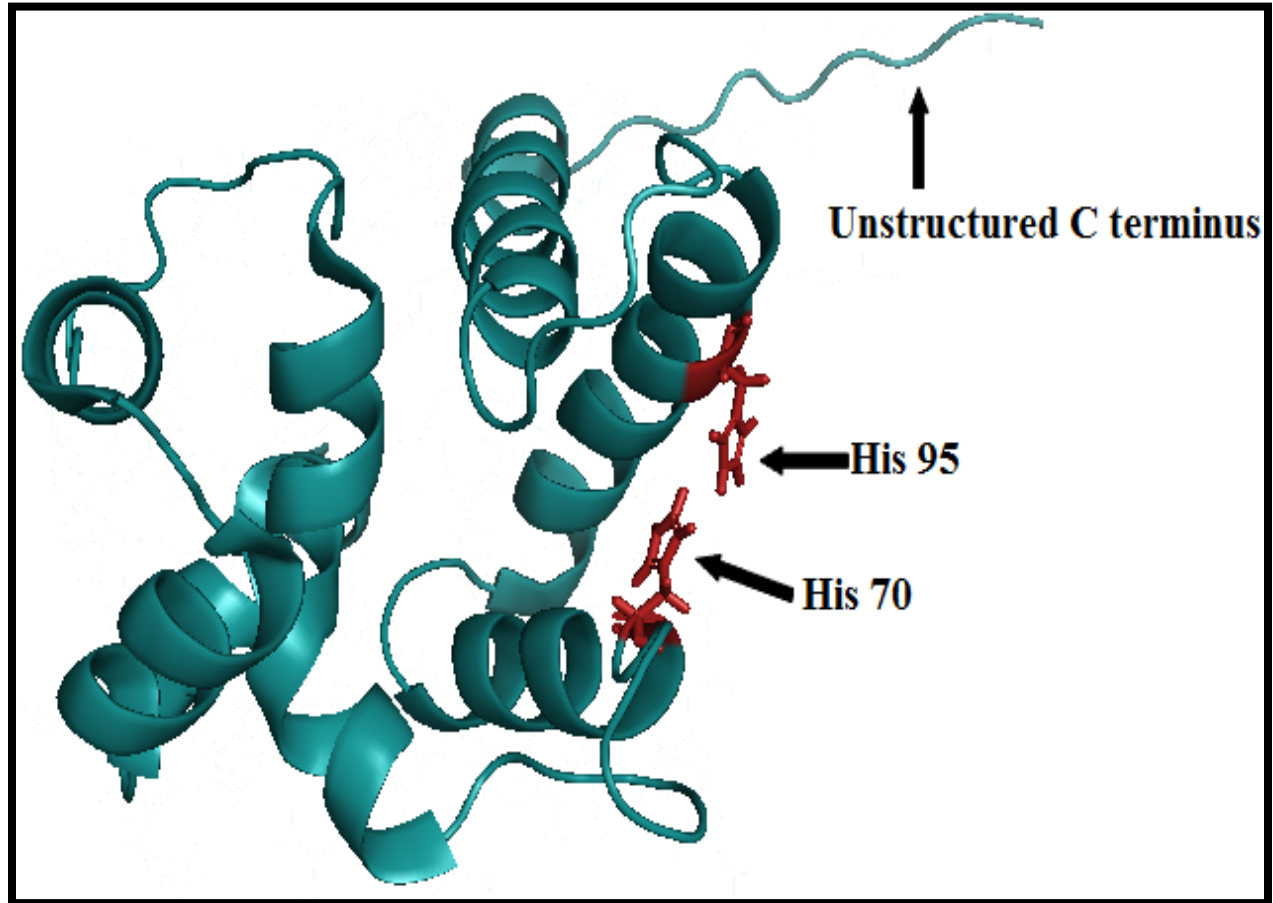


Figure 3.6 ApolPBP1 at pH 6.3, showing His-70 and His-95 at one end of the binding pocket.

Distance between the residues is 6.4 Å. From reference 23.

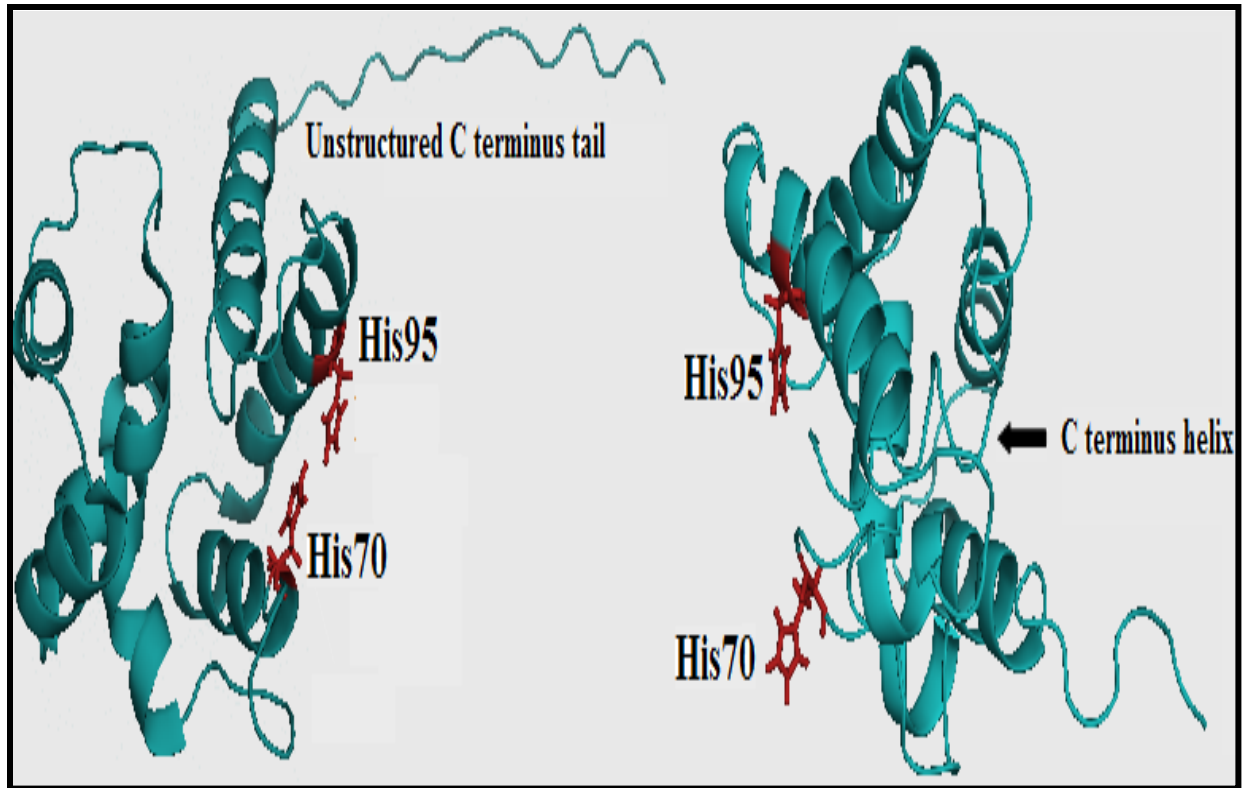


Figure 3.7 Left hand side: ApolPBP1 at pH 6.3, showing the distance between the His70 and His95 residues are very close to each other. Right hand side: ApolPBP1 at pH 4.5, showing the distance between His70 and His95 has increased.

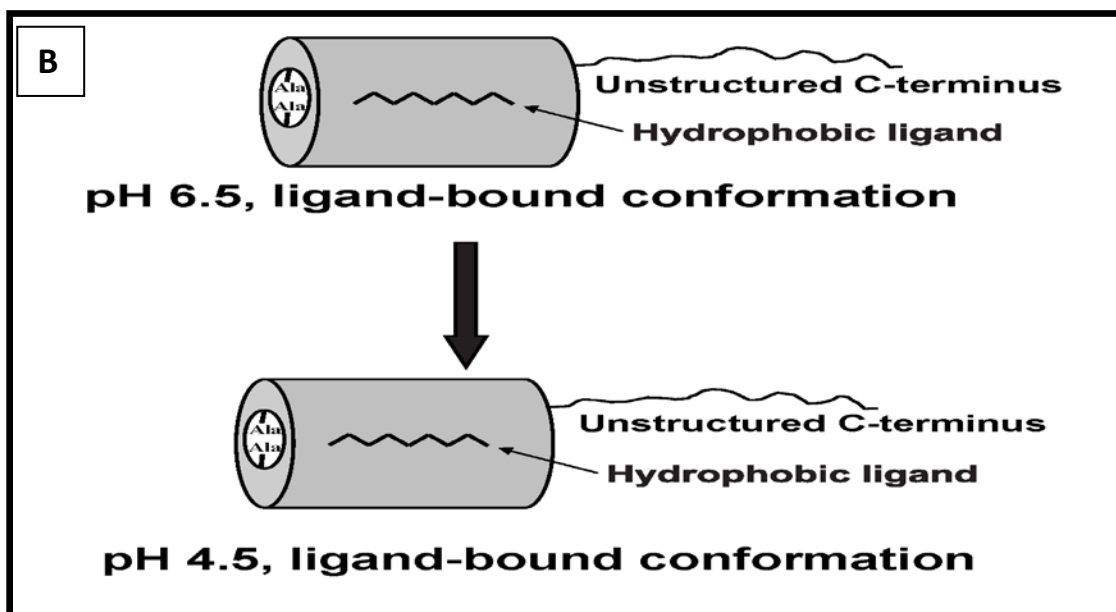
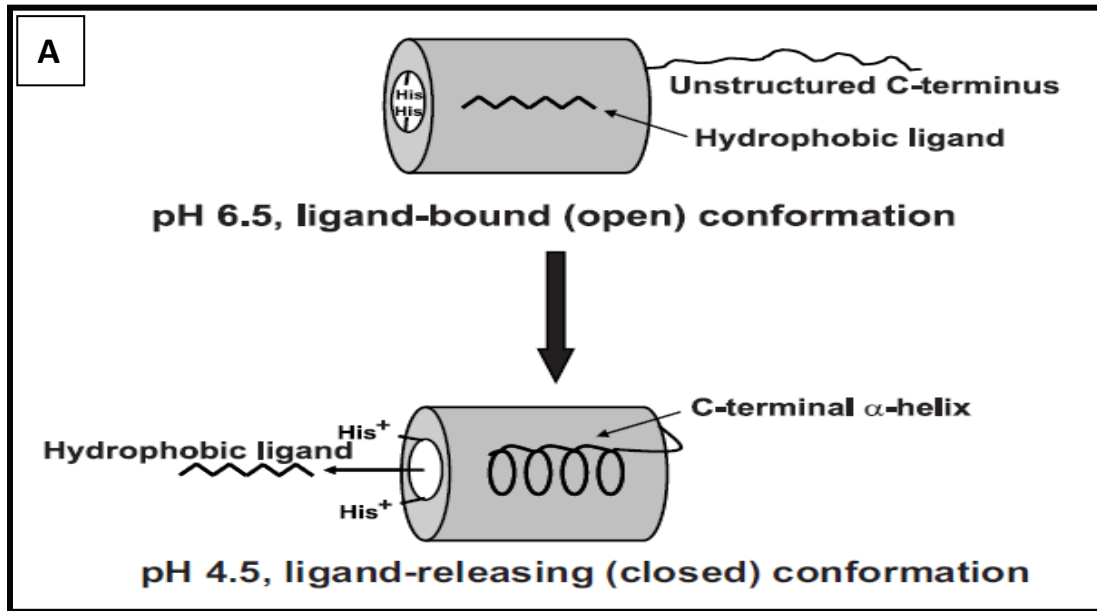


Figure 3.8 A. ApolPBP1 wild-type protein, at pH 6.5 shows the ligand-bound conformation while at low pH shows the ligand-release conformation. B. ApolPBP1H70A/H95A, at pH 6.5 and 4.5 shows the ligand-bound conformation only.

References:

- (1) Hildebrand, J. G. and Shepherd, G. M. (1997) Mechanisms of olfactory discrimination: converging evidence for common principles across phyla. *Annu. Rev. Neurosci.* 20, 595–631.
- (2) Buck, L. and Axel, R. (1991) A novel multigene family may encode odorant receptor: A molecular basis for odor recognition. *Cell* 65, 175–187.
- (3) Krieger, J. and Breer, H. (1999) Olfactory reception in invertebrates. *Science* 286, 720–723.
- (4) Agosta, W.C. (1992) Chemical Communication: The Language of Pheromones. *Scientific American Library*, New York.
- (5) Roelofs, W. L. (1995) Chemistry of sex attraction. *Proc. Natl Acad. Sci. U.S.A.* 92, 44–497.
- (6) Pelosi, P. and Maida, R. (1995) Odorant-binding proteins in insects. *Comp. Biochem. Physiol. B* 111, 503–514.
- (7) Hansson, B.S. (1995) Olfaction in lepidoptera. *Experientia* 51, 1003–1027.
- (8) Schneider, D. (1992) 100 years of pheromone research: an essay on lepidoptera. *Naturwissenschaften* 79, 241–250.
- (9) Sato, K., Pellegrino, M., Nakagawa, T., Nakagawa, T., Vosshall, L. B., and Touhara, K. (2008) Insect olfactory receptors are heteromeric ligand-gated ion channels. *Nature* 452, 1002–1006.
- (10) Wicher, D., Schäfer, R., Bauernfeind, R., Stensmyr, M. C., Heller, R., Heinemann, S. H., and Hansson, B. S. (2008) *Drosophila* odorant receptors are both ligand-gated and cyclic-nucleotide-activated cation channels. *Nature* 452, 1007–1011.

- (11) Damberger, F., Nikonova, L., Horst, R., Peng, G., Leal, W. S., and Wüthrich, K. (2000) NMR characterization of a pH-dependent equilibrium between two folded solution conformations of the pheromone-binding protein from *Bombyx mori*. *Protein Sci.* 9, 1038–1041.
- (12) Horst, R., Damberger, F., Luginbühl, P., Güntert, P., Peng, G., Nikonova, L., Leal, W. S., and Wüthrich, K. (2001) NMR structure reveals intramolecular regulation mechanism for pheromone binding and release. *Proc. Natl. Acad. Sci. U.S.A.* 98, 14374–14379.
- (13) Lee, D., Damberger, F. F., Peng, G., Horst, R., Güntert, P., Nikonova, L., Leal, W. S., and Wüthrich, K. (2002) NMR structure of the unliganded *Bombyx mori* pheromone-binding protein at physiological pH. *FEBS Lett.* 531, 314–318.
- (14) Mohanty, S., Zubkov, S., and Gronenborn, A. M. (2004) The solution NMR structure of *Antheraea polyphemus* PBP provides new insight into pheromone recognition by pheromone-binding proteins. *J. Mol. Biol.* 337, 443–451.
- (15) Zubkov, S., Gronenborn, A. M., Byeon, I.-J. L., and Mohanty, S. (2005) Structural consequences of the pH-induced conformational switch in *A. polyphemus* pheromone-binding protein: Mechanisms of ligand release. *J. Mol. Biol.* 354, 1081–1090.
- (16) Wojtasek, H., and Leal, W. S. (1999) Conformational change in the pheromone-binding protein from *Bombyx mori* induced by pH and by interaction with membranes. *J. Biol. Chem.* 274, 30950–30956.
- (17) Kowcun, A., Honson, N., and Plettner, E. (2001) Olfaction in the gypsy moth, *Lymantria dispar*: Effect of pH, ionic strength, and reductants on pheromone transport by pheromone-binding proteins. *J. Biol. Chem.* 276, 44770–44776.

- (18) Laughlin, J. D., Ha, T. S., Jones, D. N. M., and Smith, D. P. (2008) Activation of pheromone-sensitive neurons is mediated by conformational activation of pheromone-binding protein. *Cell* 133, 1255–1265.
- (19) Kaissling, K. E. (2001) Olfactory perireceptor and receptor events in moths: A kinetic model. *Chem. Senses* 26, 125–150.
- (20) Kaissling, K. E. (2009) Olfactory perireceptor and receptor events in moths: A kinetic model revised. *J. Comp. Physiol., A* 195, 895–922.
- (21) Xu, W., and Leal, W. S. (2008) Molecular switches for pheromone release from a moth pheromone-binding protein. *Biochem. Biophys. Res. Commun.* 372, 559–564.
- (22) Sandler, B. H., Nikonova, L., Leal, W. S., and Clardy, J. (2000) Sexual attraction in the silkworm moth: Structure of the pheromone binding- protein-bombykol complex. *Chem. Biol.* 7, 143–151.
- (23) Katre, U. V., Mazumder, S., Prusti, R. K., and Mohanty, S. (2009) Ligand binding turns moth pheromone-binding protein into a pH sensor: Effect on the *Antheraea polyphemus* PBP1 conformation. *J. Biol. Chem.* 284, 32167–32177.
- (24) Delaglio, F., Grzesiek, S., Vuister, G. W., Zhu, G., Pfeifer, J., and Bax, A. (1995) NMRPipe: A multidimensional spectral processing system based on UNIX pipes. *J. Biomol. NMR* 6, 277–293.
- (25) Johnson, B. A., and Blevins, R. A. (1994) NMR View: A computer program for the visualization and analysis of NMR data. *J. Biomol. NMR* 4, 603–614.

(26) Mohanty, S., Zubkov, S., and Campos-Olivas, R. (2003) Letter to the Editor: ^1H , ^{13}C and ^{15}N backbone assignments of the pheromone binding protein from the silk moth *Antheraea polyphemus* (ApolPBP) *J. Biomol.NMR* 27, 393–394.

Chapter 4

Role of the C-terminus in ligand binding and/or releasing

4.1 Introduction

Two molecular switches have been proposed to play a role in the ligand-release mechanism of moth PBPs: the first one is the pH driven protonation and deprotonation of His-70 and His-95 situated at one end of the binding pocket.¹⁻³ The second one is the switch of the unstructured C-terminus to a helix at low pH that enters the binding pocket from the opposite end of the pocket as the ligand is released through the Histidine gate.³⁻⁵ We have demonstrated the role of the two histidine residues (His-70 and His-95) in the ligand release mechanism of ApolPBP1 in chapter-3.⁶ At low pH, the repulsion between the two charged histidines opens the gate to unload the ligand.⁶ When these two histidines were mutated to alanines, the ApolPBP1H70A/H95A double mutant remained in ligand-bound conformation at all pH levels as the alanines permanently shut the gate prohibiting ligand release. Thus, the neutral forms of His-70 and His-95 shut the gate at high pH to facilitate ligand binding while the repulsion between the charged histidines opens the gate at low pH allowing ligand release. Clearly the entry and exit of a ligand is controlled by the histidine gate at one end of the binding pocket.

In this chapter, I present our investigation on the second molecular switch: the C-terminal tail of the ApolPBP1. We address here the role of the C-terminal tail or whether this C-terminal is tail absolutely necessary for pheromone unloading at the receptor site. The questions that we wanted to address is whether the ligand escapes on its own when the histidine gate opens at low pH or whether the C-terminal helix play any role in the ligand release. As we have shown in

chapter-2, the ligand free ApolPBP1 is in the closed conformation at all pH levels, where the C-terminus is internalized inside the binding pocket as the 7th helix.⁶ In BmorPBP, the C-terminus has been reported to be essential for preventing ligand-binding at low pH. The protein without the C-terminus was able to bind the ligand with same affinities at both acidic and neutral pHs as that of the wild type protein at physiological pH.⁵ Similar results have been reported for navel orangeworm moth *Amyelois transitella* PBP (AtraPBP).⁷ However, LdisPBP2 from the gypsy moth *Lymantria dispar* was found to have ~ 10X reduced affinity towards ligand after truncation of the C-terminal tail suggesting that the C-termini of moth PBPs may play an important role in ligand binding as well.⁸ These different functions of different PBPs like- BmorPBP, AtraPBP and LdisPBP2 led us to investigate the role of C-terminus in the ligand releasing as well as binding mechanisms for ApolPBP1 by fluorescence and NMR spectroscopy.

The C-terminus of ApolPBP1 has 14 residues, from Pro-129 to Val-142. There are three charged residues present in the C-terminus tail, they are: Asp-132, Glu-137 and Glu-141. To investigate the role of the C-terminal tail in the ligand releasing/binding mechanism of ApolPBP1, we deleted 14 residues (Pro129-Val142) from the C-terminus of ApolPBP1wt as well as ApolPBP1H70A/H95A. Also to examine the role of the three charged residues in the formation of the C-terminal 7th helix in the low pH induced conformational switch, we mutated them to produce the following proteins- ApolPBP1D132N, ApolPBP1E137Q and ApolPBP1E141Q. We also produced double mutants- ApolPBP1D132NE137Q and ApolPBP1E137QE141Q and triple mutant ApolPBP1D132NE137QE141Q proteins.

The effects of pH and ligand on the conformation of these mutated proteins were studied by high resolution solution NMR spectroscopy and fluorescence spectroscopy. The effects of the C-terminal deletion alone and that of both the C-terminus deletion along with the His-70 and

His-95 mutations, on the binding of ligand to these proteins at different pH values were also investigated. Our NMR data suggest that, unlike the wild type protein, both delipidated (ligand-free) and undelipidated (ligand-bound) C-terminus deleted ApolPBP1 Δ P129-V142 and ApolPBP1H70A/H95A Δ P129-V142 proteins exist only in ligand-bound conformation, without undergoing pH- or ligand-dependent conformational switch.⁹ This means ligand release at low pH by the wild-type ApolPBP1 is not possible without the C-terminus even when the His gate is opened. The ligand is not released through the His gate without the help from the C-terminal tail. Thus, the His gate at one end of the binding pocket and the C-terminal gate at the other end work together for the ligand release. Additionally, the delipidated C-terminal truncated protein exists only in ligand-bound conformation at all pH levels as the unoccupied binding pocket remains open in the absence of the C-terminus.⁹ Moreover, from the AMA binding assay carried out by fluorescence spectroscopy, we have found out that the C-terminus truncated proteins have reduced affinity towards the ligand at all pH values compared to the wild type protein.⁹ Based on these observations, we concluded that the C-terminus is not only necessary in ligand releasing mechanism but also plays an equally important role in ligand binding.⁹

NMR data of C-terminus single mutant proteins (ApolPBP1D132N, ApolPBP1E137Q and ApolPBP1E141Q) suggested that, these proteins behave same as the wild type protein indicating that point mutation has no effect on protein conformation. At pH 6.5, undelipidated ApolPBP1D132N, ApolPBP1E137Q and ApolPBP1E141Q are in the ligand-bound conformation. Whereas at pH 4.5 undelipidated ApolPBP1D132N, ApolPBP1E137Q and ApolPBP1E141Q are in the ligand-free conformation. These conformations are exactly same as that of the wild type protein. So we concluded that single mutation of any of the charged residues in the C-terminus does not affect its switch to helix at low pH. Double mutated undelipidated

proteins, ApolPBP1D132NE137Q and ApolPBP1E137QE141Q appears to have similar fingerprint in the HSQC spectra. However detailed biophysical investigation is necessary to study the effect of delipidation and pH on the conformation of ApolPBP1D132NE137Q and ApolPBP1E137QE141Q to confirm the above observation. Very interestingly, the ApolPBP1D132NE137QE141Q protein behaves completely differently than the wild type protein. At high pH, the HSQC spectrum of ApolPBP1D132NE137QE141Q appears to match the HSQC spectrum of the wild type protein. However, the HSQC spectrum of ApolPBP1D132NE137QE141Q at pH 4.5 is very different. The degradation in the spectral quality could be either due to the destabilization of the protein conformation or effect of mutation on protein solubility and stability. However, this preliminary observation must be investigated further to determine the effect of the mutation on protein conformation and stability.

4.2 Materials and Methods

4.2.1 Cloning, Overexpression & Purification of C-terminus deleted proteins

Truncation of 14 residues (Pro-129 to Val-142) from the C-terminus of ApolPBP1wt and ApolPBP1H70A/H95A was achieved using a PCR based approach. *ApolPBP1wt* and *ApolPBP1H70A/H95A* genes, cloned into a pET-21a vector, were amplified with the following primers: forward, 5' GGAATTCCA|TATGTCGCCAGAGATCATGAAG 3' & reverse, 5' GCG|GATCCCTAAACCCAGTTCAGCTTATGGATCTC 3' (restriction sites are underlined) and sub-cloned between the restriction sites of *NdeI* and *BamHI* of the pET-21a vector. The correct orientations of both constructs were determined by DNA sequencing. All plasmid constructs were transformed into *E. coli* origami cells and expressed as described previously.⁶ M9 minimal medium supplemented with ¹⁵NH₄Cl (Cambridge Isotope Laboratories, MA) was used for the expression of isotope-labeled recombinant proteins. Unlabeled and ¹⁵N labeled proteins were expressed, purified and delipidated as described earlier.⁶ The purity of the proteins was assessed by LC/ESI-MS (Figure 4.2A and 4.2B). Protein concentrations were determined spectrophotometrically using the theoretical E₂₈₀= 14230 M⁻¹ cm⁻¹.

4.2.2 Cloning, Overexpression & Purification of C-terminus mutant proteins

The C-terminus of ApolPBP1wt was mutated using site-directed mutagenesis. ApolPBP1D132N was constructed from the *ApolPBP1wt* gene using the forward primer 5' GAACTGGGTTCCTAACATGAATCTTGTAATAGGCGAGGTC 3' and the reverse primer 5' GA CCTCGCCTATTACAAGATTCATGTTAGGAACCCAGTTC 3'. Whereas ApolPBP1E137Q was constructed using the forward primer 5' CATGGACCTTGTAATAGGCCAGGTCTTAGCTG AAGTTTAG 3' and the reverse primer 5'

CTAAACTTCAGCTAAGACCTGGCCTATTACAAGG TCCATG 3' and ApolPBP1E141Q was constructed using the forward primer 5' GTAATAGGCGAGGTCTTAGCTCAAGTTTAGGGATCCGAATTC 3' and the reverse primer 5' GAATTCGGATCCCTAAACTTGAGCTAAGACCTCGCCTATTAC 3'.

ApolPBP1D132NE137Q was constructed using the *ApolPBP1E137Q* plasmid as template with the primers: forward 5' CATGAATCTTGTAATAGGCCAGGTCTTAGCTGAAGTTTAG 3' and reverse 5' CTAAACTTCAGCTAAGACCTGGCCTATTACAAGATTCATG 3'. ApolPBP1E137QE141Q was constructed using the *ApolPBP1E137Q* plasmid as template with the primers: forward 5' GTAATAGGCCAGGTCTTAGCTCAGGTTTAGGGATCCGAATTCGAG 3' and reverse 5' CTCGAATTCGGATCCCTAAACCTGAGCTAAGACCTGGCCTATTAC 3'. Finally ApolPBP1D132NE137QE141Q was constructed using the *ApolPBP1E137QE141Q* plasmid as template with the primers: forward 5' CATGAATCTTGTAATAGGCCAGGTCTTAGCTCAAGTTTAG 3' and reverse 5' CTAAACTTGAGCTAAGACCTGGCCTATTACAAGATTCATG 3'.

The correct orientations of all the constructs were determined by DNA sequencing. All plasmid constructs were transformed into *E. coli* origami cells and expressed as described previously.⁶ Unlabeled and ¹⁵N labeled proteins were expressed, purified and delipidated as described earlier.⁶ The purity of the proteins was assessed by SDS-PAGE.

4.2.3 NMR Measurements

All NMR data were collected at 35 °C on a Bruker Avance 600-MHz spectrometer at the Department of Chemistry and Biochemistry, Auburn University. pH titrations were carried out on 400 µl of uniformly ¹⁵N labeled 0.3 mM proteins in 50 mM sodium phosphate buffer, pH 6.5

or pH 4.5, 1 mM EDTA, 0.01% NaN₃, and 5% D₂O (used as a lock solvent) in a Shigemi tube. Two-dimensional {¹H, ¹⁵N} heteronuclear single quantum coherence (HSQC) spectra were collected for ¹⁵N labeled undelipidated and delipidated ApolPBP1ΔP129-V142 and ApolPBP1H70A/H95AΔP129-V142, samples at pH 4.5 and 6.5. Ligand titration studies were carried out for ¹⁵N labeled delipidated ApolPBP1ΔP129-V142 and ApolPBP1H70A/H95AΔP129-V142 at pH 4.5 and 6.5 with palmitic acid as a ligand. The proteins (310 μL of 220 μM in 50 mM phosphate buffer, pH 6.5 or 4.5, containing 5% D₂O, 1 mM EDTA, and 0.01% (w/v) NaN₃) were titrated with increasing concentrations of palmitic acid (0-2.2 mM) and the corresponding two-dimensional HSQC spectra were recorded at each titration point.

Two-dimensional {¹H, ¹⁵N} heteronuclear single quantum coherence (HSQC) spectra were collected for ¹⁵N labeled undelipidated ApolPBP1D132N, ApolPBP1E137Q and ApolPBP1E141Q at pH 6.5 and 4.5. While two-dimensional {¹H, ¹⁵N} HSQC spectra were also collected for undelipidated and delipidated ApolPBP1D132NE137Q and ApolPBP1E137QE141Q and undelipidated ApolPBP1D132NE137QE141Q at pH 6.5 and 4.5. All data were processed using NMRPipe¹⁰ and analyzed using NMRView¹¹ and Sparky.¹⁴

4.2.4 Fluorescence Spectroscopy

Fluorescence experiments were done on a 55B spectrofluorimeter (PerkinElmer Life Sciences) as described previously.⁶ All experiments were repeated at least twice to confirm reproducibility.

4.2.5 AMA Binding Studies

The binding of AMA to delipidated ApolPBP1 Δ P129-V142 and ApolPBP1H70A/H95A Δ P129-V142 at pH 6.5 and 4.5 was assessed by monitoring the increase in the AMA fluorescence at 480 nm as described previously.⁶ Phosphate buffer with the appropriate amount of AMA served as control for each data point. Binding constants for each sample were determined from the nonlinear regression of the data as discussed earlier.⁶ All PBP mutants showed maximum fluorescence intensity at 5 μ M AMA concentration hence this data point was chosen to compare the relative binding affinity of all proteins. The fluorescence intensity of ApolPBP1wt at 1:5 proteins: AMA mixture was considered as 100% binding affinity and relative binding affinities for other proteins were calculated accordingly.

4.3 Results

4.3.1 Expression and purification of C-terminus deleted proteins

Unlabeled as well as ^{15}N -labeled ApolPBP1 Δ P129-V142 and ApolPBP1H70A/H95A Δ P129-V142 were expressed and purified as mentioned in the materials and methods. The SDS-PAGE (Figure 4.1A and 4.1B) and mass-spec analysis showed the purity of the protein (Figure 4.2A and 4.2B). Unlabeled and ^{15}N -labeled ApolPBP1D132N, ApolPBP1E137Q, ApolPBP1E141Q, ApolPBP1D132NE137Q, ApolPBP1E137QE141Q and ApolPBP1D132NE137QE141Q were also expressed and purified. Purity of the proteins was showed by the SDS-PAGE (Figure 4.1C and 4.1D).

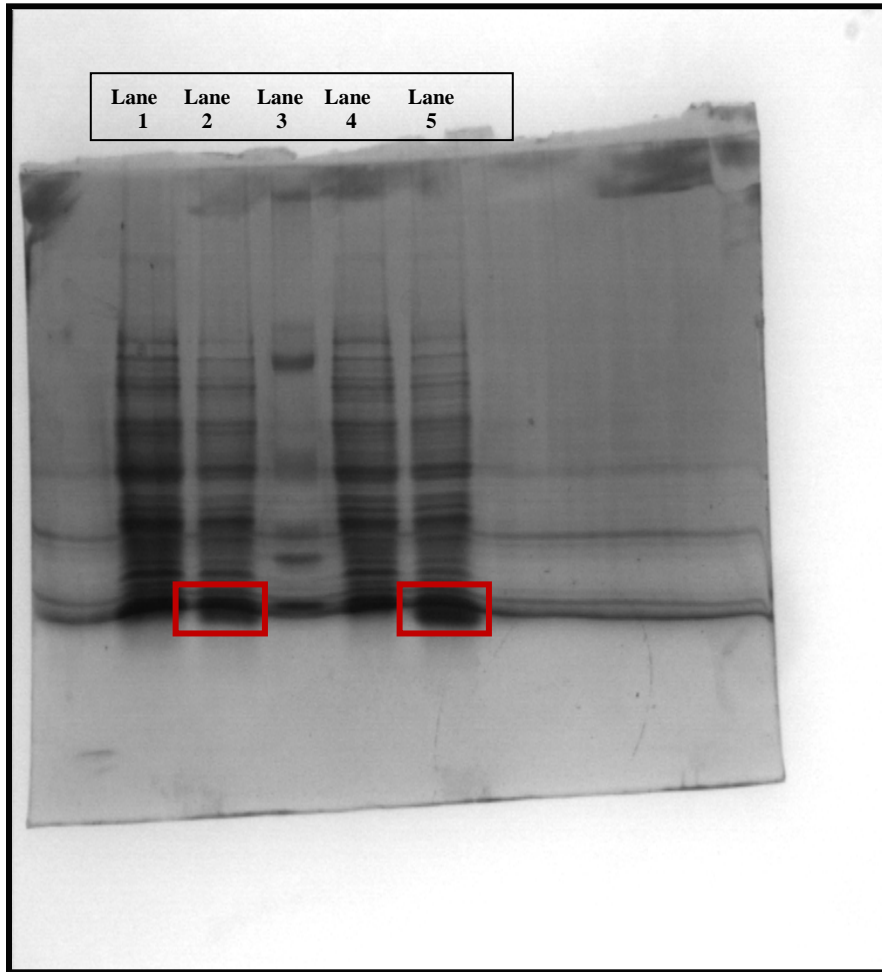


Figure 4.1 A. SDS-PAGE analysis of unlabeled ApolPBP1 Δ P129-V142. Lane 1: Protein at the time of induction with IPTG. Lane 2: Protein after 4 hours of induction, red box shows the expression of the protein. Lane 3: Protein markers. Lane 4: Protein at the time of induction with IPTG. Lane 5: Protein after 4 hours of induction.

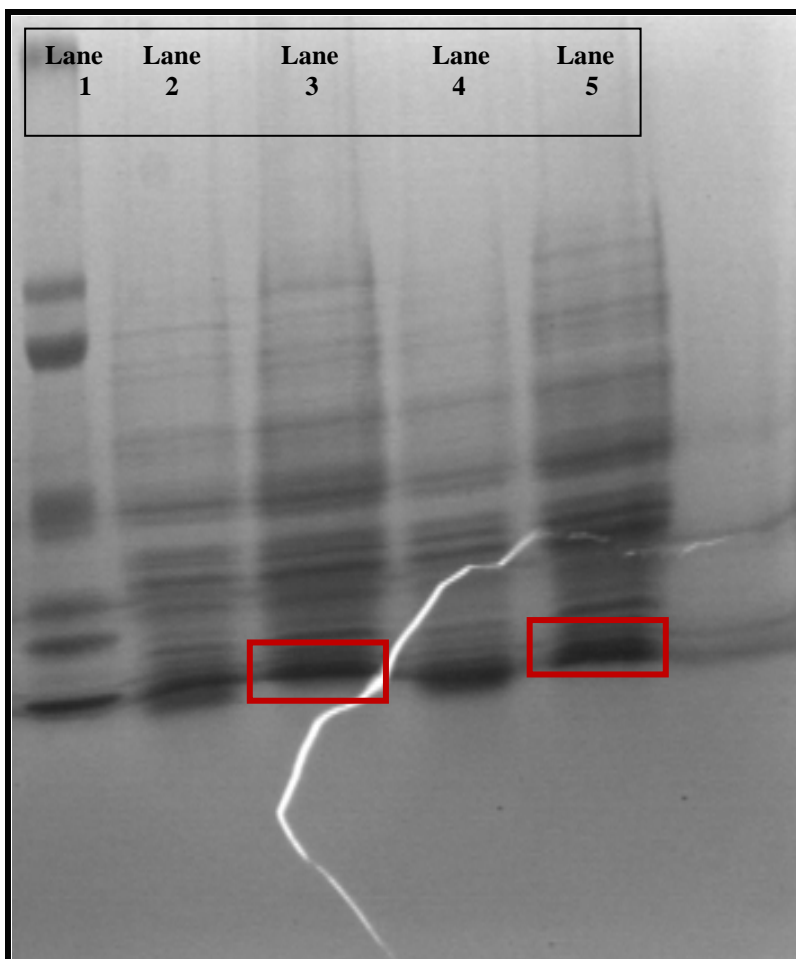


Figure 4.1 B. SDS-PAGE analysis of unlabeled ApolPBP1H70A/H95A Δ P129-V142. Lane 1: Protein Marker. Lane2: Protein at the time of induction with IPTG. Lane 3: Protein after 4 hours of induction, red box shows the expression of the protein. Lane4: Protein at the time of induction with IPTG. Lane 5: Protein after 4 hours of induction.

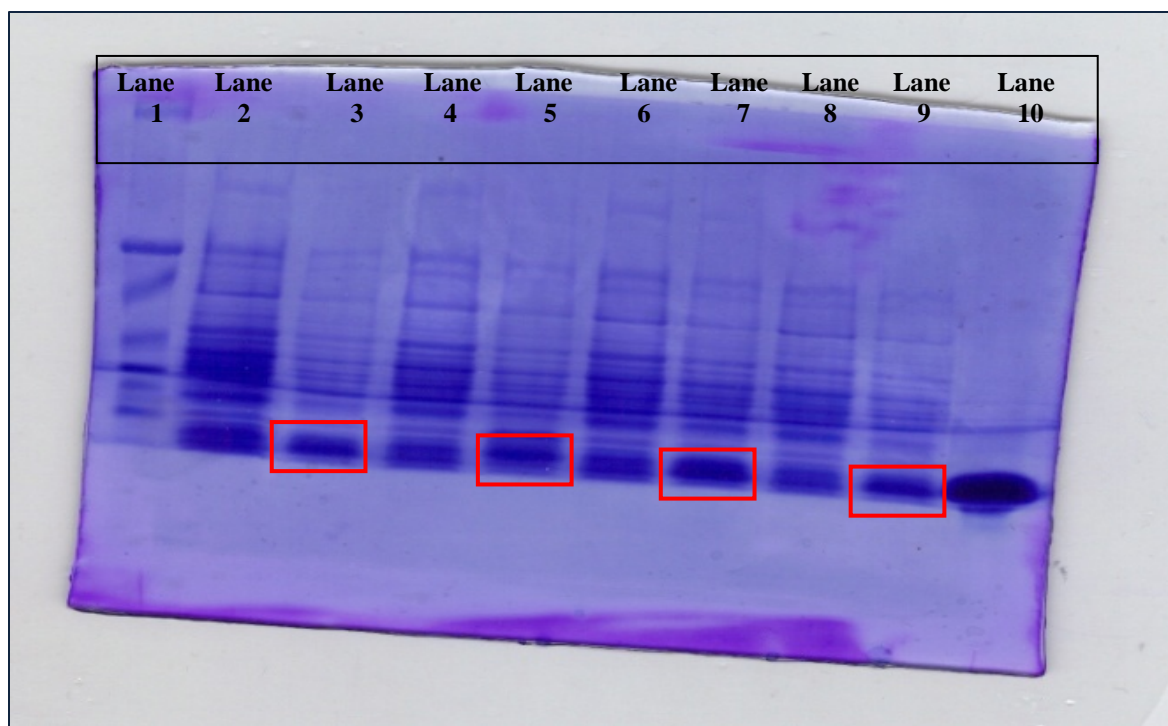


Figure 4.1 C. SDS-PAGE analysis of unlabeled ApolPBP1D132N, ApolPBP1E137Q and ApolPBP1E141Q. Lane 1: Protein Marker; Lane 2: ApolPBP1D132N at the time of induction with IPTG; Lane 3: ApolPBP1D132N after 4 hrs of induction; Lane 4: ApolPBP1E137Q at the time of induction with IPTG; Lane 5: ApolPBP1E137Q after 4 hrs of induction; Lane 6: ApolPBP1E141Q at the time of induction with IPTG; Lane 7: ApolPBP1E141Q after 4 hrs of induction; Lane 8: ApolPBP1D132N at the time of induction with IPTG; Lane 9: ApolPBP1D132N after 4 hrs of induction; Lane 10: Pure ApolPBP1 wild type protein.

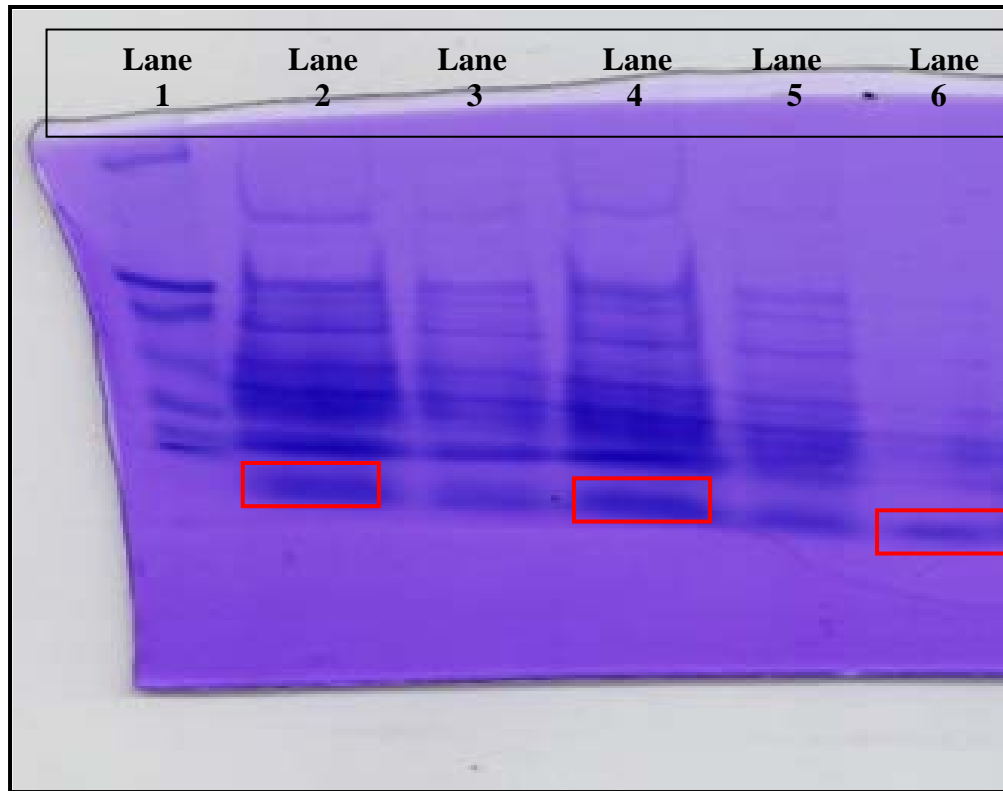


Figure 4.1 D. SDS-PAGE analysis of unlabeled ApolPBP1D132NE137Q and, ApolPBP1E137QE141Q. Lane 1: Protein Marker; Lane 2: ApolPBP1D132NE137Q after 4 hrs of induction; Lane 3: ApolPBP1D132NE137Q at the time of induction with IPTG; Lane 4: ApolPBP1E137QE141Q after 4 hrs of induction; Lane 5: ApolPBP1E137QE141Q at the time of induction with IPTG; Lane 6: Pure ApolPBP1 wild type protein.

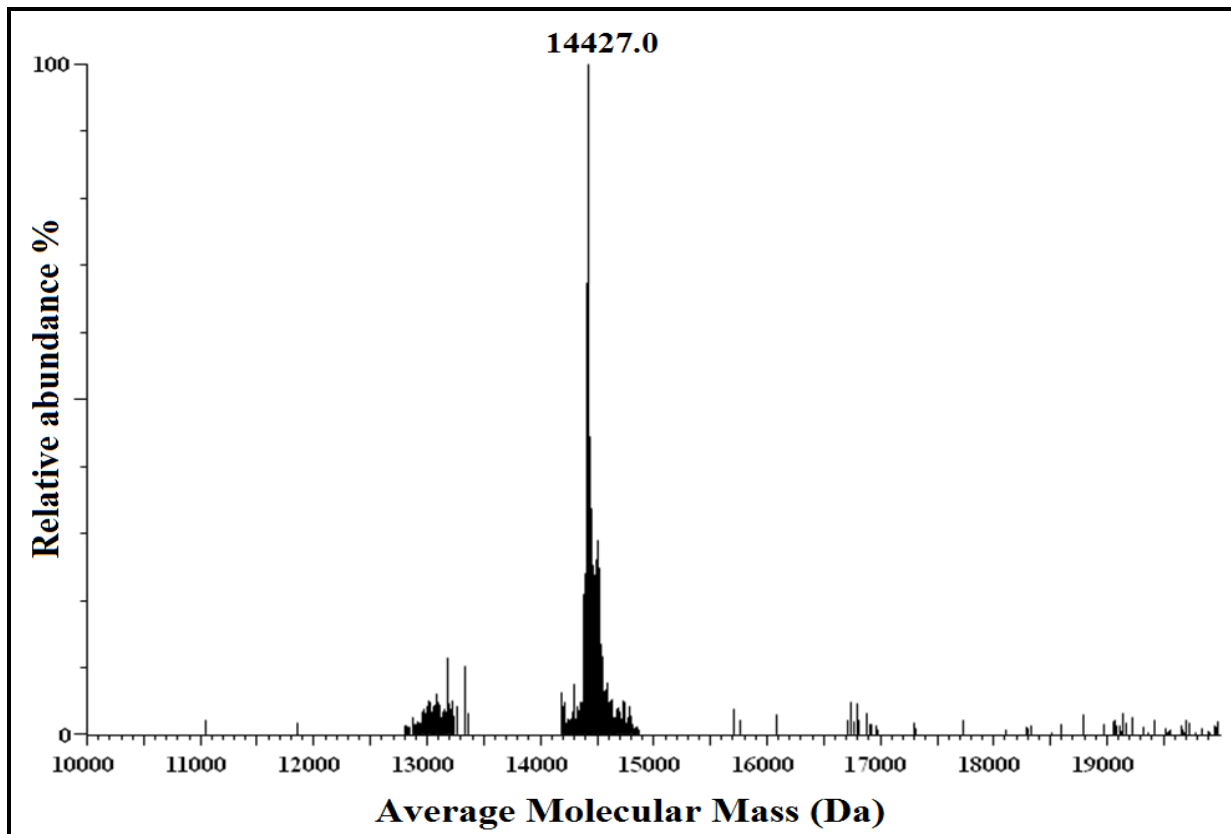


Figure 4.2 A. Mass spec analysis of pure ApolPBP1 Δ P129-V142. A sharp peak at 14427.0 Da indicates the presence of pure protein.

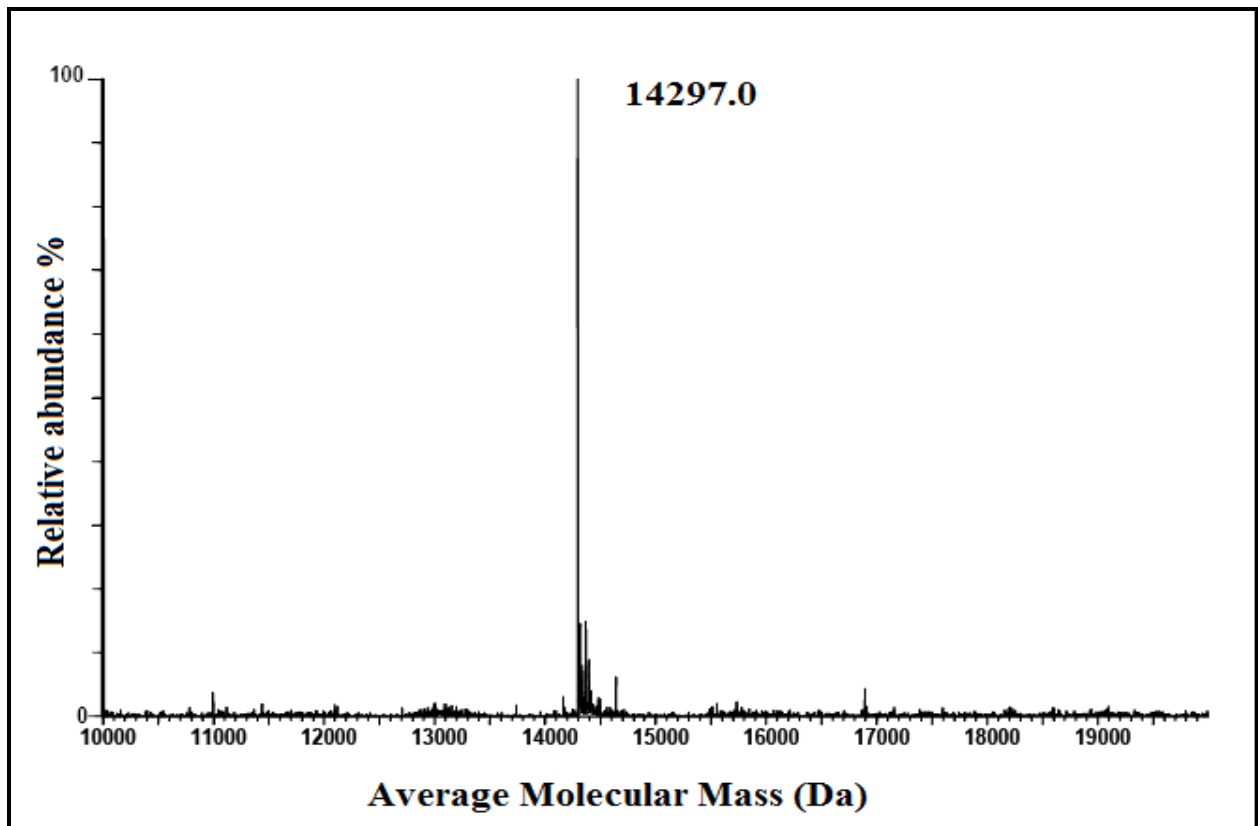


Figure 4.2 B. Mass spec analysis of pure ApolPBP1H70A/H95AΔP129-V142. A sharp peak at 14297.0 Da indicates the presence of pure protein.

4.3.2 Role of the C-terminus in Ligand Binding and Release

The PBPs release ligand at low pH near the membrane-bound receptors (ion channels) by undergoing a conformational change. This conformational change is controlled by two molecular switches: the histidine switch and the C-terminus switch. We present here our research work on the role of the C-terminus on the ligand release and binding of ApolPBP1. The two-dimensional $\{^1\text{H}, ^{15}\text{N}\}$ HSQC spectrum is considered to be the fingerprint of a protein, as it is very sensitive to the environmental changes like pH, temperature, substrate binding, mutations etc. Local or global conformational changes occurring in the protein are reflected in the HSQC spectrum as the changes in the chemical shift positions of resonances of the amino acid residues involved. The HSQC spectra of delipidated ApolPBP1 Δ P129-V142 and ApolPBP1H70A/H95A Δ P129-V142 at pH 6.5 exhibited well-dispersed resonances indicating that both proteins were properly folded. These spectra largely resembled that of the ligand-bound conformation of ApolPBP1wt, with marked disappearances of the resonances belonging to the residues in the C-terminal tetradecapeptide segment (Figure 4.3A and 4.3B). Using the assignment of undelipidated ApolPBP1wt at pH 6.5,¹² more than 80% of the original peaks could be located in the HSQC spectra of delipidated ApolPBP1 Δ P129-V142 and ApolPBP1H70A/H95A Δ P129-V142, respectively. Very interestingly, these delipidated proteins, where the endogenous ligand of the expression system has been removed through delipidation procedure, are still in ligand-bound conformation although the hydrophobic cavity is empty (Figure 4.3C and 4.3D).⁹ This data suggests that for the C-terminus truncated mutants, the binding pocket is not closed by the C-terminus anymore.⁹ Thus the protein always exhibits ligand-bound conformation even when no ligand is bound to the pocket.⁹

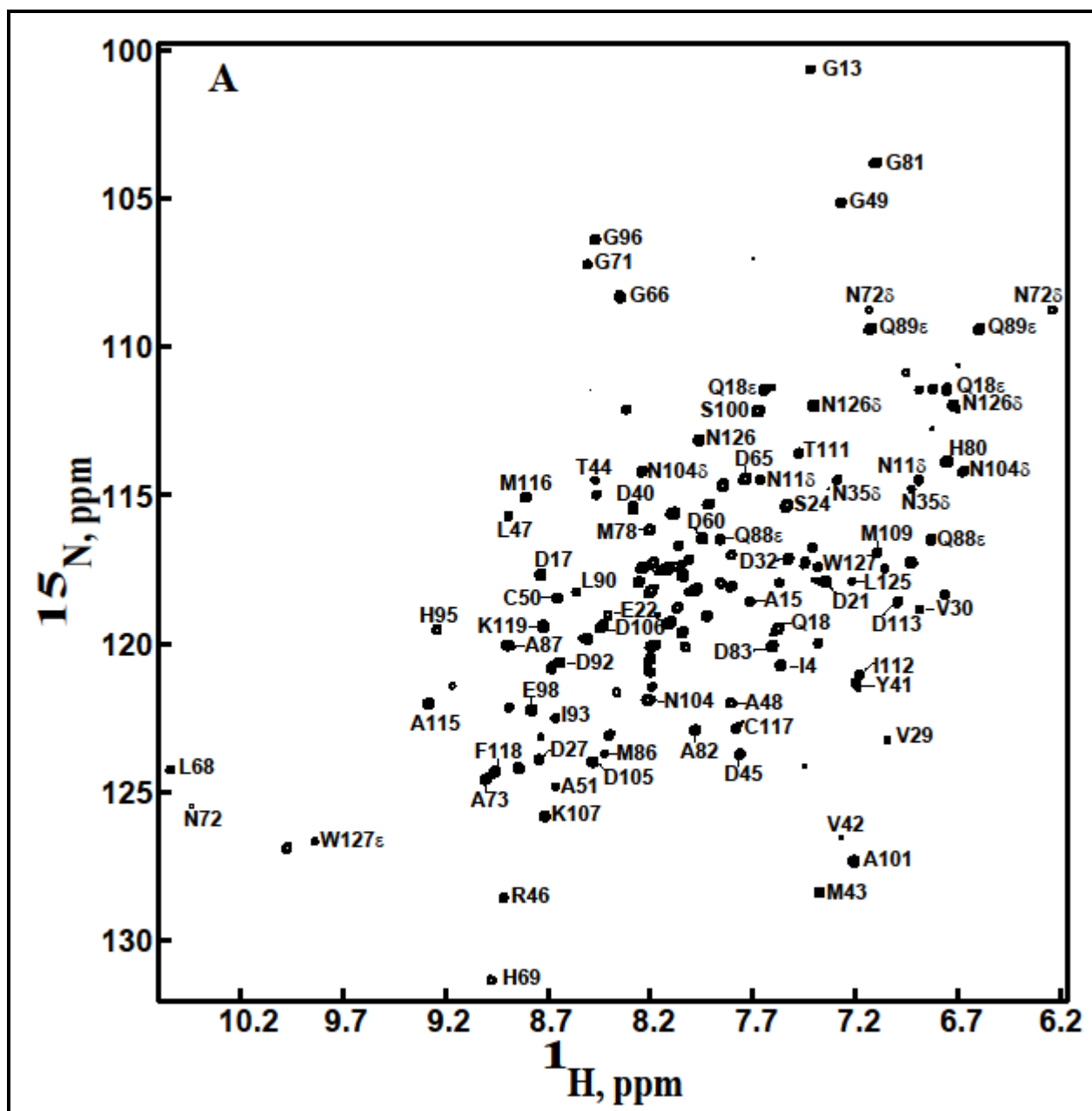


Figure 4.3 A. Two-dimensional $\{^1\text{H}, ^{15}\text{N}\}$ HSQC spectra of delipidated ApolPBP1 Δ P129-V142 in 50 mM sodium phosphate buffer at pH 6.5 containing 5% D_2O , 1M EDTA, and 0.01% sodium azide. The protein shown to have the ligand-bound conformation. From reference 9.

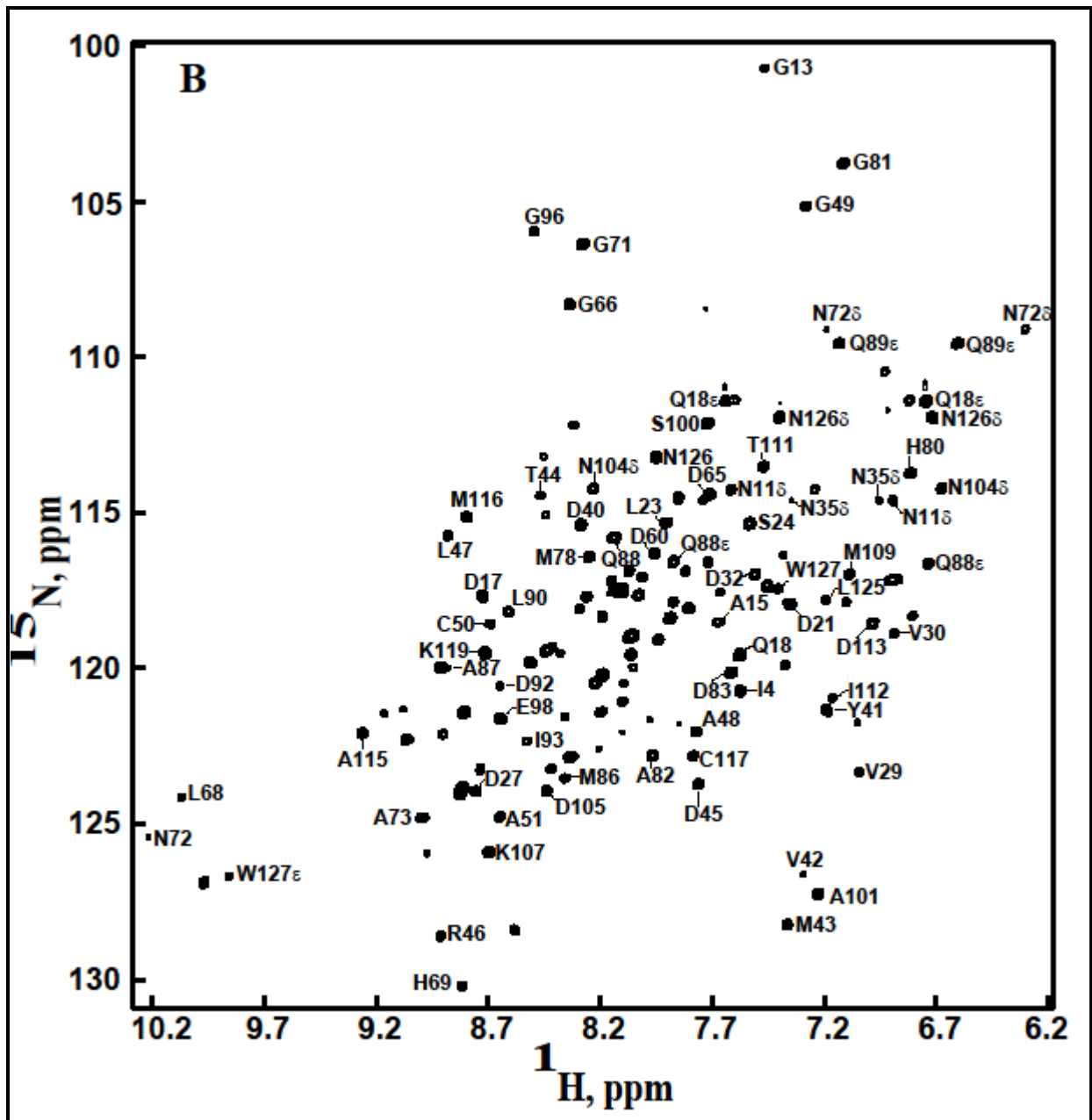


Figure 4.3 B. Two-dimensional $\{^1\text{H}, ^{15}\text{N}\}$ HSQC spectra of delipidated ApolPBP1H70A/H95A Δ P129-V142 in 50 mM sodium phosphate buffer at pH 6.5 containing 5% D_2O , 1M EDTA, and 0.01% sodium azide. The protein shown to have the ligand-bound conformation. From reference 9.

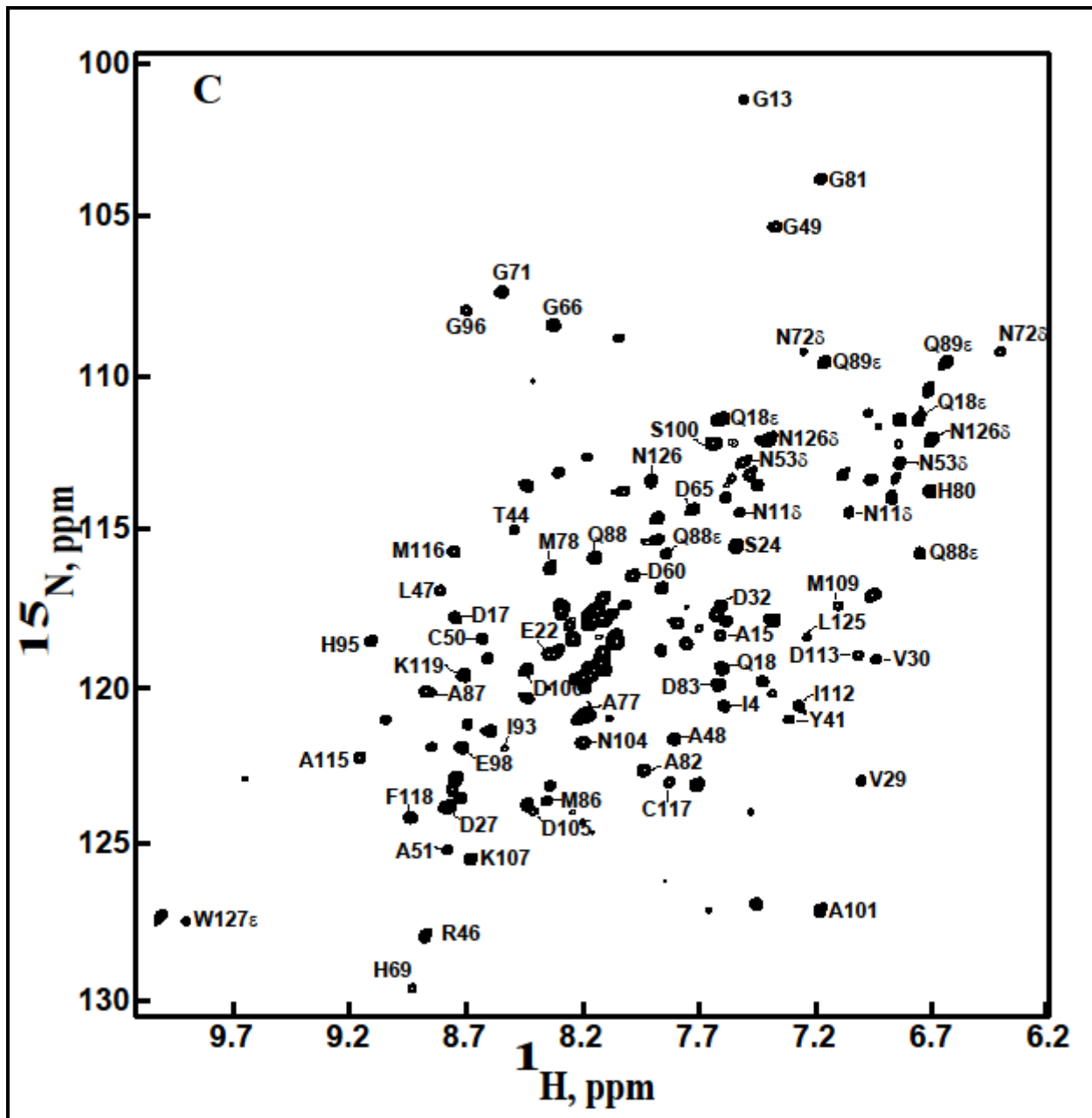


Figure 4.3 C. Two-dimensional $\{^1\text{H}, ^{15}\text{N}\}$ HSQC spectra of delipidated ApolPBP1 Δ P129-V142 in 50 mM sodium phosphate buffer at pH 4.5 containing 5% D_2O , 1M EDTA, and 0.01% sodium azide. The protein shown to have the ligand-bound conformation. From reference 9.

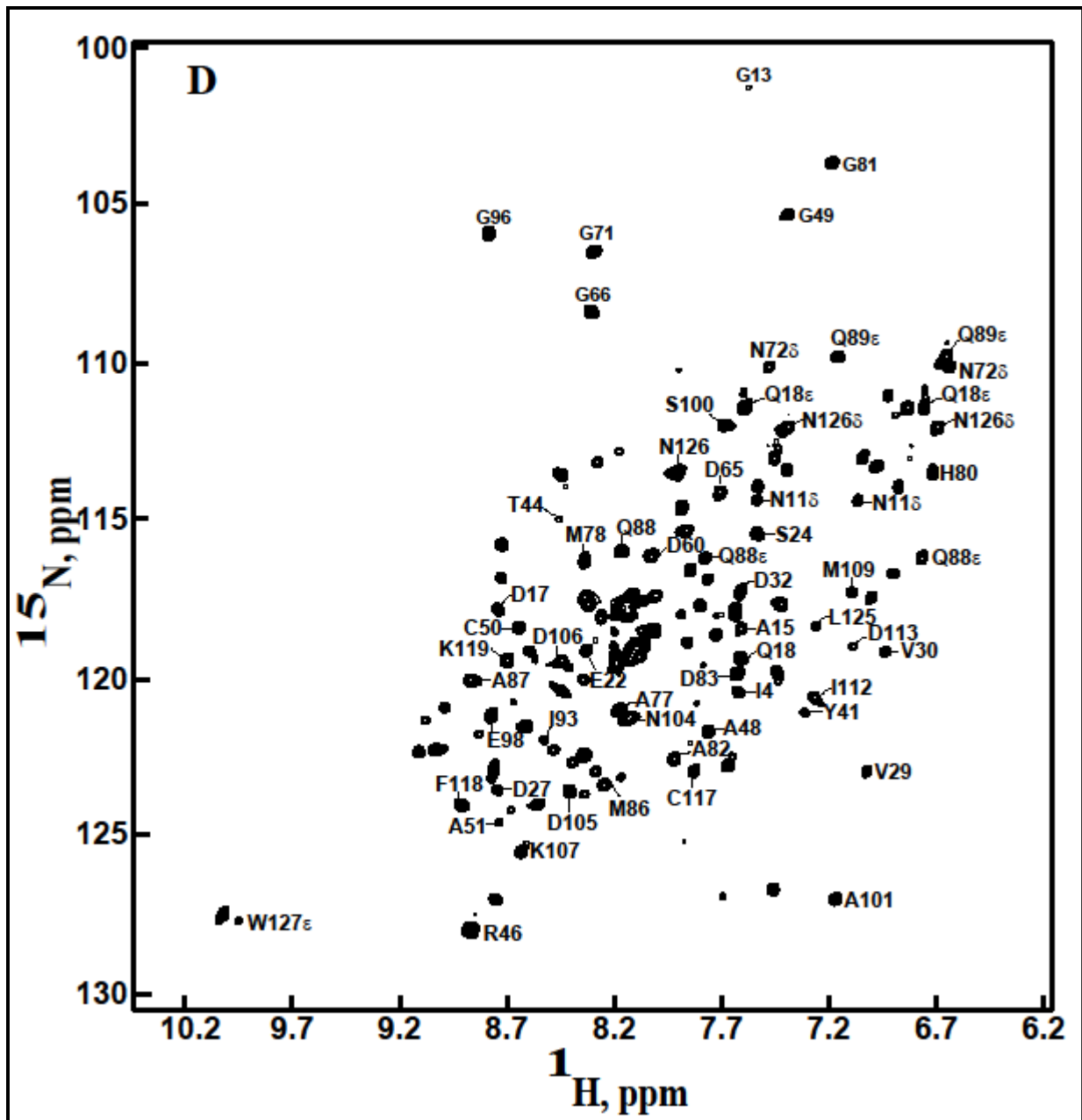


Figure 4.3 D. Two-dimensional $\{^1\text{H}, ^{15}\text{N}\}$ HSQC spectra of delipidated ApolPBP1H70A/H95A Δ P129-V142 in 50mMsodium phosphate buffer at pH 4.5 containing 5% D₂O, 1M EDTA, and 0.01% sodium azide. The protein shown to have the ligand-bound conformation. From reference 9.

2D HSQC spectra of unlipidated ApolPBP1 Δ P129-V142 and ApolPBP1H70A/H95A Δ P129-V142 at pH 6.5 matched very well with those of their delipidated counterparts (Figure 4.4A and 4.4B) and exhibited the characteristic ligand-bound conformation pattern also.⁹ Undelipidated ApolPBP1 Δ P129-V142 and ApolPBP1H70A/H95A Δ P129-V142 at pH 4.5 also showed the ligand-bound conformation same as the delipidated proteins (figure 4.4C and 4.4D).⁹ Interestingly, several resonances such as those belonging to Gly-13, Asn-53 δ , Trp-127 ϵ etc were found to be disappeared in these spectra due to line broadening. Such resonances could be readily located in the spectra of the delipidated counterparts of the same proteins, indicating that these residues must be in the intermediate-exchange regime on the NMR timescale in the ligand-bound protein.⁹

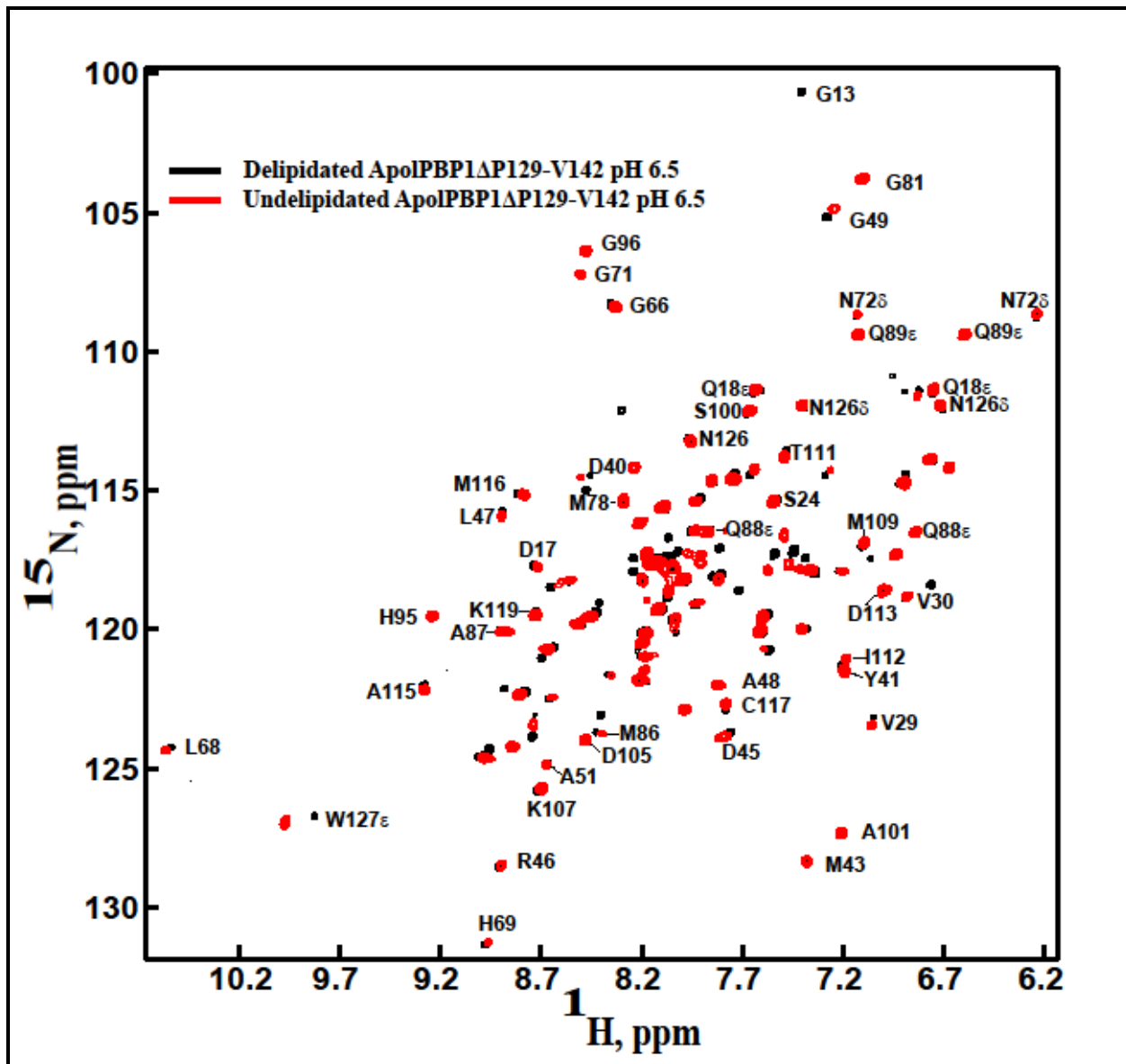


Figure 4.4 A. Two-dimensional $\{^1\text{H}, ^{15}\text{N}\}$ HSQC spectra of delipidated (black color) and undelipidated (red color) ApolPBPI Δ P129-V142 in 50 mM sodium phosphate buffer, pH 6.5, containing 5% D_2O , 1 mM EDTA, and 0.01% sodium azide. Note the disappearances of resonances such as those belonging to Gly-13, Trp-127 ϵ and several others in the spectrum of undelipidated protein. From reference 9.

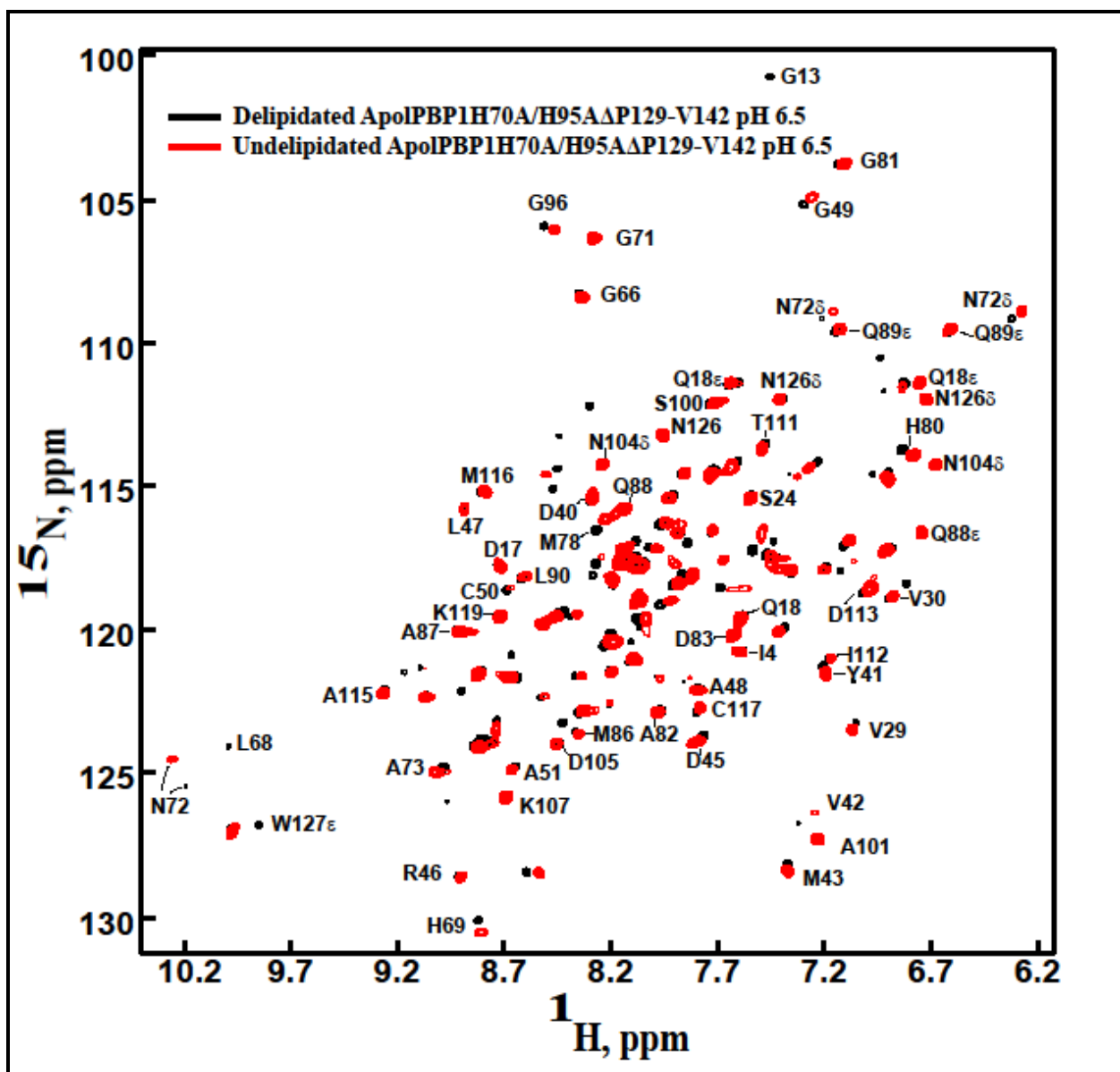


Figure 4.4 B. Two-dimensional $\{^1\text{H}, ^{15}\text{N}\}$ HSQC spectra of delipidated (black color) and undelipidated (red color) ApolPBP1H70A/H95A Δ P129-V142 in 50 mM sodium phosphate buffer, pH 6.5, containing 5% D₂O, 1 mM EDTA, and 0.01% sodium azide. Note the disappearances of resonances such as those belonging to Gly-13, Leu-68, Trp-127 ϵ and several others in the spectrum of undelipidated protein. From reference 9.

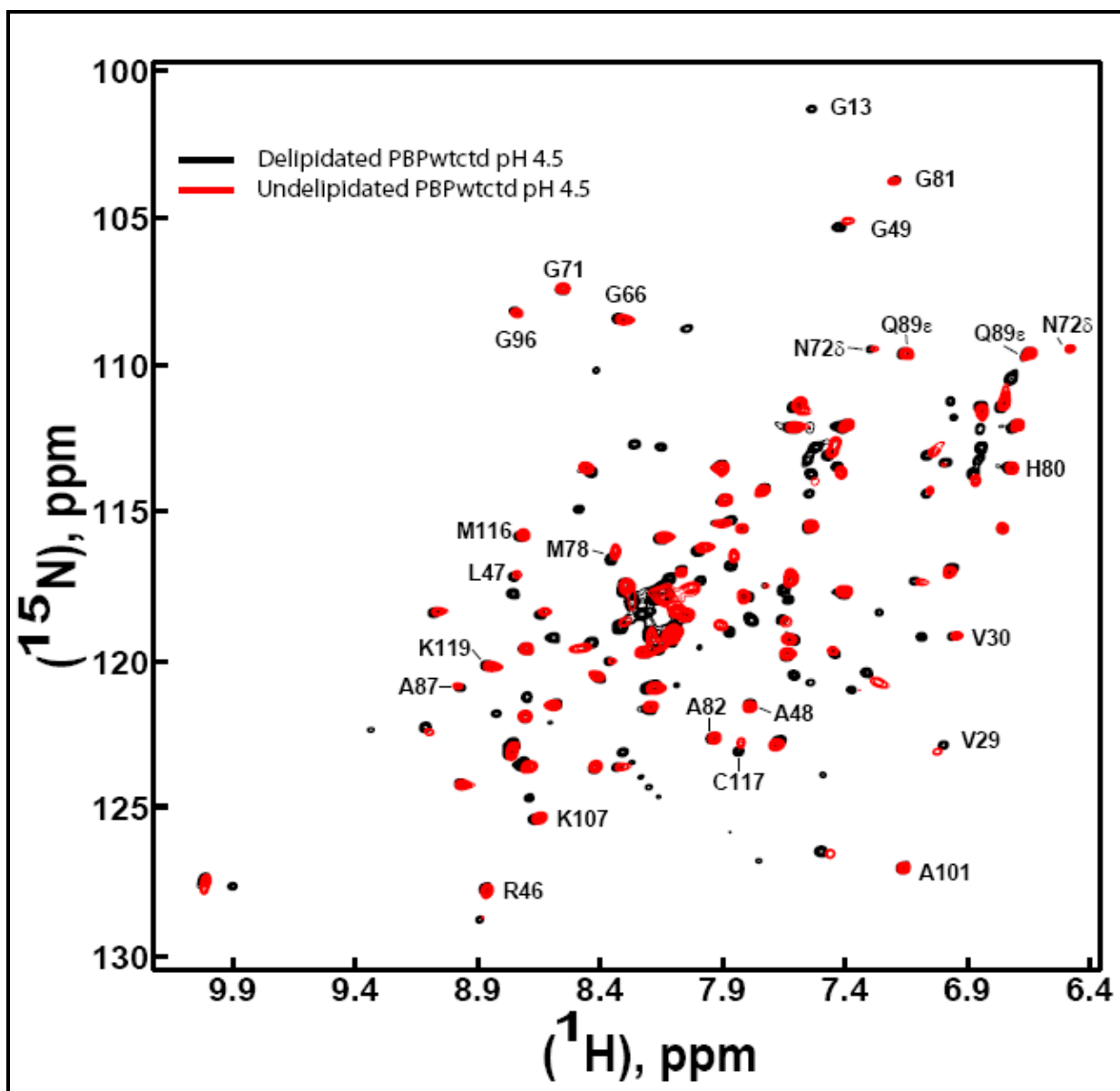


Figure 4.4 C. Two-dimensional $\{^1\text{H}, ^{15}\text{N}\}$ HSQC spectra of delipidated (black color) and undelipidated (red color) ApolPBP1 Δ P129-V142 in 50 mM sodium phosphate buffer, pH 4.5, containing 5% D₂O, 1 mM EDTA, and 0.01% sodium azide. The disappearances of resonances such as those belonging to Gly-13 and several others in the spectrum of undelipidated protein. From reference 9.

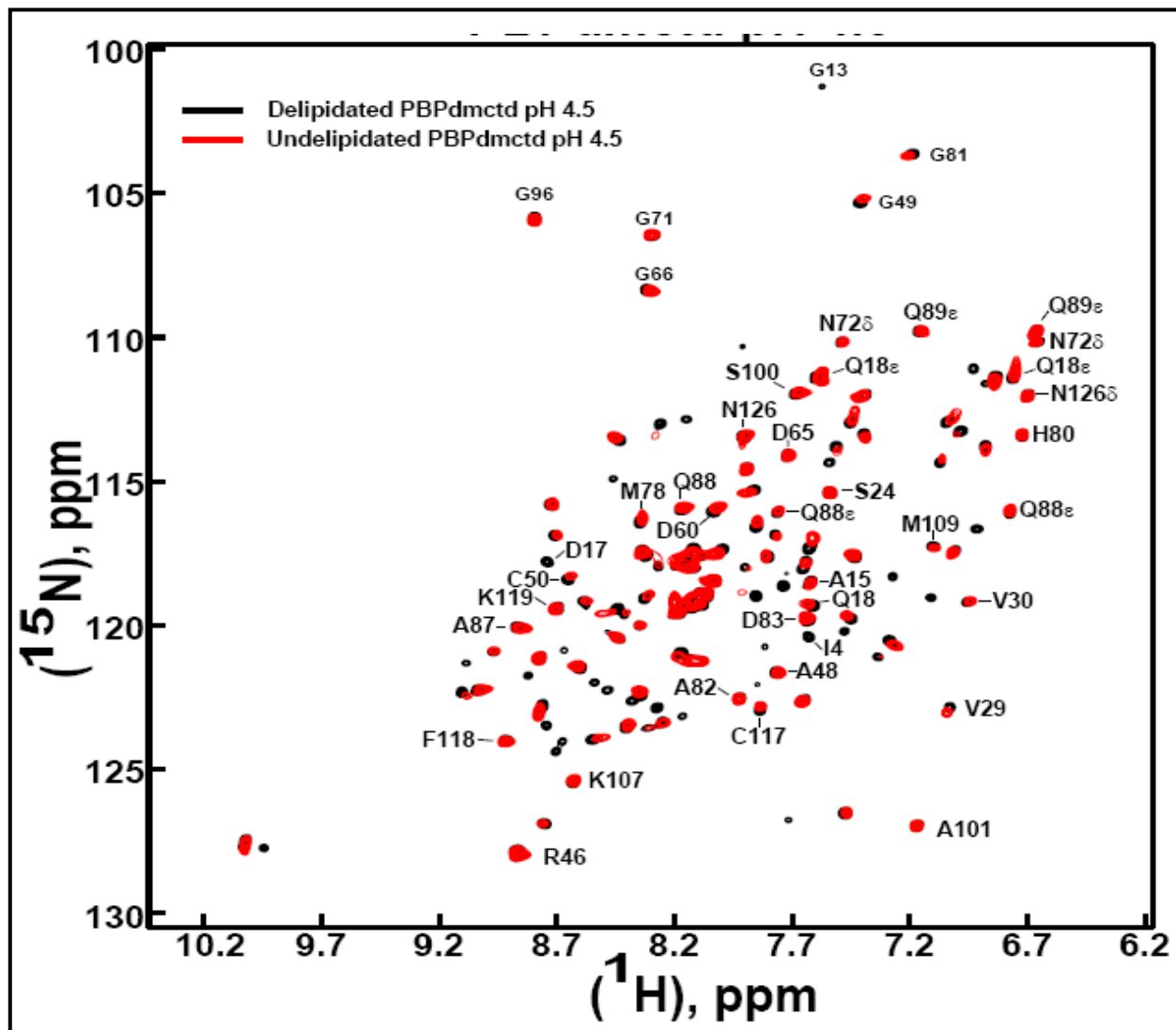


Figure 4.4 D. Two-dimensional $\{^1\text{H}, ^{15}\text{N}\}$ HSQC spectra of delipidated (black color) and undelipidated (red color) ApolPBP1H70A/H95A Δ P129-V142 in 50 mM sodium phosphate buffer, pH 4.5, containing 5% D₂O, 1 mM EDTA, and 0.01% sodium azide. The disappearances of resonances such as those belonging to Gly-13 and several others in the spectrum of undelipidated protein. From reference 9.

4.3.3 Effect of pH and ligand on the conformation of ApolPBP1 C-terminus deleted mutants

Delipidated ApolPBP1 Δ P129-V142 and ApolPBP1H70A/H95A Δ P129-V142 at pH 4.5 showed the same open conformation in HSQC spectra as observed at pH 6.5 (Figure 4.3A, 4.3B, 4.3C and 4.3D).⁹ The undelipidated proteins behaved in the similar manner. Thus these proteins did not undergo the pH-dependent conformational change as it was seen for the undelipidated ApolPBP1 wild-type protein. These results are in agreement with those reported for the C-terminus truncated BmorPBP (1-128) variant.¹³ However, several resonances (for example, those belonging to Gly13, Gly49, Gly81, Gly96 etc) displayed a moderate-to-large change in their chemical shift positions (Figure 4.5A and 4.5B) as a result of pH change.⁹ This indicated that although the conformation remains open at both pH values, local environmental changes due to change in pH affect chemical shifts of these residues.

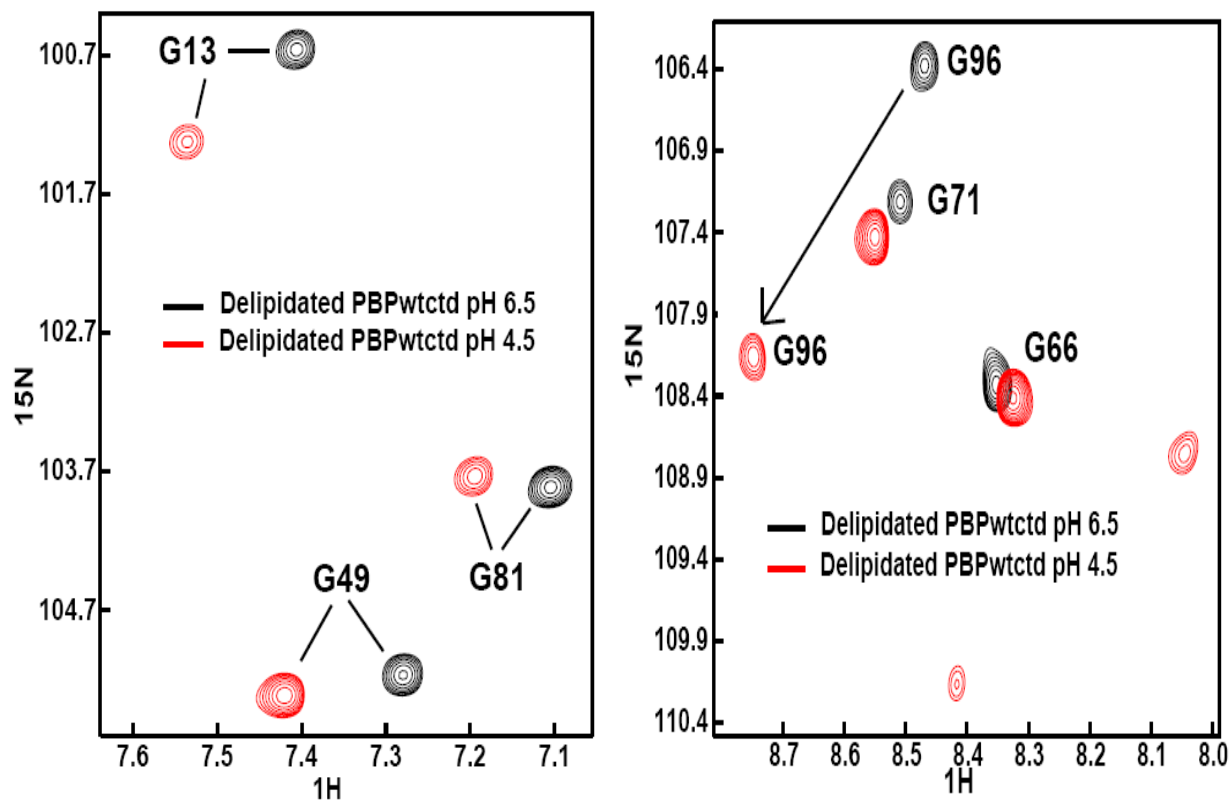


Figure 4.5 A. Expanded regions of the two-dimensional $\{^1\text{H}, ^{15}\text{N}\}$ HSQC spectra of delipidated ApolPBP1 Δ P129-V142 in 50 mM sodium phosphate buffer, showing movements of certain peaks as a result of pH. The pH of the buffer is indicated on the spectra. From reference 9.

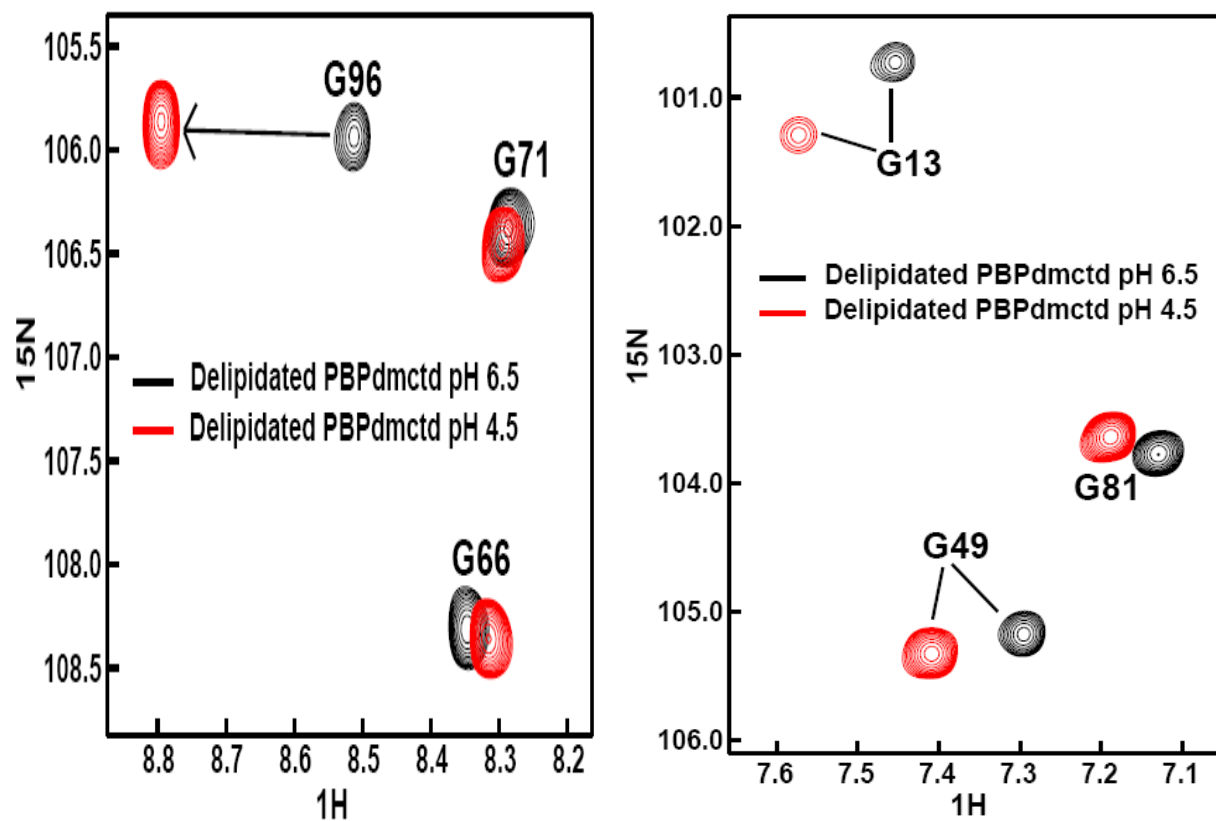


Figure 4.5 B. Expanded regions of the two-dimensional $\{^1\text{H}, ^{15}\text{N}\}$ HSQC spectra of delipidated ApolPBP1H70A/H95A Δ P129-V142 in 50 mM sodium phosphate buffer, showing movements of certain peaks as a result of pH. The pH of the buffer is indicated on the spectra. From reference 9.

To investigate the effect of ligand on the conformations of delipidated forms of ApolPBP1 Δ P129-V142 and ApolPBP1H70A/H95A Δ P129-V142, ligand titration studies were carried out using palmitic acid (a fatty acid similar to *Antheraea polyphemus* pheromone, 6E,11Z-hexadecadienyl acetate), at pH 6.5 and 4.5. Protein: palmitic acid ratios were varied from 1:0 to 1:10. Ligand titration studies revealed that there was no conformational change with the addition of ligand (Figure 4.6A, 4.6B, 4.6C and 4.6D).⁹ These delipidated proteins remained in the open conformation even after the addition of excess ligand. However, some of the resonances for example, Gly-13, Leu-68 etc. exhibited line-broadening and/or disappearance, indicating that they were in the intermediate exchange regime on the NMR time scale (Figure 4.7A and 4.7B).⁹ Several other resonances were seen to be in fast exchange regime on the NMR timescale, characterized by gradual changes in their chemical shift positions. These observations were in severe contrast to those observed earlier for the ligand titration of delipidated ApolPBP1wt and ApolPBP1H70A/H95A, in which almost all resonances were seen to be in slow exchange regime characterized by two sets of peaks for ligand-free (closed) and ligand-bound (open) conformations.⁹

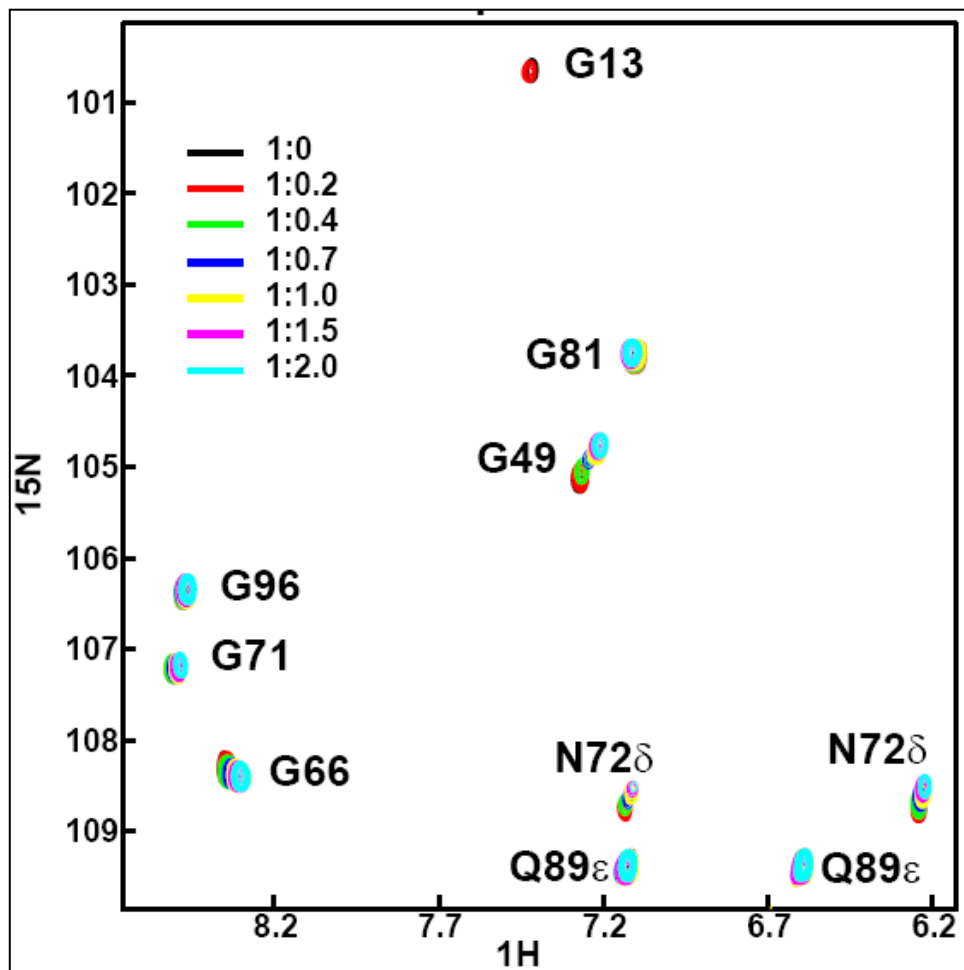


Figure 4.6 A. Expanded region of the two-dimensional $\{^1\text{H}, ^{15}\text{N}\}$ HSQC spectra of delipidated ApolPBP1 Δ P129-V142 (220 μM) in 50 mM phosphate buffer, pH 6.5, upon titration with palmitic acid. Protein: ligand ratios are indicated in the figure. Note the disappearance of the resonance belonging to Gly-13 due to line broadening. Some other resonances are in intermediate-to-fast exchange regime. From reference 9.

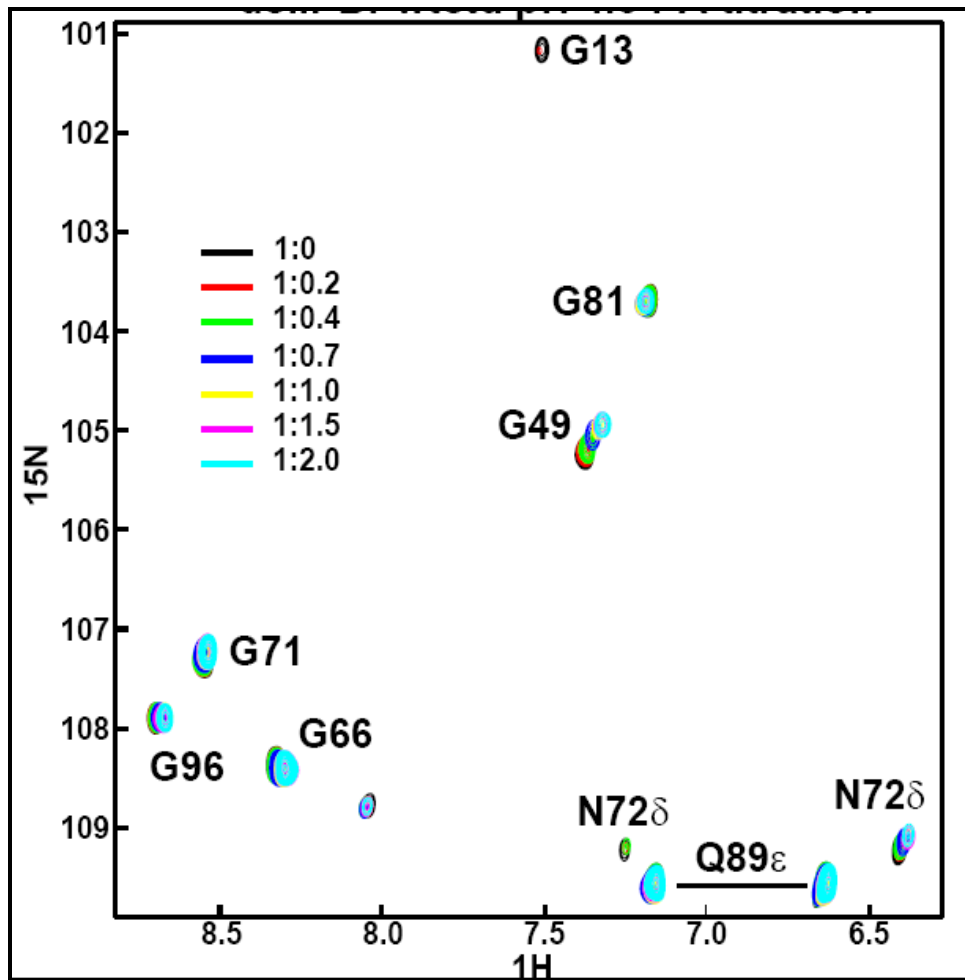


Figure 4.6 B. Expanded region of the two-dimensional $\{^1\text{H}, ^{15}\text{N}\}$ HSQC spectra of delipidated ApolPBP1 Δ P129-V142 in 50mM phosphate buffer, pH 4.5, upon titration with palmitic acid. Protein: ligand ratios are indicated in the figure. Note the disappearance of the resonance belonging to Gly-13 due to line broadening. Some other resonances are in intermediate-to-fast exchange regime. From reference 9.

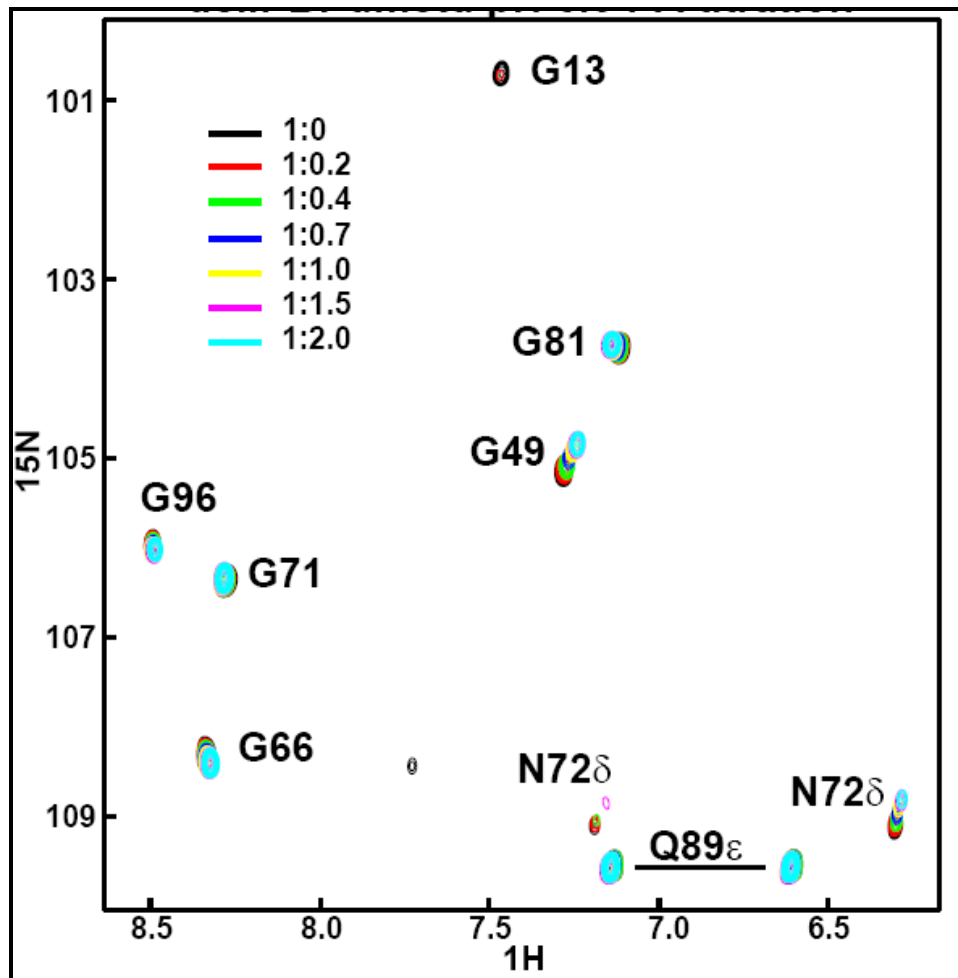


Figure 4.6 C. Expanded region of the two-dimensional $\{^1\text{H}, ^{15}\text{N}\}$ HSQC spectra of delipidated ApolPBP1H70A/H95A Δ P129-V142 in 50mM phosphate buffer, pH 6.5, upon titration with palmitic acid. Protein: ligand ratios are indicated in the figure. Note that the resonances are in intermediate-to-fast exchange regime. From reference 9.

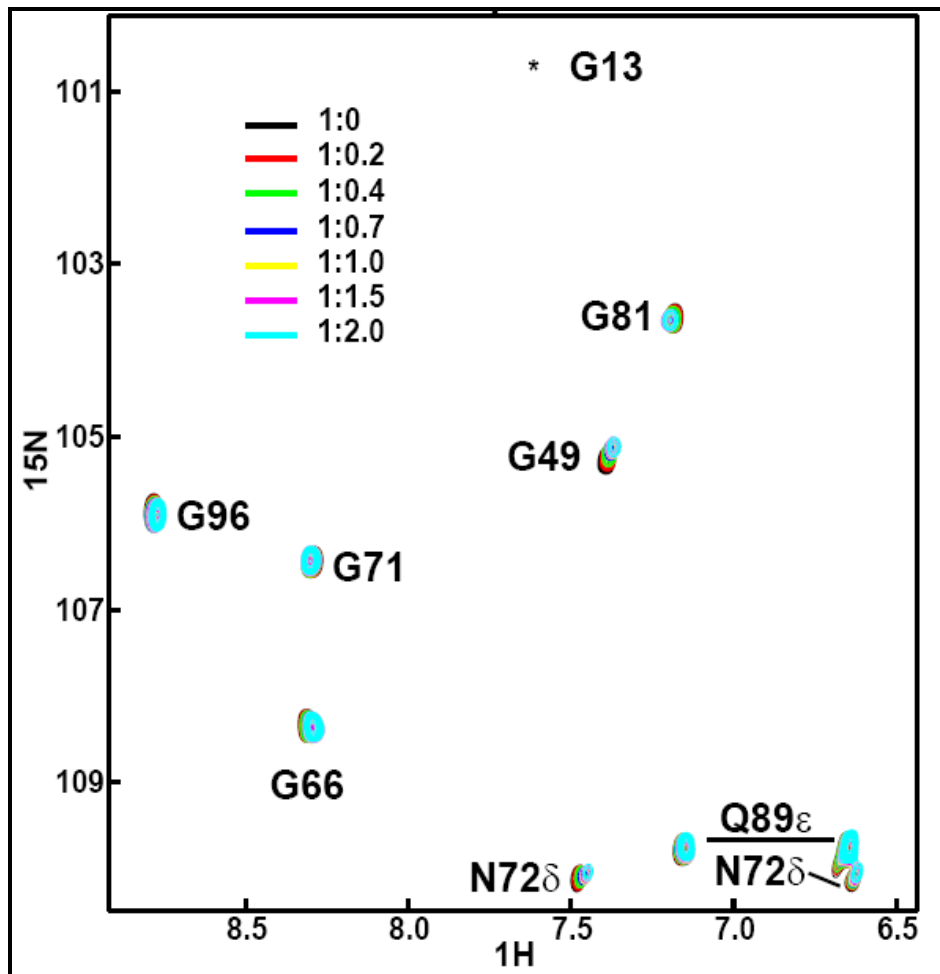


Figure 4.6 D. Expanded region of the two-dimensional $\{^1\text{H}, ^{15}\text{N}\}$ HSQC spectra of delipidated ApolPBP1H70A/H95A Δ P129-V142 in 50mM phosphate buffer, pH 4.5, upon titration with palmitic acid. Protein: ligand ratios are indicated in the figure. Note that the resonances are in intermediate-to-fast exchange regime. From reference 9.

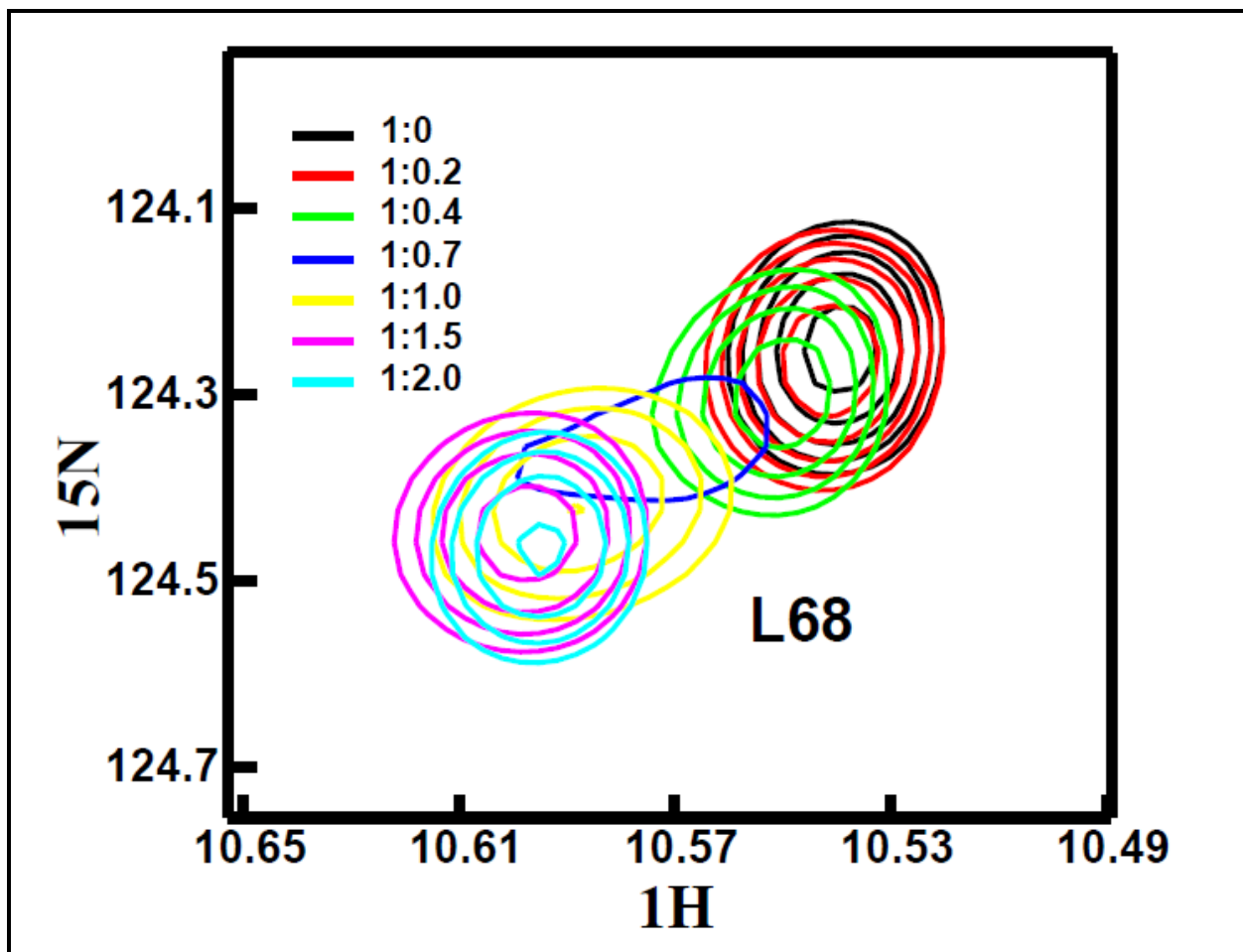


Figure 4.7 A. Resonance corresponding to Leu-68 showing the phenomenon of intermediate exchange, from the two-dimensional $\{^1\text{H}, ^{15}\text{N}\}$ HSQC spectra of delipidated ApoI PBP1 Δ P129-V142 in 50mM phosphate buffer, pH 6.5. From reference 9.

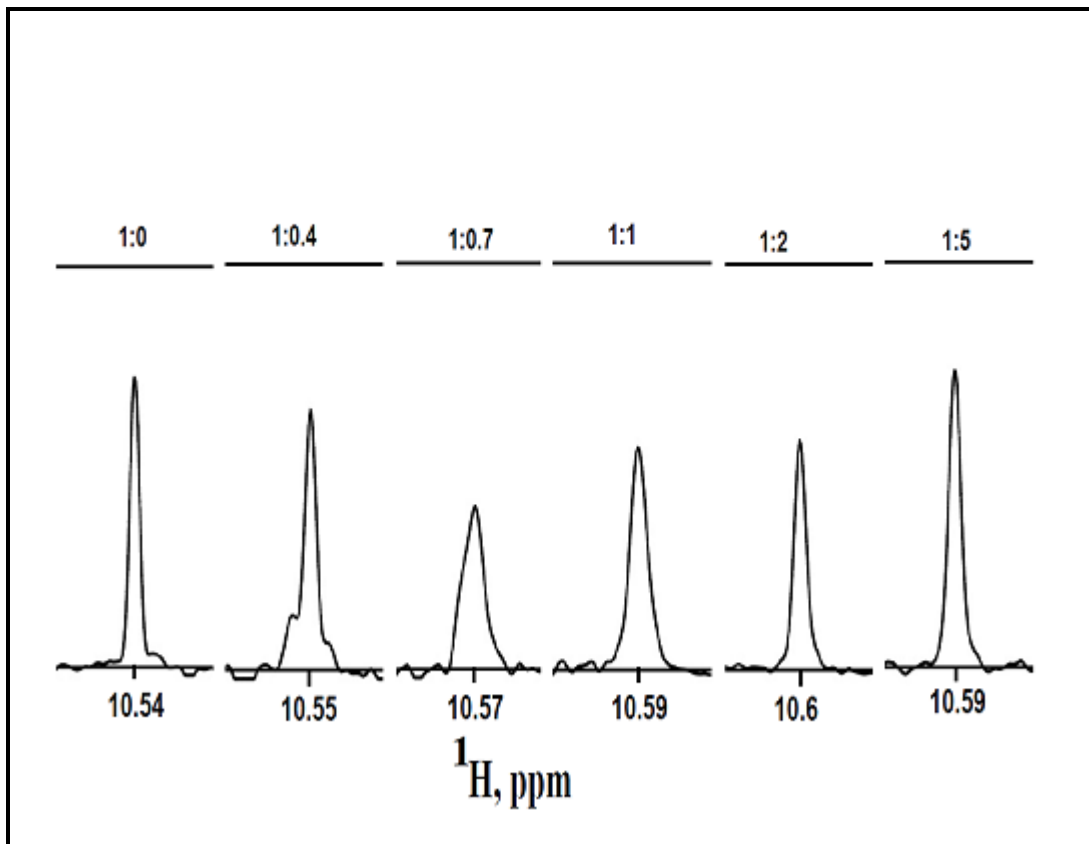


Figure 4.7 B. One-dimensional slices from the ^1H axis taken in the midpoint of the resonance corresponding to Leu-68 (same as in Figure 4.7A) showing the intermediate exchange phenomenon. Protein: ligand ratios are indicated on top of each slice. All slices are scaled relative to the same y axis. From reference 9.

4.3.4 AMA binding studies by fluorescence

The hydrophobic fluorescent dye 1-aminanthracene (AMA) fluoresces weakly in the aqueous environment after excitation at 256 or 298 nm with a λ_{max} of 563 nm. In hydrophobic environments such as the binding cavity of ApolPBP1, the fluorescence of AMA enhances considerably with a λ_{max} of ~ 480 nm. We have already used AMA titration studies to compare the binding affinities of various proteins in different conditions.⁶ In the present work, we carried out the titrations of delipidated ApolPBP1 Δ P129-V142 and ApolPBP1H70A/H95A Δ P129-V142 with AMA at pH 6.5 and 4.5. Our studies revealed that the binding of AMA to all C-terminus deleted proteins at either pH was greatly reduced as compared to ApolPBP1wt: the maximum fluorescence intensity achieved by all C-terminus deleted proteins was about 20-30 % of what was observed for the wild type protein, under the identical experimental conditions (Figure 4.8 and 4.9).⁹ The equilibrium dissociation constant (K_d) values for these proteins were 2-7 folds higher than that for the delipidated ApolPBP1wt at pH 6.5 (Table 4.1), This indicating reduced affinities of these proteins towards AMA. These results are consistent with the ligand titration studies monitored by NMR. Thus we can say that, while delipidated ApolPBP1wt and ApolPBP1H70A/H95A exhibited very strong (nanomolar) affinities for ligands, their C-terminus-deleted counterparts had much reduced affinities (in micromolar range).⁹

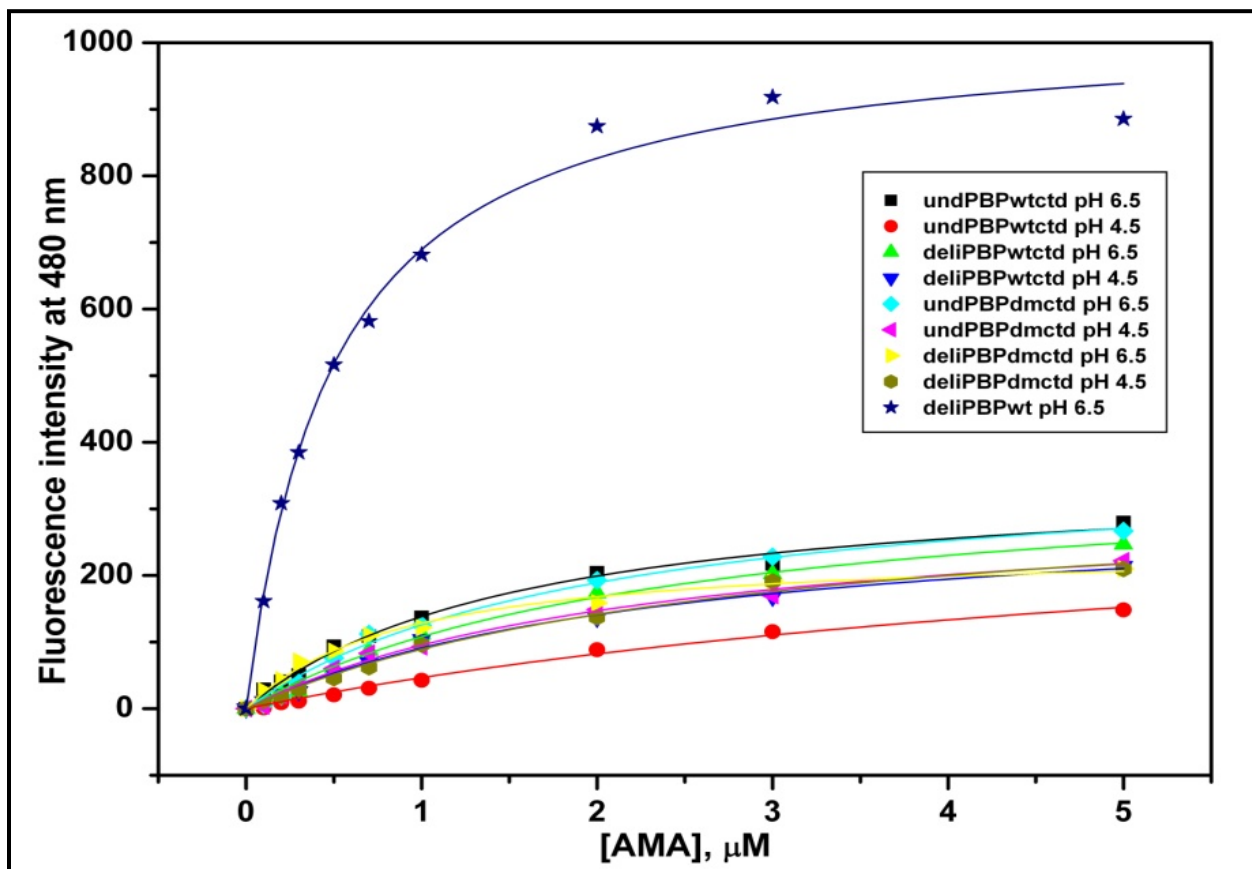


Figure 4.8 Increase in the fluorescence intensities of different ApolPBp1 samples upon addition of AMA monitored at 480 nm. Different colors corresponding to the different protein samples are indicated in the figure. From reference 9.

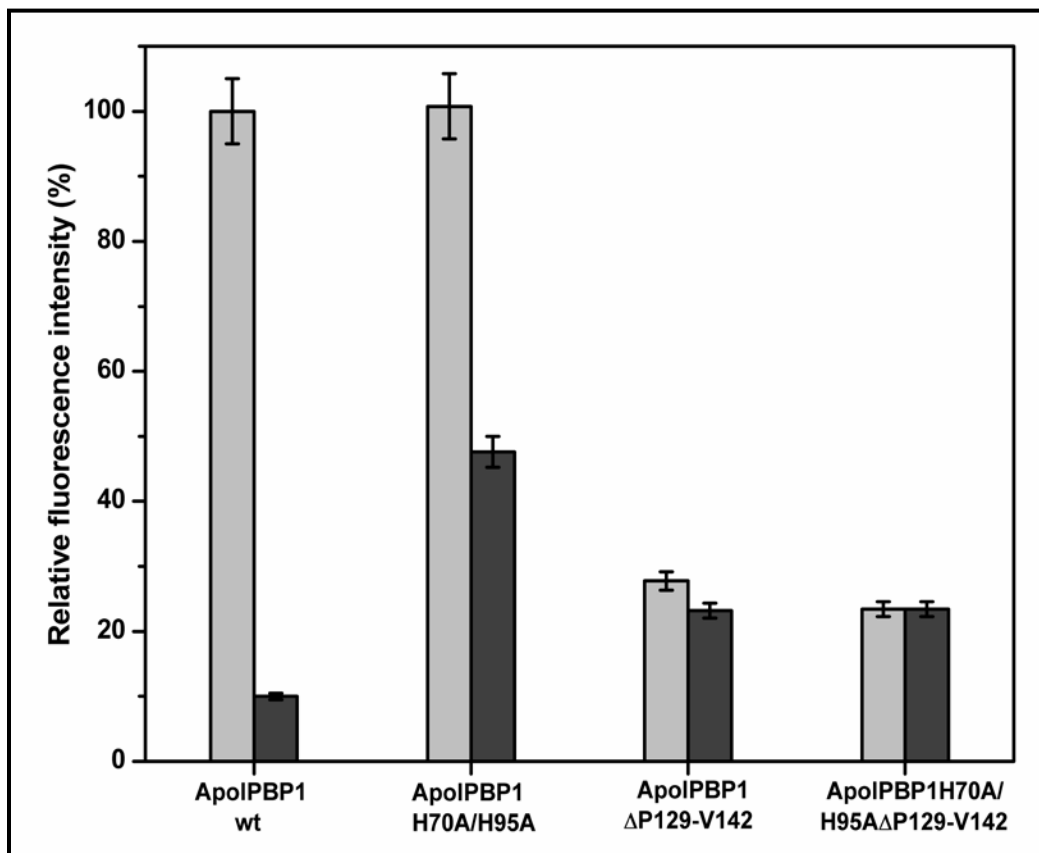


Figure 4.9 Relative fluorescence intensities of delipidated ApolPBP1 mutants upon addition of 5 μ M AMA to 1 μ M protein samples. Light grey: pH 6.5; Dark grey: pH 4.5. Error bars indicate standard deviation of the data. ApolPBP1wt and ApolPBP1H70A/H95A show similar binding at pH 6.5. ApolPBP1wt has negligible binding at pH 4.5 while ApolPBP1H70A/H95A shows considerable binding at same pH. Both ApolPBP1 Δ P129-V142 and ApolPBP1H70A/H95A Δ P129-V142 show reduced binding (20-30 % of the wild type protein at pH 6.5) at both pH 6.5 and 4.5. From reference 9.

Protein	pH	K_d (μM)
Undelipidated ApolPBP1ΔP129-V142	6.5	1.2 ± 0.16
Undelipidated ApolPBP1ΔP129-V142	4.5	3.44 ± 0.60
Delipidated ApolPBP1ΔP129-V142	6.5	2.12 ± 0.38
Delipidated ApolPBP1ΔP129-V142	4.5	2.48 ± 0.57
Undelipidated ApolPBP1H70A/H95AΔP129-V142	6.5	1.52 ± 0.21
Undelipidated ApolPBP1H70A/H95AΔP129-V142	4.5	2.13 ± 0.15
Delipidated ApolPBP1H70A/H95AΔP129-V142	6.5	2.90 ± 0.68
Delipidated ApolPBP1H70A/H95AΔP129-V142	4.5	0.92 ± 0.16
Delipidated ApolPBP1wt	6.5	0.5 ± 0.09

Table 4.1: Dissociation constant (K_d) values for the binding of AMA to various mutants of ApolPBP1, determined using the increase in AMA fluorescence at 480 nm.

4.3.5 Effect of mutations on C-terminus

To investigate whether three charged residues (Asp132, Glu137 and Glu141) located in the C-terminus of ApolPBP1 play any role in the formation of the seventh helix (C-terminus) that facilitates the ligand release, we mutated Asp132, Glu137 and Glu141 into Asn132, Gln137 and Gln141, respectively to produce single mutant proteins ApolPBP1D132N, ApolPBP1E137Q and ApolPBP1E141Q. We also produced double-mutants (ApolPBP1D132NE137Q and ApolPBP1 E137QE141Q) and triple-mutant proteins (ApolPBP1D132NE137QE141Q).

We observed that the HSQC spectrum of the undelipidated single-mutant ApolPBP1D132N at pH 6.5 resembled the undelipidated HSQC spectrum of the wild type protein (Figure 4.10B), while at pH 4.5, the HSQC of the undelipidated ApolPBP1D132N resembled to that of the delipidated spectrum of the wild type protein (Figure 4.10A). So ApolPBP1D132N behaved exactly the same at high and low pH levels as the wild type protein (Figure 4.11A and 4.11B), though a few resonances were shifted due to the effect of mutation. Two other single mutant proteins, ApolPBP1E137Q and ApolPBP1E141Q also showed the same characteristics as wild type protein (Figure 4.10C, 4.10D, 4.10E and 4.10F). All these proteins exhibited the ligand-bound conformation at pH 6.5 and the ligand-free conformation at pH 4.5 similar to the wild-type protein (Figure 4.11C, 4.11D, 4.11E and 4.11 F).

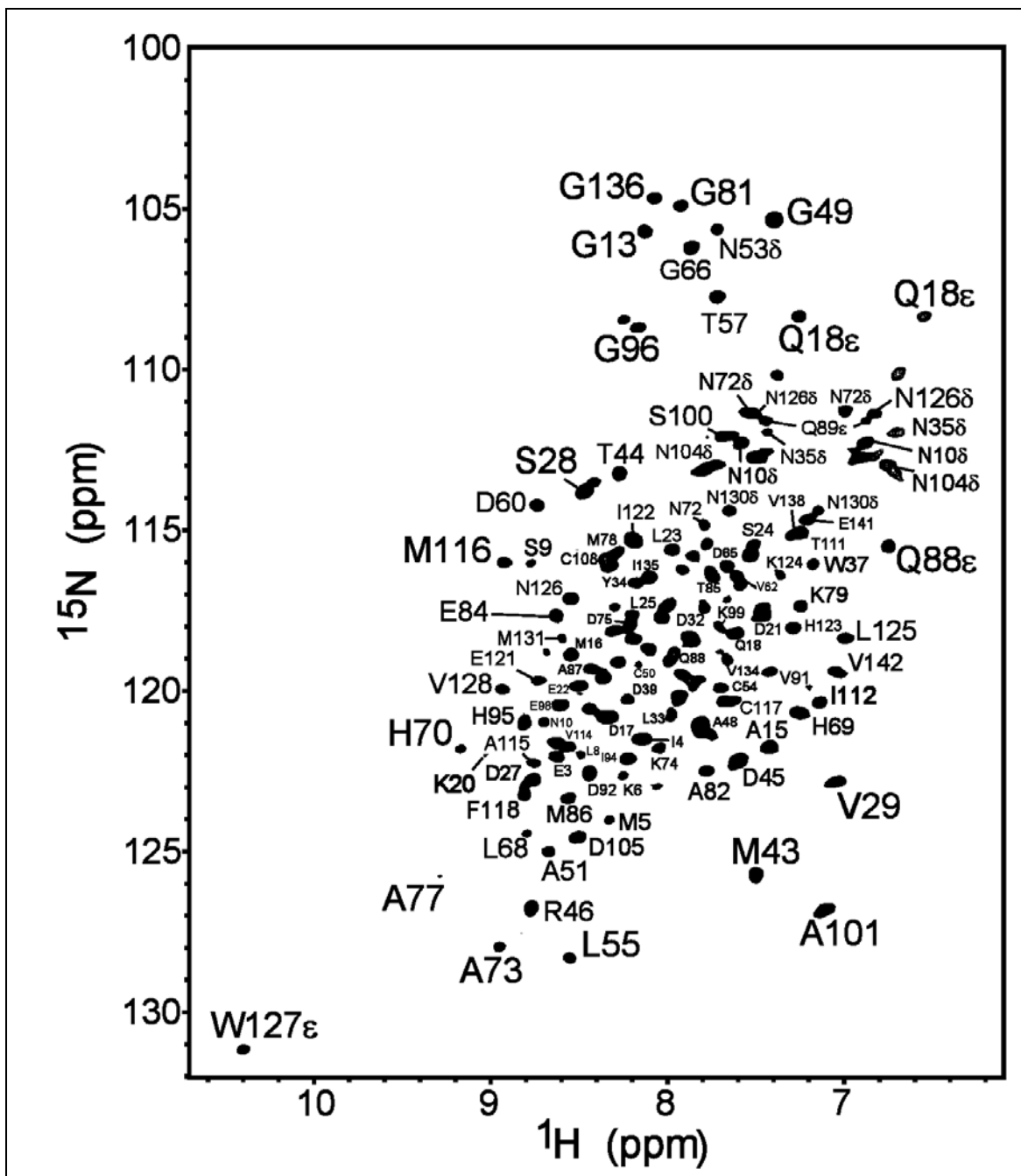


Figure 4.10 A. Two-dimensional $\{^1\text{H}, ^{15}\text{N}\}$ HSQC spectra of undelipidated ApolPBP1D132N in 50 mM sodium phosphate buffer at pH 4.5. The spectrum resembles to the ligand-free conformation of the ApolPBP1 wt protein.

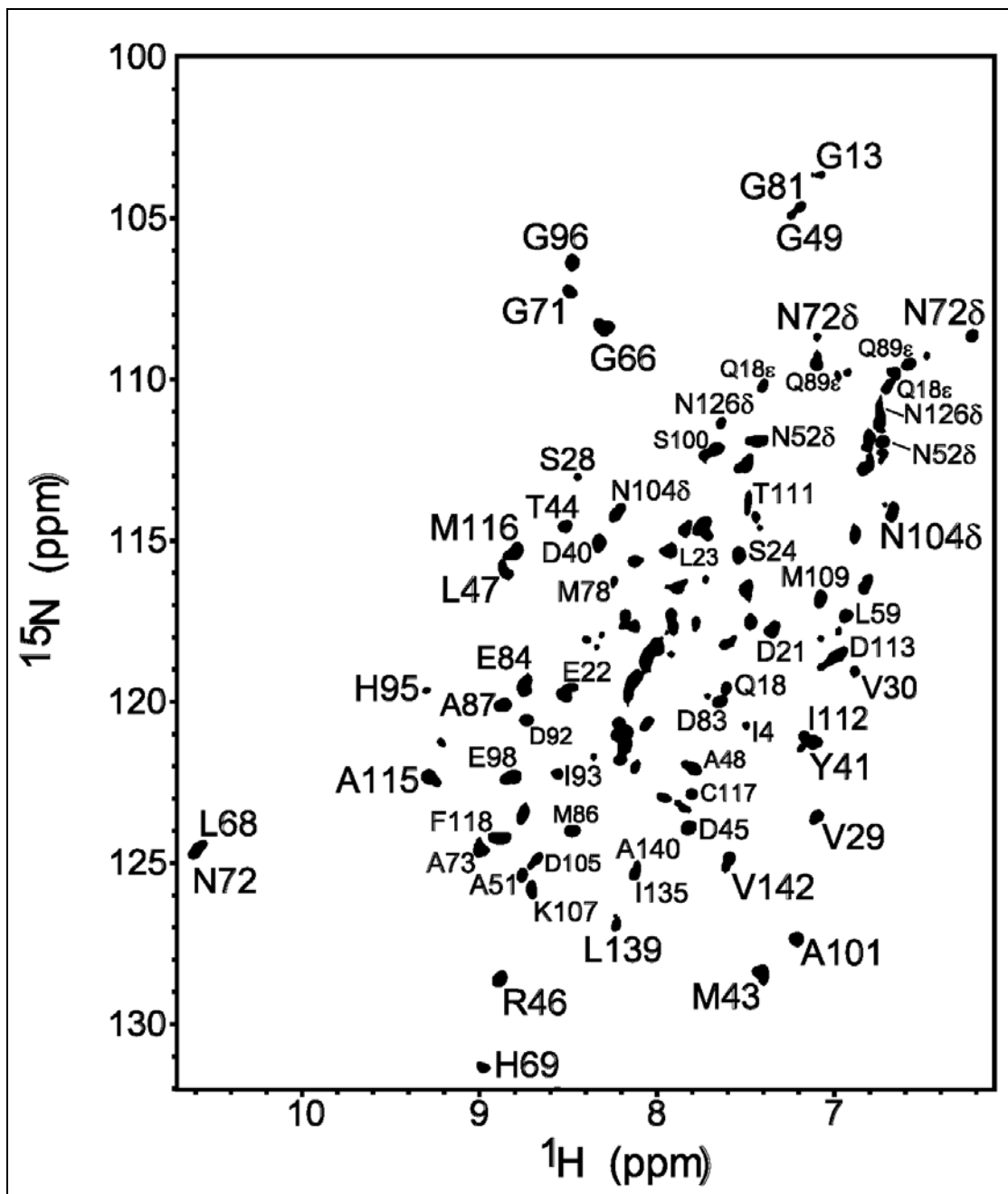


Figure 4.10 B. Two-dimensional $\{^1\text{H}, ^{15}\text{N}\}$ HSQC spectra of undelipidated ApolPBP1D132N in 50 mM sodium phosphate buffer at pH 6.5. The spectrum resembles to the ligand-bound conformation of the ApolPBP1wt protein.

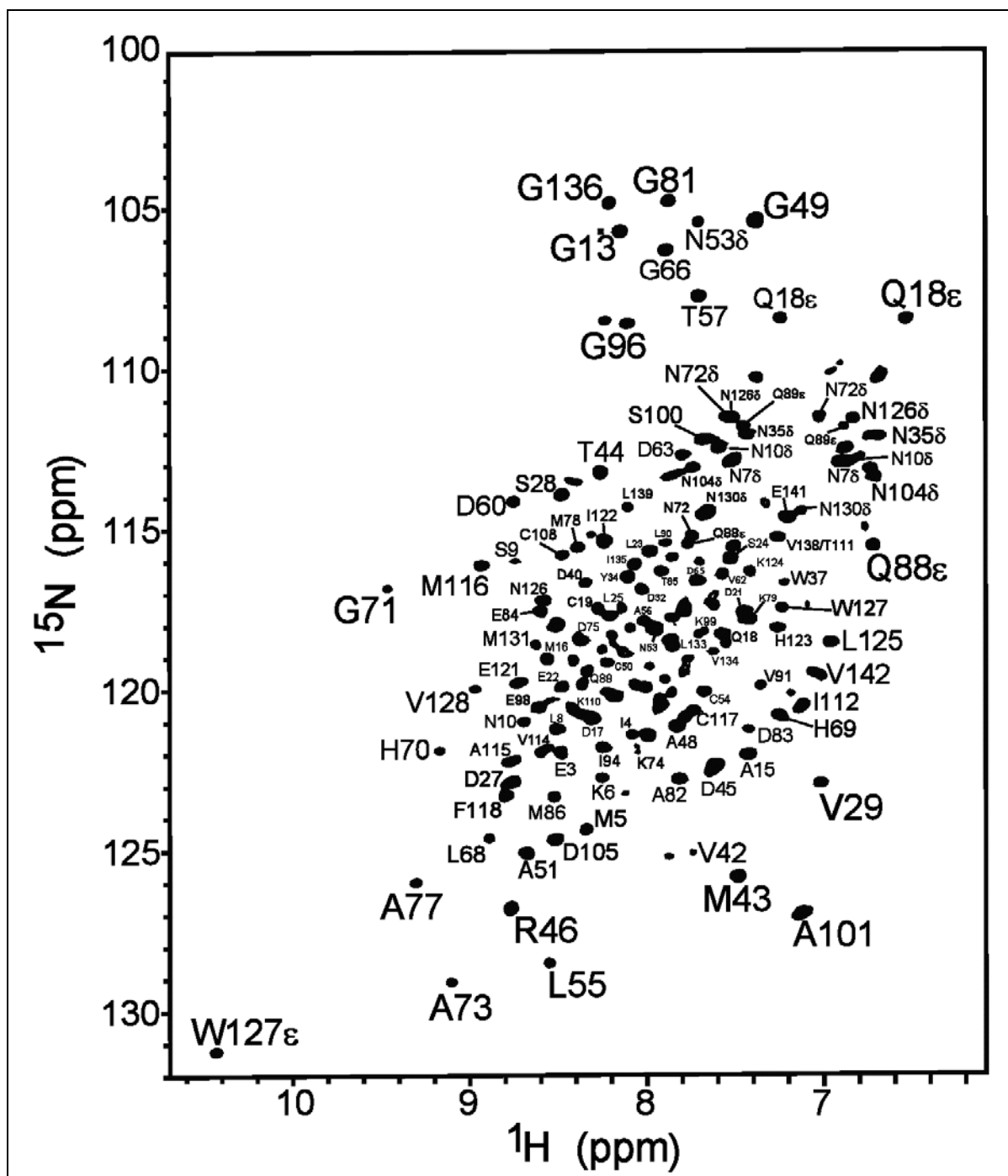


Figure 4.10 C. Two-dimensional $\{^1\text{H}, ^{15}\text{N}\}$ HSQC spectra of undelipidated ApolPBP1E137Q in 50 mM sodium phosphate buffer at pH 4.5. The spectrum resembles to the ligand-free conformation of the ApolPBP1wt protein.

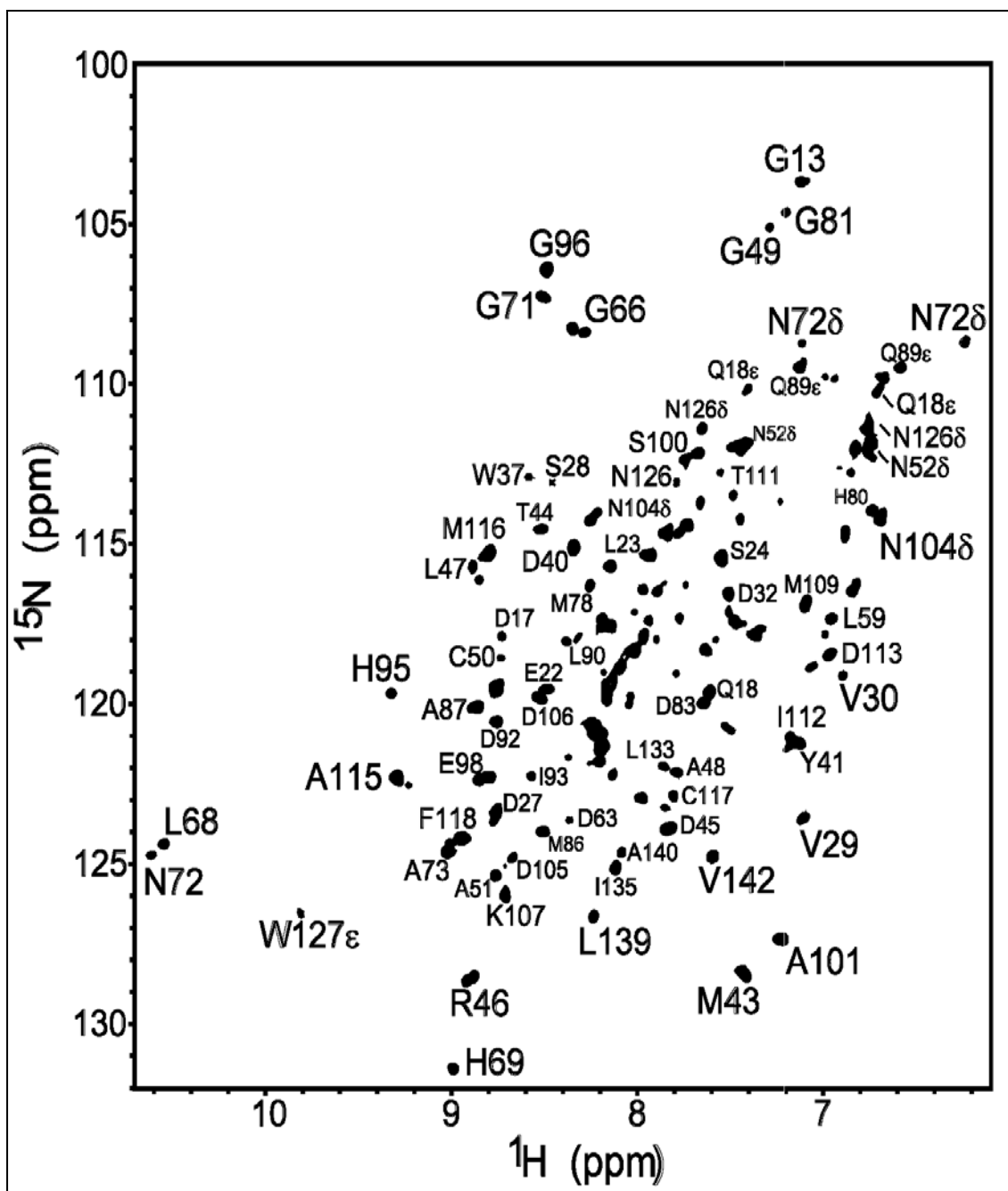


Figure 4.10 D. Two-dimensional $\{^1\text{H}, ^{15}\text{N}\}$ HSQC spectra of undelipidated ApolPBP1E137Q in 50 mM sodium phosphate buffer at pH 6.5. The spectrum resembles to the ligand-bound conformation of the ApolPBP1wt protein.

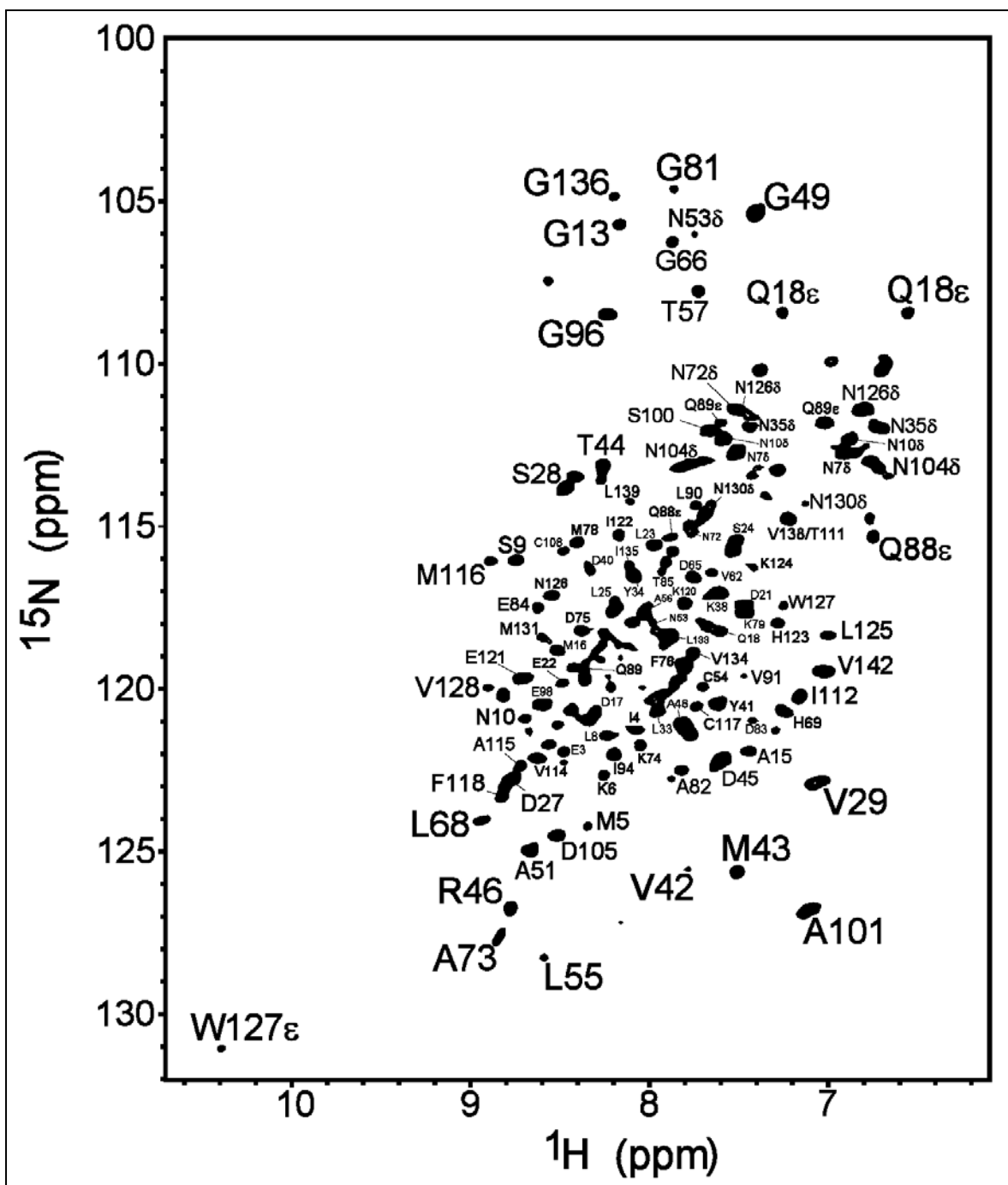


Figure 4.10 E. Two-dimensional $\{^1\text{H}, ^{15}\text{N}\}$ HSQC spectra of undelipidated ApolPBPIE141Q in 50 mM sodium phosphate buffer at pH 4.5. The spectrum resembles to the ligand-free conformation of the ApolPBPI wt protein.

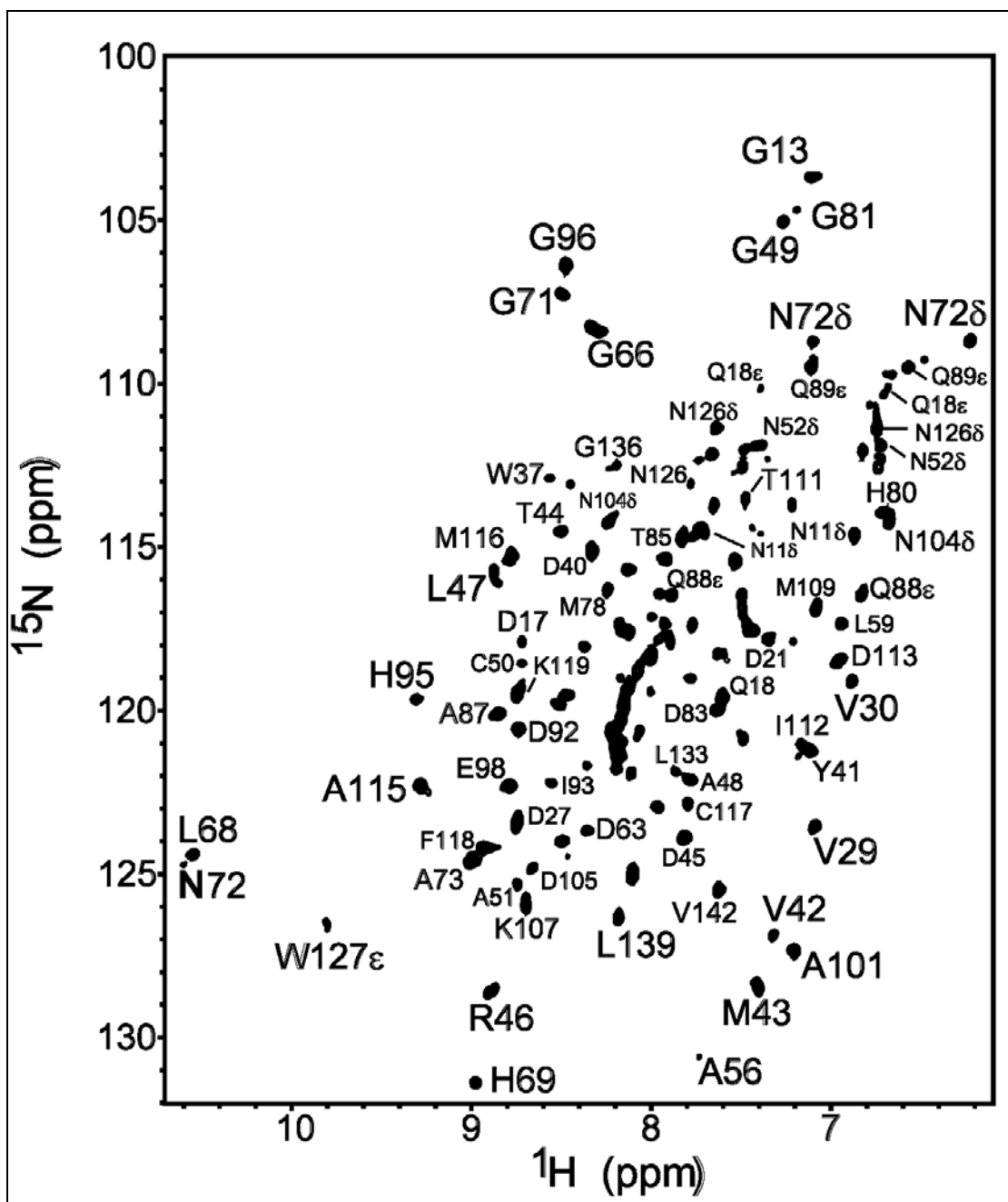


Figure 4.10 F. Two-dimensional $\{^1\text{H}, ^{15}\text{N}\}$ HSQC spectra of undelipidated ApolPBP1E141Q in 50 mM sodium phosphate buffer at pH 6.5. The spectrum resembles to the ligand-bound conformation of the ApolPBP1wt protein.

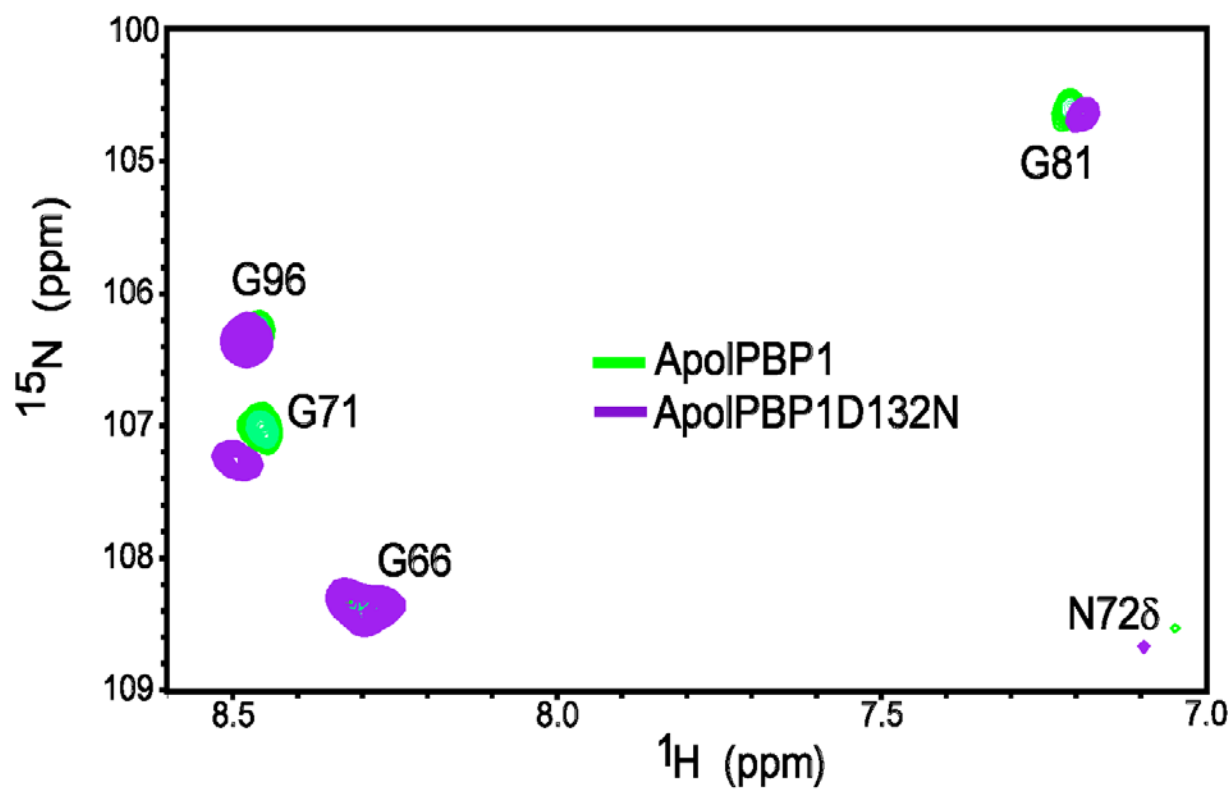


Figure 4.11 A. Expanded region of Two-dimensional $\{^1\text{H}, ^{15}\text{N}\}$ HSQC spectra of undelipidated ApolPBP1D132N and ApolPBP1wt proteins at pH 6.5. Green color: ApolPBP1wt (ligand-bound form); Violet color: ApolPBP1D132N.

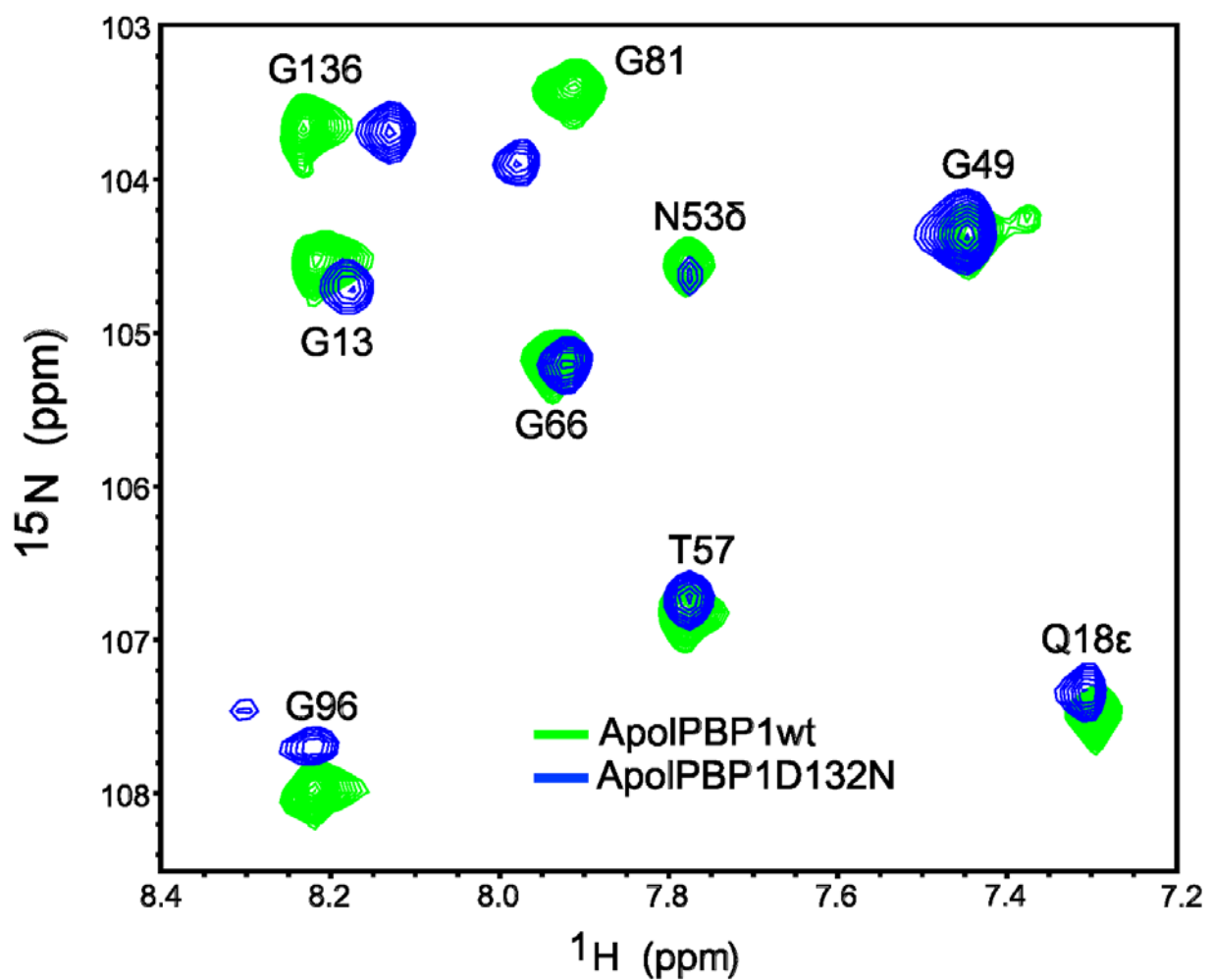


Figure 4.11 B. Expanded region of Two-dimensional $\{^1\text{H}, ^{15}\text{N}\}$ HSQC spectra of undelipidated ApolPBP1D132N and ApolPBP1wt proteins at pH 4.5. Green color: ApolPBP1wt (ligand-free form); Blue color: ApolPBP1D132N.

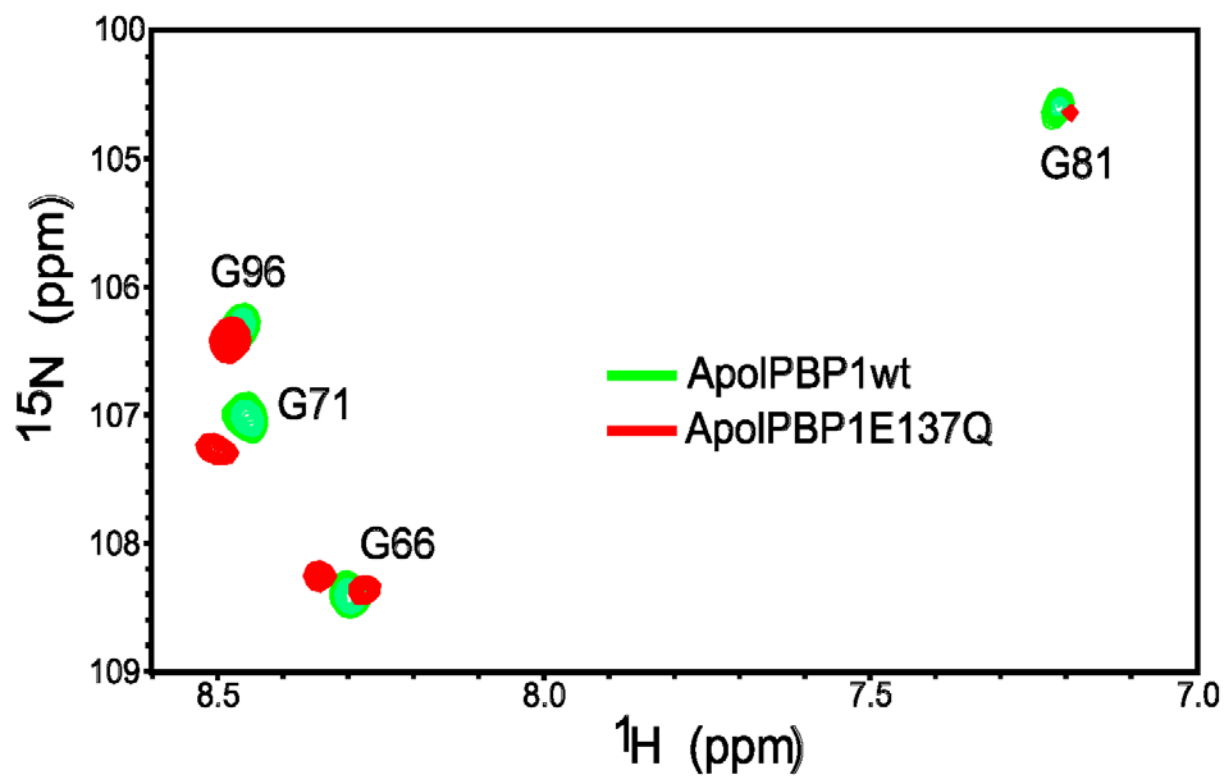


Figure 4.11 C. Expanded region of Two-dimensional $\{^1\text{H}, ^{15}\text{N}\}$ HSQC spectra of undelipidated ApolPBP1E137Q and ApolPBP1wt proteins at pH 6.5. Green color: ApolPBP1wt (ligand-bound form); Red color: ApolPBP1E137Q.

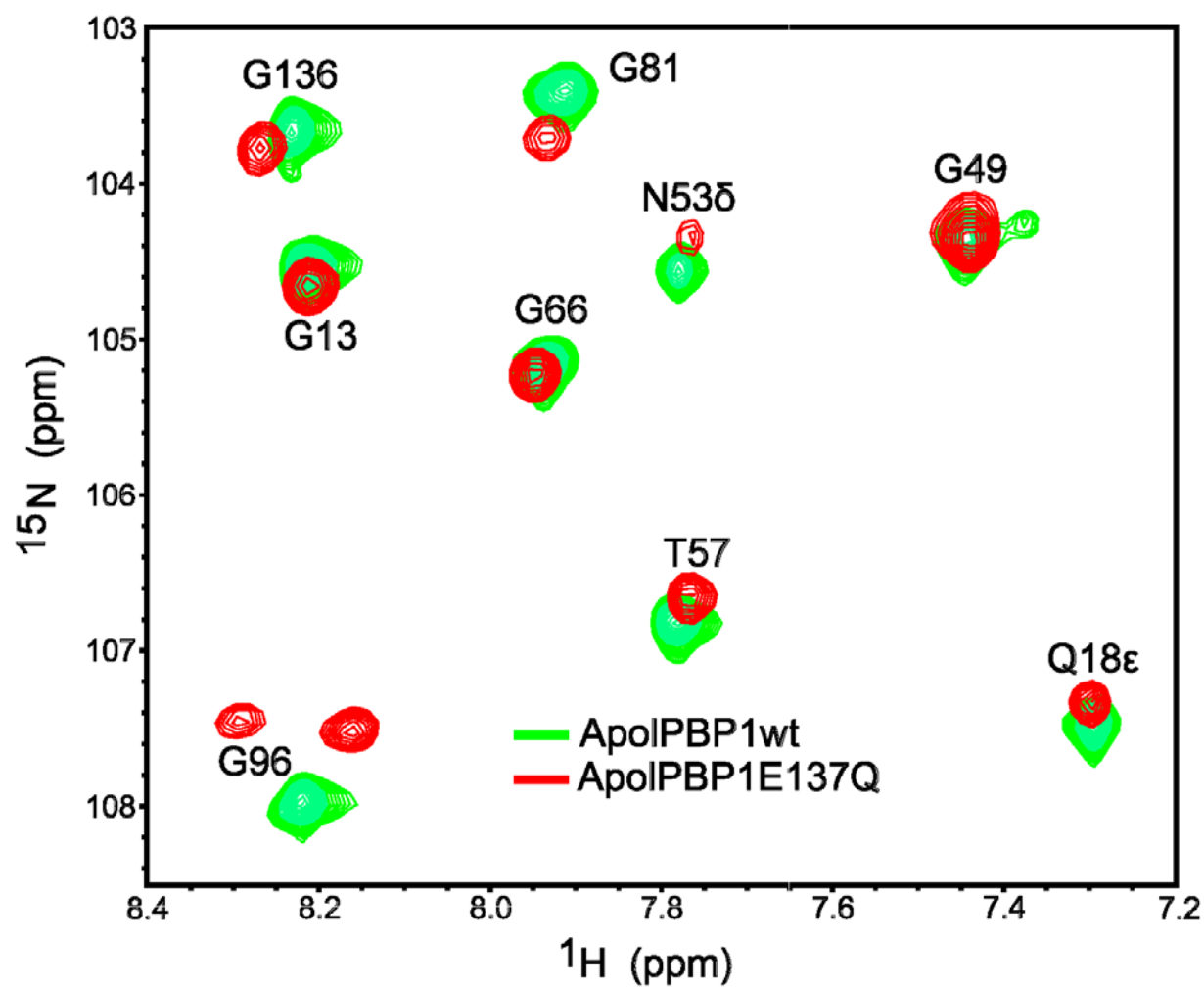


Figure 4.11 D. Expanded region of Two-dimensional $\{^1\text{H}, ^{15}\text{N}\}$ HSQC spectra of undelipidated ApolPBP1E137Q and ApolPBP1wt proteins at pH 4.5. Green color: ApolPBP1wt (ligand-free form); Red color: ApolPBP1E137Q.

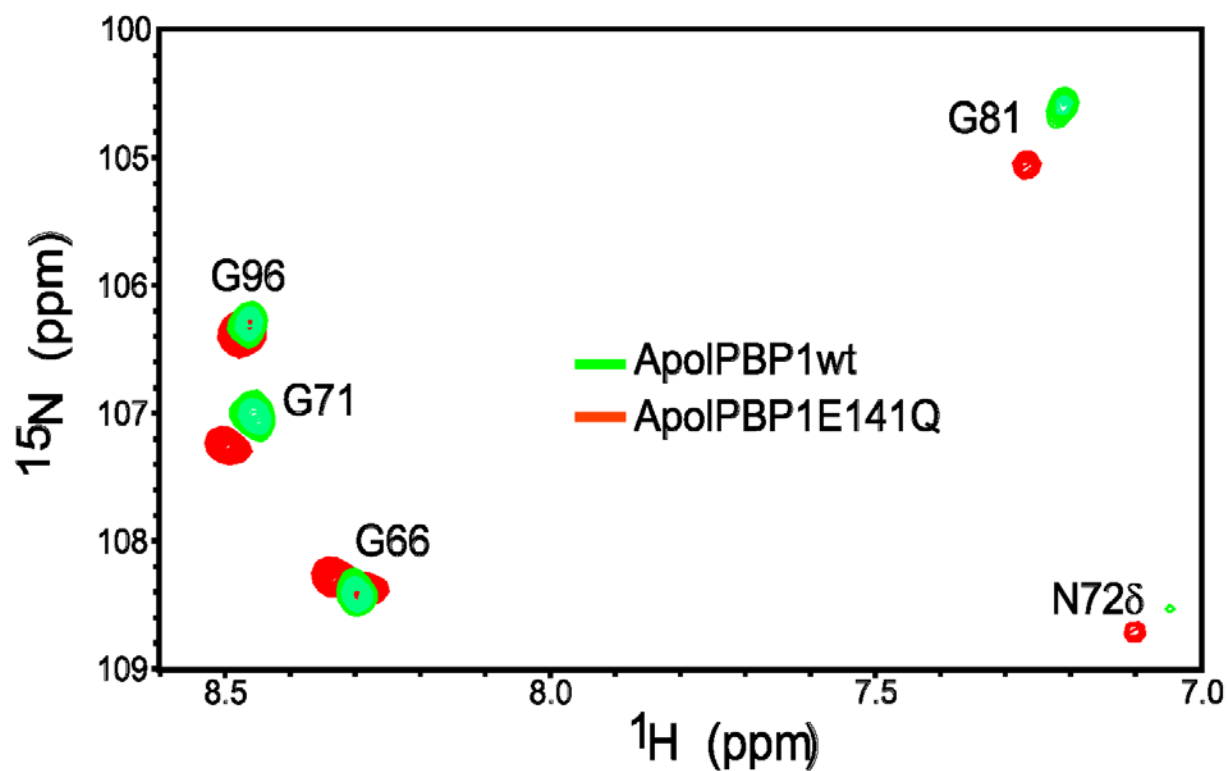


Figure 4.11 E. Expanded region of Two-dimensional $\{^1\text{H}, ^{15}\text{N}\}$ HSQC spectra of undelipidated ApolPBP1E141Q and ApolPBP1wt proteins at pH 6.5. Green color: ApolPBP1wt (ligand-bound form); Red color: ApolPBP1E141Q.

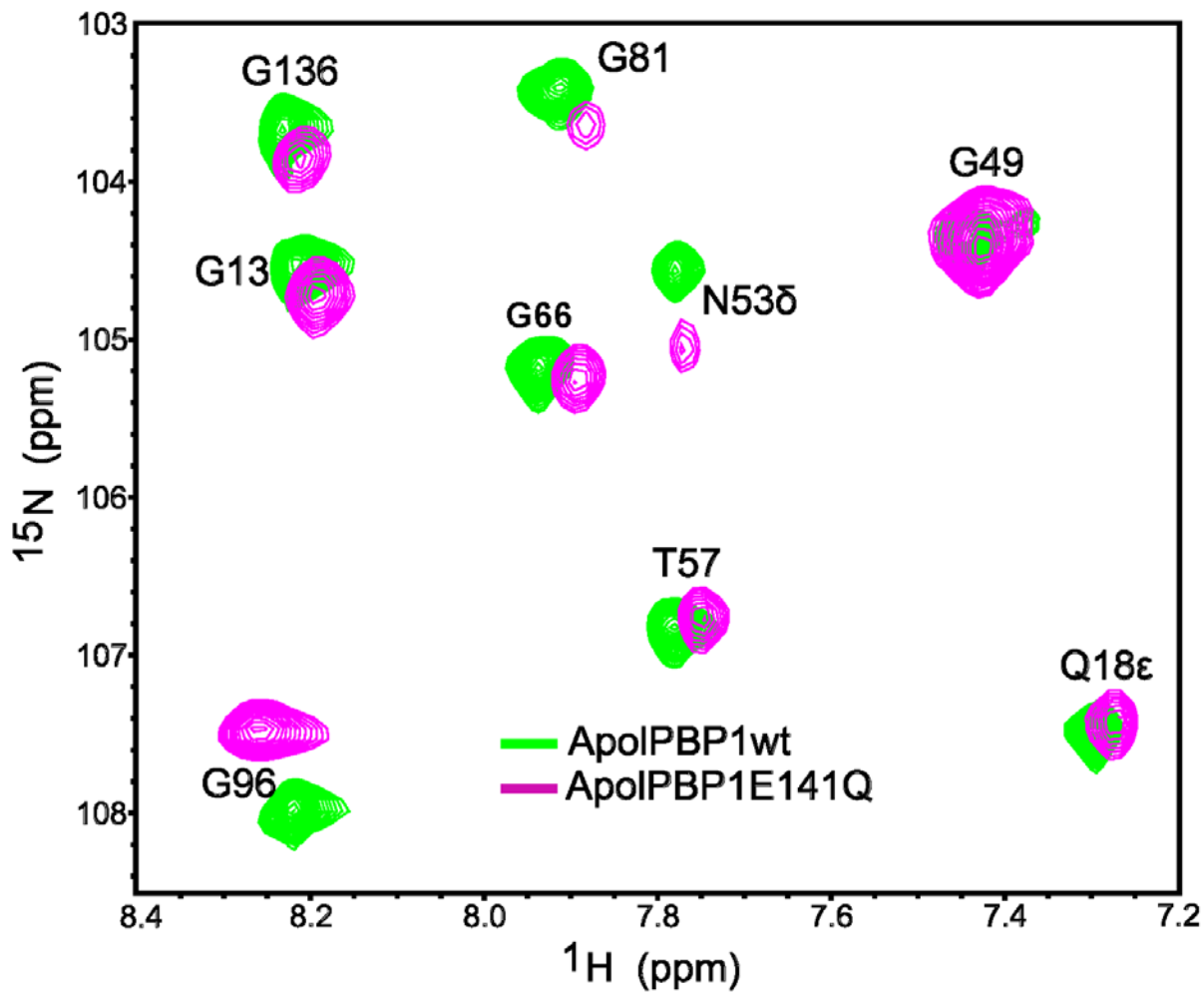


Figure 4.11 F. Expanded region of Two-dimensional $\{^1\text{H}, ^{15}\text{N}\}$ HSQC spectra of undelipidated ApolPBP1E141Q and ApolPBP1wt proteins at pH 4.5. Green color: ApolPBP1wt (ligand-free form); Magenta color: ApolPBP1E141Q.

For the undelipidated double-mutants ApolPBP1D132NE137Q and ApolPBP1E137QE141Q, similar phenomena were observed as for the single mutant proteins (Figure 4.12A, 4.12B, 4.12C, 4.12D, 4.13A, 4.13B, 4.13C and 4.13D). However, these preliminary observations must be investigated further to determine the effect of the mutation, pH and delipidation on protein conformation. For delipidated double-mutants ApolPBP1D132NE137Q and ApolPBP1E137QE141Q, similar phenomena were observed as for the single mutant proteins (Figure 4.14A, 4.14B, 4.14C, 4.14D, 4.15A and 4.15B), again any final conclusion is not possible until further detailed biophysical studies are carried out.

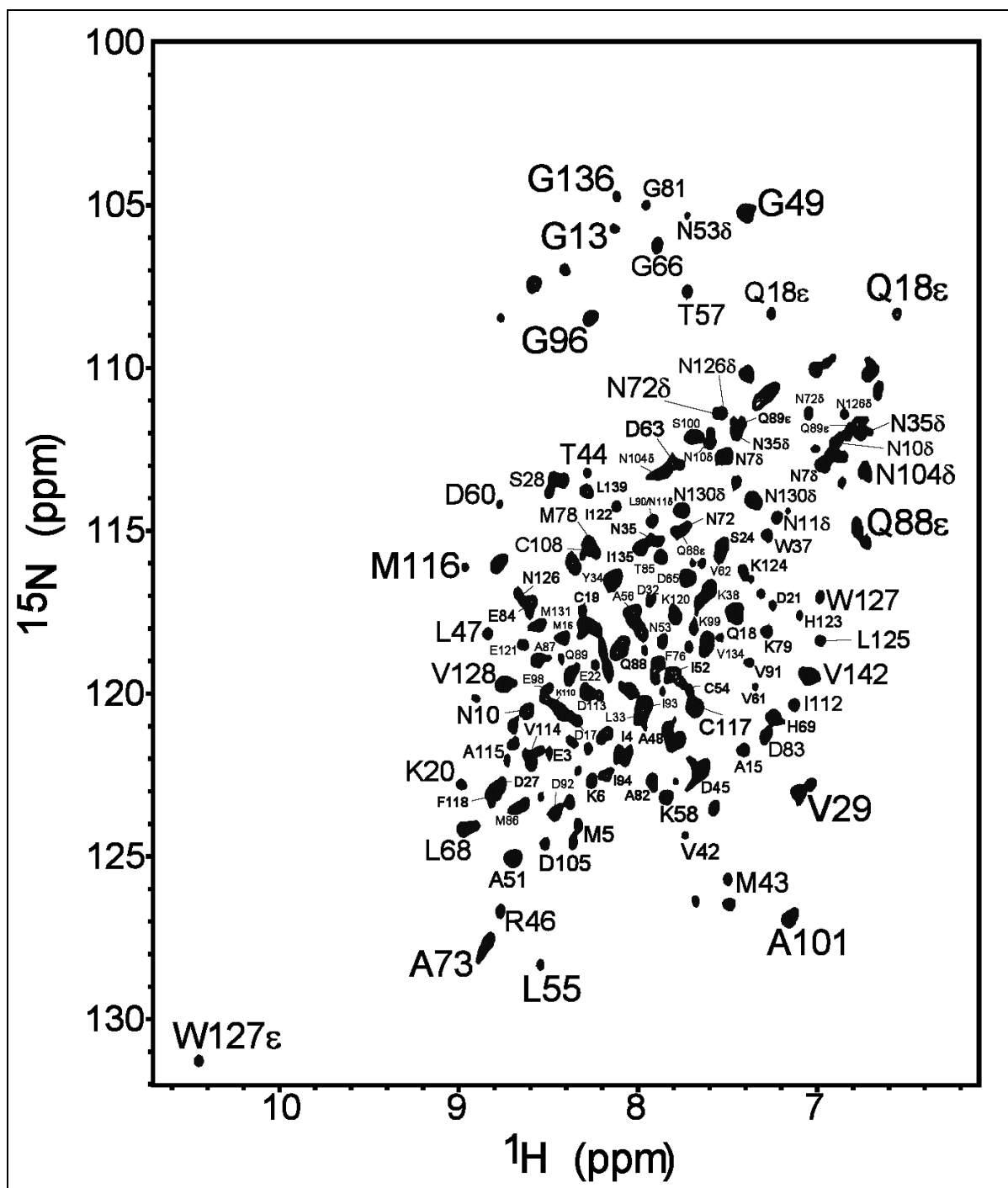


Figure 4.12 A. Two-dimensional $\{^1\text{H}, ^{15}\text{N}\}$ HSQC spectra of undelipidated ApolPBP1D132NE137Q in 50 mM sodium phosphate buffer at pH 4.5. The spectrum resembles to the ligand-free conformation of the ApolPBP1wt protein.

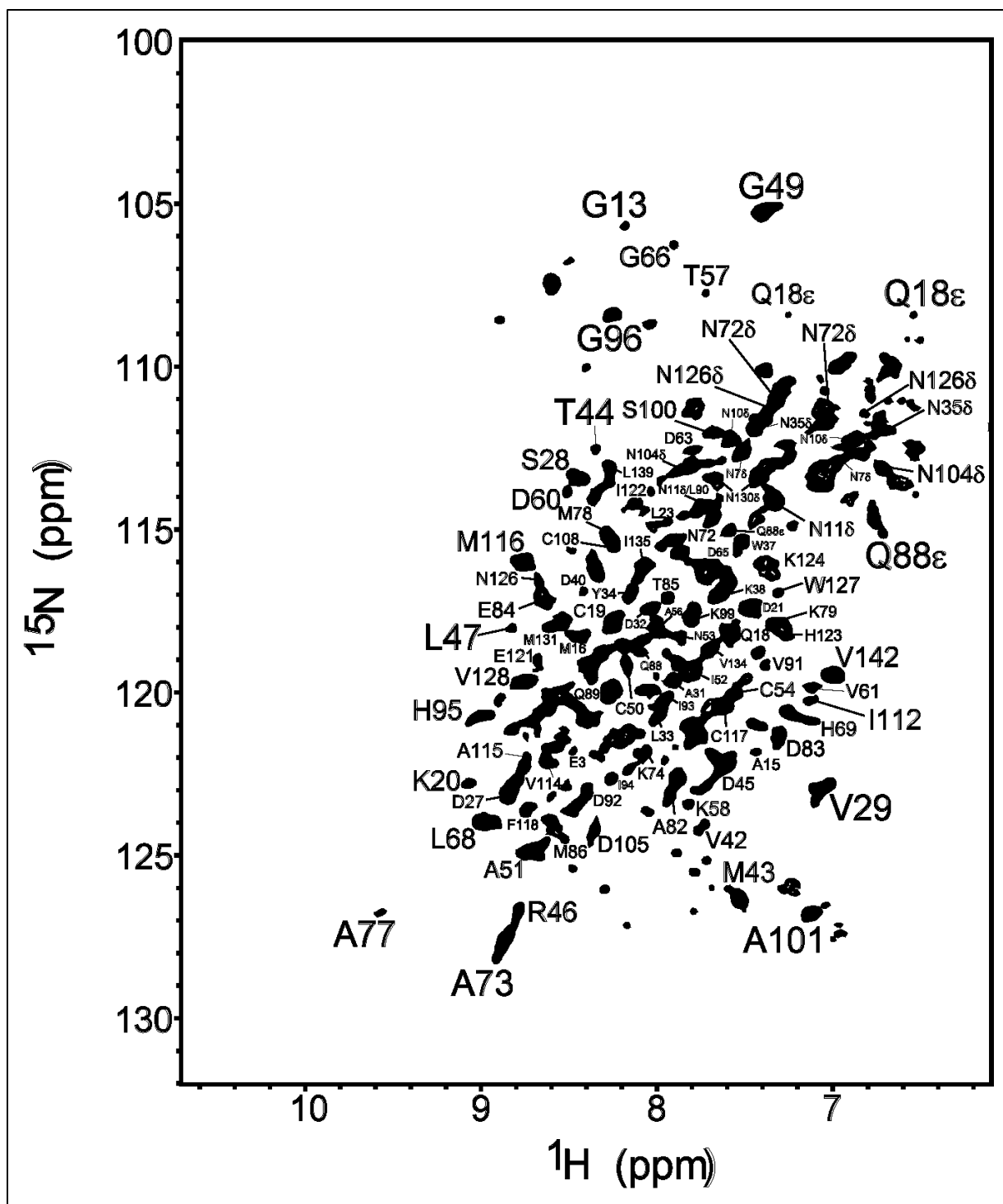


Figure 4.12 B. Two-dimensional $\{^1\text{H}, ^{15}\text{N}\}$ HSQC spectra of undelipidated ApolPBP1E137QE141Q in 50 mM sodium phosphate buffer at pH 4.5.

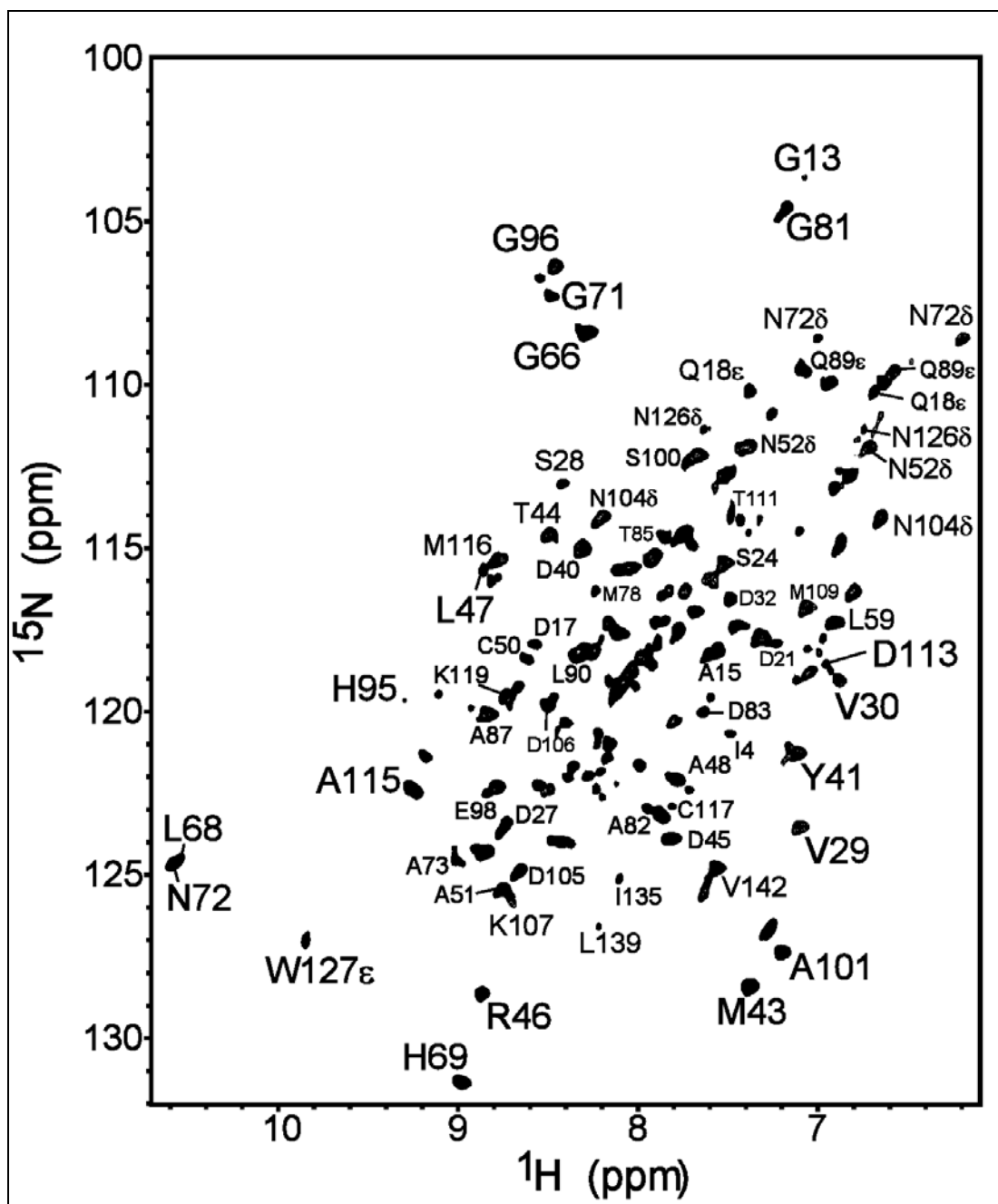


Figure 4.12 C. Two-dimensional $\{^1\text{H}, ^{15}\text{N}\}$ HSQC spectra of undelipidated ApolPBP1D132NE137Q in 50 mM sodium phosphate buffer at pH 6.5. The spectrum resembles to the ligand-bound conformation of the ApolPBP1wt protein.

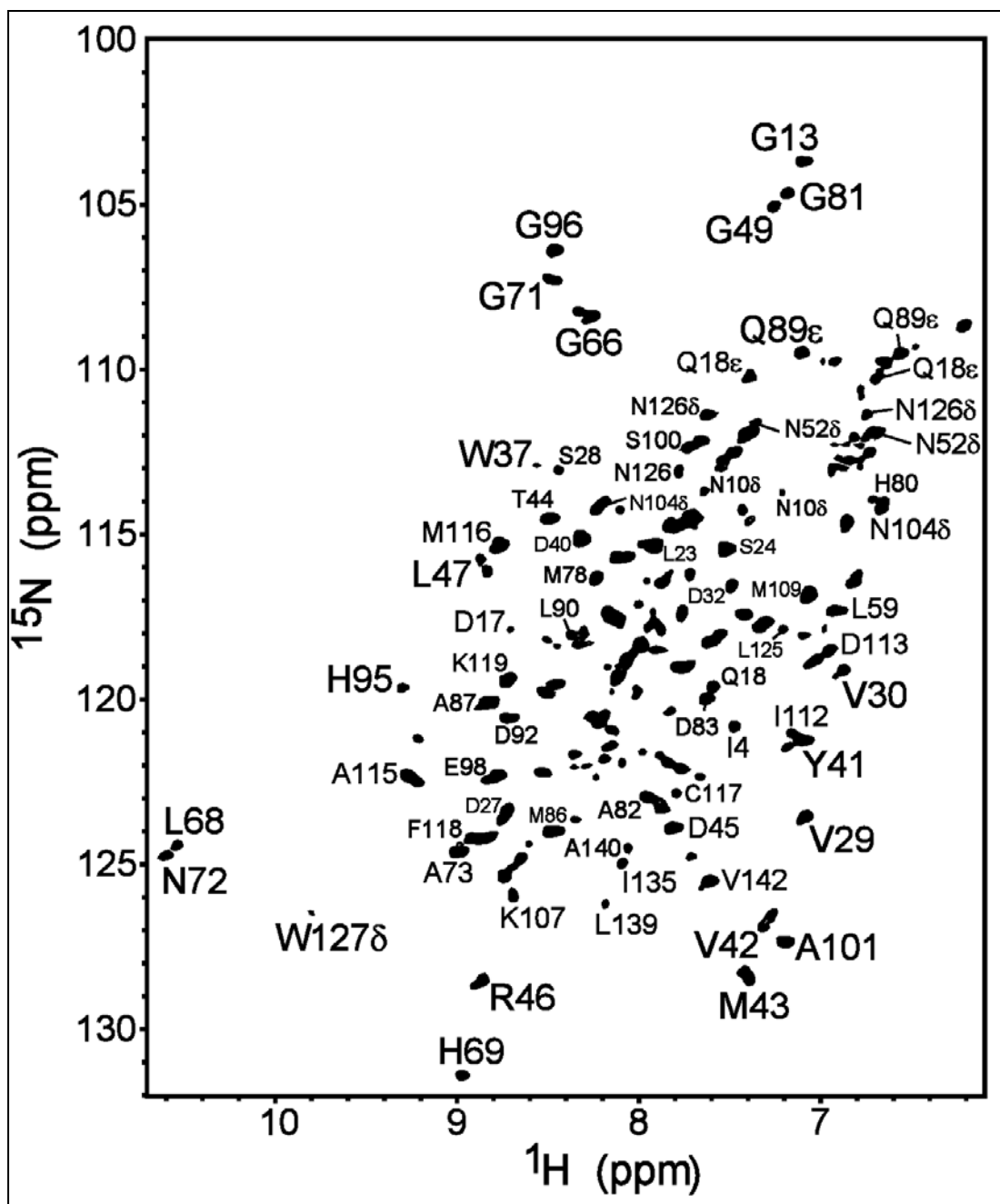


Figure 4.12 D. Two-dimensional $\{^1\text{H}, ^{15}\text{N}\}$ HSQC spectra of undelipidated ApolPBP1E137QE141Q in 50 mM sodium phosphate buffer at pH 6.5. The spectrum resembles to the ligand-bound conformation of the ApolPBP1wt protein.

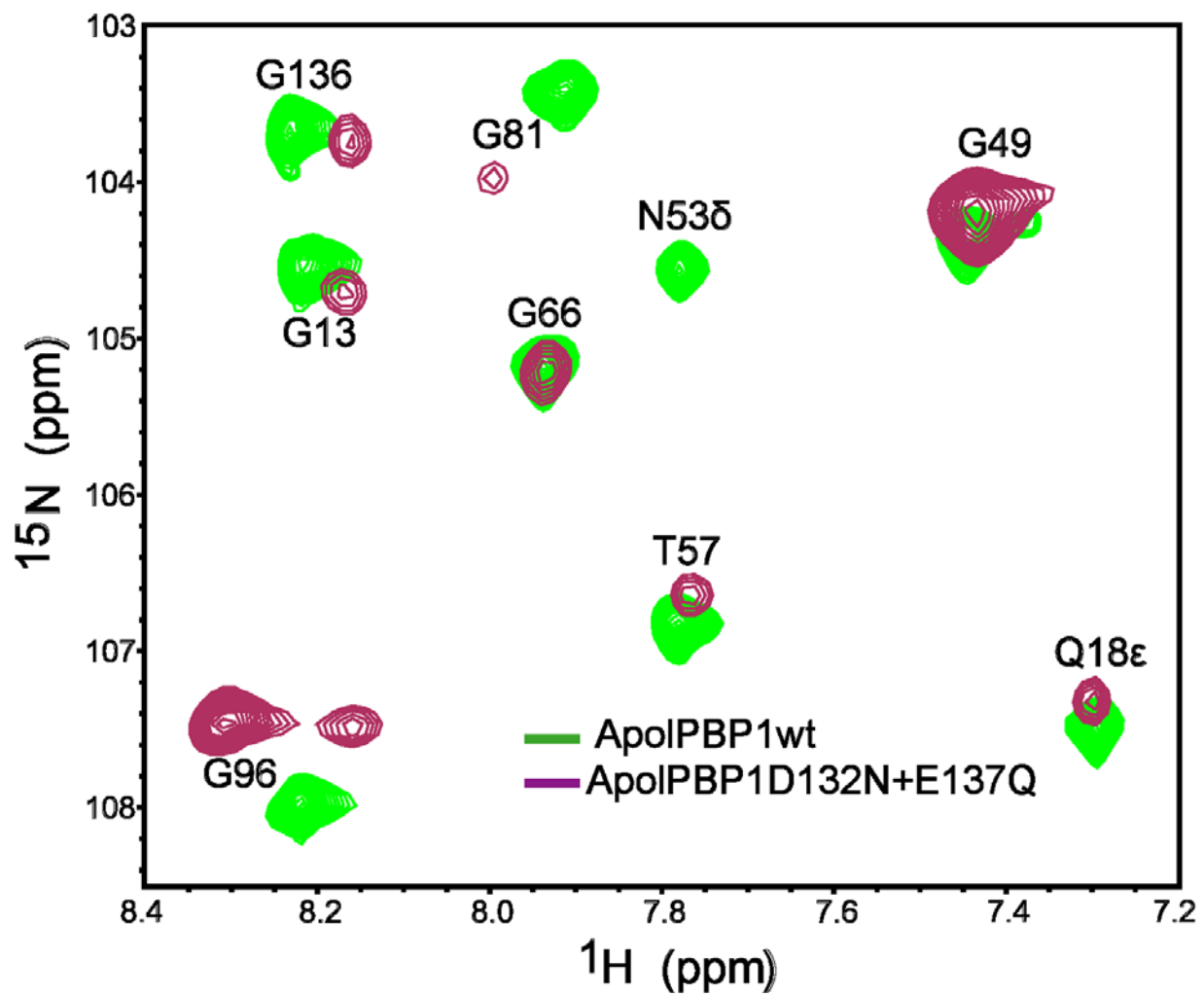


Figure 4.13 A. Expanded region of Two-dimensional $\{^1\text{H}, ^{15}\text{N}\}$ HSQC spectra of undelipidated ApolPBP1D132NE137Q and ApolPBP1wt proteins at pH 4.5. Green color: ApolPBP1wt (ligand-free form); Magenta color: ApolPBP1D132NE137Q.

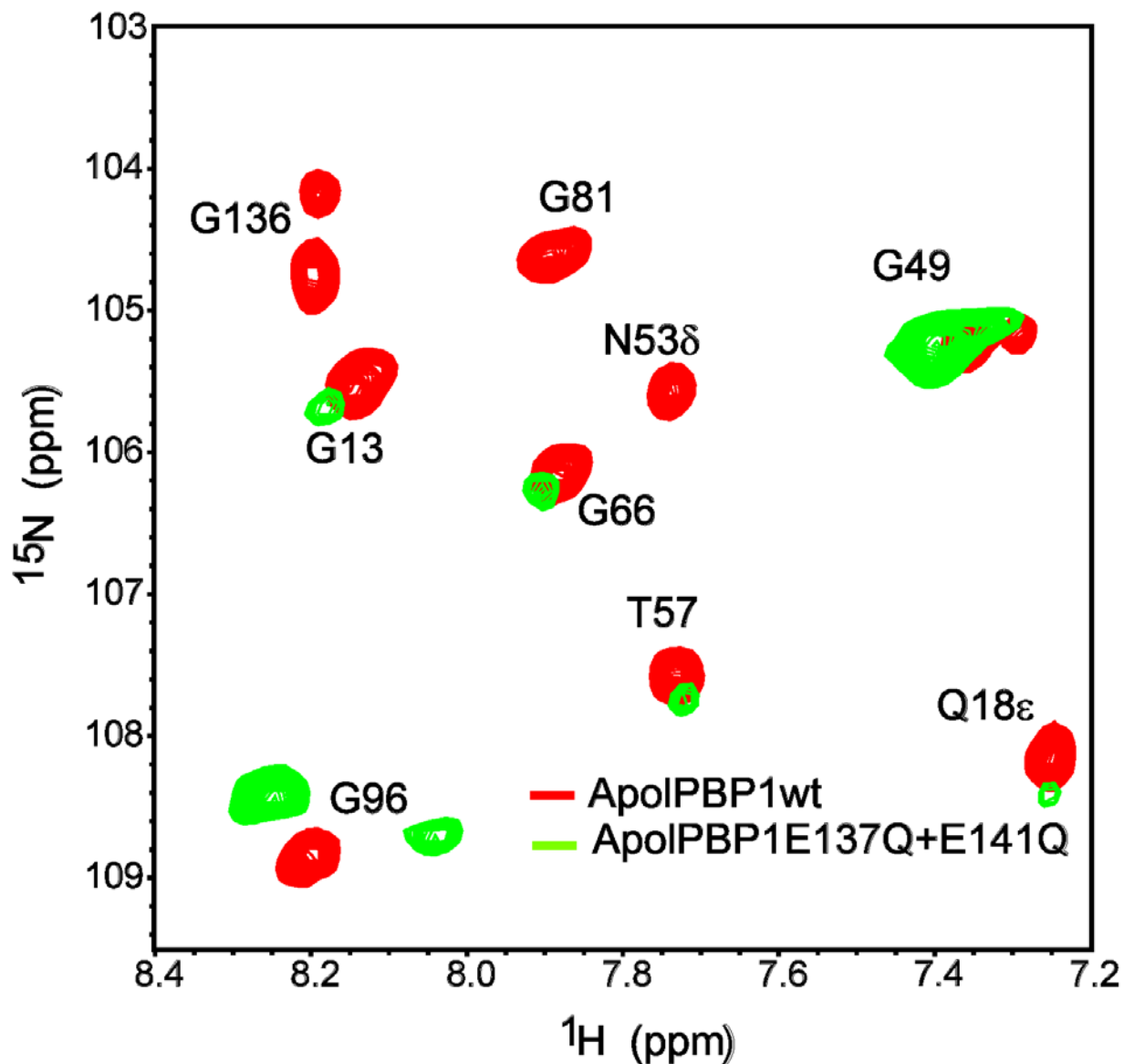


Figure 4.13 B. Expanded region of Two-dimensional $\{^1\text{H}, ^{15}\text{N}\}$ HSQC spectra of undelipidated ApolPBP1E137QE141Q and ApolPBP1wt proteins at pH 4.5. Red color: ApolPBP1wt (ligand-free form); Green color: ApolPBP1E137QE141Q.

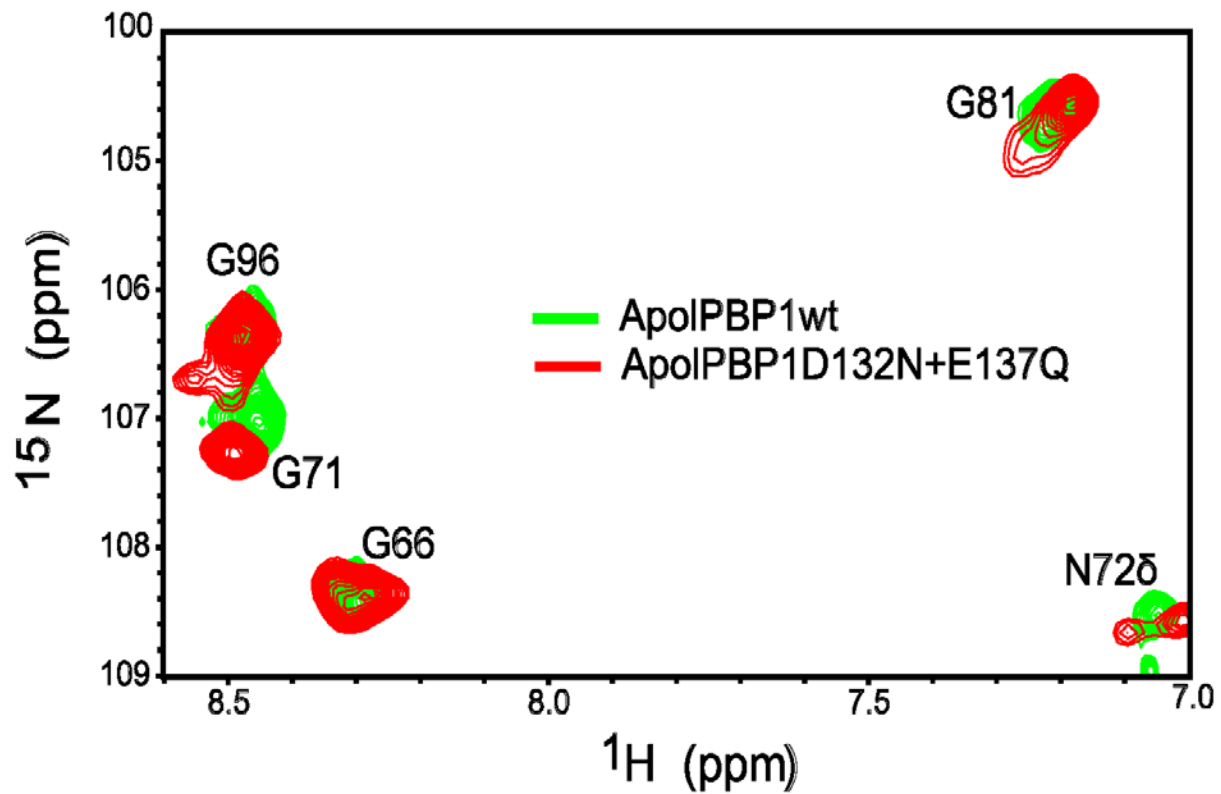


Figure 4.13 C. Expanded region of Two-dimensional $\{^1\text{H}, ^{15}\text{N}\}$ HSQC spectra of undelipidated ApolPBP1D132NE137Q and ApolPBP1wt proteins at pH 6.5. Green color: ApolPBP1wt (ligand-bound form); Red color: ApolPBP1D132NE137Q.

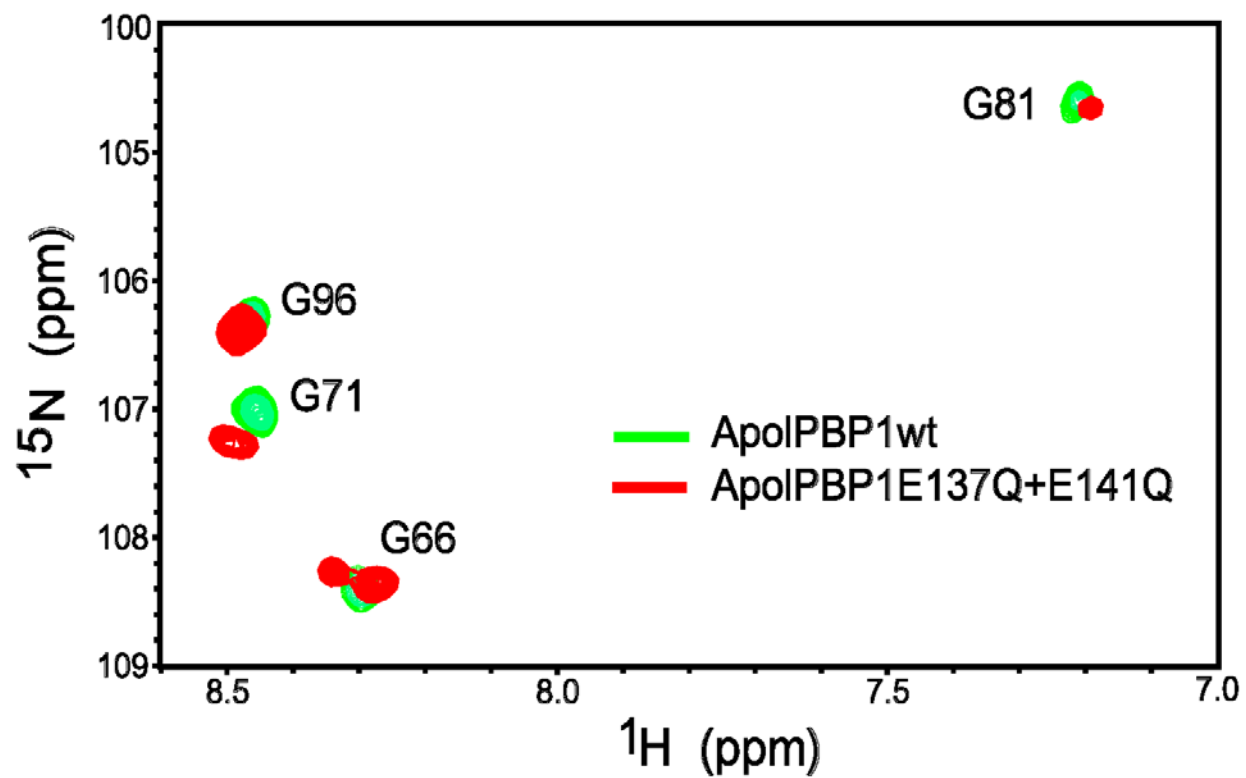


Figure 4.13 D. Expanded region of Two-dimensional $\{^1\text{H}, ^{15}\text{N}\}$ HSQC spectra of undelipidated ApolPBP1E137QE141Q and ApolPBP1wt proteins at pH 6.5. Green color: ApolPBP1wt (ligand-bound form); Red color: ApolPBP1E137QE141Q.

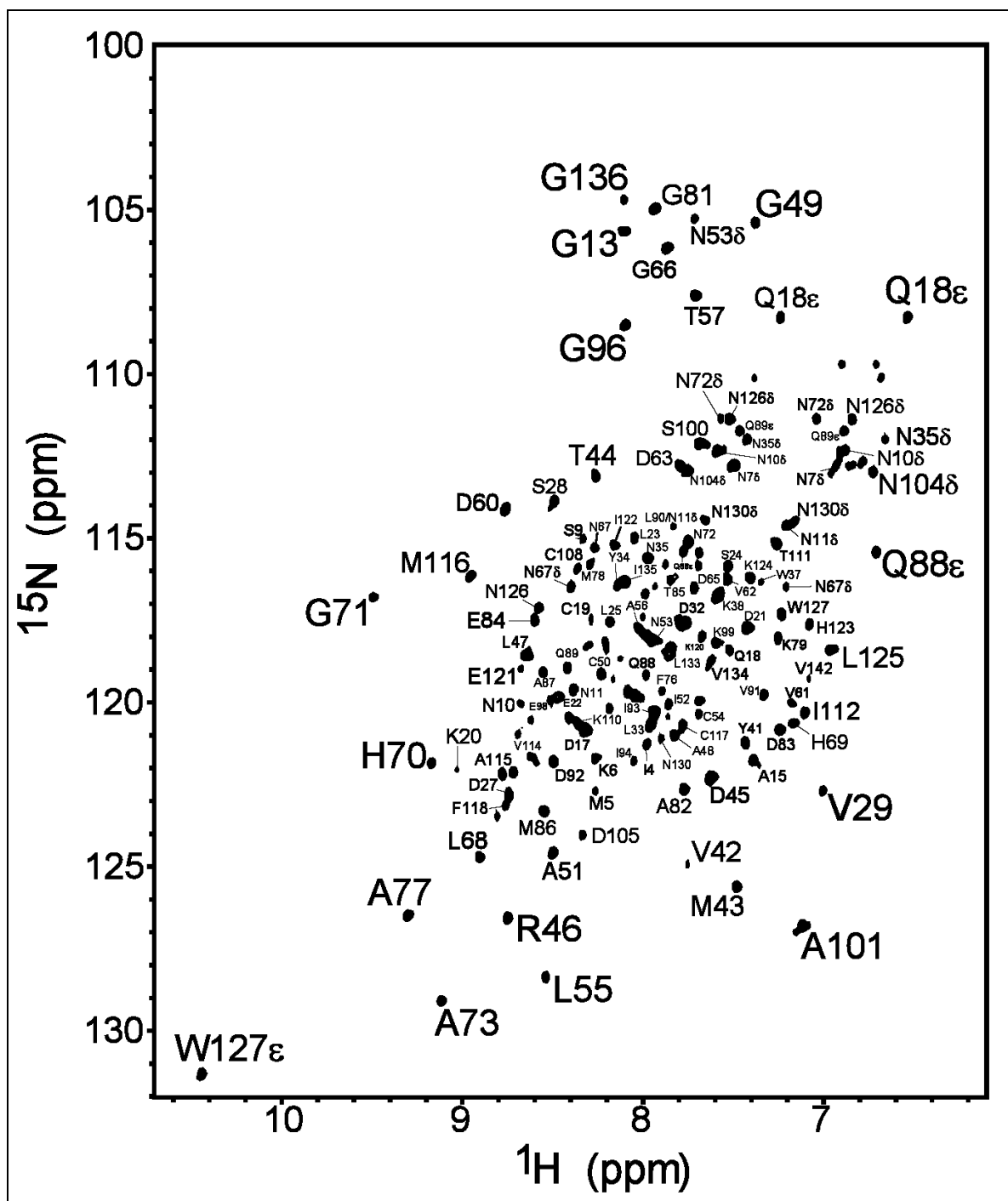


Figure 4.14 A. Two-dimensional $\{^1\text{H}, ^{15}\text{N}\}$ HSQC spectra of delipidated ApolPBP1D132NE137Q in 50 mM sodium phosphate buffer at pH 4.5. The spectrum resembles to the ligand-free conformation of the ApolPBP1wt protein.

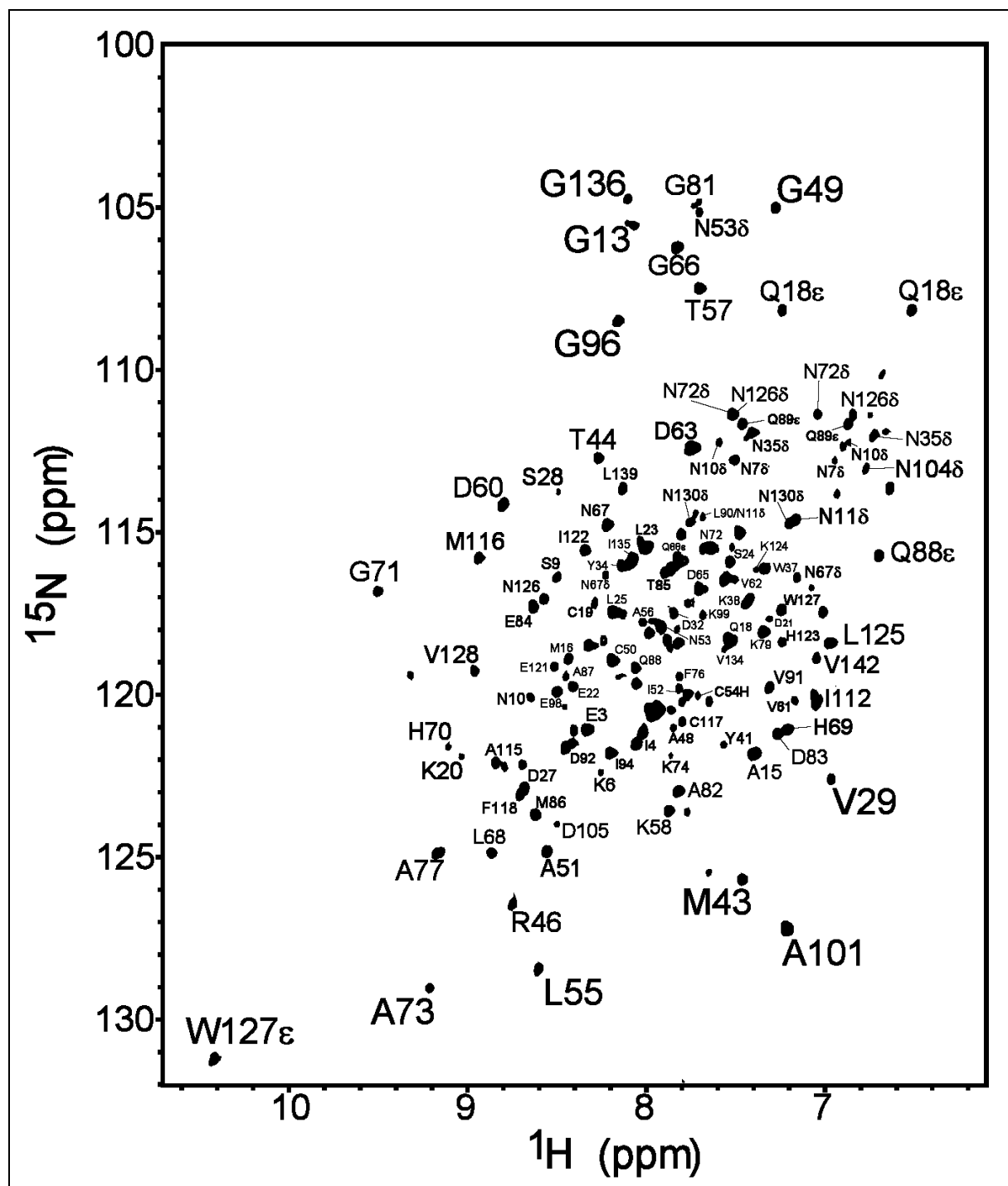


Figure 4.14 B. Two-dimensional $\{^1\text{H}, ^{15}\text{N}\}$ HSQC spectra of delipidated ApolPBP1D132NE137Q in 50 mM sodium phosphate buffer at pH 6.5. The spectrum resembles to the ligand-free conformation of the ApolPBP1wt protein.

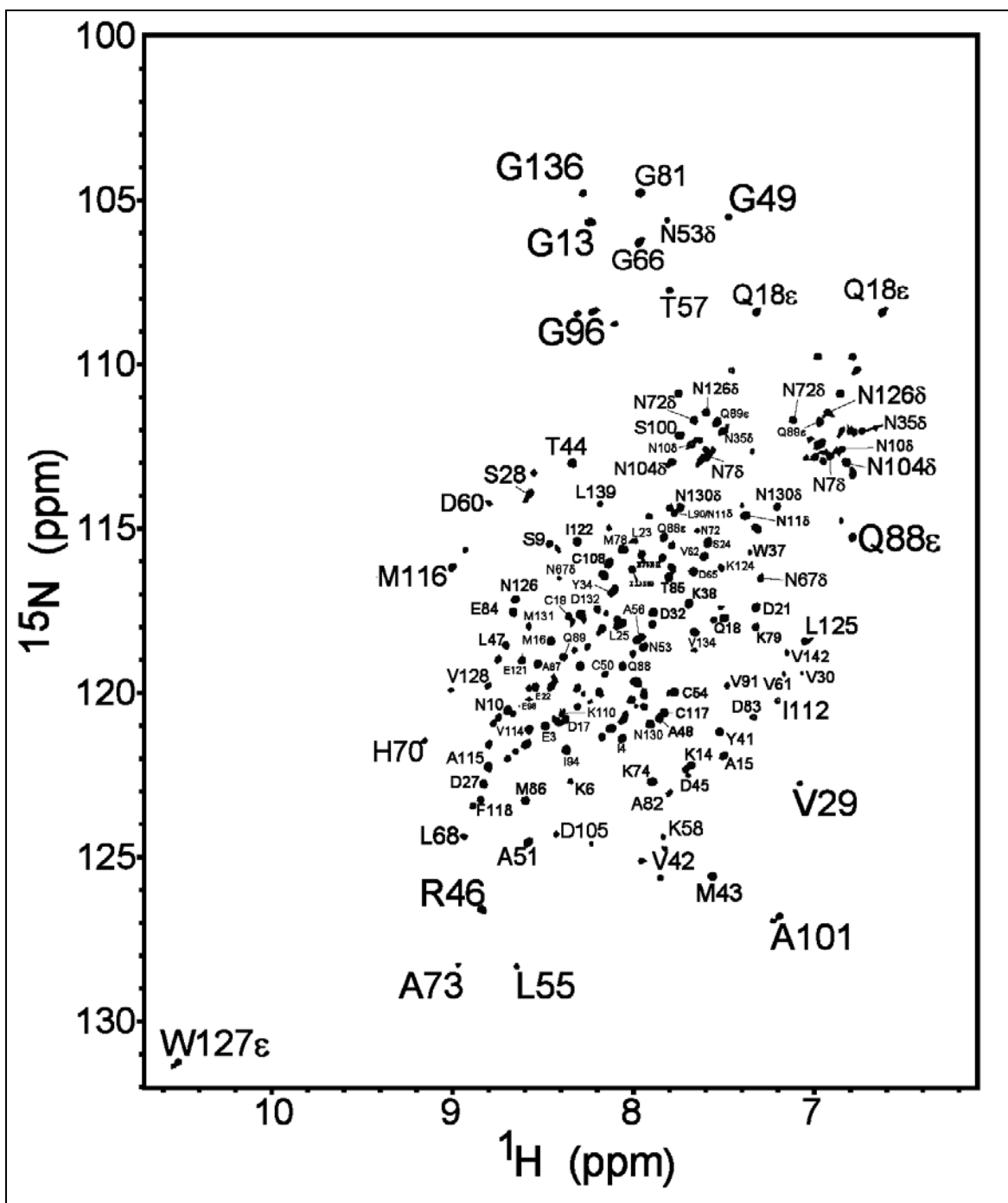


Figure 4.14 C. Two-dimensional $\{^1\text{H}, ^{15}\text{N}\}$ HSQC spectra of delipidated ApolPBP1E137QE141Q in 50 mM sodium phosphate buffer at pH 4.5. The spectrum resembles to the ligand-free conformation of the ApolPBP1wt protein.

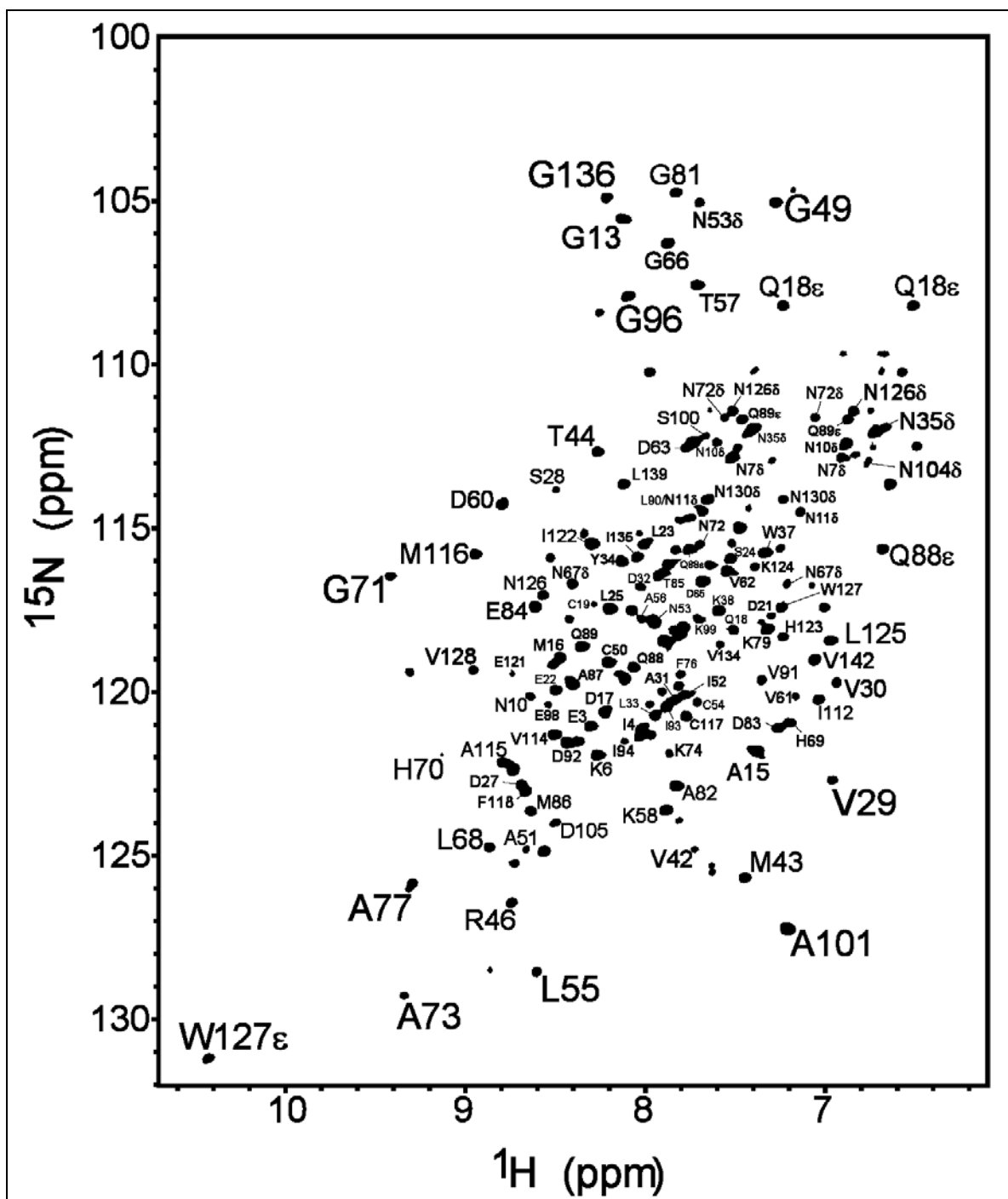


Figure 4.14 D. Two-dimensional $\{^1\text{H}, ^{15}\text{N}\}$ HSQC spectra of delipidated ApolPBP1E137QE141Q in 50 mM sodium phosphate buffer at pH 6.5. The spectrum resembles to the ligand-free conformation of the ApolPBP1wt protein.

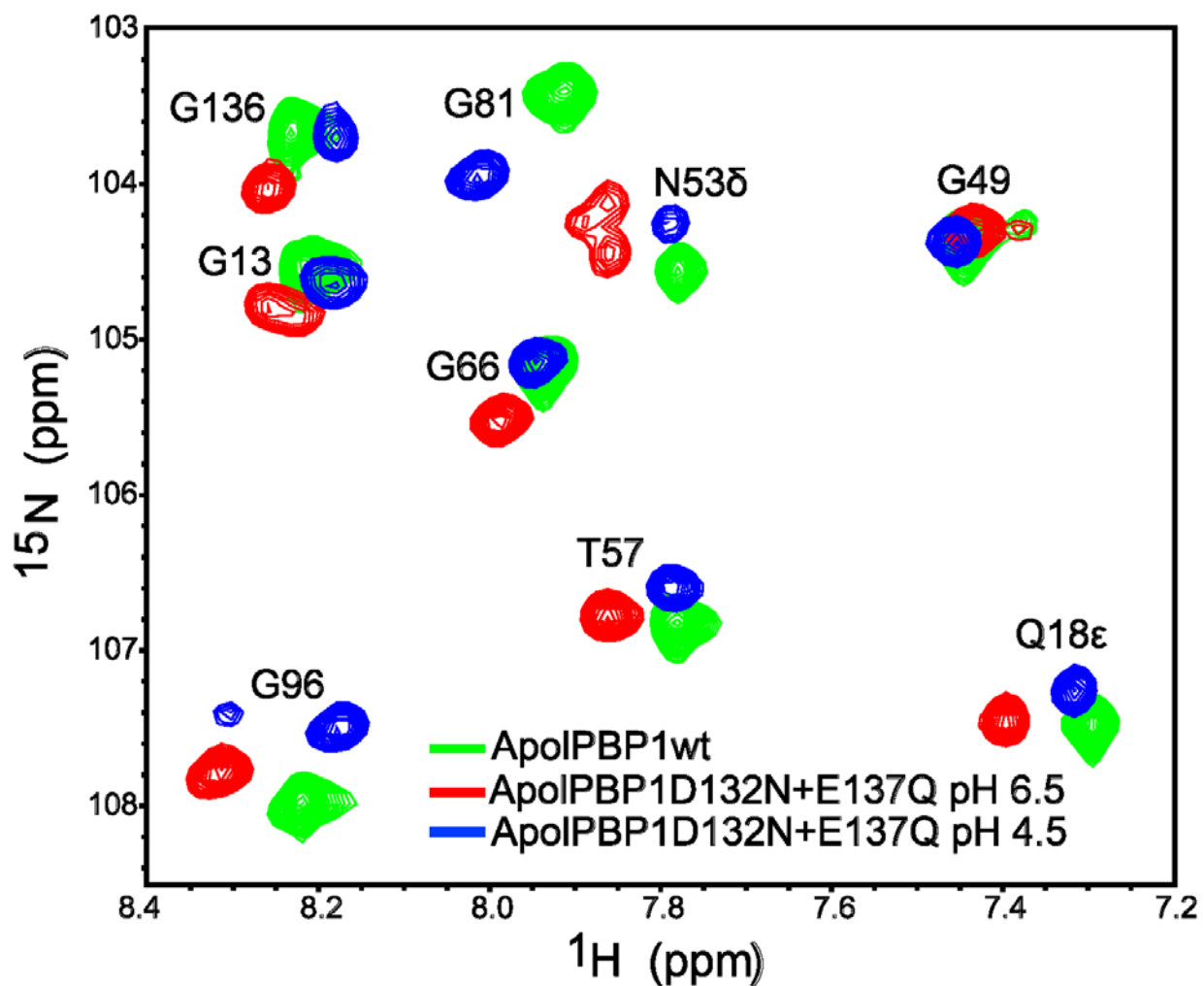


Figure 4.15 A. Expanded region of Two-dimensional $\{^1\text{H}, ^{15}\text{N}\}$ HSQC spectra of delipidated ApolPBP1D132NE137Q at pH 4.5 and 6.5 and ApolPBP1wt protein at pH 4.5. Green color: ApolPBP1wt (ligand-free form); Red color: ApolPBP1D132NE137Q at pH 6.5; Blue color: ApolPBP1D132NE137Q at pH 4.5.

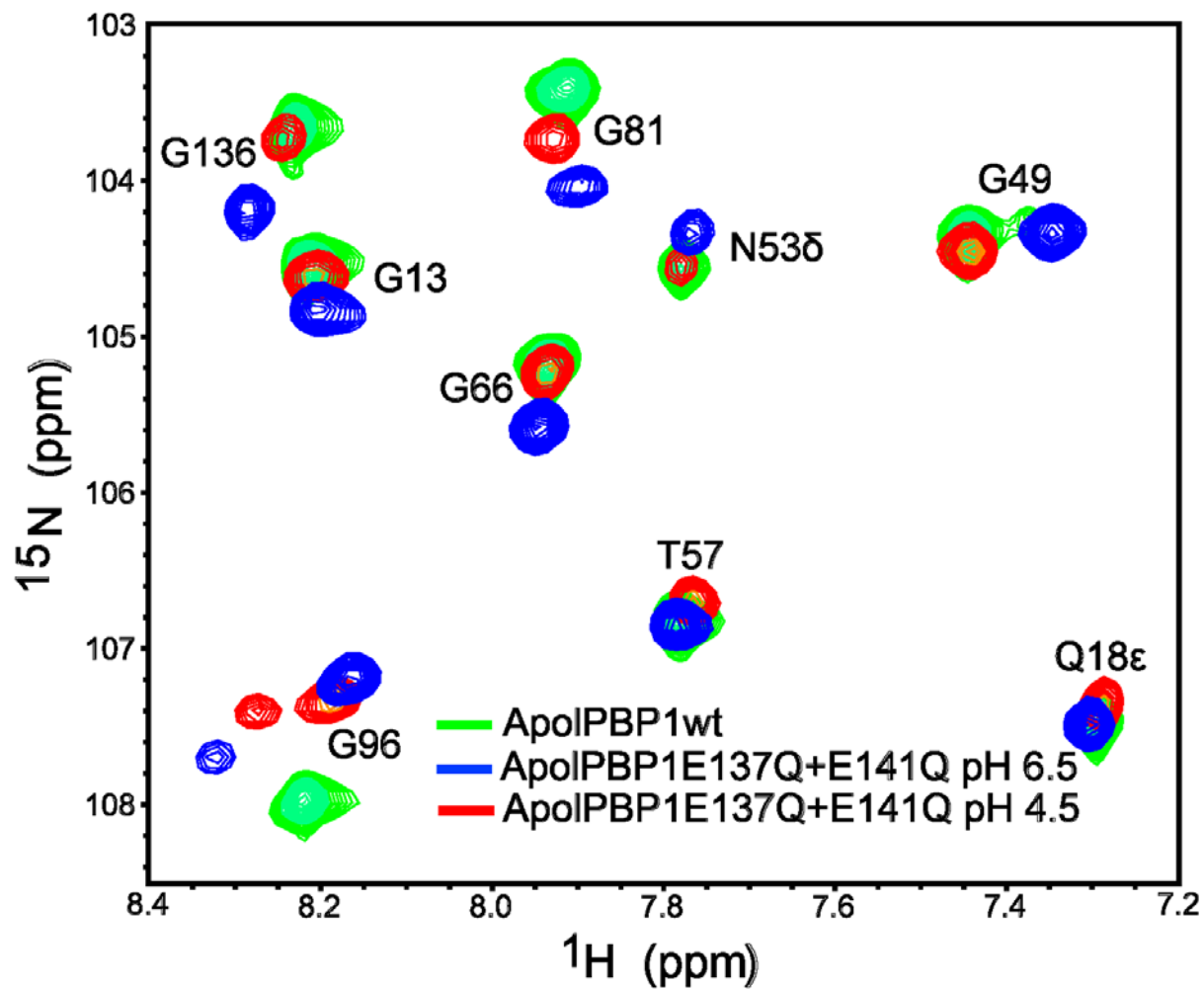


Figure 4.15 B. Expanded region of Two-dimensional $\{^1\text{H}, ^{15}\text{N}\}$ HSQC spectra of delipidated ApolPBP1E137QE141Q at pH 4.5 and 6.5 and ApolPBP1wt protein at pH 4.5. Green color: ApolPBP1wt (ligand-free form); Blue color: ApolPBP1E137QE141Q at pH 6.5; Red color: ApolPBP1E137QE141Q at pH 4.5.

But, the triple mutant protein, ApolPBP1D132NE137QE141Q, behaved in a completely different manner. The undelipidated triple mutant protein at pH 6.5 appeared to be quite different than the wild-type ApolPBP1 (Figure 4.16A). Although, it is not similar, the chemical shift positions of several residues showed closeness to the respective residues in the HSQC spectrum of the ligand-bound conformation of the wild type protein (Figure 4.16B and 4.16C). However, we cannot confirm with certainty that this is the ligand-bound conformation until further investigation. At pH 4.5, the protein appeared to be denaturing (Figure 4.17A). We observed that the resonances in the HSQC spectrum of ApolPBP1D132NE137QE141Q at low pH were not well dispersed; they were confined in the middle of the spectrum (Figure 4.17A). ApolPBP1D132NE137QE141Q at pH 4.5 shows no resembles to the conformation of wild type either at pH 6.5 (ligand bound form) (Figure 4.17B) or at pH 4.5 (ligand free form) (Figure 4.17C). However, this preliminary observation must be investigated further to determine the effect of the mutation on protein conformation including that of pH, and delipidation.

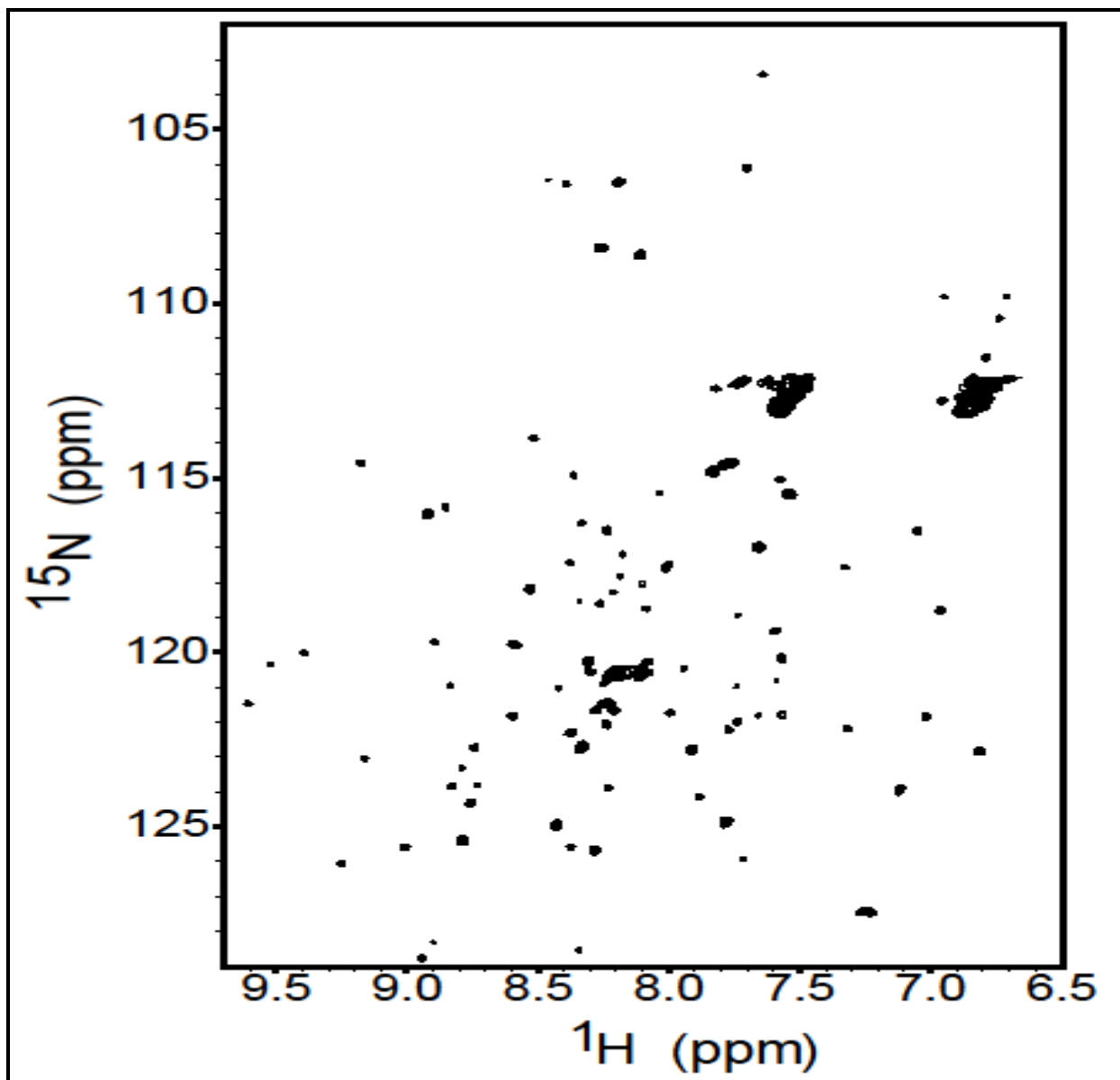


Figure 4.16 A. Two-dimensional $\{^1\text{H}, ^{15}\text{N}\}$ HSQC spectra of undelipidated ApolPBP1D132NE137QE141Q in 50 mM sodium phosphate buffer at pH 6.5.

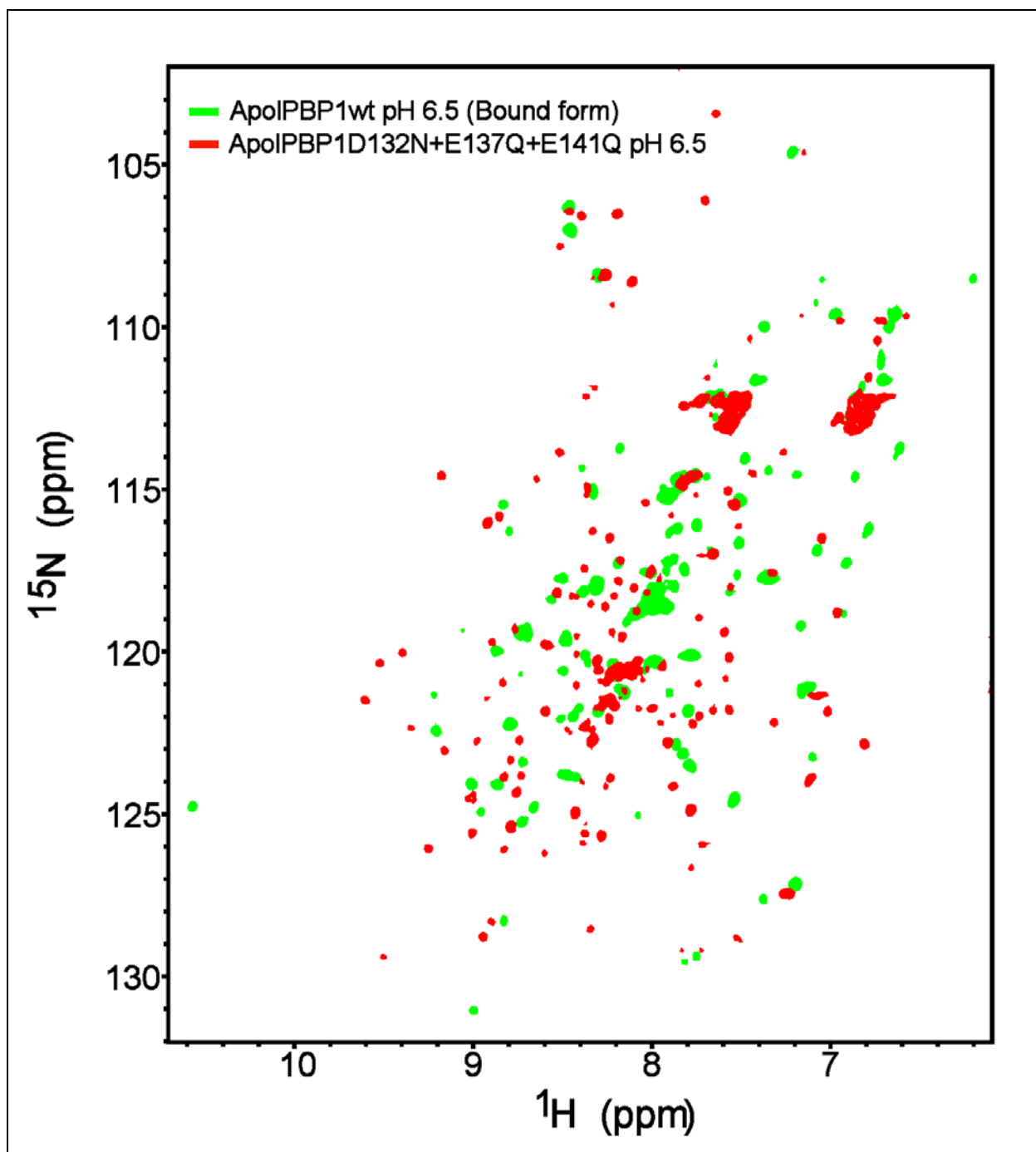


Figure 4.16 B. Overlapping between the HSQC spectra of Undelipidated ApolPBP1 at pH 6.5 and ApolPBP1D132NE137QE141Q at pH 6.5. Different proteins are indicated by the colors inside the picture.

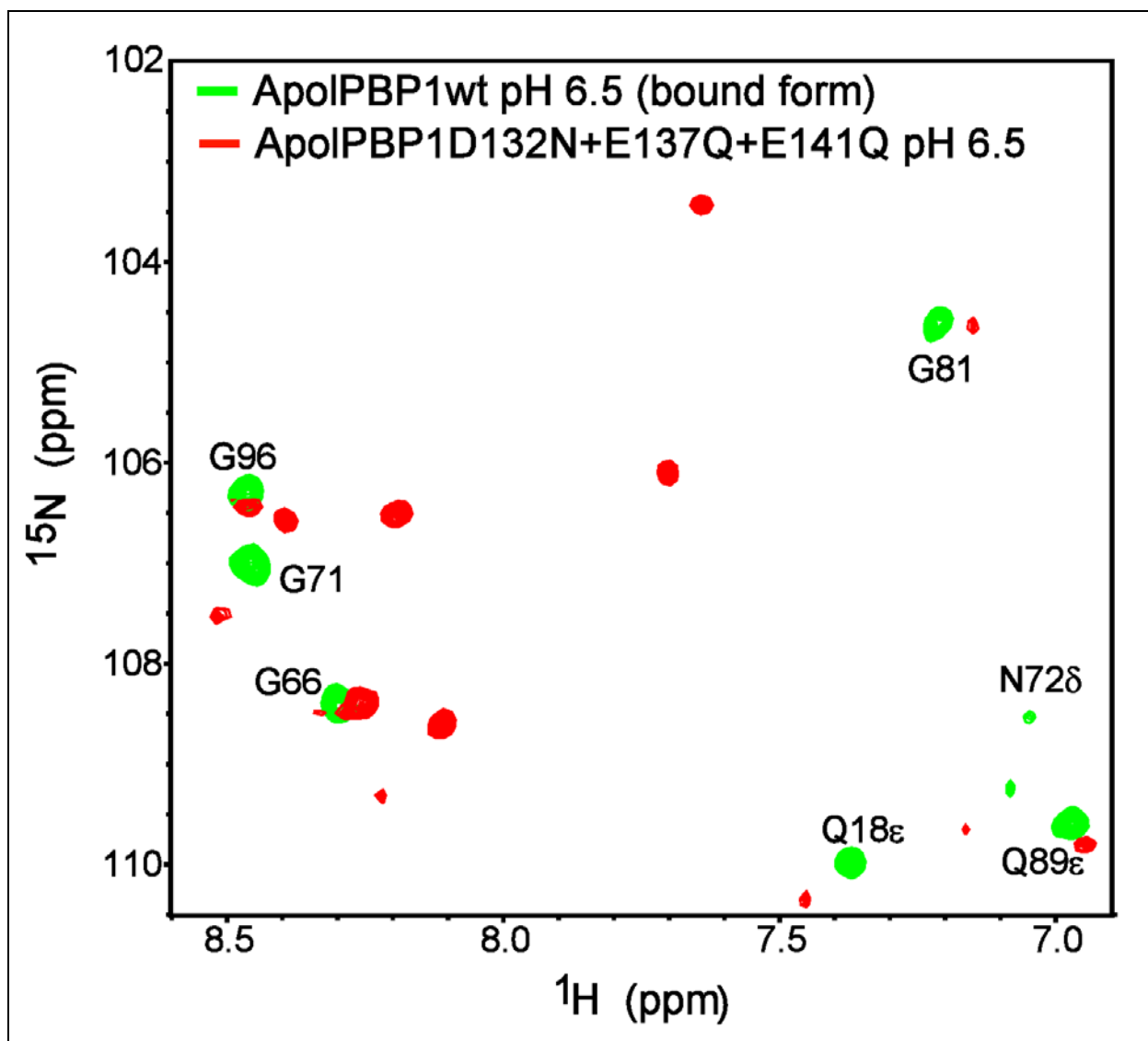


Figure 4.16 C. Extended region of HSQC spectra of Undelipidated ApolPBP1 at pH 6.5 and ApolPBP1D132NE137QE141Q at pH 6.5. Different proteins are indicated by the colors inside the picture.

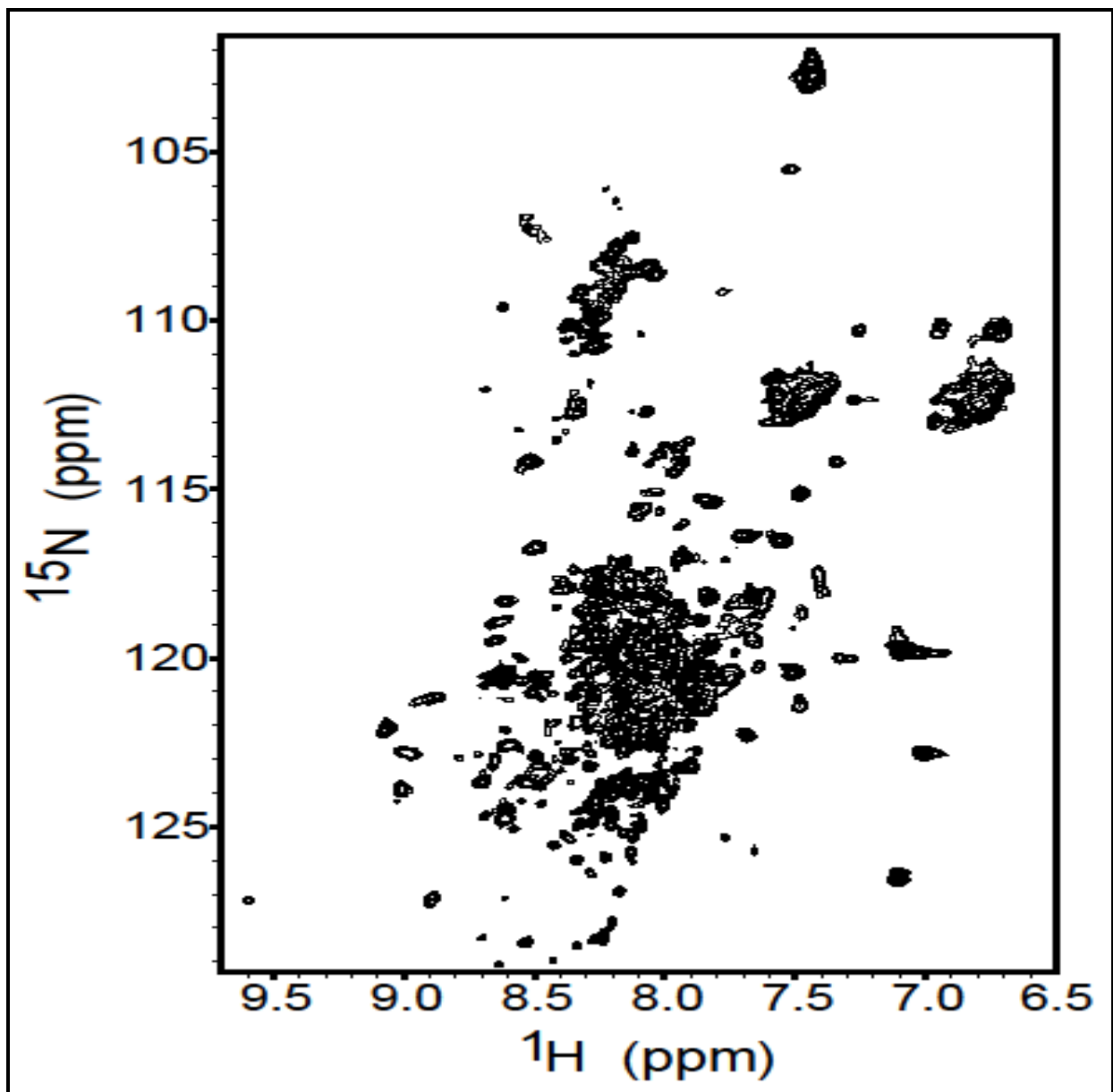


Figure 4.17 A. Two-dimensional $\{^1\text{H}, ^{15}\text{N}\}$ HSQC spectra of undelipidated ApolPBP1D132NE137QE141Q in 50 mM sodium phosphate buffer at pH 4.5.

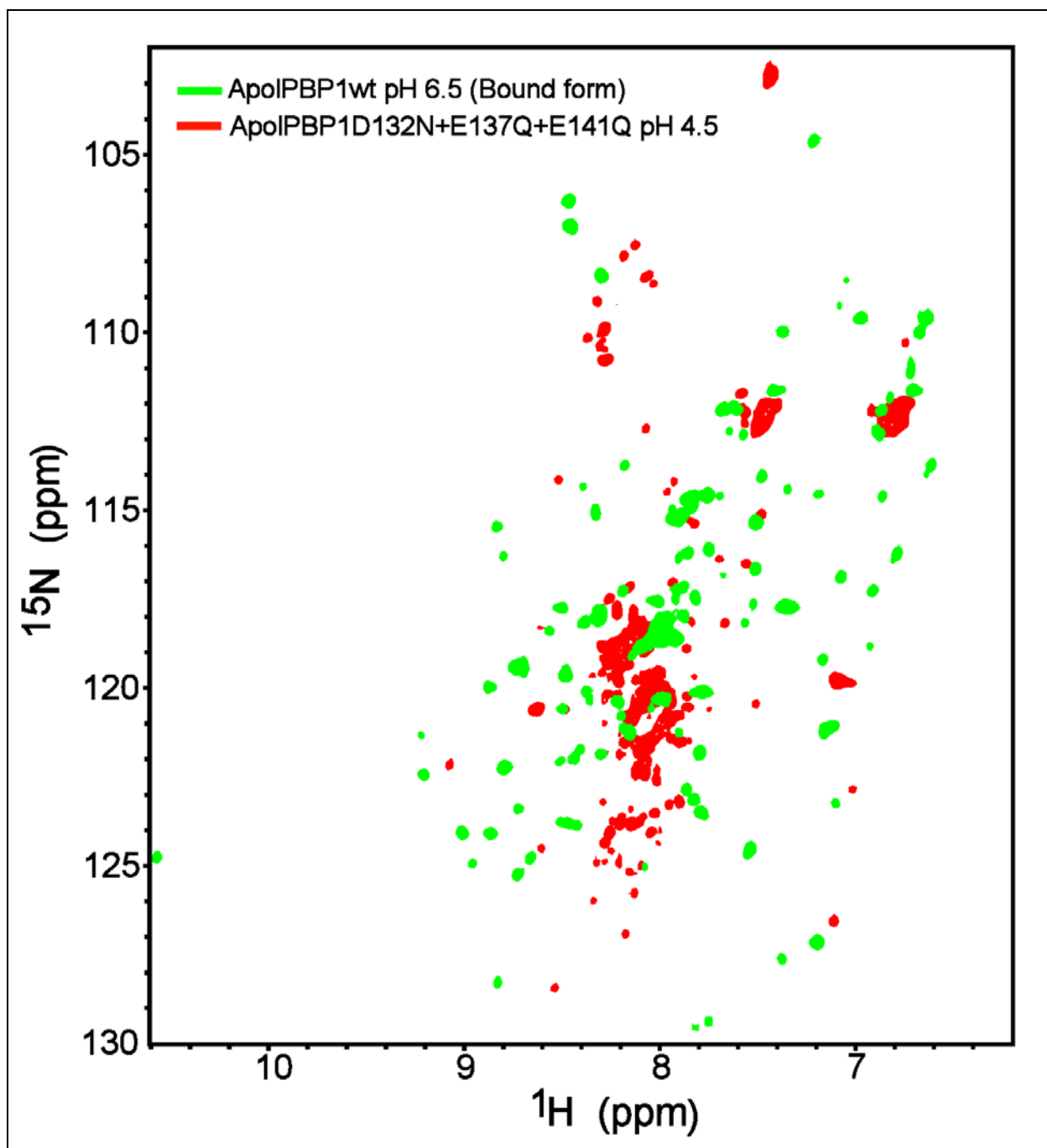


Figure 4.17 B. Overlapping between the HSQC spectra of Undelipidated ApolPBP1 at pH 6.5 and ApolPBP1D132NE137QE141Q at pH 4.5. Different proteins are indicated by the colors inside the picture.

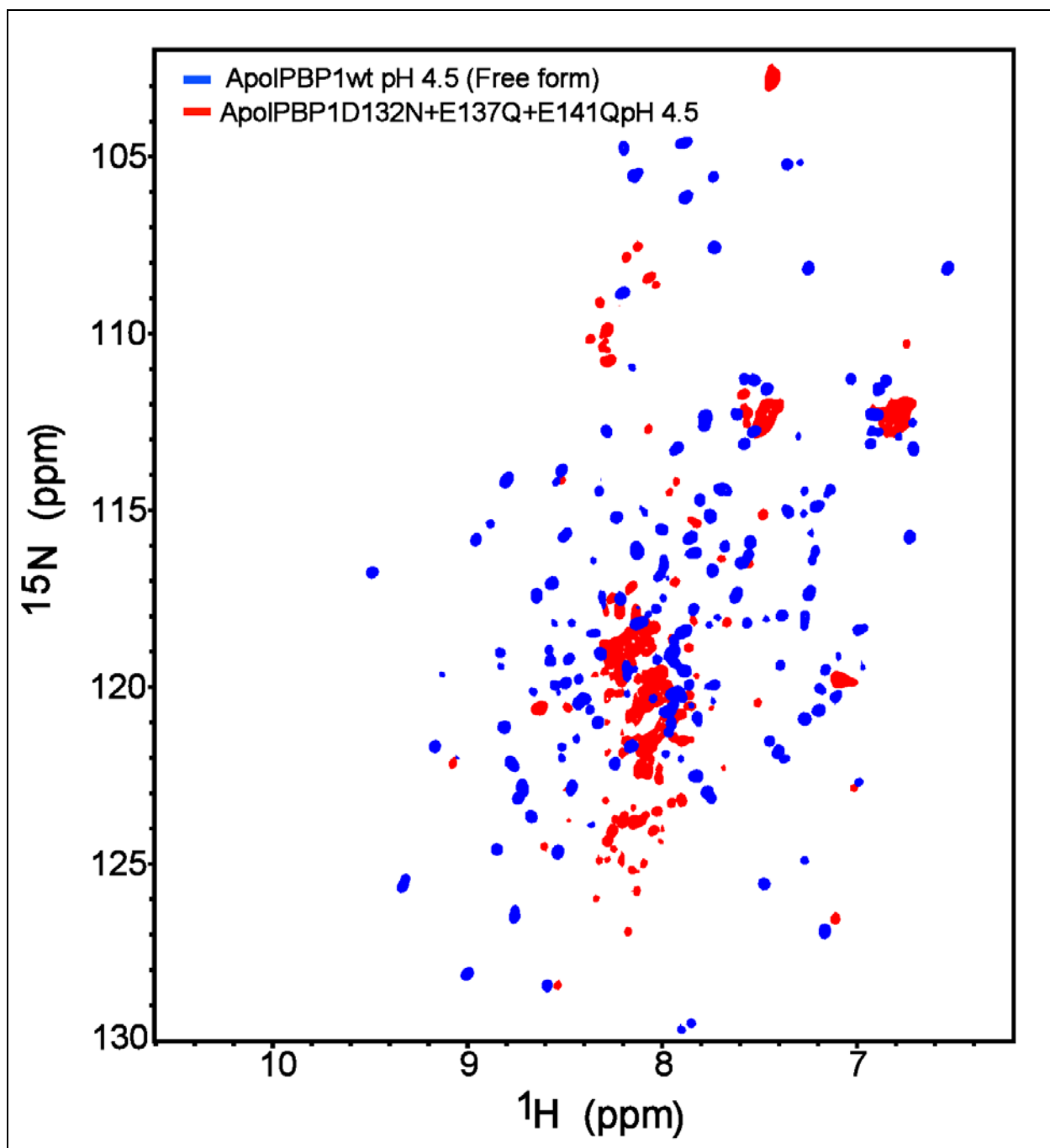


Figure 4.17 C. Overlapping between the HSQC spectra of Undelipidated ApoIPBP1 at pH 4.5 and ApoIPBP1D132NE137QE141Q at pH 4.5. Different proteins are indicated by the colors inside the picture.

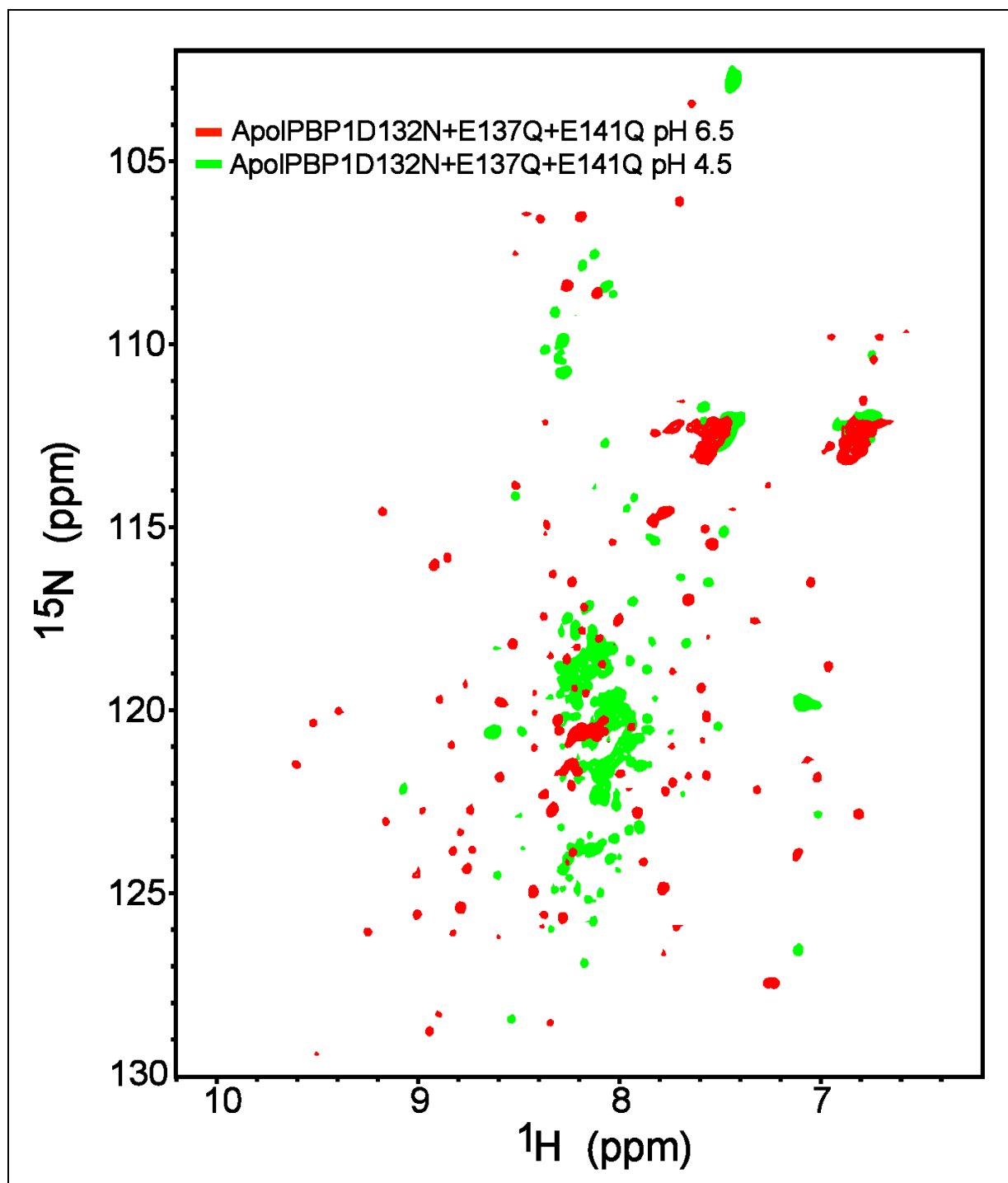


Figure 4.17 D. Overlapping between the HSQC spectra of Undelipidated ApoIPBP1D132NE137QE141Q at pH 6.5 and ApoIPBP1D132NE137QE141Q at pH 4.5. Different proteins are indicated by the colors inside the picture.

4.4 Discussion

In this work, we have investigated the role of the C-terminus in the ligand binding and releasing mechanism of ApolPBP1. Truncation of C-terminus in ApolPBP1wt as well as ApolPBP1H70A/H95A resulted in proteins which exhibited the ligand-bound conformation regardless of pH and presence/absence of ligand (Figure 4.3, 4.4, 4.5 and 4.6). Although change of pH did not cause any drastic conformational change in these proteins from ligand-bound to free conformation as was observed for undelipidated (ligand-bound) ApolPBP1wt, it did affect chemical shifts of several resonances indicating that local changes due to the effect of pH occurred in the protein (Figure 4.5 and 4.6). Delipidation also did not bring any major conformational change in these proteins (Figure 4.4) in stark contrast to what was seen earlier for the ApolPBP1wt and ApolPBP1H70A/H95A at pH 6.5.⁶ Several resonances that had disappeared in the spectra of undelipidated proteins could be easily located in the spectra of delipidated proteins. These resonances again underwent line broadening and/or disappearance during ligand titration (Figure 4.7). Most of the resonances in all C-terminus truncated proteins exhibited intermediate-to-fast exchange phenomena on the NMR time scale during ligand titration (Figure 4.7), implying less affinity towards the ligand than the wild type protein. Thus, while ApolPBP1wt and ApolPBP1H70A/H95A had nanomolar affinities towards ligands (characterized by the slow exchange seen for almost all resonances in HSQC during ligand titration), their C-terminus truncated counterparts had much lesser affinities. In fluorescence spectroscopic studies, ApolPBP1 Δ P129-V142 and ApolPBP1H70A/H95A Δ P129-V142 showed the ability to bind AMA even at low pH; unlike the wild type protein (Figure 4.8 and 4.9). However, their binding affinities at both pH 6.5 and 4.5 were greatly reduced by 2-6 folds as compared to ApolPBP1wt and ApolPBP1H70A/H95A (Table 4.1). Our results are in contrast to

those reported for BmorPBP and AtraPBP using cold binding assay.^{5,7} For BmorPBP, the C-terminus deleted mutant retained its binding ability at pH 7 nearly identical to that of the wild type and displayed significant binding at pH 5.⁵ In the case of AtraPBP, the C-terminus truncated mutant showed a 1.5 fold increase in the binding at pH 7 and retained the binding at pH 5 albeit lesser than at pH 7.⁷ However, C-terminus truncated LdispPBP2 showed higher K_d (and hence, lesser affinity) than that of wild type protein⁸ in a GC assay, which is consistent with our observations.

The reduced binding affinities of the delipidated C-terminus-truncated proteins could have been attributed to inefficient delipidation due to the absence of the C-terminus that helps in ejecting the ligand out at low pH. It is possible that the delipidation is not as effective in C-terminus-truncated proteins as in ApolPBP1wt and ApolPBP1H70A/H95A. As a result, the endogenous ligand would have competed with the added ligand resulting in lesser binding affinities, as observed in the case of ApolPBP1wt and ApolPBP1H70A/H95A. However, based on the following observations we conclude that this is not the case: (i) even undelipidated proteins showed much reduced ligand binding affinity at any pH than their counterparts with intact C-terminus and (ii) we see disappearance of certain resonances in the undelipidated samples in the HSQC spectrum (iii) addition of palmitic acid to the delipidated proteins caused the same resonances to broaden and disappear resulting in the spectra which matched those of undelipidated proteins. This indicates that the delipidation of these proteins was quite effective and complete.

Thus it is important to note that even when the C-terminus is missing, the ligand removal is possible at low pH by the delipidation procedure. This is quite surprising especially for ApolPBP1H70A/H95A Δ P129-V142 where both molecular switches forming the ligand release

mechanism (histidines as well as C-terminus) are removed. Thus even though these two switches are very important for ligand release; there might be some other residues playing a minor role in this mechanism. It is also possible that the protein loses its overall binding affinity at acidic pH, or that the affinity of Lipidex resin towards the hydrophobic ligand is more than that of the protein at low pH. This phenomenon was observed even in the case of ApolPBP1H70A/H95A, where the affinity of the protein at pH 4.5 was lower than that at pH 6.5.⁶

The histidines are important only in the ligand releasing mechanism. As seen in our earlier work,⁶ their substitution to alanines confers the protein the ability to bind ligand even at low pH. However this substitution does not affect the ligand binding affinity of the protein, as the delipidated forms of both ApolPBP1wt and ApolPBP1H70A/H95A have similar binding affinities towards AMA and acetate pheromone at pH 6.5.⁶ This does not seem to be the case with the C-terminal tail. Although C-terminus truncated proteins can bind the ligand at low pH, their affinities at both high and low pH are drastically reduced as compared to the wild type and double mutant proteins. Indeed, one could expect a considerably tight protein-ligand association in the case of ApolPBP1H70A/H95A Δ P129-V142 even at low pH, where both molecular switches have been removed, indicated by K_d values lesser or at least similar to the ApolPBP1wt or ApolPBP1H70A/H95A. Our results, on the contrary, indicate reduced ligand binding affinities for both C-terminus deleted proteins in all of the conditions tested. Thus, it is evident that C-terminus plays a major role in the ligand-release mechanism at low pH as well as some role in the ligand-binding to the protein. It is also possible that in addition to helping the translocation of the ligand in the binding pocket, the C-terminus also acts as a gate to “lock” the ligand in the binding pocket,⁸ until released by the protonation of histidines at low pH. Hence removal of C-

terminus might be resulting in hampered association and faster dissociation of the ligand from the protein, reducing the overall K_d .

Further investigation on the role of C-terminus tail in the release of the ligand through the mutation of the three charged residues of the C-terminus was done (Figure 4.10- 4.17). The hypothesis behind such mutation study was that mutations of those charged residues into uncharged ones could disrupt the formation of the 7th C-terminal helix at low pH resulting in no ligand release at low pH. However, the single mutants had no effect on the protein and behaved very similar to the wild type protein as indicated by the ligand-free conformation exhibited in the HSQC spectra at low pH of these proteins. However, the HSQC spectra for the double and triple mutant proteins both at low and high pH require further investigation.

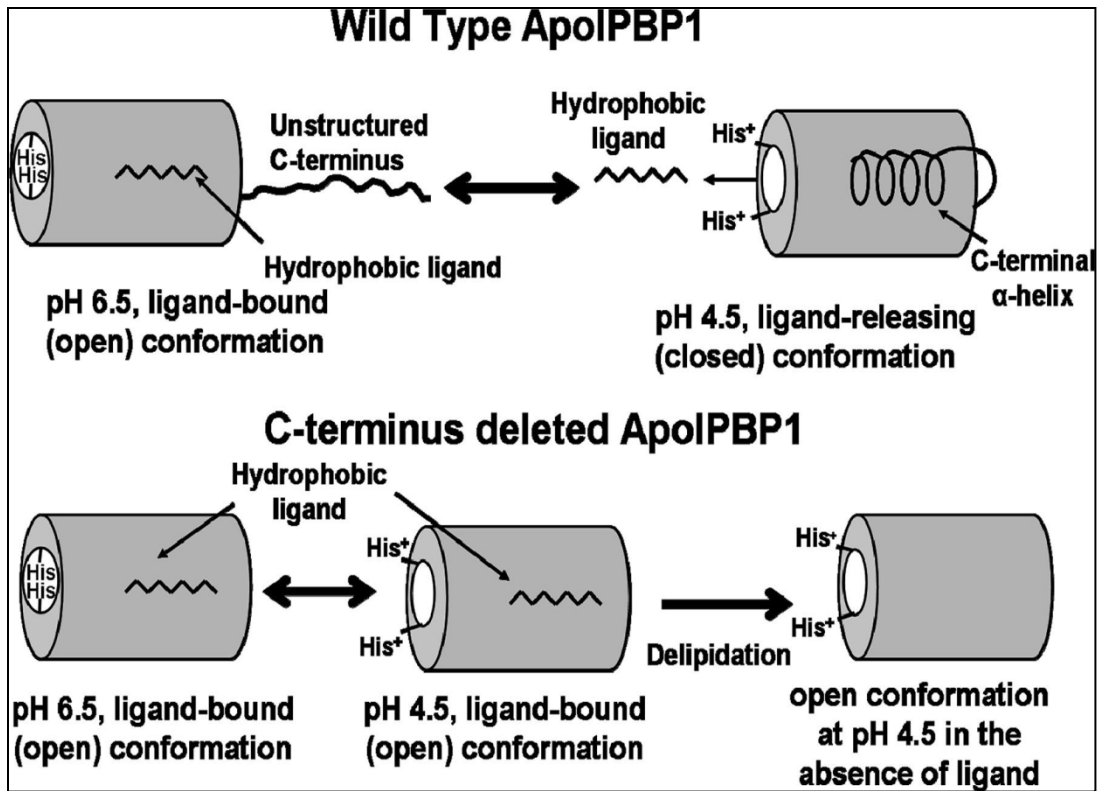


Figure 4.18 Schematic representation of the c-terminus deleted (ApoIPBP1 Δ P129-V142 and ApoIPBP1H70A/H95A Δ P129-V142) proteins with compared to the ApoIPBP1wt protein.

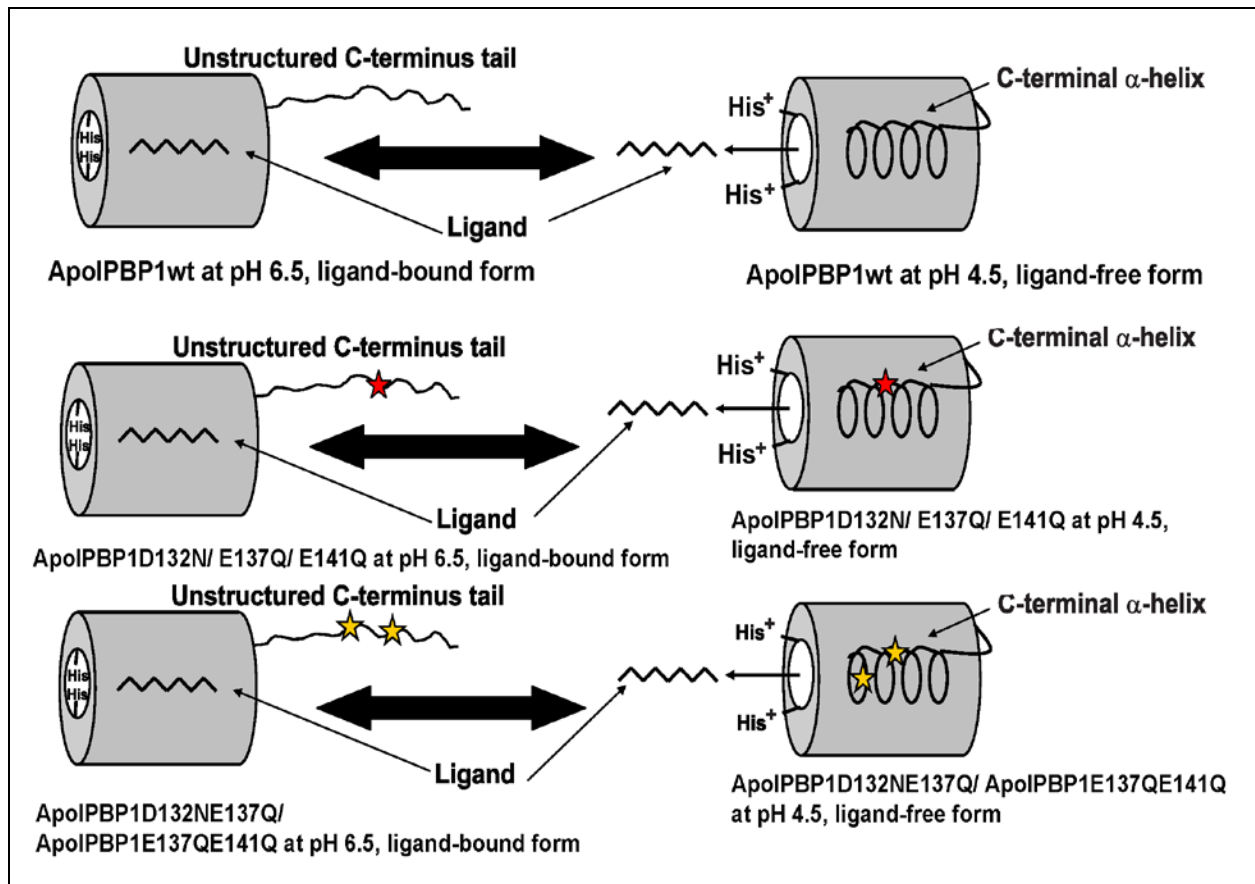


Figure 4.19 Schematic representation of the single mutant (ApoIPBP1D132N, ApoIPBP1E137Q and ApoIPBP1E141Q) and double mutant (ApoIPBP1D132NE137Q and ApoIPBP1E137QE141Q) proteins with compared to the ApoIPBP1wt protein.

Reference:

- (1) Zubkov, S., Gronenborn, A. M., Byeon, I. J., and Mohanty, S. (2005) Structural Consequences of the pH-induced Conformational Switch in *A. polyphemus* Pheromonebinding Protein: Mechanisms of Ligand Release. *J. Mol. Biol.* 354, 1081-1090.
- (2) Sandler, B. H., Nikonova, L., Leal, W. S., and Clardy, J. (2000) Sexual attraction in the silkworm moth: structure of the pheromone-binding-protein–bombykol complex. *Chem Biol* 7, 143-151.
- (3) Xu, W., and Leal, W. S. (2008) Molecular switches for pheromone release from a moth pheromone-binding protein. *Biochem. Biophys. Res. Commun.* 372, 559-564.
- (4) Lautenschlager, C., Leal, W. S., and Clardy, J. (2005) Coil-to-helix transition and ligand release of *Bombyx mori* pheromone-binding protein. *Biochem. Biophys. Res. Commun.* 335, 1044-1050.
- (5) Leal, W. S., Chen, A. M., Ishida, Y., Chiang, V. P., Erickson, M. L., Morgan, T. I., and Tsuruda, J. M. (2005) Kinetics and molecular properties of pheromone binding and release. *Proc. Natl. Acad. Sci. U. S. A.* 102, 5386-5391.
- (6) Katre, U. V., Mazumder, S., Prusti, R. K., and Mohanty, S. (2009) Ligand Binding Turns Moth Pheromone-binding Protein into a pH Sensor: EFFECT ON THE ANTHERAEA POLYPHEMUS PBP1 CONFORMATION. *J. Biol. Chem.* 284, 32167-32177.
- (7) Xu W., Xu X., Leal W. S., and Ames J. B. (2011) Extrusion of the C-terminal helix in navel orangeworm moth pheromone-binding protein (AtraPBP1) controls pheromone binding. *Biochem. Biophys. Res. Commun.* 404, 335-338.

- (8) Gong, Y., Pace, T. C., Castillo, C., Bohne, C., O'Neill, M. A., and Plettner, E. (2009) Ligand-Interaction Kinetics of the Pheromone-Binding Protein from the Gypsy Moth, *L. dispar*: Insights into the Mechanism of Binding and Release. *Chem. Biol.* 16, 162-172.
- (9) Katre U. V., Mazumder S., and Mohanty S. (2013) Structural Insights into the Ligand Binding and Releasing Mechanism of *Antheraea polyphemus* Pheromone-Binding Protein1: Role of the C-Terminal Tail. *Biochemistry* 52, 1037-1044.
- (10) Delaglio, F., Grzesiek, S., Vuister, G. W., Zhu, G., Pfeifer, J., and Bax, A. (1995) NMRPipe: A multidimensional spectral processing system based on UNIX pipes. *J. Biomol. NMR* 6, 277–293.
- (11) Johnson, B. A., and Blevins, R. A. (1994) NMRView: A computer program for the visualization and analysis of NMR data. *J. Biomol. NMR* 4, 603–614.
- (12) Mohanty, S., Zubkov, S., and Campos-Olivas, R. (2003) Letter to the Editor: ^1H , ^{13}C and ^{15}N backbone assignments of the pheromone binding protein from the silk moth *Antheraea polyphemus* (ApolPBP). *J. Biomol. NMR* 27, 393-394.
- (13) Michel E., Damberger F. F., Ishida Y., Fiorito F., Lee D., Leal W. S., and Wüthrich K. (2011) Dynamic Conformational Equilibria in the Physiological Function of the *Bombyx mori* Pheromone-Binding Protein. *J. Mol. Biol.* 408, 922-931.
- (14) Goddard, T. D., and Kneller, D. G. SPARKY 3, University of California, San Francisco.

Chapter 5

Exploring the nickel proteome

5.1 Introduction

5.1.1 Exploring the nickel proteome in *Methanothermobacter marburgensis*

Most of the bacteria require different trace metals (like Ni, Zn, Ca, Cu, and Cd) for conducting different biological processes. Many of these bacteria use nickel for the production of key enzymes present in the cell. Microorganisms have evolved to utilize nickel ions in several different enzyme systems that enable these organisms to survive and proliferate in various environments. The enzymes include urease, hydrogenase, methyl coenzyme M reductase (MCR), some dehydrogenases and acetyl-coenzyme A synthase. The metal ion is quite important for the proper function of these enzymes.^{1,2} Moreover, pathogenic bacteria like *Escherichia coli*, *Helicobacter pylori*, *Salmonella*, *Shigella*, and *Mycobacterium tuberculosis* rely on nickel for their pathogenicity.^{1,3} *H. pylori* produces a nickel-containing hydrogenase and urease and *E. coli* also requires nickel for a NiFe-hydrogenase.⁴⁻⁹

Most of the bacteria have a dedicated set of proteins to import and export the nickel and regulate the cellular distribution and incorporation of nickel into different enzymes. These groups of proteins are called the nickel trafficking proteins. The key proteins involved in nickel trafficking have been identified in various organisms over the past years. In *E. coli*, the nickel is imported by an ABC-type permease, NikABCDE, through an energy driven process.¹⁰ Whereas the *E. coli* has a protein called RcnAB (formerly known as YohM and YohN) which acts as nickel exporter to balance the nickel concentration inside the cells.^{11, 12} *E. coli* has several other

nickel chaperones and accessory proteins present, like HypA, HypB, both of which are important for the insertion of nickel into hydrogenases.¹³ An overview of the nickel trafficking system in *E. coli* is shown in Figure 5.1.

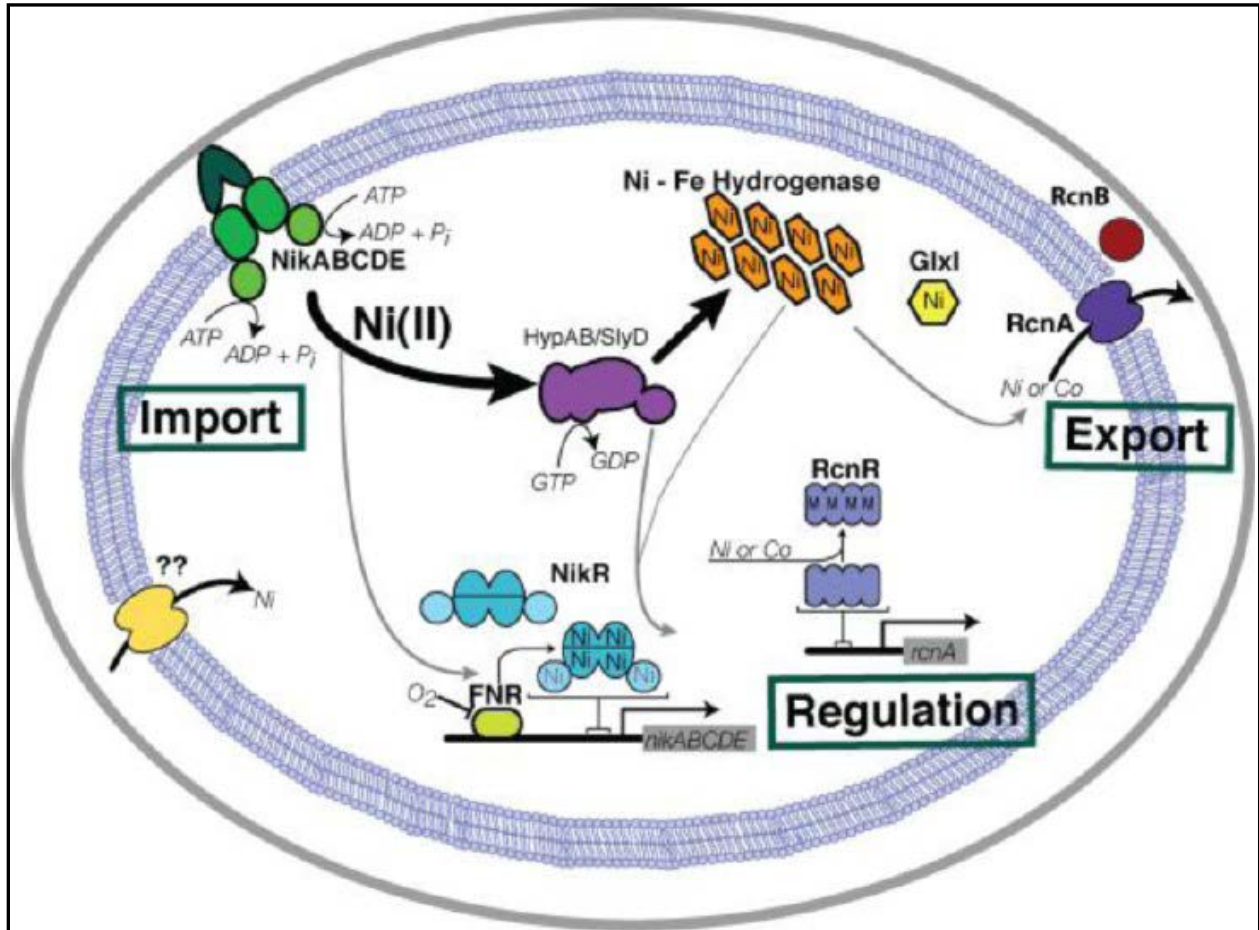


Figure 5.1 Overview of the nickel trafficking proteins in *E. coli*. NikABCDE is the importer of the nickel; HypA, HypB and SlyD are acting as chaperons and accessory proteins, which help to deliver the nickel to NiFe-hydrogenase. NikR is the regulator to importer protein (NikABCDE). RcnA is the exporter of the nickel. Copied from reference 14.

Many studies have been done in the past to isolate and characterize nickel trafficking proteins from various organisms. It has been found that many proteins are involved in the nickel intake, localization or export out of the bacterial cell; most of these proteins are well characterized.¹⁴

Methanothermobacter marburgensis is a member of the Archaea. This organism belongs to a member of the order Methanobacteriales under the class Methanobacteria and was isolated from anaerobic sewage sludge in Marburg, Germany in 1978.^{15, 16} This organism was formerly known as *Methanobacterium thermoautotrophicum* strain Marburg. This methanogen is well known for the production of enzymes and co-enzymes involved in the reduction of CO₂ to methane in the presence of H₂. The complete genome sequence of *M. marburgensis* has been reported.¹⁷ It has been found that approximately 200 protein coding sequences were identified that are essential for the synthesis of the required enzymes, coenzymes, and prosthetic groups involved in the reduction of CO₂ to methane coupled with energy conservation.¹⁸

M. marburgensis contains several nickel-containing hydrogenases that are important for the cell metabolism. On top of that, it contains the unique nickel-containing methyl-coenzyme M reductase (MCR) where the nickel is present in the tetrapyrrole factor 430 (F₄₃₀). When either MCR or F₄₃₀ was isolated from whole cells it was discovered that a majority of the F₄₃₀ was not bound to MCR but apparently present 'freely' in the cytosol (R. Thauer, personal communication). At the same time it was found that isolated F₄₃₀ in aqueous solutions would epimerize to the 12, 13-diepimere form. Since this diepimerization does not happen in the cytosol this could indicate that a chaperone could be bound to the F₄₃₀ that prevents this conformational change since in vitro this is a non-reversible event. Oxygen will convert the

diepimere into the F₅₆₀ form, but this is a process that would not happen in the cells under growth conditions. Here we will try to find the hypothetical F₄₃₀ chaperone.

5.1.2 Exploring the nickel proteome in the plant *Streptanthus polygaloides*

Plants and animals rely heavily on the macronutrients such as Na, K, Cl₂, and Ca for most of their cellular functions. However micronutrients like Ni, Cd, Mn, Mo, Cu, and Fe are also an integrated part of the different important enzymes in both plants and animals and therefore equally essential for their survival. However most of the metal ions are extremely toxic at higher concentrations, as they can inhibit the function of several essential enzymes, block functional groups of important metabolic molecules, and cause oxidative damage by producing reactive oxygen species.¹⁹⁻²² Some plants, however, have evolved the ability to survive in metal rich soils where they sequester and store exceptionally high amount of metal ions. These plants are called hyperaccumulating plants. These hyperaccumulator plants have a series of defense mechanisms that controls the import, export, accumulation and localization of the metal ions and release of the free ionic forms from the cytoplasm (Figure 5.2).²² About 450 plant species have been identified so far as heavy metal hyperaccumulators, which is less than 0.2% of all known plant species. Among these, most of the plants are nickel-hyperaccumulators (almost 75%).²³⁻³¹ Hyperaccumulating plants are found in South Africa, Latin America, North America and Europe.²⁵ The metal hyperaccumulator plant species are distributed in a wide range of unrelated families; so far 34 plant families have been reported as hyperaccumulators. Among them the Brassicaceae family, in particular the genera *Alyssum* and *Thlaspi* are known for relatively high internal nickel concentrations.^{32,33} Nickel is the metal which showed the highest concentration present in a plant among the other metals. In New Caledonia, a plant named *Sebertia acuminata* (from Sapotaceae family), can accumulate up to 26% Ni (dry weight) in its latex.³⁴ A picture of

Sebertia acuminata is shown below (Figure 5.3).³⁵ The reasons behind the evolution of hyperaccumulating plants are still unknown. Defense against predators seems the most logical explanation, but at the same time insects have coevolved that can handle the high amount of metal ions in their diets.

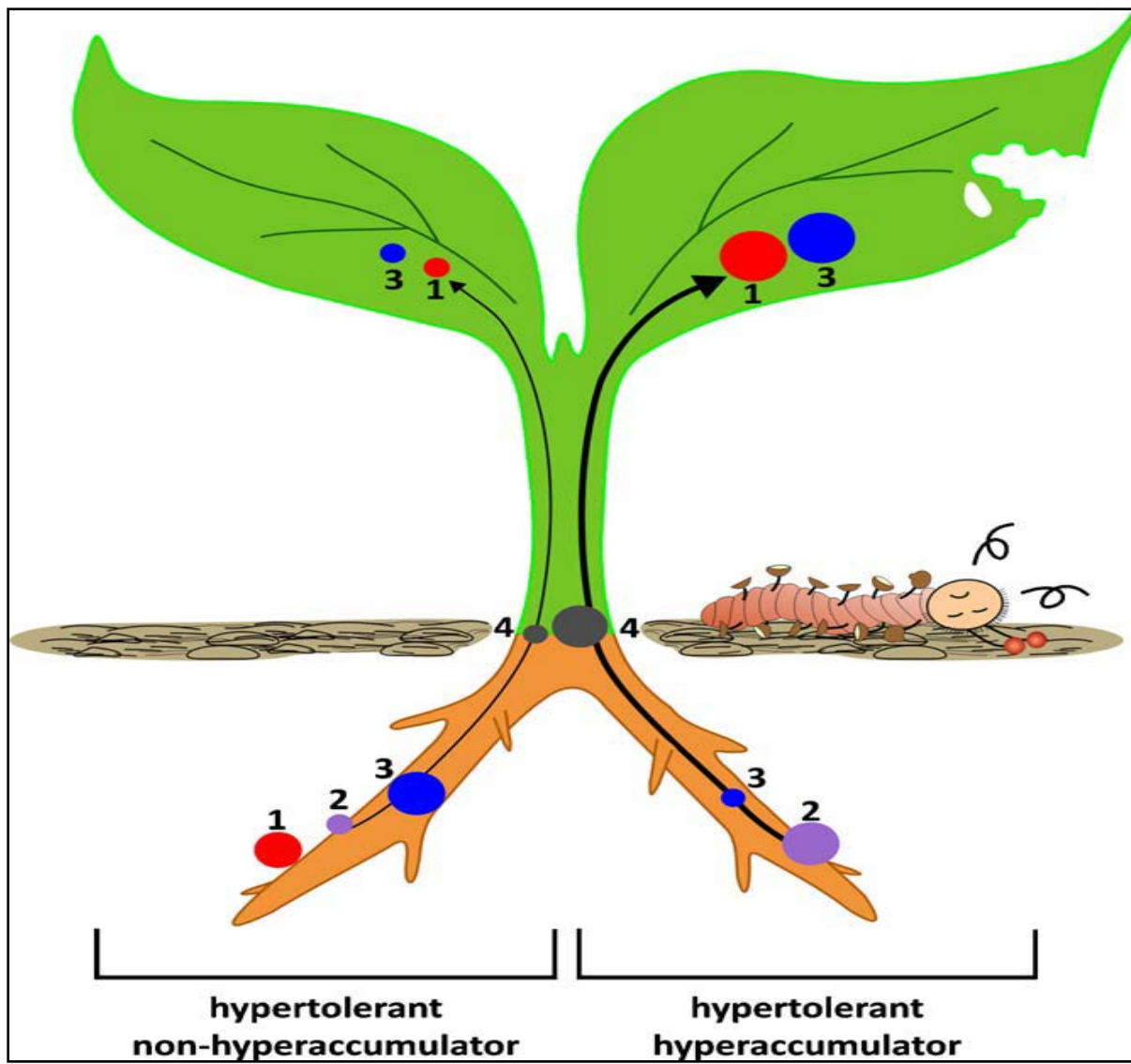


Figure 5.2 Schematic representations of different mechanisms for metal intake and distribution for non-hyperaccumulator (left) and hyperaccumulator (right) plants. No 1 indicates heavy metal binding to the cell walls, no 2 shows uptake via the roots, no 3 represents chelation in the cytosol and/or sequestration in vacuoles, and no 4 represents the root-to-shoot translocation. The spots indicate the plant organ in which the different mechanisms occur and the spot sizes indicate the intensity of each of them. Copied from reference 22.



Figure 5.3 The latex of *Sebertia acuminata*. The green color is due to the high Ni concentration.

Copied from reference 35.

Streptanthus polygaloides is a flowering plant. This plant belongs to the Brassicaceae family. The common name of this plant is milkwort jewelflower. This plant is native and endemic to the western foothills of California's Sierra Nevada.^{36,37} This plant is a nickel hyperaccumulating plant. Specimens from *Streptanthus polygaloides* showed nickel measurements in above-ground tissues ranging between 1100 to 16400 µg of Ni/g dry mass of the plant, while root tissue has Ni concentrations that ranged between 2000 to 2460 µg of Ni/g dry mass of the plant.³⁶ The most important role of Ni hyperaccumulation is to serve as the elemental defense of *Streptanthus polygaloides*. Several studies have shown the role of Ni is to serve as an effective defensive mechanism against many herbivores.³⁸⁻⁴²

Although there is extensive information known about where the nickel is taken up and where it ends up in the plants there is still a lack in knowledge about the nickel trafficking proteins. Most plants store the nickel as nickel citrate or nickel histidine complexes in the vacuoles but it is not clear how the nickel gets there since it has to cross important barriers in the plants to be able to get from the roots to the stems and leaves. Also the complete genetic map of *Streptanthus polygaloides* is not available. In this study we tried to use a metallobiome approach to see if we can detect any nickel-containing proteins that have not been characterized before.

5.2 Materials and methods

Growing of *M. marburgensis* cells required anaerobic conditions. Cells were grown in an air-tight fermenter and all the purification steps were done in a glove box (Coy Laboratory Products, Inc., Grass Lake, USA) filled with a gas mixture consisting of 95% N₂ and 5% H₂. All the buffers and solutions used in the procedures were filtered with a 0.45 µm Millipore filter to remove any particles, then degassed by boiling them first and then flushed with nitrogen gas and subsequent cooled down followed by overnight equilibration inside the glove box. Purification from the plant sample though didn't require maintaining any such anaerobic condition. So the purification steps were done on the bench top.

5.2.1 Growth of *Methanothermobacter marburgensis* cells

Methanothermobacter marburgensis was grown at 65 °C in a glass fermenter (New Brunswick) containing 10 L of growth medium for 13 hrs. Growing of *M. marburgensis* cells used the protocol described previously.⁴³ The growth medium contained 90 g KH₂PO₄, 27 g NH₄Cl, 33 g Na₂CO₃, 15 mL trace elements (contains nitrilotriacetic acid, MgCl₂, FeCl₂, CoCl₂, NaMoO₄ and NiCl₂) and 0.5 ml of 0.2% resazurin. The anaerobic condition of the growth medium was maintained by gassing with 80% H₂/20% CO₂ and 0.1% H₂S at a rate of 1,200 mL/min. Resazurin was added to the medium as an indicator, so that change in the color (from blue to colorless) would indicate when sufficient anaerobic conditions were reached and the medium was ready for inoculating. After 1-2 hour, when the optimum temperature and anaerobic condition were reached, the medium was inoculated with about 200 mL of cell culture from the earlier prepared stock. The stirring motor speed was set at 1000 rpm. After 13 hrs of incubation the OD of the medium was checked. If the OD₅₆₈ of the medium was about ~4, the cells were ready to harvest.

5.2.2 Harvest and sonication of *M. marburgensis* cells

The cells were harvested anaerobically by centrifugation at 15,000 rpm using a flow-through centrifuge (Sorvall[®] Biofuge, Stratos) until almost all the growth medium was passed through the centrifuge. The anaerobic condition of transfer tubes and flow-through rotor was maintained by passing degassed Potassium phosphate buffer (KPP buffer) and pre-filling the rotor. The rotor along with the cells was brought inside the anaerobic tent. The cells were then suspended in Buffer A containing 50 mM Tris-HCl at pH 7.6. The suspended cells were then sonicated on ice 3 times for a total of 3.5 mins for each cycle (pulsing on for 0.5 second and off for 0.5 second). The cells were allowed to cool down in between each run for a few minutes at the end of the procedure. The sonicated cells were then centrifuged anaerobically at 35000 rpm for 20 minutes at 4°C using a Type 45 Ti rotor in a Beckman XL-70 Ultracentrifuge. The supernatant after the centrifugation was carefully poured into a beaker inside the anaerobic tent.

5.2.3 Protein purification and metal ion detection

The supernatant after the sonication was collected and concentrated by filtration using a 10 kDa filter to 10-11 mL and was subsequently applied to a Sephacryl[™] 300 column equilibrated with Buffer C containing 50 mM Tris-HCl, pH 7.6 and 100 mM NaCl. The protein fractions were then analyzed for the presence of metal ions using Inductively-Coupled Plasma: Optical Emission Spectrophotometry (ICP-OES) present in the laboratory of Dr Paul Cobine in the Biological Science Department at Auburn University. Only the smaller-size protein fractions having nickel were then collected and applied to a Q-Sepharose column equilibrated with Buffer A containing 50 mM Tris-HCl, pH 7.6. A NaCl step gradient was used to elute the proteins from the column by using Buffer D containing 50 mM Tris-HCl, pH 7.6 and 1 M NaCl. Again the protein fractions were analyzed to determine the nickel ion content using ICP-OES. The different

protein fractions, having nickel in them, were further purified separately on a Mono-Q column. Different fractions from each run of the Mono-Q column were further analyzed to determine the nickel ion concentration using ICP-OES. The different fractions collected from the Mono-Q run were then analyzed for purity on a 15% SDS-PAGE gel.

5.2.4 Purification from the plant material

The plant material we were working with was provided by Dr. Robert Boyd of the Biological Science Department at Auburn University. A plant sample from *Streptanthus polygaloides* was frozen in liquid nitrogen. The dried plant material was then ground heavily using a mortar and pestle. A suspension was created by adding ~200 mL of buffer containing 50 mM Sodium phosphate, pH 7.5 with 1 mM polyethylene glycol (m.w. 8000), 0.01% (v/v) Triton X-100 and 1 mM phenylmethylsulfonyl fluoride (PMSF). The suspension was centrifuged at 35000 rpm for 20 minutes at 4°C using a Type 45 Ti rotor in a Beckman XL-70 Ultracentrifuge. The supernatant after the centrifuge was poured carefully into a beaker. The supernatant was applied to a DEAE-sepharose column equilibrated with Buffer A containing 50 mM sodium phosphate, pH 7.5. A NaCl gradient was applied using Buffer B containing 50 mM sodium phosphate, pH 7.5 with 1 M NaCl to elute the proteins. The different protein fractions were then analyzed for nickel ion content by ICP-OES. The protein fractions contain nickel were pooled together and concentrated to 2-3 mL using a 10 kDa filter. The concentrated solution was then applied to a Superdex™ 100 column equilibrated with Buffer C containing 50 mM sodium phosphate, pH 7.5 and 100 mM NaCl. The flow through from the DEAE-sepharose column step was also lyophilized and dissolved into 3 mL of Buffer A. This lyophilized flow-through sample was also applied to the Superdex™ 100 column equilibrated with Buffer C. The protein fractions from both the runs were analyzed to determine the nickel ion content. Only the fractions

containing nickel in them were analyzed further on a 15% SDS-PAGE gel. The bands on the gel that looked 'pure' were sequenced using mass spectrometry. We have performed NCBI-BLAST searches with the obtained sequences.

5.2.5 Sequencing of protein bands

Protein bands from SDS-PAGE gel was sequenced in the Mass Spectrometry Facility at the Department of Chemistry and Biochemistry, Auburn University.

5.3 Results

5.3.1 Purification of different protein fractions from *M. marburgensis*

This work was carried out in Dr. E. C. Duin's laboratory at Auburn University. After a centrifugation step, *M. marburgensis* cell extract was applied to a Sephacryl™ 300 column. The chromatography profile looked promising with many different protein peaks. The fractions no. 15-70 (high absorbance at 280 nm) were used to do the metal ion determination. The nickel content for two runs is shown in Figure 5.4A. We also analyzed for some other metals as well (Figure 5.4B). The protein fractions 21-45 have different enzymes in them, these are most likely (for the nickel enzymes), F₄₂₀-non-reducing hydrogenase (MVH), methyl coenzyme M reductase (MCR), and the hydrogenase/heterodisulfide reductase complex. These fractions were used for other studies going on in the Duin laboratory. We were interested in the smaller-sized proteins: Fractions 46-60 (Figure 5.5).

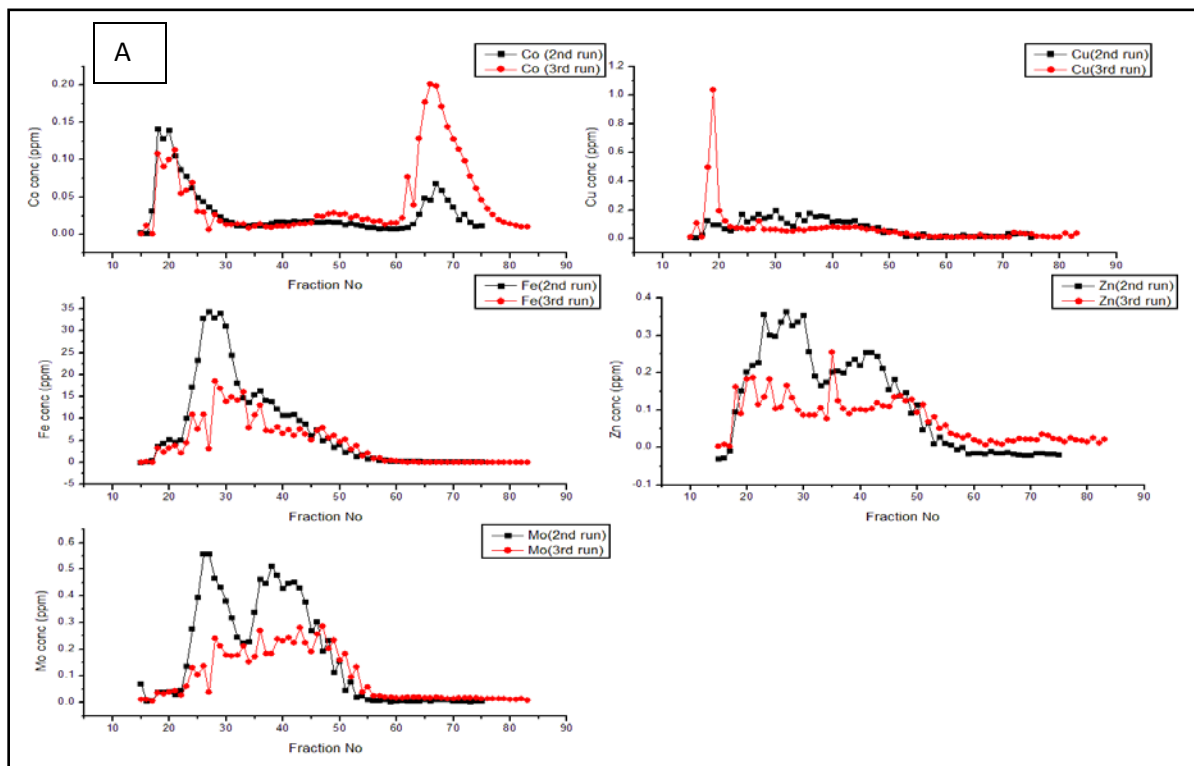
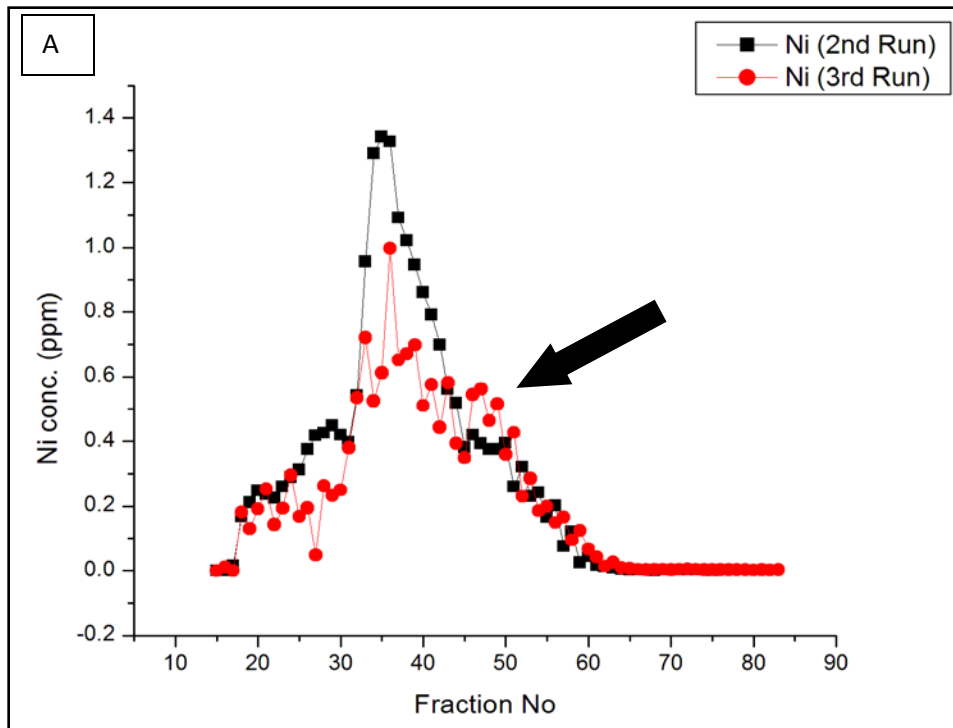


Figure 5.4 Metal concentrations from different run of *M. marburgensis* after Sephacryl run. A.

Showing the Ni concentration. B. Showing the concentrations of Cu, Co, Mo, Zn and Fe.

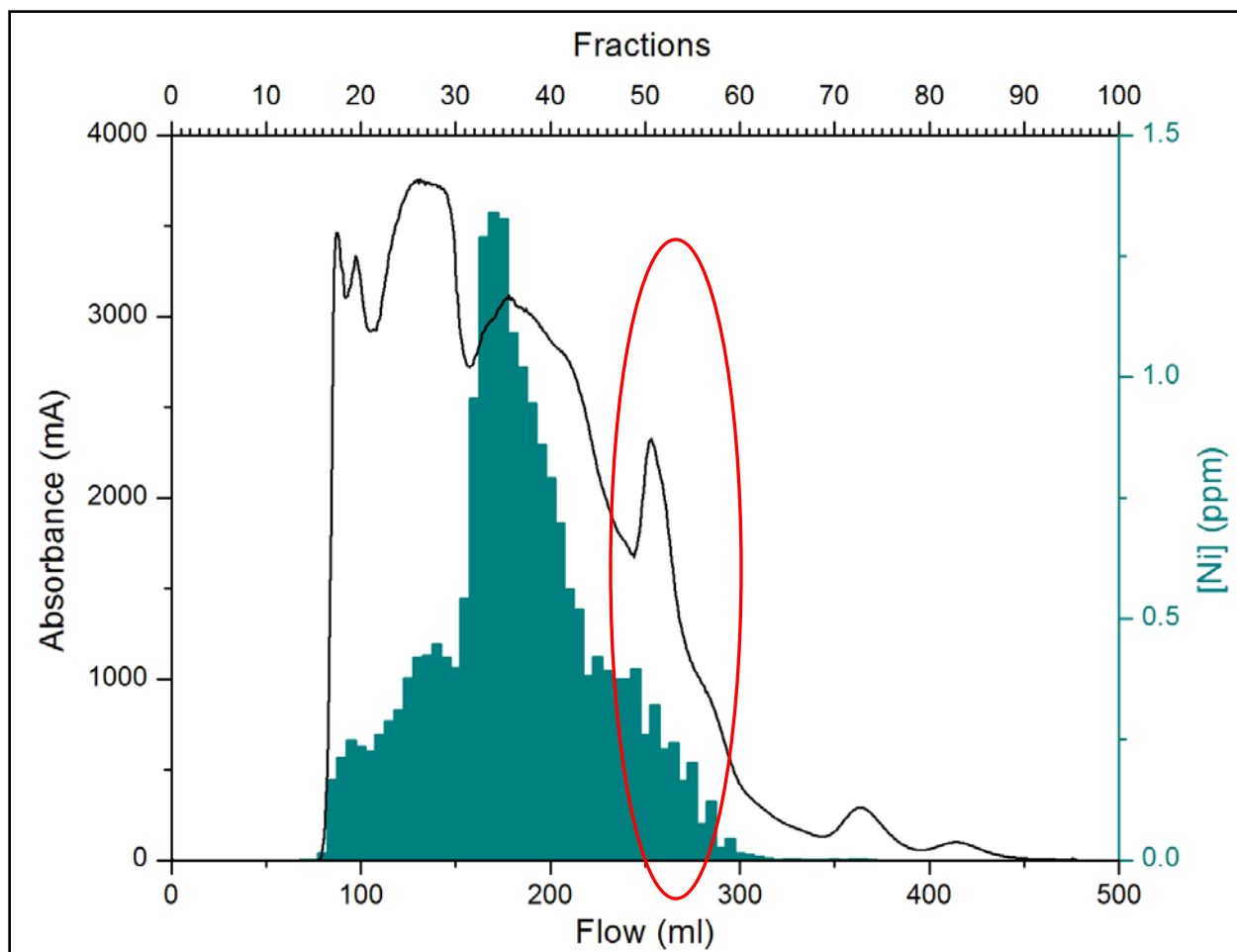


Figure 5.5 Ni profile of the different protein peaks with the after Sephacryl column run. The black line is the absorbance at 280 nm. The columns in dark cyan are the indicators for the nickel ion content.

The protein fractions 46-60 were pooled together and then applied to the Q-sepharose column. Different protein peaks appeared on the chromatography profile (Figure 5.6). All the different protein peaks were analyzed to determine the nickel ion content. Two major protein peaks (indicated as A & B) have a considerable amount of nickel present (Figure 5.6). So we decided to further purify peak A (fraction no 28-31) and B (fraction no 44-49).

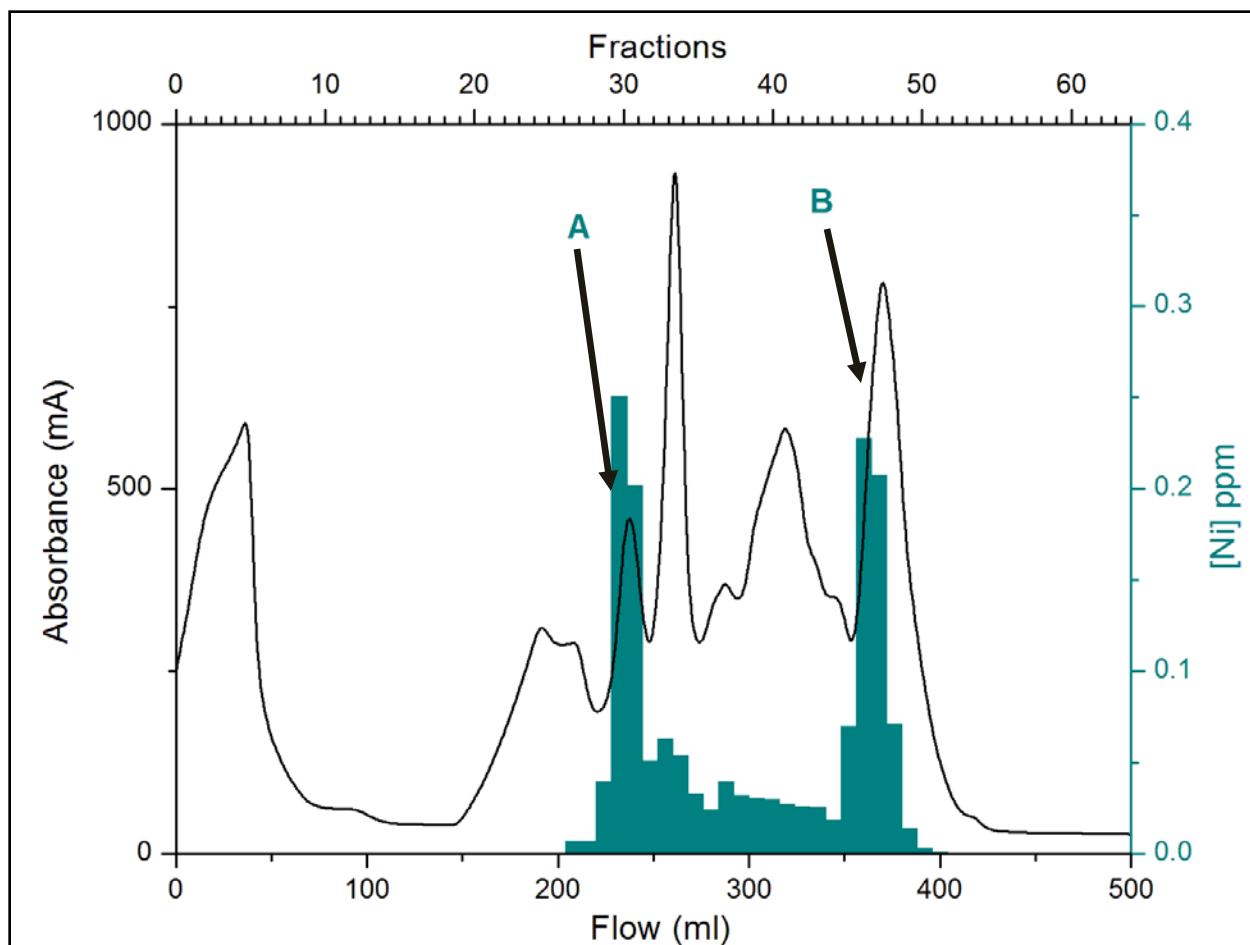


Figure 5.6 Ni profile of the different protein peaks with the after the Q-sepharose column. The black line is the absorbance at 280 nm. The columns in dark cyan are the indicators for the nickel ion content. Peak A and B (marked by the arrows) have considerable amount of nickel ions present.

We pooled Peak A and Peak B separately. Both of the peaks A and B were then applied to a Mono-Q column. The chromatography profile for protein sample B has only one main protein peak (Figure 5.6). The 15% SDS-PAGE gel showed the presence of three major bands in all the fractions that were of similar size of the three subunits of MCR (Figure 5.7). Therefore this sample was not studied any further. The mono-Q chromatographic profile of peak A from the Q-sepharose column step yielded lots of different peaks (Figure 5.8). Here we did determine the nickel ion content for the different fractions (no 15-26) and found out that fractions 18-24 have considerable amounts of nickel present (Figure 5.8). These fractions were analyzed on a 15% SDS-PAGE gel (Figure 5.9). Fractions 21-23 clearly show the presence of several protein bands indicating that additional purification steps will be needed. The three concentrated bands were partially sequenced. The BLAST search showed that the two bands at around 30-35 kDa are probably due to translation elongation factor EF 1 α while the 22 kDa band is probably due tungsten-containing formylmethanofuran dehydrogenase II, subunit C. This indicates that one of the minor bands has to be the nickel-containing protein and further purification is needed.

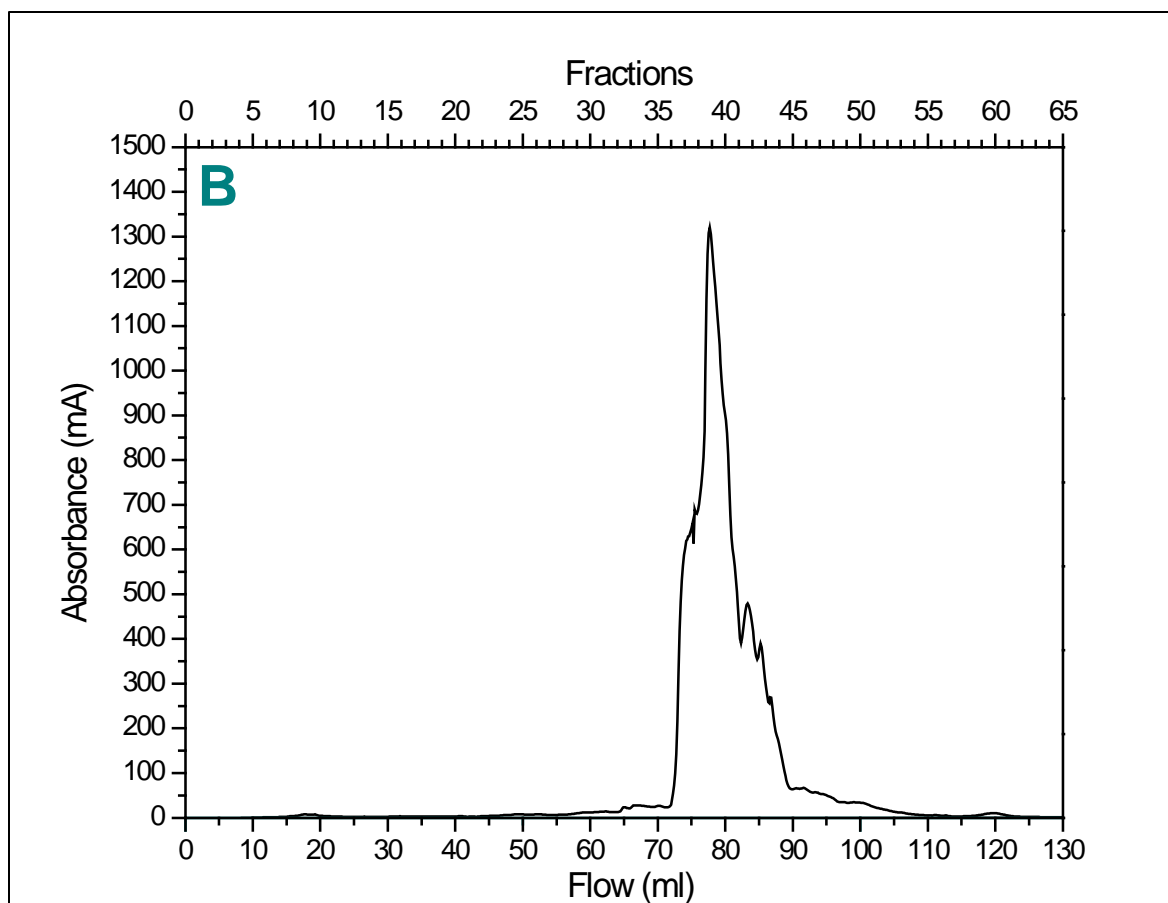


Figure 5.6 Mono-Q profile for the B peak obtained from the Q-sepharose column step. The black line is the absorbance at 280 nm. Nickel ion content was not determined.

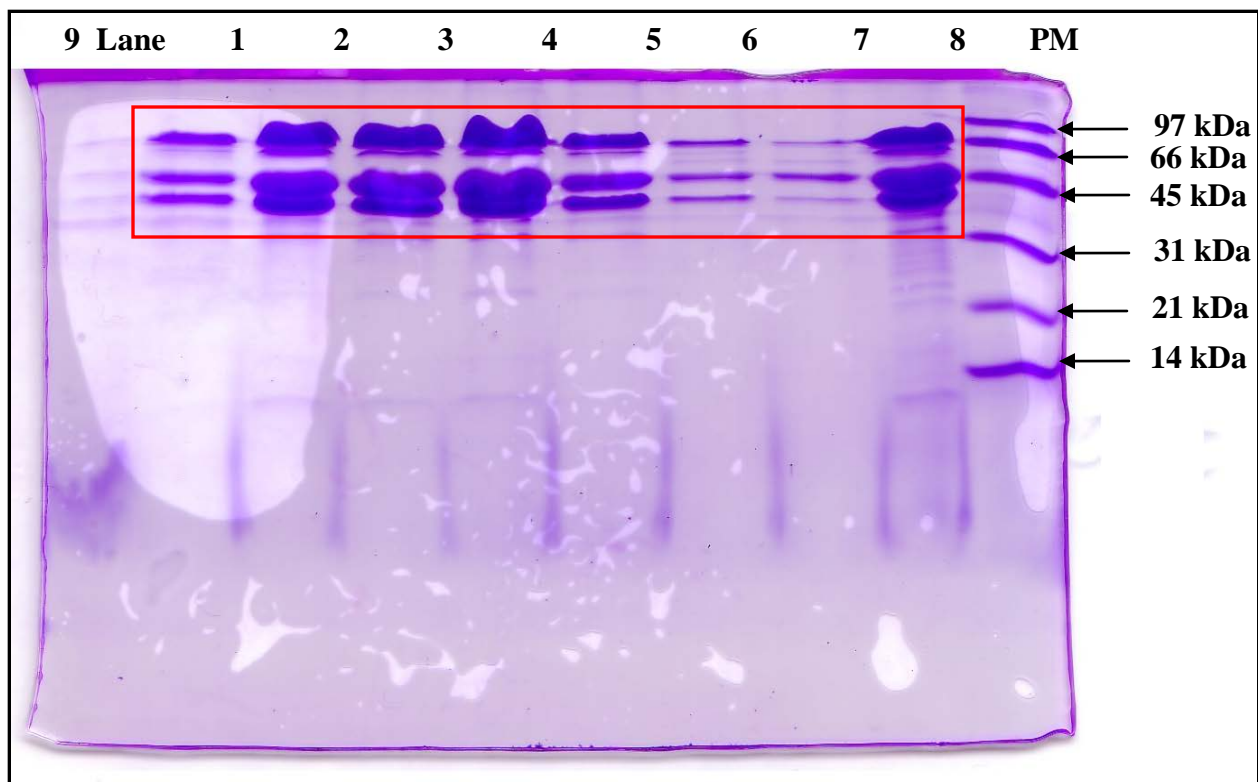


Figure 5.7 15% SDS-PAGE analysis of the fractions of peak B (from Q-sepharose column) after Mono-Q run. Lane 1-8 corresponds to different proteins fractions number from 38-45. Lane 9 corresponds to the protein marker (Molecular weights of the marker are leveled on the side). The bands (lane 1-8) shown in the red box corresponds to the methyl co-enzyme M reductase (MCR).

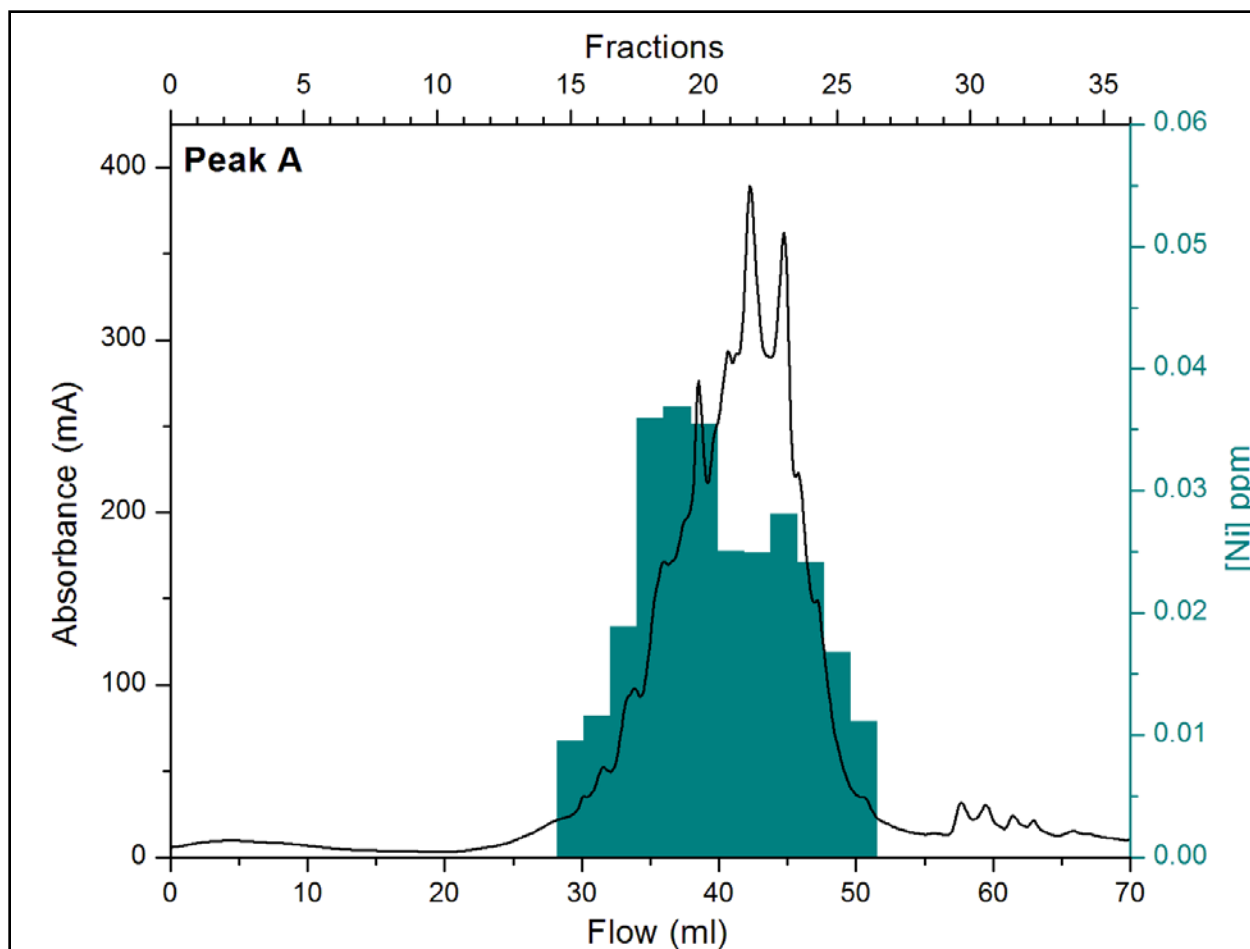


Figure 5.8 Ni profile of different protein peaks of Peak A (from Q-sepharose) after Mono-Q run. The red circle is showing fractions 20-24, which are distinct protein peaks with considerable amount of Ni in them, which we further analyzed in 15% SDS-PAGE gel.

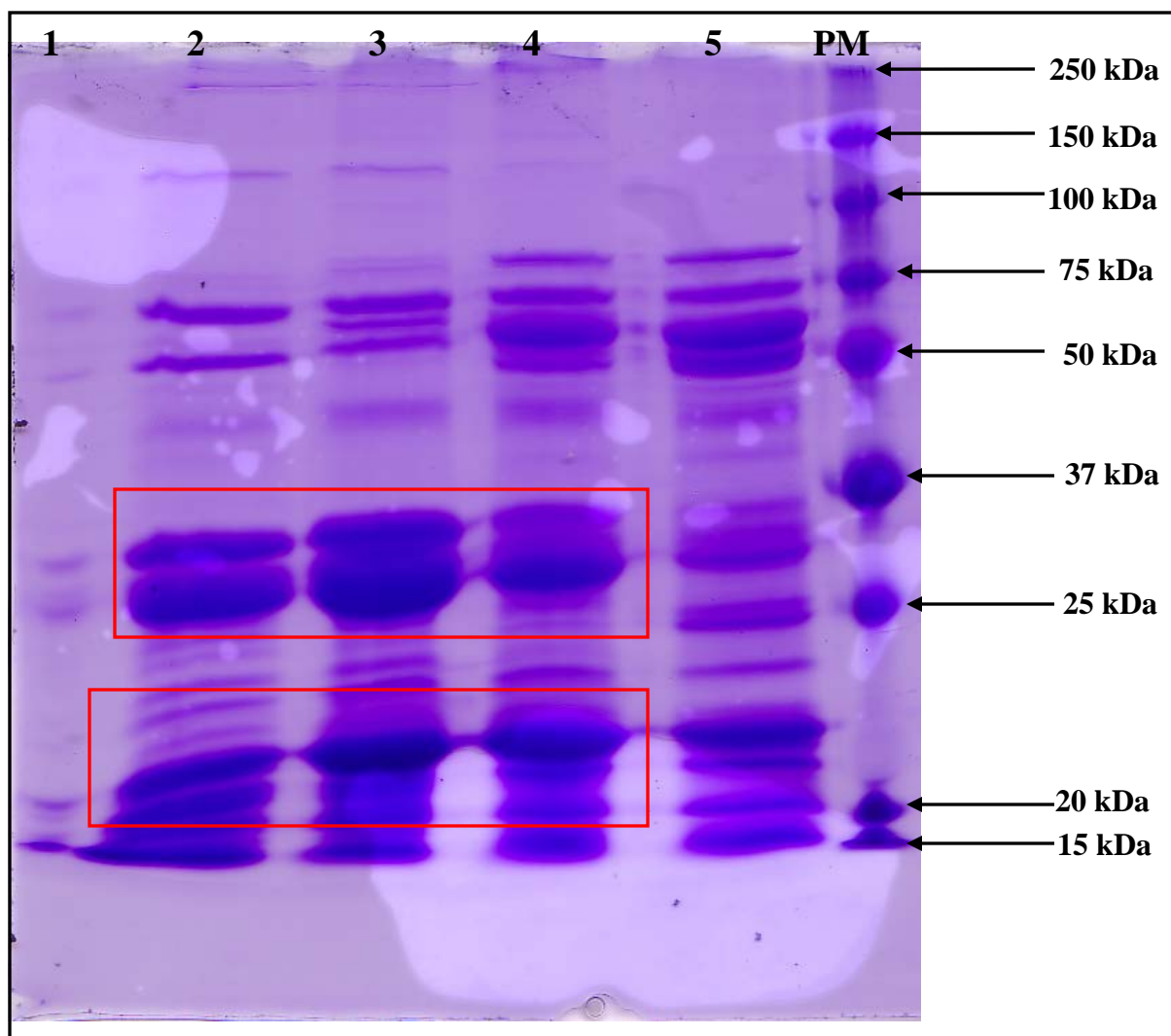


Figure 5.9 15% SDS-PAGE analysis of different protein peaks from peak A (from Q-sepharose) after Mono-Q run. Lane 1-5 corresponds to different proteins fractions number from 20-24. Lane 6 corresponds to protein marker (Molecular weights of the marker are leveled on the side). Protein fraction from 21-23 are showing same pattern of protein bands (showing in red box).

5.3.2 Purification of different protein fractions from plant material

The supernatant obtained from the centrifugation of the cell extract of the plant sample from *Streptanthus polygaloides* was applied onto the DEAE-sepharose column. The chromatographic profile has two big protein peaks in it. We ignored the early protein peaks (Peak B, fraction nos. 1-10) for the time being, as they didn't bind to the column (Figure 5.10). We kept those fractions for later analysis. A large peak with high nickel content was detected in the middle of the profile (Peak A, Figure 5.10). We pooled the fractions 29-37 and applied them onto a Superdex™ 100 column.

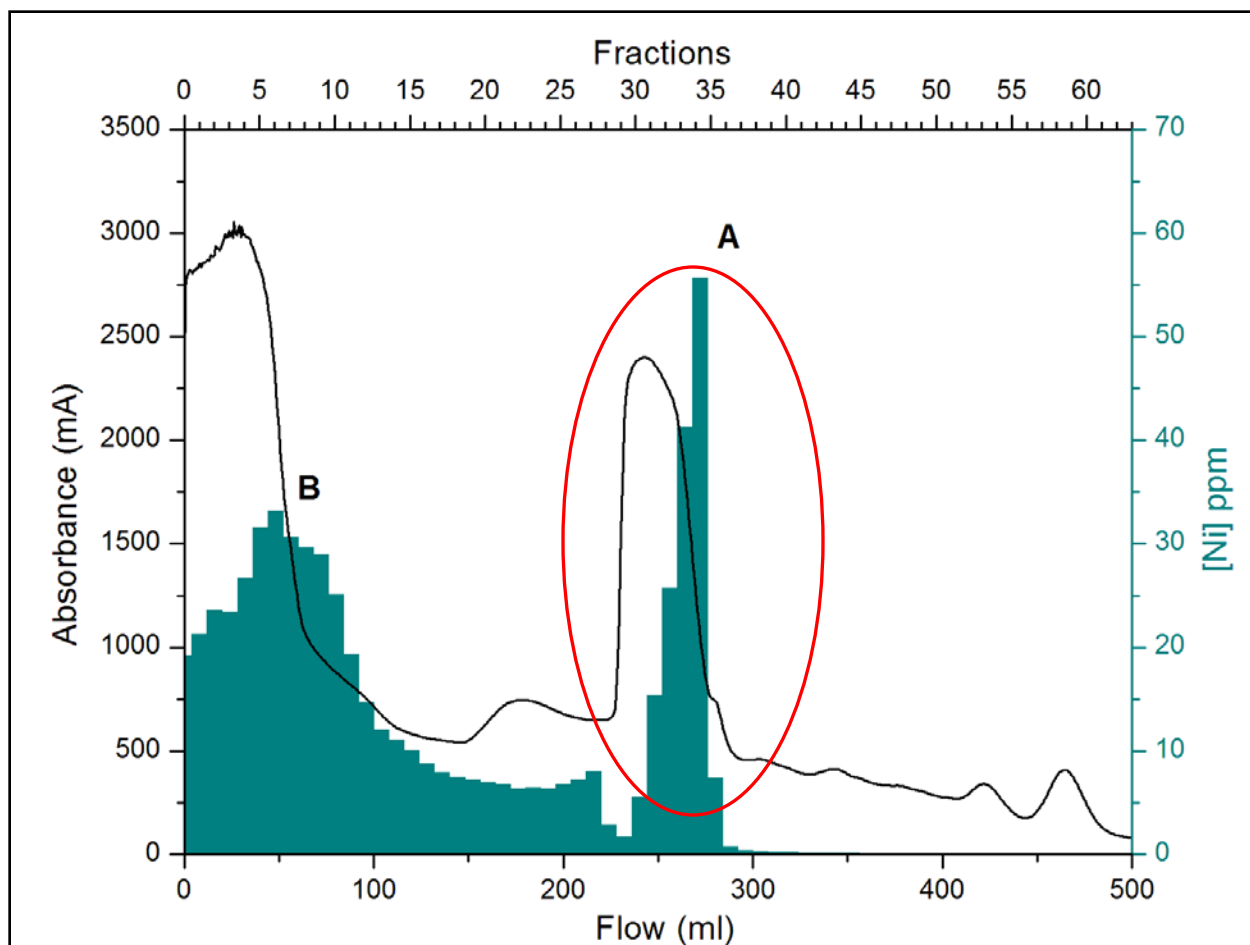


Figure 5.10 Ni profile of different protein fractions from *Streptanthus polygaloides* after running into DEAE-sepharose column. The protein fraction 29-37 (indicated by red circle) was pooled for the further purification.

The protein fractions 29-37 from the DEAE run were pooled and concentrated using a 10 kDa filter to a volume of 2 mL. This concentrated sample was then applied to the Superdex™ 100 column. The chromatographic profile has three distinctive protein peaks (Figure 5.11). The nickel concentration for all the three peaks was determined and only the middle peak (fractions 27-31) contained a large amount of nickel (Figure 5.11). These fractions were analyzed by 15% SDS-PAGE gel (Figure 5.12). The main fractions seem to be pretty pure and only 5 clear bands can be detected on the gel. All five bands were sent in for sequencing. The sequencing was done by Dr. Yonnie Wu of the Mass Spec Facility at the Department of Chemistry & Biochemistry at Auburn University. Except for band 2, due to low concentration, data were obtained. The coverage maps for gel bands 1, 3, 4, and 5 are shown in Figure 5.13. These sequences were entered into NCBI-BLAST to find out the sequence similarities with known sequences. We used the non-redundant protein sequences (nr) database against *Arabidopsis thaliana* (also a member from Brassicaceae family). The matches are summarized in Table 5.1. Band 3 could be from a putative ATP-dependent transporter, while band 5 is from an unknown protein. Bands 1 and 4 are definitely not from nickel-containing proteins.

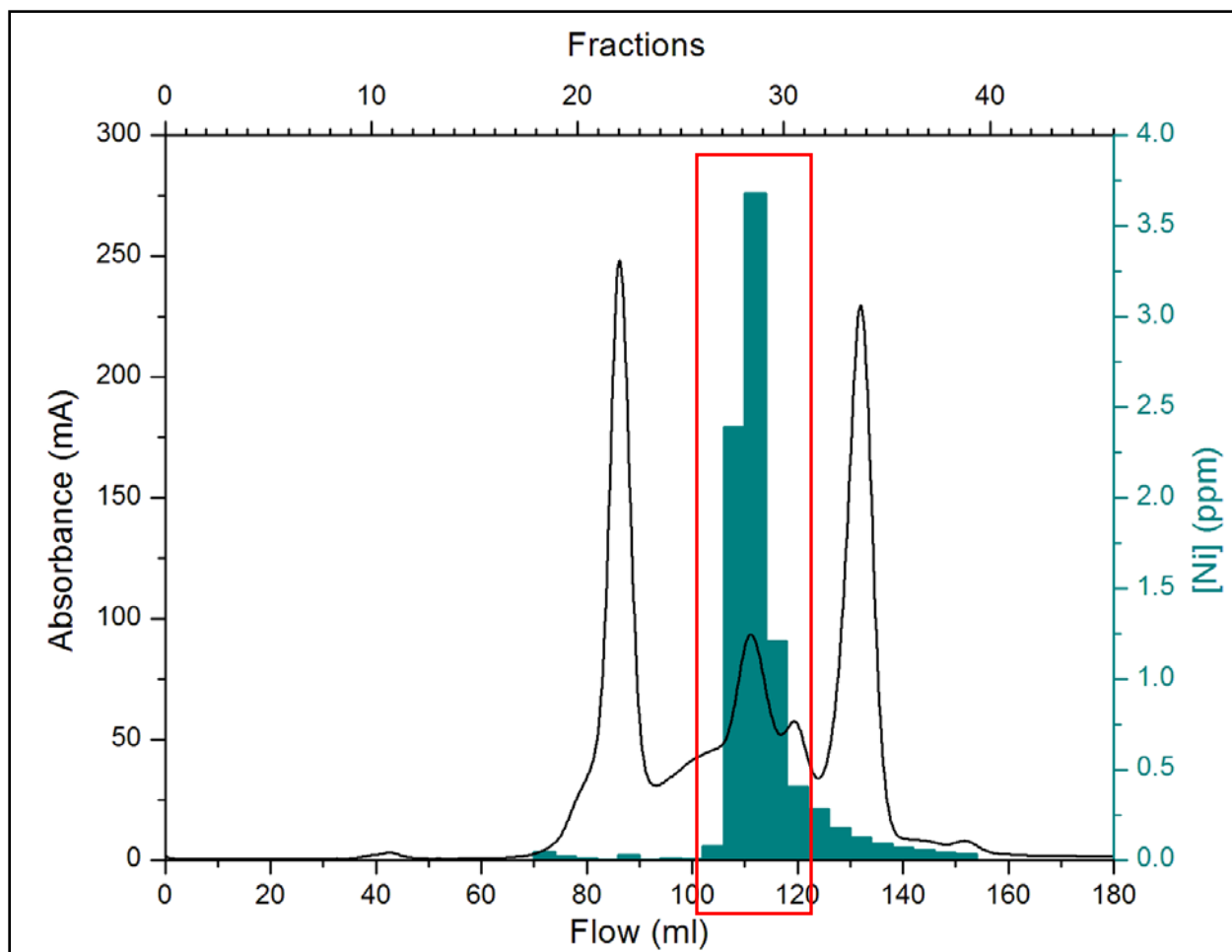


Figure 5.11 Ni profile of the protein peaks after running into Superdex™ 100 column. The protein peak (fraction no 27-31) indicated in red has a large amount of nickel in it.

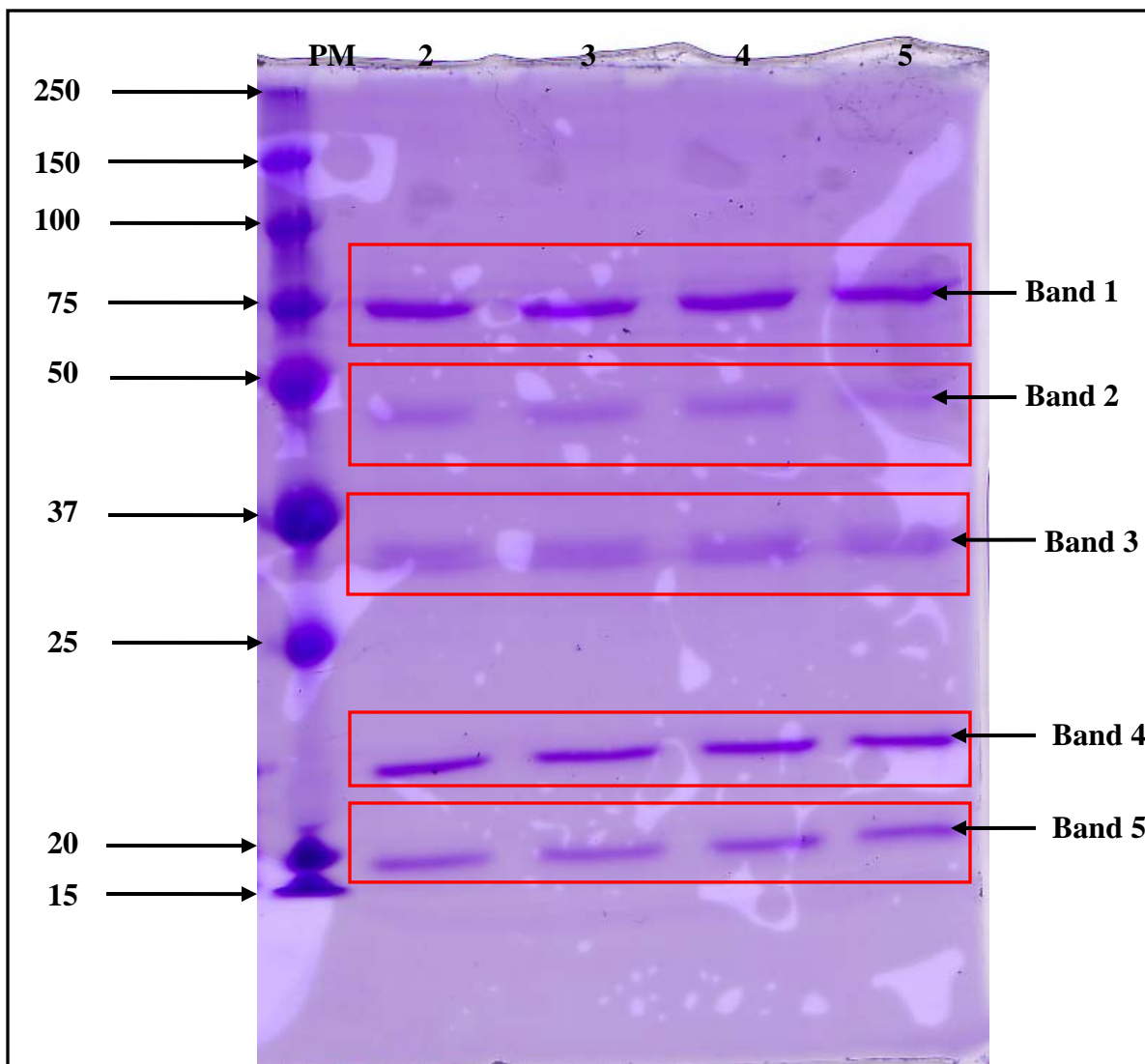


Figure 5.12 15% SDS-PAGE gel analysis of the fractions 28 and 30 (after the Superdex column run). Lane 1: Protein marker (Molecular weight in the side in kDa). Lane 2 & 3: Fraction 28. Lane 4 & 5: Fraction 30. Both the fractions have five separate protein bands (Band 1-5) shown in red box.

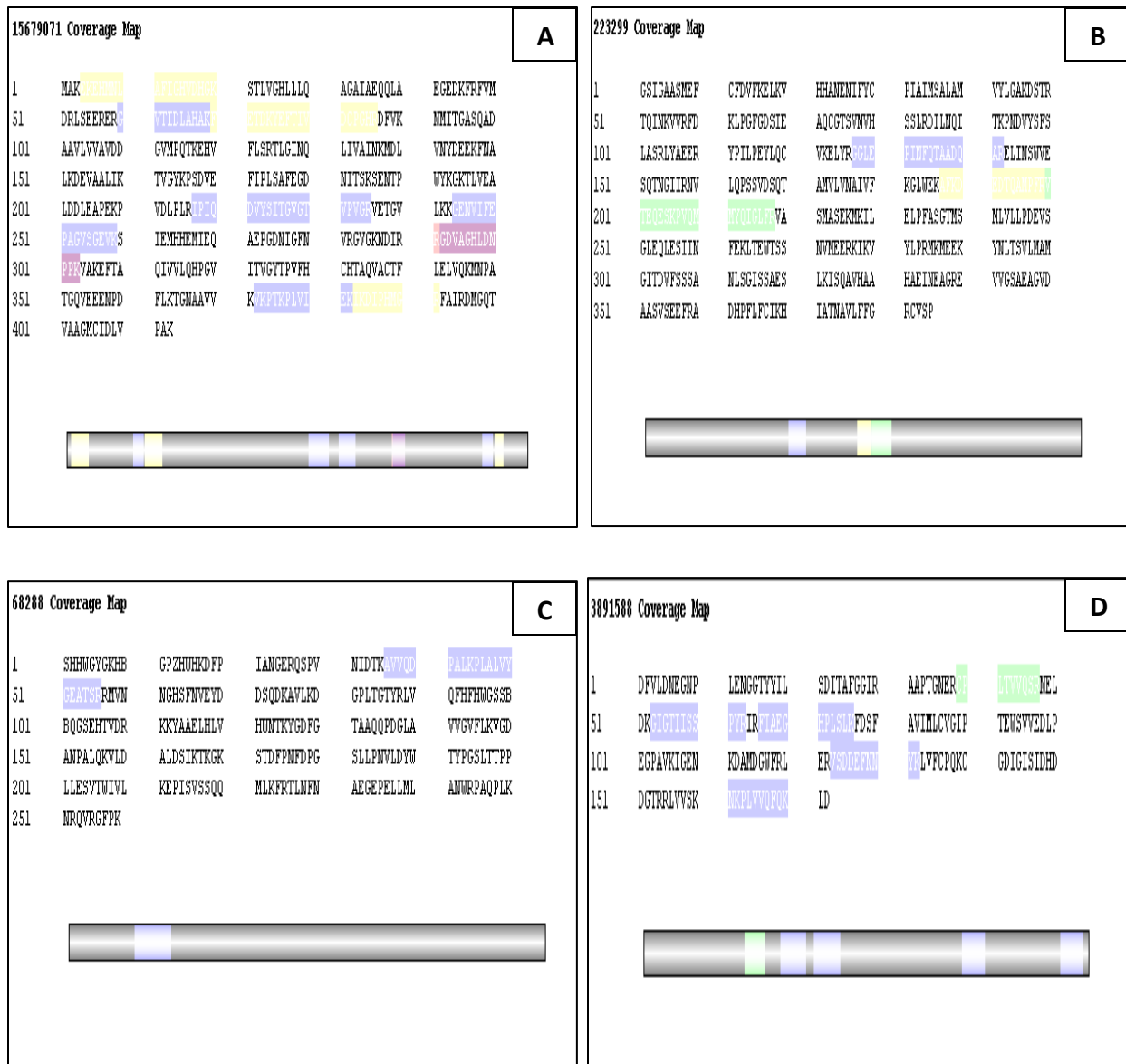


Figure 5.13 Coverage map of Band 1, 3, 4 and 5 (of the fractions 28 and 30) from SDS-PAGE gel. A. Band 1. B. Band 3. C. Band 4 and D. Band 5.

Band from 15% gel	Matches found
Band 1	Translation elongation factor EF1A/initiation factor IF2gamma family protein [<i>Arabidopsis thaliana</i>]
Band 3	Putative calcium-transporting ATPase [<i>Arabidopsis thaliana</i>] Hypothetical protein [<i>Arabidopsis thaliana</i>]
Band 4	MIRO-related GTP-ase 1 [<i>Arabidopsis thaliana</i>]
Band 5	Uncharacterized protein [<i>Arabidopsis thaliana</i>]

Table 5.1 NCBI-BLAST search for the protein bands from 15% gel.

When the DEAE fraction was concentrated down, using a 10 kDa filter, the filtrate, however, could also contain protein or even the small sized Ni-His₆ complex. Therefore this filtrate was lyophilized and subsequently dissolved in 50 mM sodium phosphate buffer, pH 7.5. This sample was then loaded onto the SuperdexTM 100 column. The chromatographic profile has two very distinct protein peaks (Figure 5.14). We also determined the nickel concentration in them and saw that fractions 28-31 contain a large amount of nickel ion (Figure 5.14). This peak has not been fully analyzed yet. No bands were detected on a 15% SDS-PAGE which could be in line with the presence of Ni-His₆ in the sample.

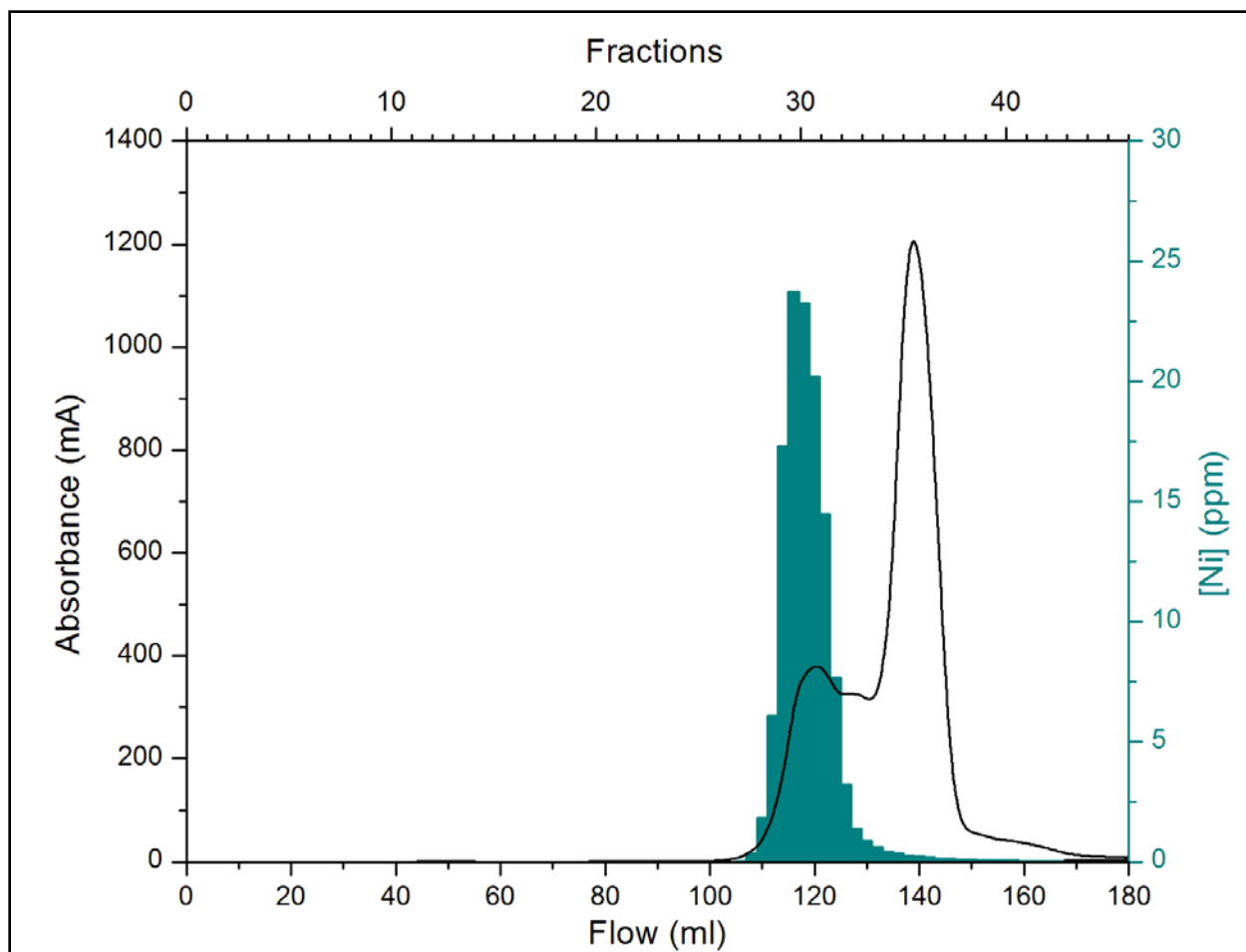


Figure 5.14 Ni ion profile after the Superdex-100 run for the DEAE-filtrate. The black line is the absorbance at 280 nm. The columns in dark cyan are the indicators for the nickel ion content.

5.4 Discussion and Future direction

In all cases, both *M. marburgensis* and *S. polygaloides*, the obtained protein fractions are not pure yet and further purification is needed. For some of the fractions, however, well separated protein bands of SDS-PAGE gels could be obtained and these have been sent in for sequencing. Some of these bands could be due to the nickel containing enzymes we are hoping to find. One way to do that is to solubilize that individual gel bands and check their nickel-content directly.

This project is clearly a work in progress and a lot more fractions and bands have to be further characterized. However, these initial results indicate that with the followed procedures and application of ICP-OES we should be successful in finding and characterizing these proteins in the near future.

References:

- (1) Mulrooney, S. B., and Hausinger, R. P. (2003) Nickel uptake and utilization by microorganisms. *FEMS Microbiol. Rev.* 27, 239–261.
- (2) Ragsdale, S. W. (2009) Nickel-based Enzyme Systems. *J. Biol. Chem.* 284, 18571–18575.
- (3) Maier, R. J. (2005) Use of molecular hydrogen as an energy substrate by human pathogenic bacteria. *Biochem. Soc. Trans.* 33, 83–85.
- (4) Olson, J. W., and Maier, R. J. (2002) Molecular hydrogen as an energy source for *Helicobacter pylori*. *Science* 298, 1788–1790.
- (5) Böck, A., King, P. W., Blokesch, M., and Posewitz, M. C. (2006) Maturation of hydrogenases. *Adv. Microb. Physiol.* 51, 1–71.
- (6) Forzi, L., and Sawers, R. G. (2007) Maturation of [NiFe]-hydrogenases in *Escherichia coli*. *BioMetals* 20, 565–578.
- (7) Eaton, K. A., Brooks, C. L., Morgan, D. R., and Krakowka, S. (1991) Essential role of urease in pathogenesis of gastritis induced by *Helicobacter pylori* in gnotobiotic piglets. *Infect. Immun.* 59, 2470–2475.
- (8) Evans, D. J., Jr., Evans D. G., Kirkpatrick S. S., and Graham. D. Y. (1991) Characterization of the *Helicobacter pylori* urease and purification of its subunits. *Microb. Pathog.* 10, 15–26.
- (9) Maier, R. J., Fu C., Gilbert J., Moshiri F., Olson J., and Plaut A. G. (1996) Hydrogen uptake hydrogenase in *Helicobacter pylori*. *FEMS Microbiol. Lett.* 141, 71–76.

- (10) Schneider, E., and Hunke, S. (1998) ATP-binding-cassette (ABC) transport systems: Functional and structural aspects of the ATP-hydrolyzing subunits/domains. *FEMS Microbiol. Rev.* 22, 1–20.
- (11) Rodrigue, A., Effantin, G., and Mandrand-Berthelot, M. A. (2005) Identification of *rcnA* (*yohM*), a nickel and cobalt resistance gene in *Escherichia coli*. *J. Bacteriol.* 187, 2912–2916.
- (12) Blériot, C., Effantin, G., Lagarde, F., Mandrand-Berthelot, M. A., and Rodrigue, A. (2011) RcnB is a periplasmic protein essential for maintaining intracellular Ni and Co concentrations in *Escherichia coli*. *J. Bacteriol.* 193, 3785–3793.
- (13) Hube, M., Blokesch, M., and Bock, A. (2002) Network of hydrogenase maturation in *Escherichia coli*: Role of accessory proteins HypA and HybF. *J. Bacteriol.* 184, 3879–3885.
- (14) Higgins, K. A., Carr, C. E., and Maroney, M. J. (2012) Specific Metal Recognition in Nickel Trafficking. *Biochemistry* 51, 7816–7832.
- (15) Boone, D. R., Whitman, W. B., and Rouvière, P. (1993) Diversity and taxonomy of methanogens. In J. G. Ferry (ed.), *Methanogenesis*. Chapman & Hall, New York, NY, 35-80.
- (16) Fuchs, G., Stupperich, E., and Thauer, R. K. (1978) Acetate assimilation and the synthesis of alanine, aspartate and glutamate in *Methanobacterium thermoautotrophicum*. *Arch. Microbiol.* 117, 61-66.
- (17) Liesegang, H., Kaster, A. K., Wiezer, A., Goenrich, M., Wollherr, A., Seedorf, H., Gottschalk, G., and Thauer R. K. (2010) Complete Genome Sequence of *Methanothermobacter marburgensis*, a Methanoarchaeon Model Organism. *J Bacteriol.* 192, 5850–5851.
- (18) Kaster, A. K, Goenrich, M., Seedorf, H., Liesegang, H., Wollherr, A., Gottschalk, G., and Thauer RK. (2011) More than 200 genes required for methane formation from H₂ and CO₂ and

energy conservation are present in
Methanothermobacter marburgensis and *Methanothermobacter thermautotrophicus*. *Archaea*
2011, 1-23.

(19) Anderson, C., Deram, A., Petit, D., Brooks, R., Stewart, R. and Simcock, R. (2001). In:
Trace elements in soil: bioavailability, flux, and transfer. (Eds. I.K. Iskandar and M.B. Kirkham)
Lewis, Washington DC, 63-76.

(20) Pagliano, C., Raviolo, M., Vecchia, F. D., Gabbrielli, R., Gonnelli, C., Rascio,
N., Barbato, R., and Rocca, N. La (2006) Evidence for PSII-donor-side damage and
photoinhibition induced by cadmium treatment on rice (*Oryza sativa* L.). *J. Photochem.*
Photobiol. B: Biol. 84, 70–78.

(21) Rocca, N. La, Andreoli, C., Giacometti, G.M., Rascio, N., and Moro, I. (2009) Responses
of the Antarctic microalga *Koliella antartica* (Trebouxiophyceae, Chlorophyta) to cadmium
contamination. *Photosynthetica* 47, 471–479.

(22) Rascio, N., and Navari-Izzo, F. (2011) Heavy metal hyperaccumulating plants: How and
why do they do it? And what makes them so interesting? *Plant Science* 180, 169–181.

(23) Brooks, R. R., Lee, J., and Jaffré, T. (1974) Some New Zealand and New
Caledonianvplant accumulators of nickel. *Journal of Ecology* 62, 493–499.

(24) Brooks, R. R., Lee, J., Reeves, R. D., and Jaffré, T. (1977) Detection of nickeliferous
rocks by analysis of herbarium specimens of indicator plants. *Journal of Geochemical*
Exploration 7, 49–57.

(25) Baker, A. J. M., and Brooks, R. R. (1989) Terrestrial higher plants which
hyperaccumulate metallic elements. A review of their distribution, ecology and phytochemistry.
Biorecovery 1, 81–126.

- (26) Reeves, R. D., and Baker, A. J. M. (2000) Metal-accumulating plants. In: Raskin I, Ensley BD, eds. *Phytoremediation of toxic metals: using plants to clean up the environment*. New York, NY, USA: John Wiley, 193–229.
- (27) Reeves, R. D. (2003) Tropical hyperaccumulators of metals and their potential for phytoextraction. *Plant and Soil* 249, 57–65.
- (28) Ellis, D. R., and Salt, D. E. (2003) Plants, selenium and human health. *Current Opinion in Plant Biology* 6, 273–279.
- (29) Sors, T. G., Ellis, D. R., Na, G. N., Lahner, B., Lee, S., Leustek, T., Pickering, I. J., and Salt, D. E. (2005) Analysis of sulfur and selenium assimilation in *Astragalus* plants with varying capacities to accumulate selenium. *Plant Journal* 42, 785–797.
- (30) Milner, M. J., and Kochian, L. V. (2008) Investigating heavy-metal hyperaccumulation using *Thlaspi caerulescens* as a model system. *Annals of Botany* 102, 3–13.
- (31) Verbruggen, N., Hermans, C., and Schat, H. (2009) Molecular mechanisms of metal hyperaccumulation in plants. *New Phytol.* 181, 759–776.
- (32) Macnair, M. R. (2003) The hyperaccumulation of metals by plants. *Advances in Botanical Research* 40, 63–105.
- (33) Brooks, R. R. (1998) (Ed.) *Plants that Hyperaccumulate Heavy Metals*, CAB International, Wallingford, UK, 380.
- (34) Sagner, S., Kneer, R., Wanner, G., Cosson, J. P., Deus-Neumann, B., and Zenk, M. H. (1998) Hyperaccumulation, complexation and distribution of nickel in *Sebestia acuminata*. *Phytochemistry* 47, 339–347.
- (35) Callahan, D. L., Baker, A. J. M., Kolev, S. D., and Wedd, A. G. (2006) Metal ion ligands in hyperaccumulating plants. *J Biol. Inorg. Chem.* 11, 2–12.

- (36) Reeves, R. D., Brooks, R. R., and Macfarlane, R. M. (1981) Nickel uptake by Californian *Streptanthus* and *Caulanthus* with particular reference to the hyperaccumulator *S. polygaloides* Gray (Brassicaceae). *American Journal of Botany* 68, 708–712.
- (37) Kruckeberg, A. R. (1984) California serpentines: flora, vegetation, geology, soils and management problems. Berkeley, CA, USA: University of California Press.
- (38) Boyd, R. S., and Martens, S. N. (1994) Nickel hyperaccumulated by *Thlaspi montanum* var *montanum* is acutely toxic to an insect herbivore. *Oikos* 70, 21–25.
- (39) Boyd, R. S., and Martens, S. N. (1999) Aphids are unaffected by the elemental defense of the nickel hyperaccumulator *Streptanthus polygaloides* (Brassicaceae). *Chemoecology* 9, 1–7.
- (40) Boyd, R. S. and Moar, W. J. (1999) The defensive function of Ni in plants: response of the polyphagous herbivore *Spodoptera exigua* (Lepidoptera: Noctuidae) to hyperaccumulator and accumulator species of *Streptanthus* (Brassicaceae). *Oecologia* 118, 218–224.
- (41) Jhee, E. M., Boyd, R. S., and Eubanks, M. D. (2005) lackwell Publishing, Ltd. Nickel hyperaccumulation as an elemental defense of *Streptanthus polygaloides* (Brassicaceae): influence of herbivore feeding mode. *New Phytologist* 168, 331-344.
- (42) Jhee, E. M., Boyd, R. S., Eubanks, M. D., and Davis, M. A. (2006) Nickel hyperaccumulation by *Streptanthus polygaloides* protects against the folivore *Plutella xylostella* (Lepidoptera: Plutellidae). *Plant Ecology* 183, 91–104.
- (43) Schonheit, P., Moll, J., and Thauer, R. K. (1980) Growth-Parameters (Ks, Mu-Max, Ys) of *Methanobacterium-Thermoautotrophicum*. *Arch Microbiol* 127, 59-65.